SEISMIC DESIGN OF OUTRIGGER SYSTEMS FOR TALL BUILDINGS

by

Jeremy Charles Harry Atkinson

B.A.Sc., The University of British Columbia, 2013

A THESIS SUBMITTED IN PARTIAL FULFILLMENT OF
THE REQUIREMENTS FOR THE DEGREE OF

MASTER OF APPLIED SCIENCE
in
THE FACULTY OF GRADUATE AND POSTDOCTORAL STUDIES
(Civil Engineering)

THE UNIVERSITY OF BRITISH COLUMBIA
(Vancouver)

April 2017

© Jeremy Charles Harry Atkinson, 2017

Abstract

Outrigger systems are an effective structural scheme that is commonly used in high-rise construction to increase stiffness and distribute the moment demand within the core to the exterior columns. Despite the on-going use of outrigger structural systems around the world, a formal seismic design procedure for outrigger system is missing. This thesis presents an equivalent energy-based design procedure (EEDP) to design outrigger systems for seismic applications. Using the concept of an energy balance, elastic single-degree of freedom systems are equated to equivalent nonlinear systems, and plastic mechanisms are used to derive design forces for the outrigger systems. EEDP allows engineers to design the outrigger-wall buildings to achieve different performance objectives at different seismic hazard levels, which is desirable for creating earthquake-resilient buildings. Three prototype outrigger-wall buildings of various heights were designed using the proposed procedure for a hypothetical site in Vancouver, Canada. Detailed finite element models were developed using OpenSees to assess the seismic performance of the prototype buildings. The results of the nonlinear time history analyses show that the prototypes can meet the performance objectives specified during the design procedure. Lastly, incremental dynamic analyses were conducted using the FEMA P695 methodology to quantify the seismic safety of outrigger systems designed using EEDP. The results show that the proposed EEDP is an effective method to design outrigger systems, where the structure can achieve sufficient margin of safety against collapse and satisfy multiple performance objectives at different hazard levels without iteration.

Preface

This thesis is original, unpublished work by the Author. The Author was responsible for implementing, analyzing, documenting, and discussing all aspects of the presented research except where noted otherwise. Parts of this thesis are being reworked into a peer-reviewed journal paper which will be completed after the publication of this thesis. Notably, Chapters 3, 4, and 5 will be altered and condensed to compose the bulk of the publication.

Table of Contents

Abstract ii

Preface iii

Table of Contents iv

List of Tables vi

List of Figures vii

List of Symbols x

List of Abbreviations xii

Acknowledgements xiii

Dedication xiv

Chapter 1 Introduction 1

1.1 Literature Review 3

1.2 Objective and Scope 10

1.3 Thesis Organization 11

Chapter 2 Behavior of Outrigger Systems 13

2.1 Theoretical Solution of Elastic Outrigger System Response Under Static Load 13

2.2 Theoretical Solution of Elastic Outrigger System Response Under Dynamic Loads 20

Chapter 3 Design Methodology for Outrigger Systems 32

3.1 Conventional Design Approach 32

3.2 Equivalent Energy-Based Design Approach 37

Chapter 4 Performance Assessment of Outrigger System 52

4.1 Seismic Hazard 52

4.2 Ground Motion Selection 56

4.3 Prototype Buildings 57

4.4 Nonlinear Modelling Technique 62

4.5 Nonlinear Time-History Analysis Results 71

4.6 Comparison to Performance Objectives 84

Chapter 5 Verification of Design Procedure for Outrigger Systems 89

5.1 Overview of FEMA P695 methodology 89

5.2 Application to prototype outrigger buildings 93

Chapter 6 Conclusion 102

6.1 Conclusions and Significance 103
6.2 Future Research........ 103
Bibliography 105
Appendices........ 108
Appendix A: Design Calculations for 20-Story Prototype Building........ 108
Appendix B: Design Calculations for 30-Story Prototype Building........ 113
Appendix C: Design Calculations for 40-Story Prototype Building........ 118
Appendix D: Reinforcing Schedule for Prototype Buildings 123
Appendix E: Additional results from seismic performance assessment 124
E.1 Tower A........ 124
E.2 Tower B........ 136
E.3 Tower C........ 148

List of Tables

Table 1: Properties of existing outrigger buildings 7

Table 2: Comparison of theoretical and finite element models 19

Table 3: Properties of buildings used for parameter study 25

Table 4: Predicted first-mode periods from model and formula 30

Table 5: Example of performance objectives and structural response characteristics 39

Table 6: Values for modification factor C_0 (ASCE/SEI, 2014) 43

Table 7: Parameters for the C_0 Study 44

Table 8: Ground motions for the C_0 Study 44

Table 9: Ground motion properties for nonlinear analysis 56

Table 10: EEDP Displacements at each hazard and energy modification factors 58

Table 11: Wall cross-sectional properties for each prototype 59

Table 12: Summary of wall reinforcing at base and below outrigger 60

Table 13: Summary of outrigger fuse and member sizes on each prototype 60

Table 14: Modal periods for the prototype buildings 61

Table 15: Summary of concrete material properties for analysis 65

Table 16: Summary of steel material properties for analysis 66

Table 17: Material Properties from Wall Test (Thomsen & Wallace, 1995) 68

Table 18: Ground Motions from the FEMA P695 Far-Field Record Set (2009) 91

Table 19: Summary of key parameters from pushover analysis of each prototype building 95

Table 20: Comparison of ACMR to acceptable values for each prototype building 101

List of Figures

Figure 1: A selection of structural schemes used in tall buildings (From Ali & Moon, 2007) 2

Figure 2: Diagram of outrigger system 3

Figure 3: Tour de la Bourse (CTBUH, 2012). 4

Figure 4: MNP Tower in Vancouver BC (RJC Engineers, 2016) 5

Figure 5: Wilshire Grand (Nieblas, 2017) 6

Figure 6: Simplified outrigger model 14

Figure 7: Outrigger moment for different outrigger locations and stiffness ratios 17

Figure 8: Overturning moment in the core wall for different outrigger locations and stiffness ratios 18

Figure 9: Roof deflection for different outrigger locations and stiffness ratios 19

Figure 10: Simplified Conventional and Outrigger Models 20

Figure 11: Mode shapes obtained from theoretical model for (a) k_r=4EI/L and (b) k_r=0 24

Figure 12: Design spectrum for Vancouver, BC used in parametric studies 26

Figure 13: Relative effect of outrigger on an example building 27

Figure 14: Effect of outrigger stiffness at roof level of hypothetical building 28

Figure 15: Relation between height and first-mode period from simplified model 29

Figure 16: Higher mode factors for a range of building configurations 31

Figure 17: Flow chart for conventional design of outrigger 33

Figure 18: Energy Balance Concept (Yang et al., 2016) 38

Figure 19: Generic EEDP System Design 39

Figure 20: Nonlinear mechanisms in the outriggered-wall system 41

Figure 21: Spectral Acceleration and Displacement for a Site in Downtown Vancouver, BC 42

Figure 22: C_0 factors determined from linear analysis of outriggered-walls 45

Figure 23: Forces acting on the intermediate wall segment 51

Figure 24: West Coast Tectonic Setting (Cassidy et al., 2010) 53

Figure 25: Seismic hazard deaggregation for Vancouver (National Resources Canada, 2016) 55

Figure 26: Response spectra of selected ground motions and target scaled to each hazard level........ 57

Figure 27: Prototype building elevations 58

Figure 28: Prototype building floor plan........ 59

Figure 29: Flexural design at the base for each of the prototype buildings 61

Figure 30: Mode shapes of Tower A prototype 62

Figure 31: Conceptual configuration of nonlinear model 64

Figure 32: Concrete02 material behavior (Filippou & Mazzoni, 2009a)........ 65

Figure 33: Steel02 Material Behavior (Filippou & Mazzoni, 2009b)........ 67

Figure 34: Shear wall specimen RW1 (Thomsen & Wallace, 1995) 69

Figure 35: Loading protocol for test specimen RW1 (Thomsen and Wallace, 1995)........ 69

Figure 36: Comparison of model and experimental result of Thomsen and Wallace (1995) 70

Figure 37: Comparison of model and experimental result of a BRB test (Black et al., 2004) 71

Figure 38: Peak moment vs height in Tower A wall for all GMs and hazards 72

Figure 39: Peak shear force vs height in Tower A wall for all GMs and hazards 73

Figure 40: Peak and mean story displacements in Tower A for each hazard level........ 73

Figure 41: Peak and mean interstory drifts in Tower A for each hazard level 74

Figure 42: Sample moment-curvature plot at base of Tower A wall 74

Figure 43: Sample moment-curvature plot of Tower A wall at outrigger 75

Figure 44: Sample force-deformation response of outrigger fuses in Tower A........ 75

Figure 45: Peak moment vs height in Tower B wall for all GMs and hazards 76

Figure 46: Peak shear force vs height in Tower B wall for all GMs and hazards........ 77

Figure 47: Peak floor displacements in Tower B for each hazard level 77

Figure 48: Peak interstory drifts in Tower B for each hazard level 78

Figure 49: Sample moment-curvature plot at base of Tower B wall 78

Figure 50: Sample moment-curvature plot of Tower B wall at outrigger 79

Figure 51: Sample force-deformation response of outrigger fuses in Tower B 79

Figure 52: Peak moment vs height in wall of Tower C for all GMs and hazards 80

Figure 53: Peak shear force vs height in Tower C wall for all GMs and hazards 81

Figure 54: Peak floor displacements in Tower C for each hazard level 81

Figure 55: Peak interstory drifts in Tower C for each hazard level 82

Figure 56: Sample moment-curvature plot at base of Tower C wall 82

Figure 57: Sample moment-curvature plot at outrigger for Tower C wall 83

Figure 58: Sample force-deformation response of outrigger fuses in Tower C 83

Figure 59: Roof displacements normalized to EEDP targets for each tower and hazard level 84

Figure 60: Outrigger fuse force for each tower and hazard 85

Figure 61: Maximum wall moment normalized to the design moment for each tower 86

Figure 62: Maximum wall moment at outrigger normalized to the design moment for each tower 86

Figure 63: Normalized wall strains over the height of each tower for each hazard level 87

Figure 64: FEMA P695 definition of seismic performance factors (2009) 90

Figure 65: P695 acceleration response spectra anchored to the MCE spectrum for Tower C 92

Figure 66: Pushover curve showing the various parameters from the pushover analysis (ATC, 2009) 95

Figure 67: Pushover curves for the three prototype outrigger buildings 96

Figure 68: IDA response of Tower A 97

Figure 69: IDA response of Tower B 98

Figure 70: IDA response of Tower C 99

List of Symbols

A = Area

b = Width

b_f = Flange length

C_0 = Factor to convert SDOF to MDOF displacements

D = Dead load

d = depth

E = Modulus of elasticity

f’c = Specified concrete strength at 28 days

fc = Concrete stress

F_p = System base shear corresponding to Rapid Return performance objective

F_{PR} = Primary system seismic force

F_{SE} = Secondary system seismic force

f_s = Steel stress

f_y = Yield strength of steel

F_y = Yield force; Yielding base shear

H = Height

h = Height; Depth of cross section

I = Second moment of area of cross section

L = Live load

M = Moment

m = Mass

M_f = Factored moment demand

M_r = Factored moment capacity

M_n = Nominal moment capacity

M_p = Probable moment capacity

P = Axial force

S_a = Spectral acceleration

S_{CT} = Spectral acceleration that causes collapse

S_d = Spectral displacement

S_{MT} = Spectral acceleration for the fundamental period at Maximum Considered Earthquake

T = Period

T_1 = Fundamental Period

V = Shear Force

W = Weight; Seismic Weight; Work

Δ = Displacement

ΔE_{E1} = Incremental energy from SLE to DBE hazards

ΔE_{E2} = Incremental energy from DBE to MCE hazards

Δ_y = Yield displacement

Δ_p = Primary displacement

Δ_u = Ultimate displacement

λ = Ratio of primary to secondary base shears

Ω = System overstrength

μ = Ductility

θ = Rotation

γ_a = Energy modification factor to relate the monotonic to dynamic energy from SLE to DBE

γ_b = Energy modification factor to relate the monotonic to dynamic energy from DBE to MCE

List of Abbreviations

ACMR	Adjusted Collapse Margin Ratio
BRB	Buckling Restrained Brace
CMR	Collapse Margin Ratio
CP	Collapse Prevention
DBE	Design-Basis Earthquake Hazard
DCR	Demand-Capacity Ratio
EEDP	Equivalent Energy-Based Design Procedure
IO	Immediate Occupancy
LFRS	Lateral Force Resisting System
MCE	Maximum Credible Earthquake Hazard
MDOF	Multiple degree of freedom
MPC	Multi-point constraint
NBCC	National Building Code of Canada
RC	Reinforced Concrete
Rebar	Reinforcing Steel Bar(s)
RR	Rapid Return
SDOF	Single degree of freedom
SFRS	Seismic Force Resisting System
SLE	Serviceability-Level Earthquake Hazard

Acknowledgements

No thesis or significant body of research is the result of one researcher. Thousands of discussions about the various aspects of the work – some trivial and some significant – take place over the course of its development. Likewise, this thesis was the result of many such discussions, and I thank all those individuals who helped me complete it.

Specifically, I would like to thank my advisor and research supervisor, Prof. Tony Yang, for initializing this research project and providing direction throughout my years spent at UBC. I thank Bob Neville and Svetlana Uranova at Read Jones Christoffersen Consulting Engineers for their helpful guidance and insight on seismic design of conventional and outriggered concrete buildings. Finally, I also thank Frank McKenna and the other contributors to the OpenSees framework, which was used throughout this thesis.

My gratitude is also extended to the Natural Sciences and Engineering Research Council of Canada, who provided funding for this research through the Canada Graduate Scholarships-Masters (CGS M) Program.

To Lisa

For your support, encouragement, and patience

Chapter 1

Introduction

Cities around the world are seeing an increase in taller and more slender buildings due to improved building technology, analysis techniques, material science, architectural and spatial constraints, and prestige. At the same time, it is desirable to reduce the size of structural elements to maximize useable space. These contradicting objectives push engineers and material scientists to use innovative new structural systems and materials. However, the dynamic characteristics of building designed to these constraints result in large displacements and accelerations under wind excitation, and large interstory drifts under earthquake excitation. These large deformations can cause damage to the structural and non-structural elements of a building. Windstorms and earthquakes also create large forces in the form of overturning moment and shears, which must be resisted by a lateral force resisting system (LFRS). Controlling the lateral response of tall buildings to earthquake and wind excitation is a well-studied topic, and has resulted in many practical and innovative solutions.

Figure 1 summarizes a few types of LFRS used in tall buildings and their practical height limitations. At the shorter end of the spectrum are frame structures, which were favored in some of the earliest high-rises (Ali & Moon, 2007). These systems use moment connections to provide lateral stability, but the beam and column sizes become unwieldy to satisfy drift requirements as building height increases beyond 20-30 stories. Modern tall buildings in Canada and the United States are generally schemed to use a centralized core to resist lateral demands from wind and earthquake. The core also contains the elevators and stairs which must be in a fire-rated enclosure, which naturally leads to a convenient location for the LFRS. The core is often an interconnected system of reinforced concrete shear walls which resist lateral loads similarly to a cantilever. A secondary frame system can also be used to provide additional drift control. Shear walls with or without secondary frame systems allow practical designs up to around 70 stories, which is well beyond the limit of the various frame LFRS. To push beyond this height with an economical design, the outrigger system can be utilized.

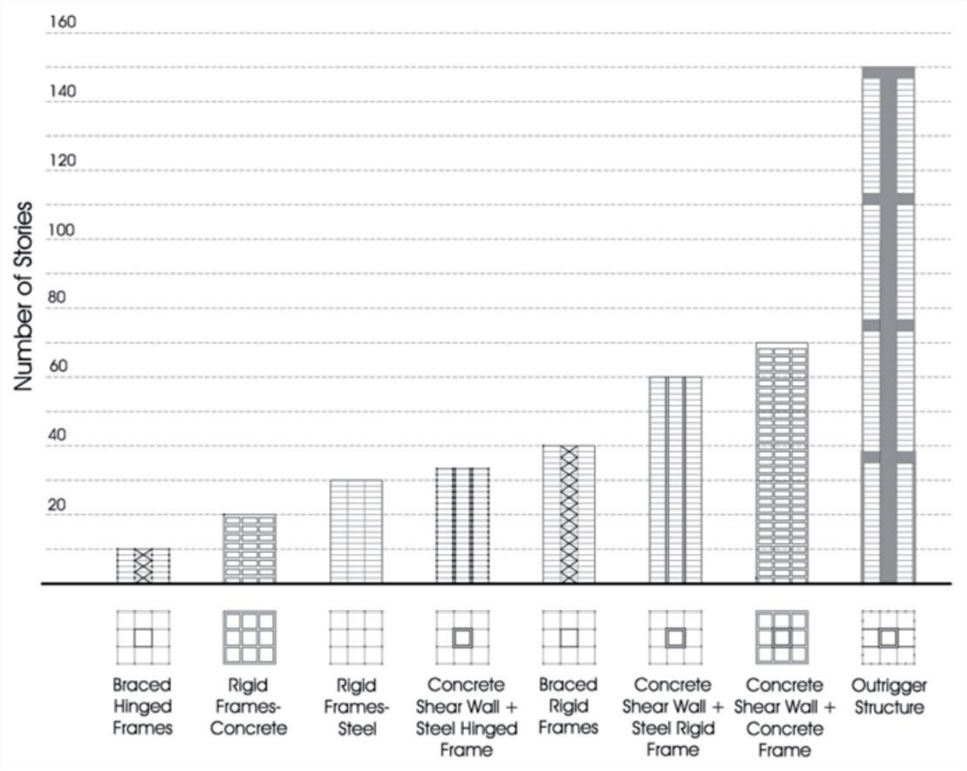

Figure 1: A selection of structural schemes used in tall buildings (From Ali & Moon, 2007)

An outrigger system is comprised of deep, stiff girders or trusses that couple the building core to exterior columns, as shown in Figure 2. This coupling can result in reduced lateral deformations for the structure and reduced overturning moment in the core. Because of the reduced demands, the outriggered core can be designed more compactly with comparable performance to a larger conventional core. Outrigger systems have been used in seismic areas for well over 30 years. However, they are not listed as a structural system in Canadian or U.S. building codes. In fact, there is little existing research on the seismic design and performance of outrigger systems. This thesis aims to investigate the seismic design and performance of outrigger systems that utilize reinforced concrete walls with steel outriggers.

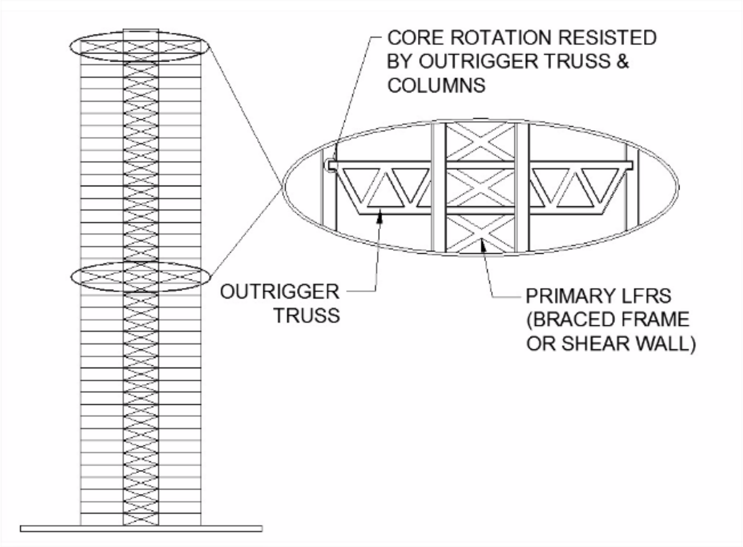
CORE ROTATION RESISTED BY OUTRIGGER TRUSS & COLUMNS
OUTRIGGER TRUSS
PRIMARY LFRS (BRACED FRAME OR SHEAR WALL)

Figure 2: Diagram of outrigger system

1.1 Literature Review

This section presents a review of literature related to the development of outrigger systems as a seismic force resisting system. First, an overview of some existing outriggered tall buildings is presented. Then important design considerations for outriggers is discussed. Finally, existing codes, guidelines and academic literature is reviewed.

History of Outrigger System

The use of outriggers in tall buildings is not a new concept. In fact, outriggers have been successfully used in tall buildings for over 50 years. The earliest examples of outriggered buildings came about at a time when modern seismic design practices were still in its infancy, and they were therefore most likely schemed only for wind effects. Using the outrigger to resist seismic demands and provide supplemental energy dissipation is a much newer development, and the topic of this thesis.

One of the earliest documented uses of an outrigger system was in the Tour de la Bourse building, in Montreal, Canada (Figure 3). This 47-story reinforced concrete tower was built in 1965 and utilizes an outrigger arrangement as shown on the floor plan in Figure 3(b). Montreal has a moderate seismic hazard, but the building design was completed before modern seismic design and analysis procedures were established. It is not known how the original designers accounted for seismic effects; the author surmises that wind forces governed the design.

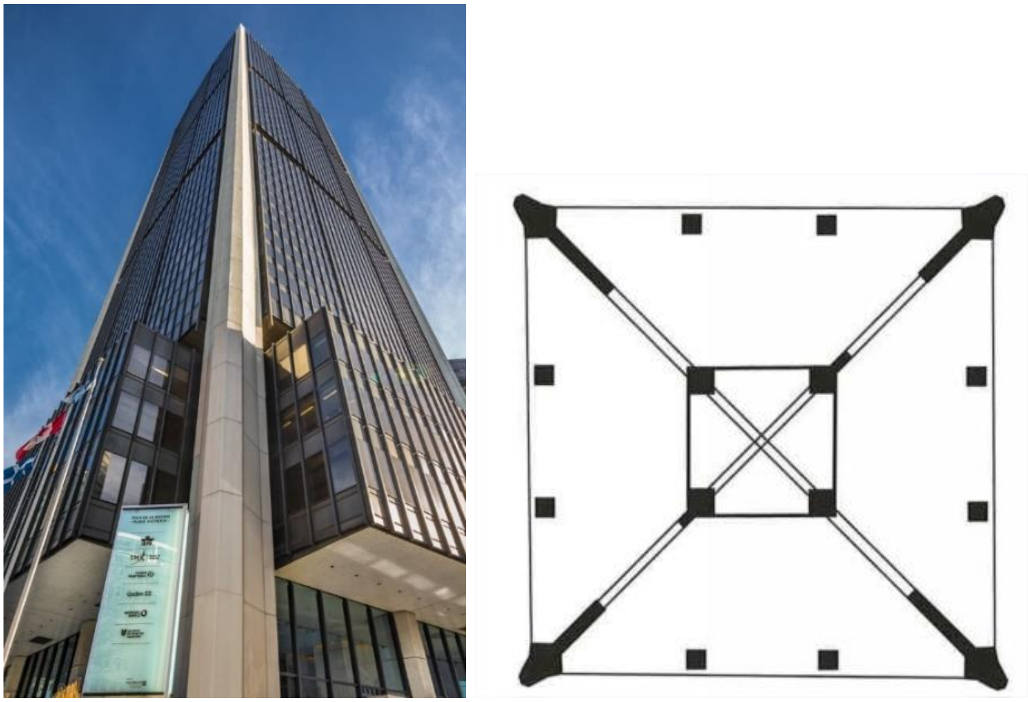

Figure 3: Tour de la Bourse (a) photo of building (Groupe Petra, 2017) and (b) Outrigger layout on plan (Council on Tall Buildings and Urban Habitat, 2012).

A more recent example of utilizing a reinforced concrete core and outrigger system is the MNP Tower in Vancouver, Canada. This 35 story office tower was built on a narrow site in a dense area of the city. It uses a steel outrigger truss at the roof level, which effectively allowed a smaller core size – a critical design constraint considering the small floor plate size (RJC Engineers, 2016). Seismic design according to the National Building Code of Canada requires a capacity design approach to enforce ductile failure mechanisms. Therefore, buckling-restrained braces were used to limit the force delivery to the outrigger columns and core walls.

Figure 4: MNP Tower in Vancouver BC (RJC Engineers, 2016)

Another notable example of combining a concrete core with a steel outrigger is the Wilshire Grand in Los Angeles, California, which was completed in 2017. The 73-story tower uses multi-story steel outrigger trusses with buckling-restrained braces at the 28th, 53rd and 70th floors to keep the core wall length down to a rather small 30 feet (Nieblas, 2017). For reference, this wall length is typical of 35-40 story concrete buildings in Vancouver. The outriggers use groups of four BRBs ranging from 800-2200 kips each at 5 points along each side of the wall, and steel mega-columns at the building perimeter. Differential settlement between core and outrigger was mitigated by adding a precompression stress to the BRBs, which will slowly dissipate as the core shrinks and settles (Nieblas, 2017).

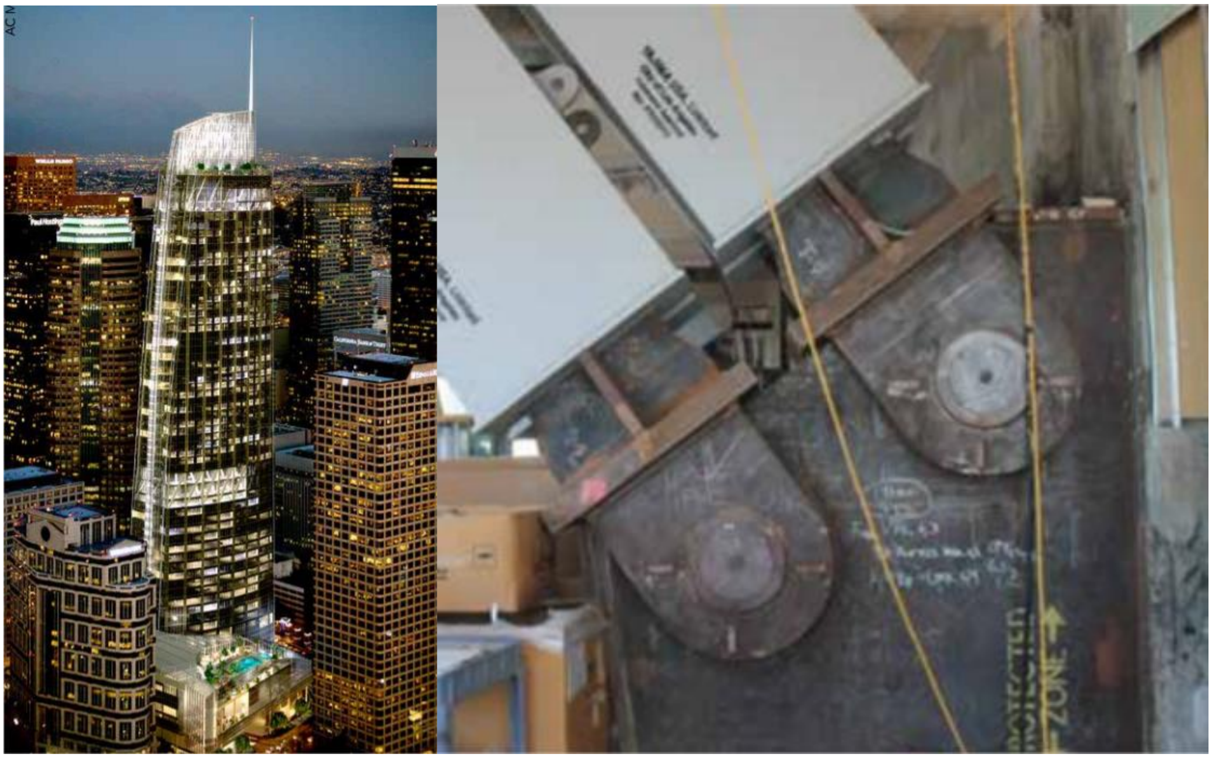

Figure 5: Wilshire Grand (a) location in downtown LA (b) outrigger connection to core wall (Nieblas, 2017)

Some other examples of outrigger systems, their heights, date of completion, and location are shown in Table 1. These examples show that outrigger systems have been effectively used on buildings ranging from 143-632m (the second tallest in the world at the time of writing). Many of the existing outrigger buildings are in areas with low seismicity but high wind demands, such as Chicago and New York. However, there are also existing outrigger building in high seismic areas like San Francisco and Vancouver. There is also variation in the chosen structural configuration: concrete cores may be designed with a steel or concrete outrigger. However, buildings with steel cores do not generally use concrete outriggers.

Table 1: Properties of existing outrigger buildings

Date Built	Name	Location	Construction Type	Height
1965	Tour de la Bourse	Montreal, Canada	Concrete Core Concrete Outriggers	190m
1973	US Bank Center	Milwaukee, Wisconsin	Steel Core Steel Outriggers	183m
1990	Waterfront Place	Brisbane, Australia	Concrete Core Concrete Outriggers	162m
1990	Two Prudential Plaza	Chicago, Illinois	Concrete Core Concrete Outriggers	303m
1999	Jin Mao Building	Shanghai, China	Concrete core Steel Outriggers	421m
1999	Cheung Kong Center	Hong Kong, China	Concrete Core Steel Outriggers	283m
2001	Plaza 66	Shanghai, China	Concrete Core Concrete Outriggers	288m
2004	Taipei 101	Taiwan	Steel Core Steel Outriggers	508m
2004	Two International Finance Center	Hong Kong, China	Concrete Core Steel Outriggers	412m
2007	New York Times Tower	New York, New York	Steel Core Steel Outriggers	220m
2008	Millennium Tower	San Francisco, California	Concrete Core Concrete Outriggers	197m
2008	One Rincon Hill	San Francisco, California	Concrete Core Steel Outriggers	180m
2008	Shanghai World Financial Center	Shanghai, China	Concrete Core Steel Outrigger	492m
2009	Trump Tower	Chicago, Illinois	Concrete Core Concrete Outriggers	432m
2009	300 North LaSalle	Chicago, Illinois	Concrete Core Steel Outriggers	239m
2014	MPN Tower	Vancouver, Canada	Concrete Core Steel Outriggers	143m
2014	Shanghai Tower	Shanghai, China	Concrete Core Steel Outriggers	632m
2017	Wilshire Grand	Los Angeles, California	Concrete Core Steel Outriggers	336m

(Source: Council on Tall Buildings and Urban Habitat, 2012)

Outrigger Design Considerations

The use of outriggers in a tall building introduce additional complexity into the design and construction process. One of the first points of contention to overcome is the coordination between architects and other trades for initial design and placement. Outriggers are often placed at mechanical floors and can potentially interfere with mechanical, electrical, and plumbing services (Choi & Joseph, 2012). If located elsewhere, the outrigger may need to be accounted for in the architectural layout of walls and openings.

There are several construction issues that arise from the use of outriggers. One such issue is the differential shortening that occurs between columns and walls. If an outrigger is located at an intermediate floor and is fully constructed, the weight of subsequent construction may cause differential deflections that will stress the outrigger. If the outrigger is not needed to resist wind during construction, it may be possible to leave the outriggers disconnected until the short-term deflections have finished. However, concrete structures also have long term deflections due to creep and shrinkage. Some care is therefore required to estimate and account for the effects of these deflection (Choi & Joseph, 2012). The inclusion of outriggers may impact the construction sequence and schedule due to the special connections and non-typical details between the wall, outrigger, columns and floors. If the outrigger is located at the roof, it may impede elevator installation which likely puts it on the critical path of the construction schedule.

Most modern building codes, including the National Building Code of Canada, contain seismic provisions restricting certain types of structural irregularities. Soft Story and Weak Story requirements attempt to limit the variation in stiffness between floors. Outrigger level tends to be stiffer and stronger due to the extra steel and reinforcing required for the connection to the wall. However, the code intent here is to avoid a uniformly stiff/strong building having a soft/weak story where excessive deformations would concentrate. Outrigger floors are the opposite situation, and the typical floors are designed to have adequate stiffness and strength (Choi & Joseph, 2012).

The modelling and analysis of outriggered buildings requires careful consideration of the interaction between the different structural components. For instance, Choi & Joseph note that incorrect assumptions about the diaphragm properties can lead to erroneous forces in the outrigger system and incorrect system deformations (2012). A commonly used assumption when modelling reinforced concrete construction is that the floor slabs act as a rigid diaphragm. However, if the outrigger chords are in the same horizontal plane as the slab, then the analysis force in chord members will be incorrect, and the stiffness of the outrigger may be overestimated.

Because the outrigger system couples the LFRS and gravity systems, it would be prudent to ensure the gravity system cannot be overloaded during extreme wind or earthquake excitation. This can be achieved using a capacity design approach or a detailed performance-based design approach. In the capacity design approach, an accurate estimate of the outrigger overstrength is determined and then capacity-protected elements are designed for amplified demands in proportion to the overstrength. The performance-based design approach would use more accurate modelling techniques such as nonlinear time history analysis to ensure there is a sufficiently small risk of overloading the gravity system.

Existing Seismic Design Guideline for Outriggers

As an accessory to existing SFRS systems, outriggers are not explicitly mentioned in Canadian or American building codes. There is some mention of them in at least one auxiliary design guideline. PEER Guidelines for Performance-Based Seismic Design of Tall Buildings (2010) outlines the importance of considering the effects of outriggers on other elements. The outrigger force-delivery to walls and columns must be carefully considered to avoid unintentional failure of these elements. The PEER guidelines are intended for projects which will use a performance-based design approach with NLTHA.

Simplified Studies of Outrigger Systems

There have been a multitude of studies on simplified outrigger models for studying the effect of outrigger systems on buildings, including the optimal outrigger location, predicting mode shapes and frequencies, and predicting peak response quantities. For example, Smith and Salim developed a mathematical model of a linear elastic core with multiple outrigger system subjected to uniform loading over the height. They use the model to determine the optimum location for reducing drifts, when one or more outriggers are present (Smith & Salim, 1983). Moudarres developed a simplified model of coupled shear walls with outrigger system subjected to static loads and used it to investigate the influence of the outrigger on building drifts and bending moments (Moudarres, 1984). Deng et al. developed a simplified model to estimate the response of outriggered buildings with hysteretic dampers. They verified the model against a finite element model using SAP2000 and found that the modal periods are predicted to within 4% error, and time-history response was predicted to within 9% error (Deng et al, 2014). These studies do not generally concern themselves with the design of outrigger systems, but rather a simplified analysis procedure for preliminary estimation of demands and deformations. Such models are useful for conceptually understanding outrigger behavior and preliminary sizing, but cannot be used directly for seismic design.

Use of Fuses and Other Innovative Structural Components in Outrigger Systems

Empirical studies have shown that the effective damping of conventional-type tall buildings generally diminishes with height (Smith and Wilford, 2007), and adding supplementary damping devices can reduce both wind and seismic demands. Smith and Wilford proposed using viscous dampers as the connection between outrigger and column (2007). They found that, although most useful for wind effects, the viscous dampers are an effective vibration mitigation technique for tall buildings. The idea of using innovative structural components, whether passive or active, has been well-explored and implemented. For example, both buckling-restrained braces and viscous dampers have been used on multiple outrigger buildings.

1.2 Objective and Scope

The objective of this thesis is to provide a *rational, efficient,* and *safe* methodology for the seismic design of outrigger systems in tall buildings. The first keyword of the objective is *rational*. To provide a rational methodology, a detailed design procedure is proposed which is consistent with the aims and provisions of the NBCC and material design codes, but also goes beyond the minimum requirements set out in the building codes by enabling the designer to set explicit performance objectives at different seismic hazard levels. This can, for example, be used to ensure that structural damage is minimized in smaller earthquakes and confined to specially-detailed regions in larger earthquakes. The chosen design methodology is Equivalent Energy-based Design Procedure (Yang et al., 2017), which is adapted where required to suit outriggered wall buildings.

The second keyword is *efficient*. To be efficient, the design procedure must avoid complex iterative tasks while still achieving the desired performance objectives. To evaluate the efficiency of the design procedure, a series of prototype outriggered wall buildings are designed using EEDP. The prototype buildings encompass a range of typical Canadian buildings. Nonlinear finite element models of the prototypes are created in the program OpenSees (McKenna & Fenves, 1997) and analyzed under earthquake excitations that correspond to the hazard levels used in the design process. The behavior of the buildings is assessed to confirm that the design procedure achieves the intended performance objectives.

The final keyword is *safe*. Seismic safety is a very broad topic, but in this thesis, the safety of the prototype buildings is evaluated by determining the margin of safety against collapse using FEMA P695 methodology (2009), whereby incremental dynamic analysis is used to develop a relation between spectral intensity and collapse, and create a fragility curve for the buildings. The adjusted collapse margin ratio is determined for each prototype building using the results of the analyses and compared to acceptability criteria.

1.3 Thesis Organization

The remainder of the thesis is organized into the following chapters:

Chapter 2 presents the development of simplified outrigger models using beam theorems. The simplified models are used in parameter studies to understand the static and dynamic behavior of outrigger systems.

Parametric plots are presented which show the relation between outrigger stiffness, location, and critical building parameters such as period, drift, and overturning moment.

Chapter 3 describes the conventional seismic design approach and a proposed alternative energy-based design approach, with specific emphasis on how it can be applied to outriggered wall systems. The detailed implementation of the procedure is discussed along with relevant design equations.

Chapter 4 presents a series of prototype models that are designed using the energy-based design procedure from Chapter 3. The nonlinear modelling assumptions, ground motion selection, time-history analysis results, and assessment of building performance are also presented.

Chapter 5 describes how the prototype designs are verified to meet the building code collapse prevention performance objective under extreme earthquake loading using FEMA P695 methodology. An overview of the methodology, the collapse assessment results, and discussion is included for each of the prototype buildings.

Chapter 6 presents a summary of the work in this thesis, the results and conclusions, and suggestions for future research.

Chapter 2

Behavior of Outrigger Systems

In this chapter, simplified outrigger models are developed to better understand the static and dynamic behavior of outriggered tall building. Section 2.1 describes the derivation of an outrigger system subjected to uniform static loading. Then, in Section 2.2, the equation of motion for cantilever and outrigger systems with uniform mass is derived. These simple models are used to generate parametric plots, which can assist the designer in evaluating the effectiveness of an outrigger system.

2.1 Theoretical Solution of Elastic Outrigger System Response Under Static Load

The theoretical solution to an elastic outrigger system under uniform static loads is presented in this section. In general, the equivalent static distribution of wind and seismic loads is not uniform, but rather some distribution which varies over the height of the structure. However, a uniformly distributed load is still useful for understanding outrigger behavior, and the same process can be used for studying the effects of other load distributions.

Consider the simplified model shown in Figure 6 which consists of an elastic wall, rigid outrigger beams, and elastic columns. The wall is fixed at the base, has a height of L, an elastic modulus of E_{wall}, and a moment of inertia of I_{wall}. At some arbitrary height, rigid outrigger elements couple the wall to flexible columns. The columns are each spaced $b/2$ from the wall centerline, have an elastic modulus of E_{col}, and an area of A_{col}. The system is subjected to a uniform load of magnitude q.

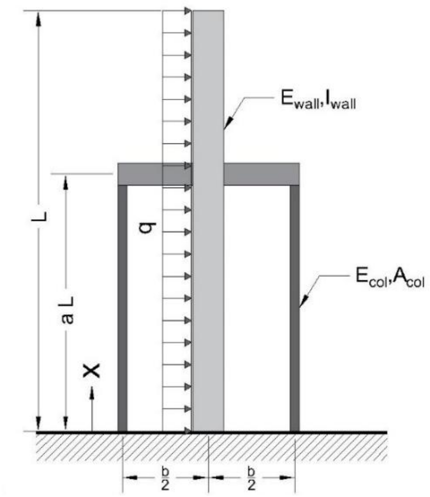

Figure 6: Simplified outrigger model

The simplified outrigger system, as shown in Figure 6, is indeterminate to two degrees. If the axial stiffness of each outrigger column is equal, symmetry dictates that the forces will also be equal, and the static indeterminacy reduces to one. The system can be solved using several structural analysis techniques. In this case, the force method is used. First, the moment connection between the wall and outrigger beams are selected as the redundant force. The redundant force is released and replaced by equal and opposite moments (M^*) on the wall and outrigger beams with magnitude 1.0. With the redundant force chosen, the system can be simplified.

When the cantilever beam is subjected to a uniformly distributed load, q, the deflection and rotation at any point can be described by Equations 2.1 and 2.2, respectively:

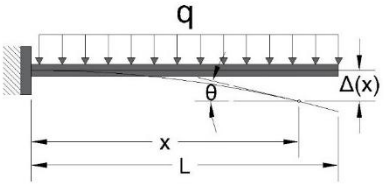

$$\Delta(x) = \frac{qL^4}{24EI}(6x^2 - 4x^3 + x^4) \qquad [2.1]$$

$$\theta(x) = \frac{qL^3}{6EI}(3x - 3x^2 + x^3) \qquad [2.2]$$

where x is the point of interest as a percentage of length.

Likewise, the deflection and rotation of a beam subjected to a concentrated moment at $x_1 = bL$ where $0 < b \leq 1$ can be described by Equations 2.3 and 2.4, respectively:

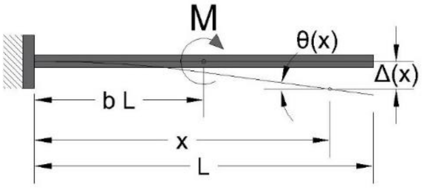

$$\Delta(x) = \begin{cases} \frac{ML^2x^2}{2EI}, \; x < b \\ \frac{ML^2b}{EI}\left(x - \frac{b}{2}\right), \; b \leq x \leq 1 \end{cases} \qquad [2.3]$$

$$\theta(x) = \begin{cases} \frac{MLx}{EI}, \; x < b \\ \frac{MLb}{EI}, \; b \leq x \leq 1 \end{cases} \qquad [2.4]$$

If the moment connection between the wall and outrigger beam is selected as a redundant, the system is reduced to two statically determinate systems: A cantilever and a frame. Each system can be subjected to a unit moment at the outrigger connection. On the cantilever, the rotation at the outrigger location is described by Equation 2.5:

$$\theta_1 = \frac{M^*La}{E_wI_w} \qquad [2.5]$$

On the outrigger frame, assuming the deformation in the outrigger beams is negligible compared to the columns, the rotation at the point of connection is described by Equation 2.6:

$$\theta_2 = \frac{2M^*La}{b^2E_cI_c} \qquad [2.6]$$

Therefore, the outrigger moment is described by Equation 2.7:

$$M_o = \frac{qL^2(a^2-3a+3)}{6+\frac{12E_wI_w}{b^2E_cA_c}} = \frac{qL^2}{2}\left(\frac{a^2-3a+3}{3\left(1+\frac{2E_wI_w}{b^2E_cA_c}\right)}\right) \qquad [2.7]$$

The moment at the base of the wall is described by Equation 2.8:

$$M_b = \frac{qL^2}{2} - M_o = \frac{qL^2}{2}\left(1 - \frac{\mathrm{a}^2-3a+3}{3\left(1+\frac{2E_wI_w}{b^2E_cA_c}\right)}\right) \qquad [2.8]$$

The deflection at the top floor is described by Equation 2.9:

$$\Delta_{roof} = \frac{qL^4}{8E_wI_w} - \frac{M_oL^2a\left(1-\frac{a}{2}\right)}{E_wI_w} = \frac{qL^4}{8E_wI_w}\left(1 - \frac{2a\left(6-9a+5a^2-a^3\right)}{3\left(1+\frac{2E_wI_w}{b^2E_cA_c}\right)}\right) \qquad [2.9]$$

The ratio of wall to outrigger rotational stiffness $\left(k = \frac{2E_wI_w}{b^2E_cA_c}\right)$ is a convenient constant which can be varied to study the system behavior. It should be noted that this simplified model will likely vary from real structures. The flexibility of the outrigger itself (which was assumed rigid in the above derivation) will lower the rotational stiffness.

2.1.1 Parameter Studies

Using the simplified system described and derived above, the behavior of outriggered buildings was studied for various configurations. The outrigger moment (Figure 7), wall base overturning moment (Figure 8), and roof deflection (Figure 9) are plotted versus different values of outrigger location and stiffness ratio.

Outrigger Contribution to Overturning

Figure 7 shows the outrigger moment as a ratio of total overturning moment at different positions and stiffness ratios. This ratio ($M_{outrigger}$ / M_{total}) is also called the Degree of Coupling (DOC) between the wall and outrigger. For a given stiffness ratio, the degree of coupling decreases as the outrigger position moves higher, due to the increased column flexibility. Conversely, as the column stiffness increases, the stiffness ratio tends to zero and the degree of coupling increases.

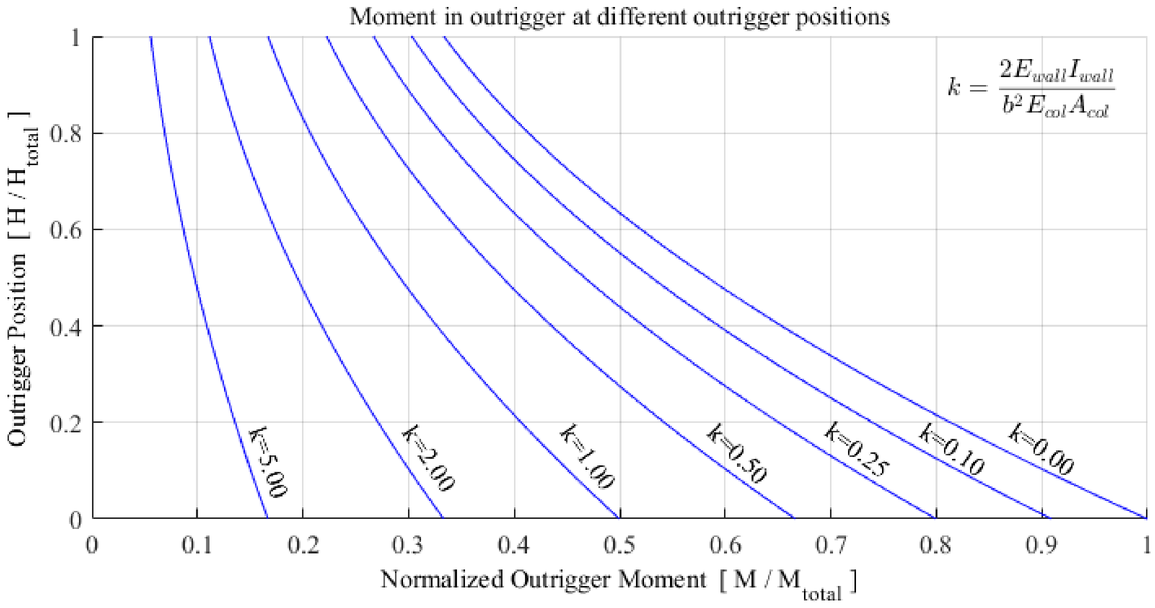

Figure 7: Outrigger moment for different outrigger locations and stiffness ratios

Wall Moment

Figure 8 shows the overturning moment in the core wall for different outrigger locations and stiffness ratios. As the outrigger is moved closer to the base it takes a larger portion of the overturning moment. Likewise, as the outrigger stiffness increases, the stiffness ratio approaches zero and the outrigger takes a larger portion of overturning moment. For an outrigger at the roof level $(a = 1)$ the reduction in wall moment can be estimated by Equation 2.10:

$$Reduction = \frac{1}{3(1+k)} = \frac{1}{3+\frac{6E_W I_W}{b^2 E_C A_C}} \qquad [2.10]$$

So, for instance, if k=1 the wall moment at the base would be reduced by approximately 17%. If the outrigger is instead located at mid height, Equation 2.10 should be multiplied by approximately 1.75.

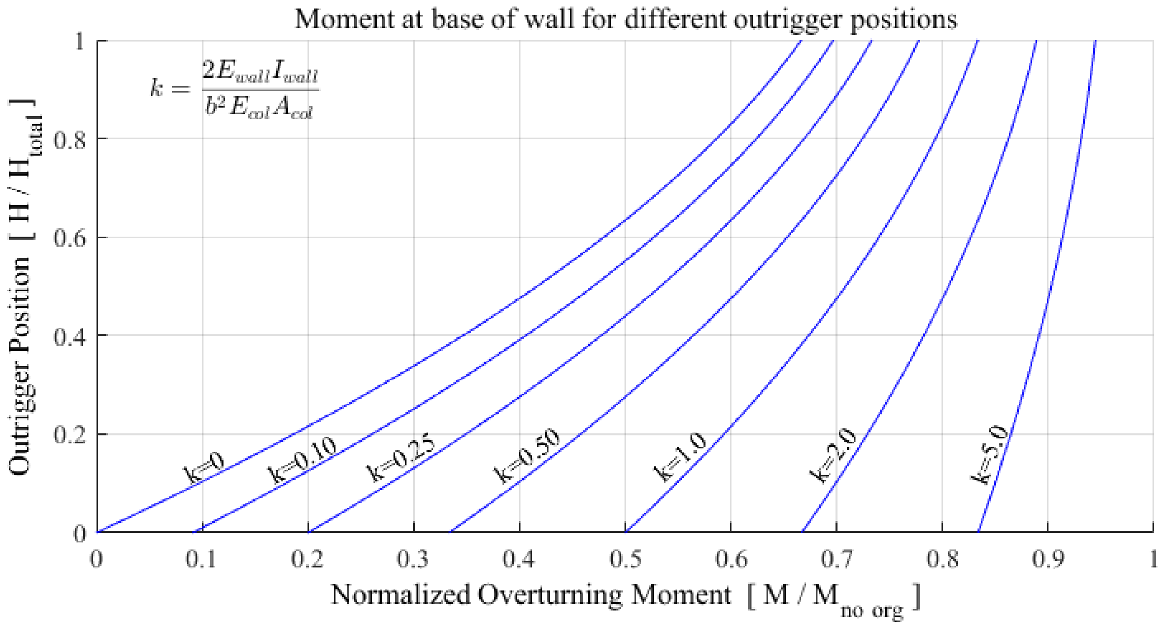

Figure 8: Overturning moment in the core wall for different outrigger locations and stiffness ratios

Roof Deflection

Figure 9 shows the roof deflection for different outrigger positions and stiffness ratios, normalized to the case where the outrigger stiffness is zero (k = ∞). The position of the outrigger which minimizes roof deflection can be found by taking the derivative of Equation 2.9 and finding the zero in the domain $0 < a \leq 1$. Doing this for any stiffness ratio will result in $a = 0.545$. Therefore, the simplified static model suggests that the optimal outrigger location is approximately 55% of the building height when subjected to a uniform static load.

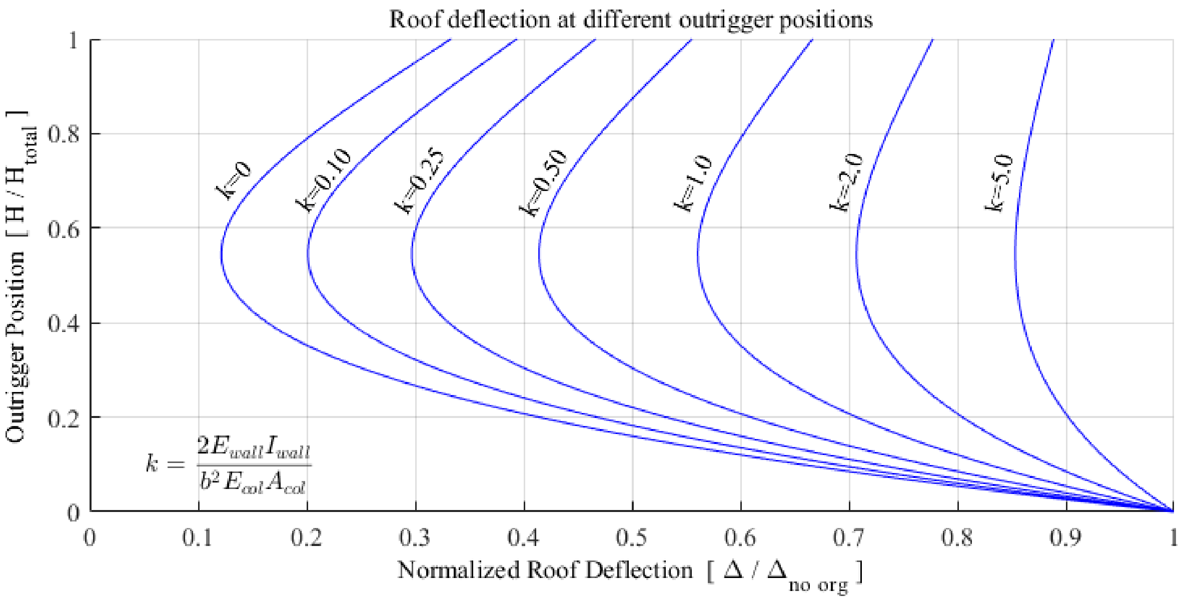

Figure 9: Roof deflection for different outrigger locations and stiffness ratios

2.1.2 Comparison to Analysis Results

The simplified model prediction was compared to a full linear analysis model in ETABS. A 40-story building was analyzed with the following properties: $E_w=E_c=35714$ MPa, b=23.8m, $I_w=223.2m^4$, k=0.5. The models were subjected to a uniformly distributed load of 10.7 kN/m, which corresponds to a uniform pressure of 0.45 kPa acting along a building face. Table 2 shows a comparison of the results.

Table 2: Comparison of theoretical and finite element models

Response Parameter	Theoretical Model	ETABS Model
Outrigger Moment [kNm]	643,900	713,600
Base Moment [kNm]	2,093,900	2,094,300
Roof Deflection [mm]	987	737
Degree of Coupling [-]	24%	25%

2.2 Theoretical Solution of Elastic Outrigger System Response Under Dynamic Loads

To understand the dynamic behavior of outrigger buildings and compare it with conventional buildings, the theoretical solution to an outrigger system and conventional beam system are derived. Both systems are composed of a Euler-Bernoulli beam with uniformly distributed mass and uniform stiffness (constant cross section). The outrigger system also contains a rotational spring with constant stiffness, located some arbitrary distance (L1) above the base.

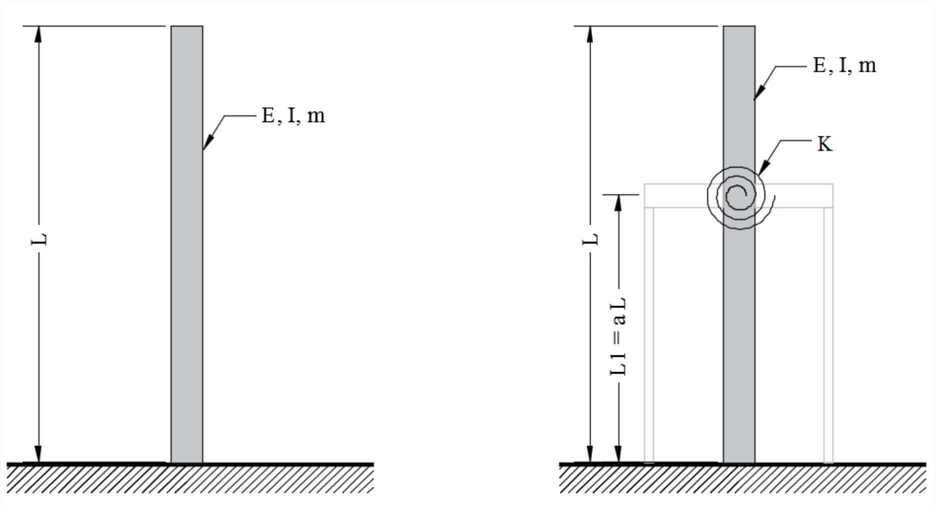

Figure 10: Simplified conventional and outrigger models

2.2.1 Conventional Beam Derivation

For the case of free vibration of a conventional cantilever beam, the governing equation of motion is given by Equation 2.11:

$$m\frac{\delta^2 w}{\delta t^2} + EI\frac{\delta^4 w}{\delta x^4} = 0 \qquad [2.11]$$

where m is the distributed mass, E is the modulus of elasticity, and I is the moment of inertia. The solution is assumed to be of the form given by Equation 2.12:

$$w(x,t) = \phi(x) e^{\sqrt{-1}\omega t} \quad [2.12]$$

Substituting Equation 2.12 into 2.11 leads to the expression given by Equation 2.13:

$$m\omega^2 \phi(x) = EI \frac{d^4}{dx^4} \phi(x) \quad [2.13]$$

The eigen function for flexible modes is assumed to be of the form of Equation 2.14:

$$\phi(x) = C_1 \cos(\beta x) + C_2 \sin(\beta x) + C_3 \cosh(\beta x) + C_4 \sinh(\beta x) \quad [2.14]$$

Where C_1, C_2, C_3, C_4 are constants which depend on the boundary conditions and where the variable β is given by equation 2.15:

$$\beta^4 = \frac{\omega^2 m}{EI} \quad [2.15]$$

The boundary conditions for a cantilever are assumed to be as follows:

1) Displacement at the base is zero: $w(x,t) = 0,\ at\ x = 0$
2) Rotation at the base is zero: $\frac{\partial w(x,t)}{\partial x} = 0,\ at\ x = 0$
3) Moment at the free end is zero: $EI \frac{\partial^2 w(x,t)}{\partial x^2} = 0,\ at\ x = L$
4) Shear at the free end is zero: $EI \frac{\partial^3 w(x,t)}{\partial x^3} = 0,\ at\ x = L$

When the above boundary conditions are inserted in Equation 2.14, the resulting system of equations can be summarized by a matrix and vector:

$$[A]\{C\} = 0 \quad [2.16]$$

Any constant of C = 0 will be a trivial solution. Therefore, the determinate of A must equal zero. By solving this gives a frequency function described by Equation 2.17:

$$1 + \cos(\beta L)\cosh(\beta L) = 0 \qquad [2.17]$$

Values of β which satisfy the frequency equation result in the fundamental frequencies of the system. The boundary conditions can also be inserted into Equation 2.14 to give the mode shape:

$$\phi(x) = C_1[\cosh(\beta x) - \cos(\beta x) - \frac{x\cosh(\beta L)+\cos(\beta L)}{\sinh(\beta L)+\sin(\beta L)}(\sinh(\beta x) - \sin(\beta x))] \qquad [2.18]$$

Where C1 is an arbitrary constant.

2.2.2 Outrigger Beam Derivation

For the case of free vibration of an outriggered beam, the governing equation of motion can be described by Equation 2.19:

$$m\frac{\delta^2 w}{\delta t^2} + EI\frac{\delta^4 w}{\delta x^4} + \mathrm{K}\frac{\partial w(x,t)}{\partial x}\delta(x - L_1) = 0 \qquad [2.19]$$

where m is the distributed mass, E is the modulus of elasticity, I is the moment of inertia, and K is the rotational stiffness of the spring. For simplicity, two equations are used to define the eigen function of the system, each having a domain over which the equation is valid. Equations 2.20 and 2.21 describe the two parts:

$$\phi_1(x) = C_1\cos(\beta x) + C_2\sin(\beta x) + C_3\cosh(\beta x) + C_4\sinh(\beta x) \quad \text{for } 0 < x < L1 \qquad [2.20]$$

$$\phi_2(x) = C_5\cos(\beta x) + C_6\sin(\beta x) + C_7\cosh(\beta x) + C_8\sinh(\beta x) \quad \text{for } L1 < x < L \qquad [2.21]$$

With twice as many constants, the number of boundary conditions for the outrigger system also double. The first four boundary conditions are the same as the conventional system. The remaining four boundary conditions enforce compatibility between the two domains:

1) Displacement at the fixed boundary is zero: $\phi_1(0) = 0$

2) Rotation at the fixed boundary is zero: $\frac{d\phi_1(0)}{dx} = 0$

3) Moment at the free end is zero: $EI\frac{d^2\phi_2(L)}{dx^2} = 0$

4) Shear at free end is zero: $EI\frac{d^3\phi_2(L)}{dx^3} = 0$

5) Displacement at spring is equal to each segment: $\phi_1(L_1) - \phi_2(L_1) = 0$

6) Rotation at L1 is equal for both segments: $\frac{d\phi_1(L_1)}{dx} - \frac{d\phi_2(L_1)}{dx} = 0$

7) Shear at L1 is equal for both segments: $EI\frac{d^3\phi_1(L_1)}{dx^3} - EI\frac{d^3\phi_2(L_1)}{dx^3} = 0$

8) Moment at each end is equal to: $E\mathrm{I}\frac{d^2\phi_1(L_1)}{dx^2} - EI\frac{d^2\phi_2(L_1)}{dx^2} - \mathrm{K}\frac{d\phi_1(L_1)}{dx} = 0$

When the boundary conditions are inserted in the equation of the eigen functions. The system of equations can be summarized by a matrix and vector:

$$[A]\{C\} = 0 \qquad [2.22]$$

Any constant of C = 0 will be a trivial solution. Therefore, the determinate of A must equal zero. The determinate of the A matrix was solved and simplified using the symbolic solver in MATLAB (The Mathworks Inc, 2016). The resulting frequency function is shown in Equation 2.23, below:

$$\frac{\mathrm{K}}{4EI\beta} * [\sin(\beta L)\cosh\big(\beta(2L_1 - L)\big) + \sinh(\beta L)\cos\big(\beta(2L_1 - L)\big) + 2\cos(L_1\beta)\sinh(L_1\beta) + 2\cosh(\beta L_1)\sin(\beta L_1) + \cos(\beta L)\sinh(\beta L) + \cosh(\beta L)\sin(\beta L) + 2\cos\big(\beta(L_1 - L)\big)\sinh\big(\beta(L_1 - L)\big) + 2\cosh\big(\beta(L_1 - L)\big)\sin\big(\beta(L_1 - L)\big)] + 1 + \cos(\beta L)\cosh(\beta L) = 0 \qquad [2.23]$$

For the case that the outrigger is located on the roof, $L_1 = L$. This simplifies the mode shapes to:

$$\phi(x) = \gamma\big(\cos(\beta x) - cosh(\beta x)\big) + si\,n(\beta x) - \sinh(\beta x) \qquad [2.24]$$

Where the parameter γ is described by Equation 2.25:

$$\gamma = \frac{\cos(\beta L)+cosh(\beta L)}{sin(\beta L)-sinh(\beta L)} \qquad [2.25]$$

The equations for the mode shapes where $L_1 \neq L$ are extensive and are not shown here for brevity. If desired, they can be determined by following the above logic and using the symbolic solver in MATLAB. Figure 11 shows the first four mode shapes obtained from this model for the case of K=4EI/L and K=0 respectively.

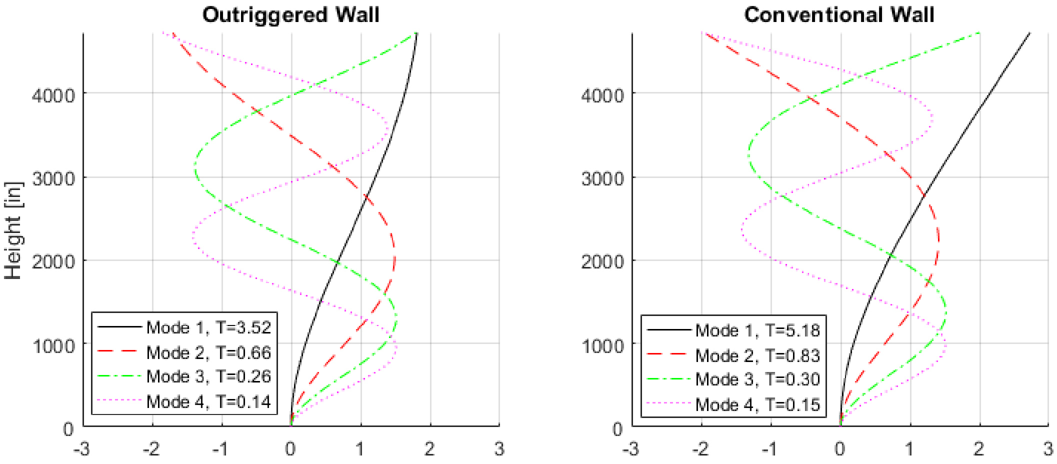

Figure 11: Mode shapes obtained from theoretical model for (a) K=4EI/L and (b) K=0

Using this method for obtaining the mode shapes and frequencies of outrigger systems, it is then possible to take it one step further and approximate the response of linear systems under arbitrary earthquake excitation using Response Spectrum Analysis (RSA). In RSA, the maximum system response is approximated by combining the peak modal responses with a combination rule such as Square-Root-Sum-of-Squares (SRSS) or Complete-Quadratic-Combination (CQC).

2.2.3 Parameter Study

Some important design parameters were studied using the theoretical model derived above. An example building was chosen with the properties listed in Table 3. These values approximately represent 20, 30, and 40-story residential buildings. The distributed mass was determined using a floor weight of 1500 kips and floor height of 10ft, which are typical of residential high-rises in Vancouver. The parametric models were subjected to RSA with the acceleration response spectrum shown in Figure 12. This spectrum was obtained from NBCC 2015 for Vancouver, BC, which has a peak S_a of approximately 0.88g at a period of 0.2 seconds. The first four model responses were combined using the SRSS method, and the resulting quantity is used in the subsequent plots.

Table 3: Properties of buildings used for parameter study

Property:	**Tower A**	**Tower B**	**Tower C**
Wall Height, Hw [m]	60	90	120
Modulus of Elasticity, Ec [MPa]	25000	25000	25000
Wall Moment of Inertia, Iw [m^4]	38.8	97.6	223.2
Distributed Mass, m [kg/m]	226.7×10^3	226.7×10^3	226.7×10^3

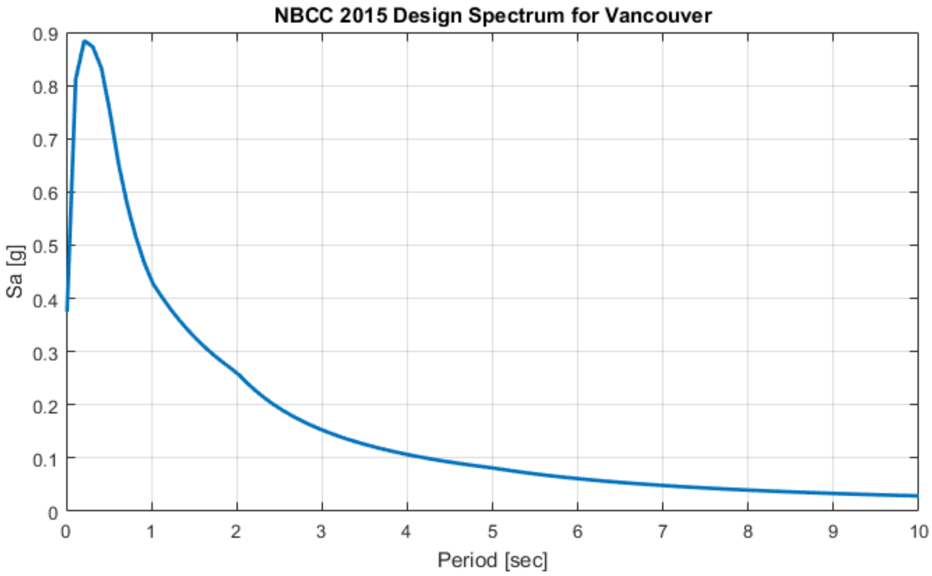

Figure 12: Design spectrum for Vancouver, BC used in parametric studies

Relation Between Basic Response Quantities and Outrigger Stiffness

Figure 13 show how the period, roof deflection, maximum interstory-drift on any story, base overturning moment, and base shear are influenced by an outrigger with various locations and stiffness. The y-axis represents the location of the outrigger along the height of the wall. The x-axis shows the response quantity. The rotational spring stiffness is given as a multiple of the rotational stiffness of the wall, using the relation $K = k_r EI/L$. Figure 13 shows the relations in relative terms; all values were normalized to the case of $K=0$, which implies the outrigger has zero stiffness (i.e. a conventional building). Using this relative figure, the designer can assess how various outrigger configurations of height and stiffness will affect some of the important design variables. These plots show the dynamic response from the design spectrum, but have not been scaled to a minimum code-specified base shear.

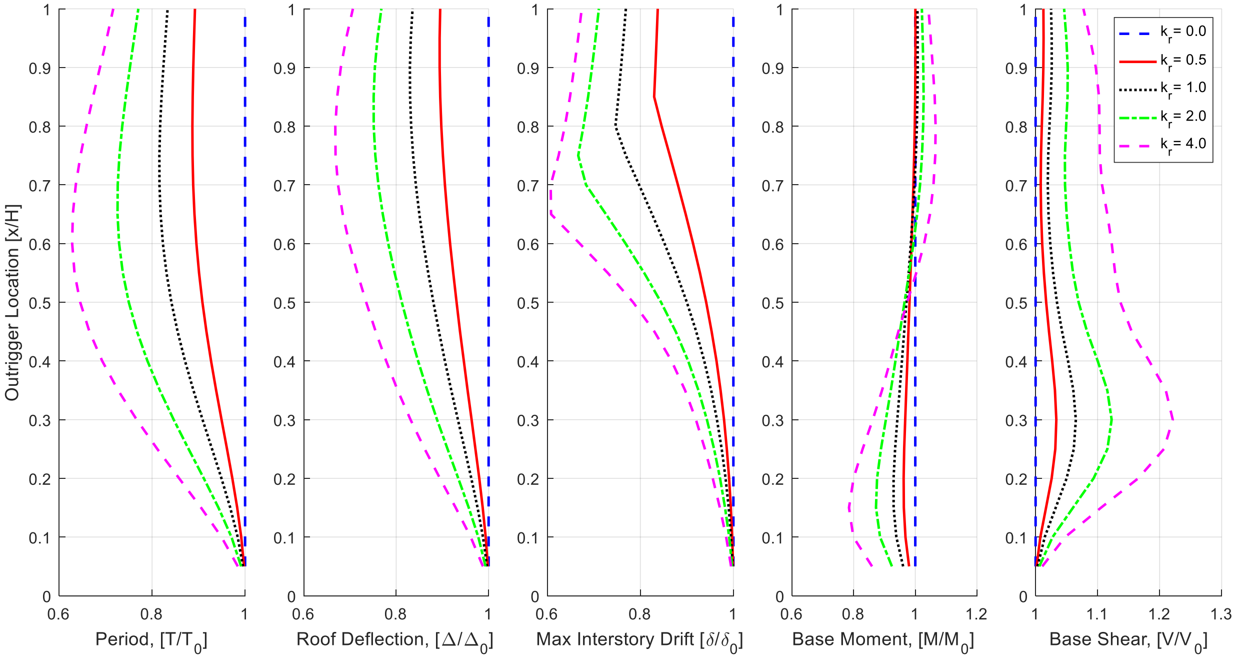

Figure 13: Relative effect of outrigger on an example building normalized to the case of zero outrigger stiffness (K = k_rEI/L)

Using a dynamic analysis with a design spectrum is an important improvement over the simple static models because it shows the effect of the outrigger in terms of actual design metrics. Adding an outrigger will decrease the period of the system (if the wall remains unchanged), and therefore, the dynamic response quantities will also change. The outrigger system generally reduces building period, story drifts and deflections. Stiffer outriggers result in greater reductions, but the effect diminishes as outrigger stiffness increases. On the other hand, adding an outrigger will slightly increase the overturning moment and shear in many cases. Figure 14 shows how five response quantities change for the three different buildings described in Table 3, with outriggers at roof levels and various outrigger stiffness ratios. All response quantities are normalized to the case of no outrigger (k_r=0). Comparing k_r=0 to k_r=2, the deflection in all buildings reduces to about 77% of the conventional building, a reduction of 33%. However, from k_r=2 to k_r=4, the deflection drops from 77% to 71%, a reduction of 6%. Clearly there is a diminishing return to the amount of deflection control the designer can get by adding outrigger stiffness. The maximum interstory drift also follows this trend. Overturning moment and base shear both increase as outrigger stiffness increases, due to the stiffer system attracting higher demands. However, the amount of change is not as drastic as it is for period and deformations. From k_r=0 to k_r=2, the moment and shear in the three buildings increased by about 1-2% and 4-7% respectively. Tower A had the lowest period and was therefore most sensitive to increasing moment and shear demands. The most active modes for Tower A correspond to the 'steeper' part of the design spectrum, while the taller building modes are on the 'flatter' portion.

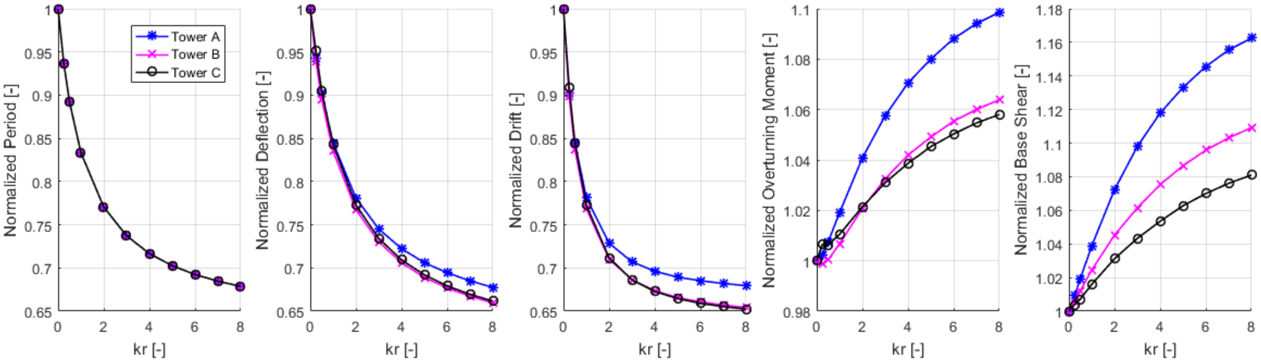

Figure 14: Effect of outrigger stiffness at roof level of hypothetical building

Range of First Mode Periods, T

The fundamental period is an important quantity for designers because it is used to calculate the minimum design base shear. It is also a comparative metric to quickly assess how flexible a building is relative to others. The simplified model was used to study a range of buildings by varying the outrigger location, outrigger stiffness, concrete modulus of elasticity, height, and mass. The outrigger was positioned between 40-100% of the total building height with a stiffness ratio (k_r) between 0.0 – 2.0. The modulus of elasticity was set to 35714 MPa which corresponds to a specified concrete strength of 65MPa. An effective flexural stiffness factor of 0.70 was used to account for cracked concrete behavior by modifying the modulus of elasticity. Building heights were varied between 60-140 m, which is approximately 20-50 stories. The distributed weight was assumed to be 2225 kN per meter (height) with a uniform random variation between 0.75 and 1.25 of this value. Figure 15 shows the results of this parameter study.

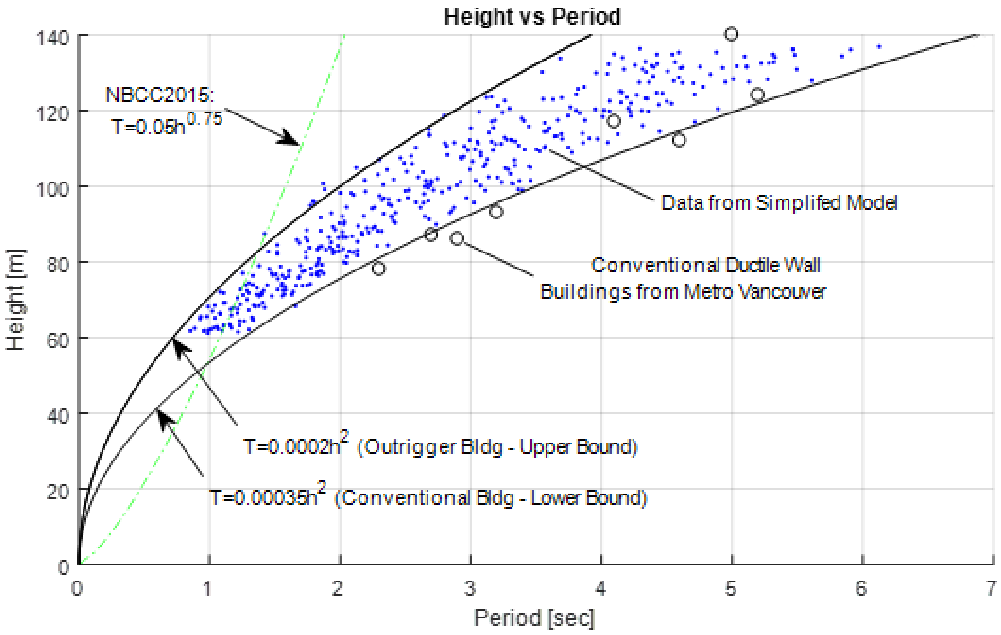

Figure 15: Relation between height and first-mode period from simplified model and a selection of real structures

NBCC 2015 provides a power law formula to estimate building period based on height, given as $T=0.05h^{0.75}$ where *h* is in meters and *T* is in seconds. It is permitted to use a period obtained using a rational model, but that period is limited to twice the code formula or 4 seconds, whichever is smaller. The shape of the code power law does not fit well to the simplified model prediction.

Two alternative equations have been fitted to the simplified model data. The first equation is a lower bound for tall cantilever wall buildings without outriggers. The proposed lower bound equation is:

$$T = 0.00035h^2 \qquad [2.26]$$

where *h* is the building height in meters and *T* is the first-mode period in seconds. The second equation is an upper bound for a stiff outriggered wall system. The proposed upper bound equation is:

$$T = 0.0002h^2 \qquad [2.27]$$

where h is the building height in meters and T is the first-mode period in seconds. These equations appear to be valid for taller, flexible concrete cantilever wall structures but have not been verified for short period structures.

The first-mode period from a variety of cantilevered wall buildings in the Metro Vancouver area are also plotted versus their respective heights, and summarized in Table 4. The periods were obtained from elastic models which used the A23.3-2004 stiffness modification factors and included the gravity system. Figure 15 shows that the lower bound equation generally does predict the period of Vancouver-style residential buildings which utilize reinforced concrete ductile wall systems.

Table 4: Predicted first-mode periods from elastic model and formula

Height	**Elastic Model Period**	**Formula Period (Lower Bound)**
385ft = 117m	4.1	4.8
285ft = 87m	2.7	2.7
366ft = 112m	4.6	4.4
407ft = 124m	5.2	5.4
257ft = 78m	2.3	2.1
282ft = 86m	2.9	2.6
305ft = 93m	3.2	3.0
462ft = 140m	5.0	6.8

Range of Higher Mode Factors, M_v

NBCC 2015 and various other building codes use a higher mode factor to transform the base shear obtained from a single degree of freedom (SDOF) system to a value suitable for multiple-degree-of-freedom (MDOF) systems. The relation between the two systems depends on the type and configuration. The simplified model was again used to see this relation for outrigger systems. The same variation of parameters described in the previous section was used. The higher mode factor was determined for each run by taking the ratio of the RSA combined base shear to the first-mode base shear. The results of this parameter study are shown in Figure 16. The recommended M_v factors for *Walls and Wall-Frame Systems* in NBCC 2015 are also plotted.

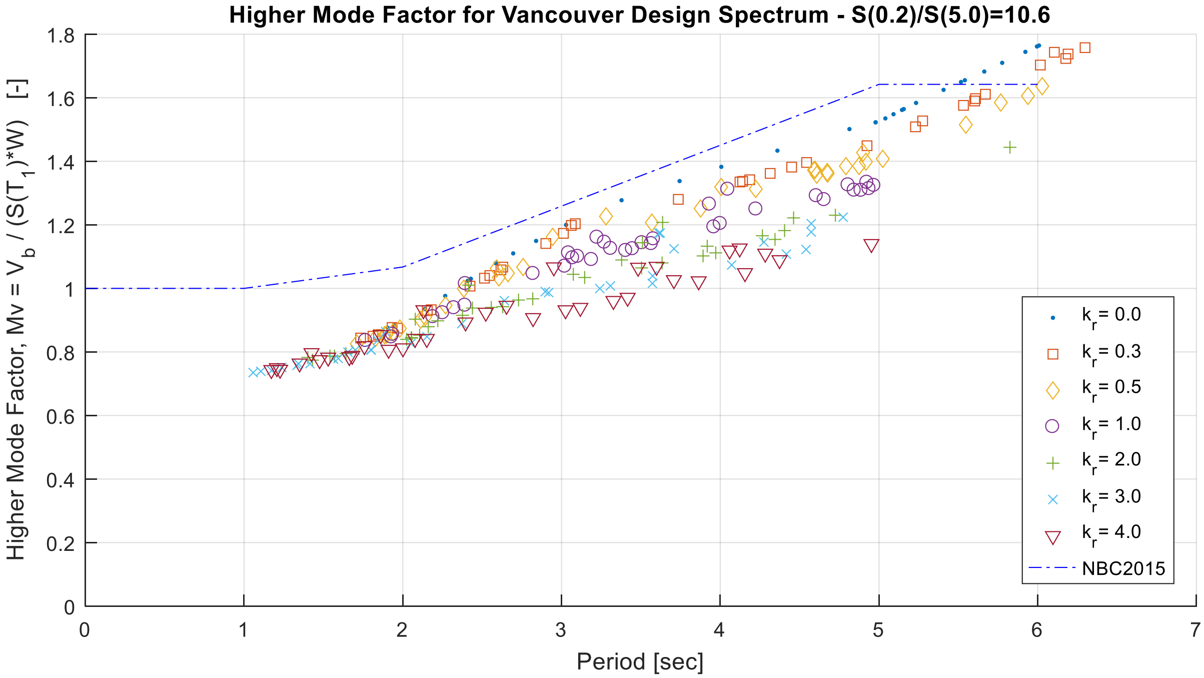

Figure 16: Higher mode factors for a range of building configurations using Vancouver design spectrum

In general, the analysis shows a negative correlation between outrigger stiffness and higher mode factor – that is, as outrigger stiffness increases the higher mode amplification decreases. The NBCC 2015 higher mode factors for *Walls and Wall Frame Systems* with Vancouver's spectral ratio, S(0.2)/S(5.0)=10.6, appear to give a conservative estimate for outrigger systems with all stiffness ratios and locations. Note that NBCC 2015 requires that wall systems with periods greater than 4 seconds be designed for the value at 4 seconds. That is, S(T)*M_v(T) is limited to S(4)*M_v(4).

Chapter 3

Design Methodology for Outrigger Systems

This chapter describes conventional and equivalent energy-based design methodology that can be used to design outriggered-wall systems.

3.1 Conventional Design Approach

Conventional design philosophy in NBCC 2015 attempts to achieve collapse prevention performance under a very rare seismic event (less than 10% probability of collapse from an event with a return period of 2475 years). This philosophy aims to prevent loss of life from structural collapse under severe earthquakes. The conventional design approach recognizes that structures can be detailed to exhibit large ductility, that is, they can undergo large displacements after yielding while maintaining structural integrity. System specific ductility (R_d) and overstrength (R_o) modification factors are used in the conventional design approach to reduce elastic seismic demands to inelastic demands. It is assumed that the displacement of the elastic system will be equal to the displacement of the inelastic system using the aptly named "Equal Displacement Principal," but this may not be true for all structures. In general, higher force modification factors are allowed by following more stringent detailing requirements. SFRS members are sized to have sufficient strength for the reduced seismic demands, and detailed to ensure they have sufficient ductility. Interstory drifts are limited to some benchmark number, usually 2.5% for regular structures. Preliminary sizing of the structural system must therefore consider both the individual member strengths as well as the system displacement response. Figure 17 shows a typical flow of tasks when undertaking a conventional design.

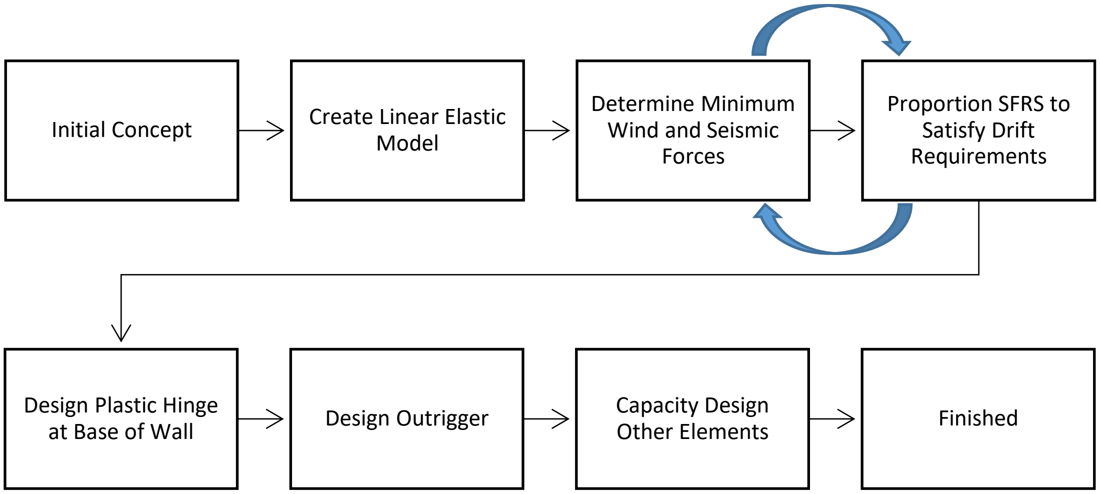
Initial Concept
Create Linear Elastic Model
Determine Minimum Wind and Seismic Forces
Proportion SFRS to Satisfy Drift Requirements
Design Plastic Hinge at Base of Wall
Design Outrigger
Capacity Design Other Elements
Finished

Figure 17: Flow chart for conventional design of outrigger

Canadian seismic design stipulates that a kinematic failure mechanism must be selected and enforced through capacity design. The promoted mechanism in this research is plastic hinging at the critical wall section and yielding of designated 'fuse' elements in the outrigger truss. Buckling restrained braces (BRBs) or other suitable energy dissipating devices can be inserted into the outrigger truss to act as a reliable fuse. All other elements in the system (non-fuse outrigger truss, mega columns, and wall regions outside the plastic hinge) are capacity designed to enforce this chosen mechanism.

Model and Analysis

NBCC utilizes two methods of analysis for seismic design, namely the Dynamic Analysis Procedure and Equivalent Static Force Procedure. The latter procedure is only applicable for (a) regions of low seismicity where I_e F_a $S_a(0.2) < 0.35$, (b) regular structures less than 60m high that have a fundamental period, Ta, less than 2sec in each principal direction, and (c) irregular structures (type 1,2,3,4,5,6,8) less than 20m high and Ta < 0.5sec in each principal direction (NBCC 2010 cl. 4.1.8.7). For buildings not meeting the requirements of Equivalent Static Force Procedure, the Dynamic Analysis Procedure is utilized. This includes practically all tall buildings, and is the procedure used for all subsequent design in this thesis.

The Dynamic Analysis Procedure is most commonly carried out with Response Spectrum Analysis (RSA). In RSA, multiple modes of vibration are combined with a set of rules (eg. Absolute Sum, Square Root Sum of Squares, or Complete Quadratic Combination) to arrive at a set of forces and deflections that approximate the demand that would be obtained through time history analysis. A suitable structural model which accounts for the spatial distribution of mass and stiffness is required for RSA. To account for the inherent nonlinearity of concrete elements, cracked sectional properties are used as specified in A23.3-14 (CSA, 2004). The stiffness of BRB elements in linear elastic design models also requires some consideration to arrive at realistic forces, due to the nonprismatic sectional properties typical in most BRBs (Bruneau, Uang, & Sabelli, 2011). An effective stiffness can be derived from a 'springs in series' analogy, and the following equation has been suggested by Tsai & Hsiao (2008):

$$K_{eff} = E \,/\, \left(\frac{L_{ysc}}{A_{ysc}} + \frac{L_{nysc}}{A_{nysc}} + \frac{L_{conn}}{A_{conn}}\right) \qquad [3.1]$$

where E, L, A are the elastic modulus of steel, Length, and Area, respectively, and the subscript *ysc* denotes yielding steel core, *nysc* denotes non-yielding steel core (outside yield zone), and *conn* is the connection. The ratio of the effective stiffness to that of the prismatic core alone has been found to be in the range of 1.3 - 1.8. Shorter braces tend to move towards the upper limit of the range because a greater proportion of length is dedicated to connection and non-yielding zones (Bruneau et al., 2011).

NBCC requires the designer to consider accidental torsion forces that could arise from discrepancies between the assumed and actual distribution of mass and stiffness. For regular buildings (that is, buildings that are not torsionally-sensitive), this can be achieved by offsetting the center of mass from the center of rigidity at each floor by an eccentricity of ±0.05b, where b is the diaphragm extent perpendicular to the direction under consideration. The final set of elastic forces is the envelope of these three analyses (except for capacity design, it is conservative to use the lower value for calculating over strength).

Elastic forces obtained by RSA must be reduced by the system ductility and over strength force modification factors, R_d and R_o, and increased by the importance factor, I_e. For ductile concrete walls designed in accordance with CSA A23.3-14, these factors are equal to 3.5 and 1.6, respectively. As previously mentioned, no values of R_d and R_o are provided for an outriggered-wall system, and therefore appropriate values have yet to be determined. The importance factor is normally taken as 1.0 for most structures.

For structures with no structural irregularities, the design base shear, V_d, must be at least 80% of the code-calculated base shear. This precludes almost all residential high-rises in the Vancouver region, which typically have various forms of mass and stiffness irregularities. These structures must therefore be designed for at least 100% of the code base shear, or RSA-determined base shear, whichever governs. The RSA forces and deformations are linearly scaled to this design base shear.

Design of Plastic Hinge

The plastic hinge is a specially-detailed region of wall where significant nonlinear behavior is expected. CSA A23.3 requires special detailing in this region around the critical section for a length equal to the estimated plastic hinge length, calculated per Equation 3.2:

$$L_p = 0.1H_w + 0.5L_w \tag{3.2}$$

where L_p is the length of plastic hinge region, H_w is the height of the wall, and L_w is the length of the wall (CSA, 2004). The hinge is designed for the scaled RSA forces at the critical section. The wall geometry, concrete strength, and reinforcing steel must be constant throughout the plastic hinge region.

Design of Outrigger

The outrigger truss is designed for the scaled RSA forces. If desired, designated fuse elements such as BRBs can be used at a convenient location in the outrigger, such as near the connection to the mega column. The remaining elements in the truss can be capacity designed for the fuse element(s), such that outrigger has a well-defined yield mechanism. Regardless of whether a fuse was used or not, it is necessary to determine the maximum probable capacity of the outrigger truss to protect other elements using capacity design. The maximum probable force in a BRB is calculated by considering the expected steel core strength, overstrength, cyclic strain hardening, compression overstrength, and safety factor. Similarly, the probable strength of truss elements can be calculated and used to determine the outrigger overstrength.

Capacity-Design

A modified demand envelope is used for flexural design of wall sections outside of the plastic hinge region. This envelope takes into consideration the choice of kinematic mechanism and overstrength of the chosen yielding elements. As is the case for ductile walls, the moment envelope is amplified by the system overstrength to limit the amount of ductility demand outside of the hinge regions.

The wall shear demand must also be increased beyond the scaled analysis forces to account for the system overstrength. The probable flexural overstrength is used for walls designed to CSA A23.3. It is calculated by making material factors (φ_c, φ_s) equal to 1.0 and boosting the steel yield strength (f_y) by 1.25. In conventional ductile wall systems, the overstrength only depends on the probable capacity of the hinge region, as hinge yielding creates a kinematic mechanism for the system. Outriggered walls should be treated differently. In an outriggered wall system, a kinematic mechanism is not formed until both the base of the wall and the outrigger (or the wall at the outrigger location) yield. If the base of the wall yields but the outrigger has residual strength (or vice versa), shear demands can still increase until both locations have yielded. Hence, the *system overstrength*, and not just the wall overstrength, is appropriate for calculating the design forces for wall shear.

The system overstrength is the ratio of the total probable overturning resistance to the factored demands. The total overturning resistance is the sum of the probable wall and outrigger contribution to overturning:

$$\gamma_{p,system} = \frac{M_{p,system}}{M_{f,system}} = \frac{M_{p,wall} + M_{p,org}}{M_{f,system}} \qquad [3.3]$$

Columns that attach to the outrigger need to be designed for axial loads that correspond to the probable capacity of the outrigger system, along with induced moments from the building drift. Limiting the outrigger force through a fuse with low overstrength is therefore beneficial.

3.2 Equivalent Energy-Based Design Approach

The conventional design approach is simple in concept and easy to codify - however, it is not without flaws. For instance, very flexible structures may require multiple design iterations if drift criteria are exceeded. The equal displacement approximation may not hold true for certain structures, leading to designs which exceed intended displacement criteria. More importantly, the conventional approach is limited to a single performance objective. It does not enable the designer to consider multiple objectives, such as keeping the structure operational under a frequent earthquake, and preventing collapse under a rare earthquake. It includes an arbitrary importance factor for post-disaster structures, but using an importance factor greater than 1 does not actually ensure the building will be functional after an earthquake. Because there are no intermediate performance objectives, a conventionally-designed structure could require costly repairs and downtime when subjected to earthquakes, even if the intensity of such events is below the design intensity.

Performance-Based Earthquake Engineering was proposed as one method of moving away from simple strength-based design and towards performance objectives which, when used correctly, could lead to more resilient structural designs. Building displacements receive much more attention in PBEE methodologies because they are better correlated to damage of structural and nonstructural components. Equivalent Energy-Based Design Procedure (EEDP) was developed by Yang et al. and is one such methodology (2017). As shown in Figure 18, EEDP uses an energy balance concept, where the energy of an elastic linear single degree of freedom (ELSDOF) system will be equated to an equivalent nonlinear single degree of freedom system (ENLSDOF). Detailed derivation of EEDP can be found in Yang et al. (2017).

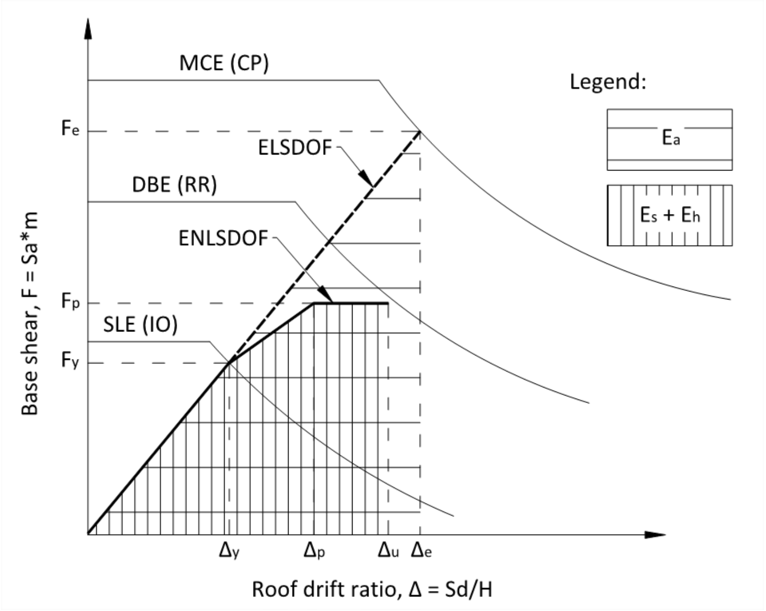

Figure 18: EEDP energy balance concept (Yang et al., 2017)

EEDP is an energy-based methodology which takes into consideration the nonlinear collapse mechanism of a structure. It uses an energy balance concept with plastic analysis to design structural systems that satisfy both strength and drift requirements. The procedure was developed specifically for designing fused-structures with a trilinear backbone as shown in Figure 19. The intention of incorporating structural fuses is to create more resilient structures by meeting multiple performance objectives while still taking advantage of system ductility. In such structures, the primary system (fuse) is designed to yield at some low or intermediate seismic hazard, while the secondary system remains essentially elastic. Then, at a higher seismic hazard, the designer allows the secondary system to yield. Finally, in a very rare seismic event it is ensured that displacements are controlled and collapse is prevented when both the primary and secondary systems have yielded. The overall structural response will resemble a trilinear curve if the primary and secondary systems have bilinear force-deformation responses.

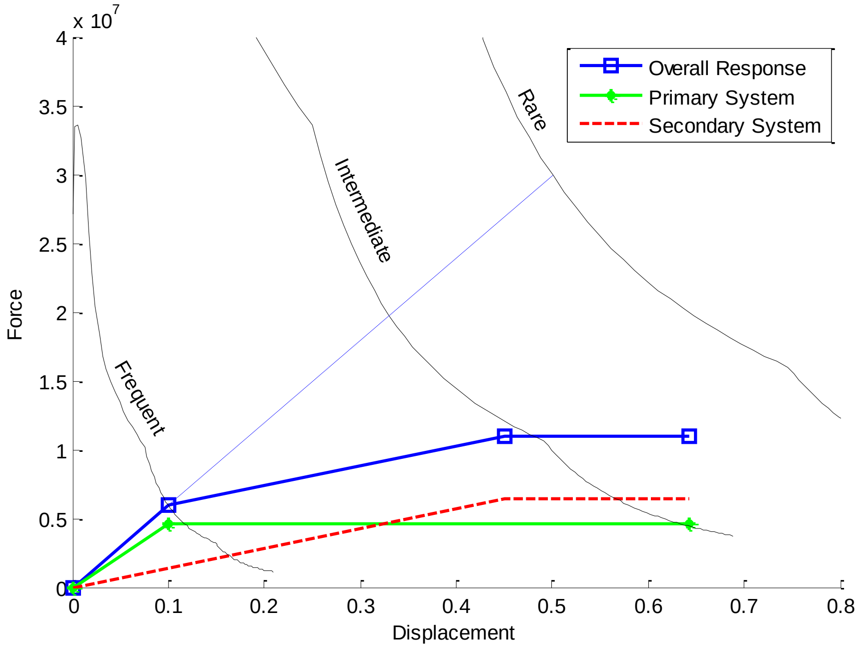

Figure 19: Generic EEDP system design

When the design methodology works as intended, three performance objectives exist. These are: Immediate Occupancy (IO) for frequent earthquakes, Rapid Return (RR) for intermediate earthquakes, and Collapse Prevention (CP) for rare earthquakes. Table 5 summarizes how these performance objectives could be matched with structural responses.

Table 5: Example of performance objectives and structural response characteristics

Performance Objective	**Seismic Event**	**Structural Response Characteristics**
Immediate Occupancy	Frequent	-Primary and secondary systems essentially elastic -Little to no non-structural damage
Rapid Return	Intermediate	-Primary system yields, while secondary system remains essentially elastic -Little to no non-structural damage
Collapse Prevention	Rare	-Primary and secondary systems yield -Drifts controlled to prevent collapse and limit non-structural damage

In a general sense, implementing EEDP involves the following steps:

1. Select performance objectives and corresponding hazards
2. Select a primary and secondary SFRS
3. Select the roof drift at which the primary system yields
4. Select the roof drift at which the secondary system yields
5. Calculate the ultimate drift of the system
6. Distribute forces to the primary and secondary SFRS
7. Select plastic mechanisms and design structural members
8. Capacity design other non-yielding structural members.

For this research, the focus is on structures which use an outrigger as the primary (fuse) system, and structural walls as the secondary system. In such a scheme, there are several important considerations for the designer. For the design of the outrigger, there needs to be sufficient stiffness to assist with overturning resistance. There also needs to be sufficient ductility and stable hysteretic response of the designated yielding elements to dissipate energy at earthquakes beyond IO hazard level. The wall needs to be sufficiently flexible to enable load-sharing with the outrigger and to allow outrigger to yield before wall. It also should be designed to avoid yielding outside of specially detailed regions for all hazard levels. Excessive ductility demands should be avoided at all hazard levels, and shear failure should be prevented through capacity design at all hazard levels

Define Performance Objectives

A major advantage of the EEDP method is the ability for the designer to select the performance objectives explicitly. This transparency ensures that building stakeholders are aware of intended building performance and associated risks. In an outriggered wall system, the primary system for resisting overturning is the outrigger and the secondary system is the structural walls. The desired system performance is to have the outrigger yield at the Service Level Earthquake (SLE) and for the wall to yield at the Design Basis Earthquake (DBE). The maximum interstory drift should be below 2.5% at the Maximum Credible Earthquake (MCE).

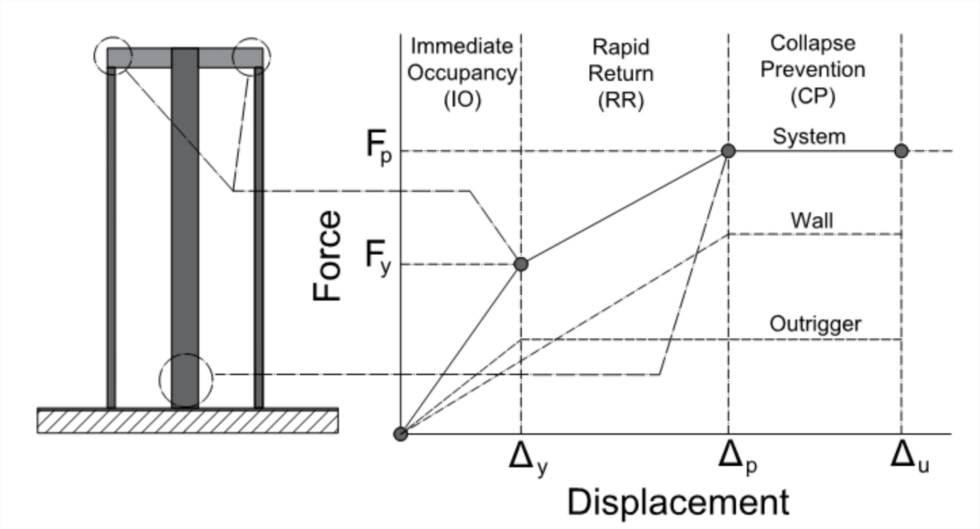

Immediate Occupancy (IO)
Rapid Return (RR)
Collapse Prevention (CP)
F_p
System
Wall
F_y
Force
Outrigger
Δ_y
Δ_p
Δ_u
Displacement

Figure 20: Nonlinear mechanisms in the outriggered-wall system

For the purposes of designing the prototypes in Vancouver, BC, the spectral accelerations for the MCE were obtained from the National Building Code of Canada (NRC, 2015) for the 2% in 50 year hazard. The DBE and SLE were then determined as ratios of the MCE. The SLE was taken as 10% of MCE hazard, and DBE was taken as 50% of MCE hazard. Figure 21 shows the spectral acceleration plotted against the spectral displacement for a location located downtown Vancouver, British Columbia. The SLE shaking intensity is primarily dependent on the desired performance. NBCC 2015 does not require designing for serviceability earthquakes. However, stakeholders may decide on a specific intensity or hazard for which they do not want any damage to occur.

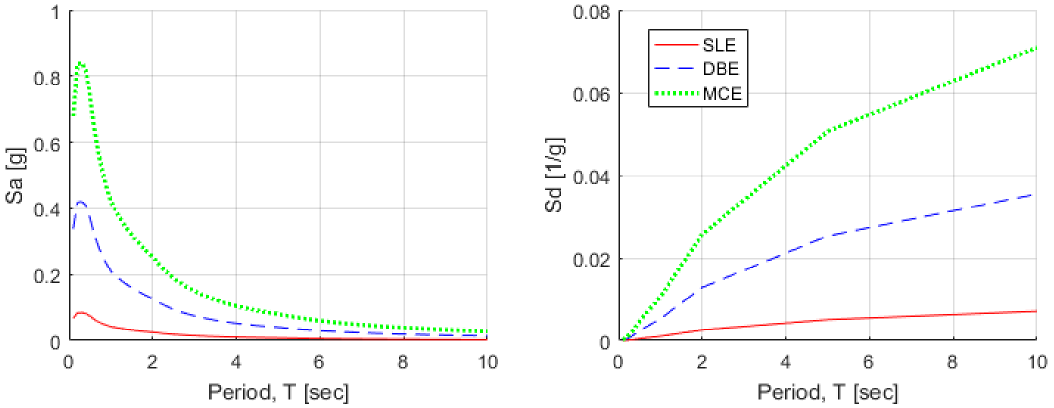

Figure 21: Spectral acceleration and displacement for a site in downtown Vancouver, BC

For design, the seismic hazards are more conveniently visualized as a modified S_a-S_d plot. The vertical axis is equal to Sa multiplied by the seismic mass to represent a base shear, and the horizontal axis is equal to S_d multiplied by a displacement modification factor (C_0) to represent a displacement. Any elastic system can be represented by a straight line passing through the origin with slope and period related by Equation 3.4:

$$T = 2\pi\sqrt{\frac{S_d}{S_a}} = 2\pi\sqrt{\frac{\Delta_y/C_0}{F_y/m}} \tag{3.4}$$

Displacement Modification Factor

An empirical factor (C_0) is used to convert displacements from a single-degree-of-freedom (SDOF) system to a multi-degree-of-freedom (MDOF) system. As shown in Table 6, ASCE-41 recommends $C_0 = 1.3$ for shear-type buildings with more than 10 stories and a triangular load pattern, and $C_0 = 1.5$ for other types of buildings greater than 10 stories.

Table 6: Values for modification factor C_0 (ASCE/SEI, 2014)

Number of Stories	Shear Buildings[1]		Other Buildings
	Triangle Load Pattern	Uniform Load Pattern	Any Load Pattern
1	1.0	1.0	1.0
2	1.2	1.15	1.2
3	1.2	1.2	1.3
5	1.3	1.2	1.4
10+	1.3	1.2	1.5

1. Buildings in which, for all stories, interstory drift decreases with increasing height

A reasonably accurate prediction of displacements is necessary for design, and therefore a parameter study was conducted to determine appropriate displacement modification factors for outriggered-wall structures. Various building configurations were modeled elastically and subjected to ground motion time histories. For each time history, the displacement response spectrum was also determined. The C_0 factor for that trial run was calculated as the ratio of max roof displacement from time-history analysis to pseudo-displacement at the fundamental period of vibration.

$$C_0 = \frac{\max(\Delta_{roof})}{S_d(T_1)} \tag{3.5}$$

The 2D models consisted of elastic beam-column elements for the wall and mega columns. The gross section properties of the wall were calculated by assuming two C-shaped wall piers with 65 MPa concrete and length, l_w=10000mm; flange width, b_f=4200mm; web thickness, t_w=600mm; flange thickness, t_f=750mm. Elastic outrigger truss elements were placed in a “kingpost” configuration for simplicity, with a very large stiffness (approximating a rigid condition). Therefore, all outrigger flexibility was concentrated in the elastic column elements. The column area was varied to achieve the desired outrigger stiffness ratio. The wall was fixed at the base while the columns were pinned. All models used a constant floor-to-floor height of 3000mm and a constant floor width of 31500mm. Stiff truss elements were used at each floor level to enforce displacement compatibility between the wall and columns (approximating a rigid diaphragm). The building configurations for the study are summarized in Table 7.

Table 7: Parameters for the C_0 study

Parameter	**Values**	**Comment**
Number of Stories	30, 40, 50, 60	3m story height used
Story Mass (kg)	1041000, 208300	
Outrigger Level	Roof, Mid height	
Outrigger Stiffness Ratio, k_r	0.5, 1, 2	$K = k_r EI/L$

The unique permutations of the above parameters result in 48 models. First mode periods ranged from 1.57 – 12.22 seconds, though the models with longer periods (T > 8.0 or so) represent unrealistic geometry configurations from a design point-of-view. Each model was subjected to 12 ground motion time-histories, for a total of 576 analysis runs. The ground motions were selected from the "Basic Far-Field Set" of the FEMA P695 project. Only the first 12 ground motions (out of 22 in total) were used to give a representative (but not overly cumbersome) spread of responses, and these are summarized in Table 8.

Table 8: Ground motions for the C_0 study

NGA#	**Event**	**Year**	**Mag**	**Mechanism**	**Station**
953	Northridge	1994	6.7	Blind thrust	Beverly Hills - 14145 Mulhol
960	Northridge	1994	6.7	Blind thrust	Canyon Country - W Lost Canyon
1602	Duzce, Turkey	1999	7.1	Strike-slip	Bolu
1787	Hector Mine	1999	7.1	Strike-slip	Hector
169	Imperial Valley	1979	6.5	Strike-slip	Delta
174	Imperial Valley	1979	6.5	Strike-slip	El Centro Array #11
1111	Kobe, Japan	1995	6.9	Strike-slip	Nishi-Akashi
1116	Kobe, Japan	1995	6.9	Strike-slip	Shin-Osaka
1158	Kocaeli, Turkey	1999	7.5	Strike-slip	Duzce
1148	Kocaeli, Turkey	1999	7.5	Strike-slip	Arcelik
900	Landers	1992	7.3	Strike-slip	Yermo Fire Station
848	Landers	1992	7.3	Strike-slip	Coolwater

C_0 factors were calculated for each analysis run using Equation 3.5. The results are plotted against the fundamental period of the model in Figure 22.

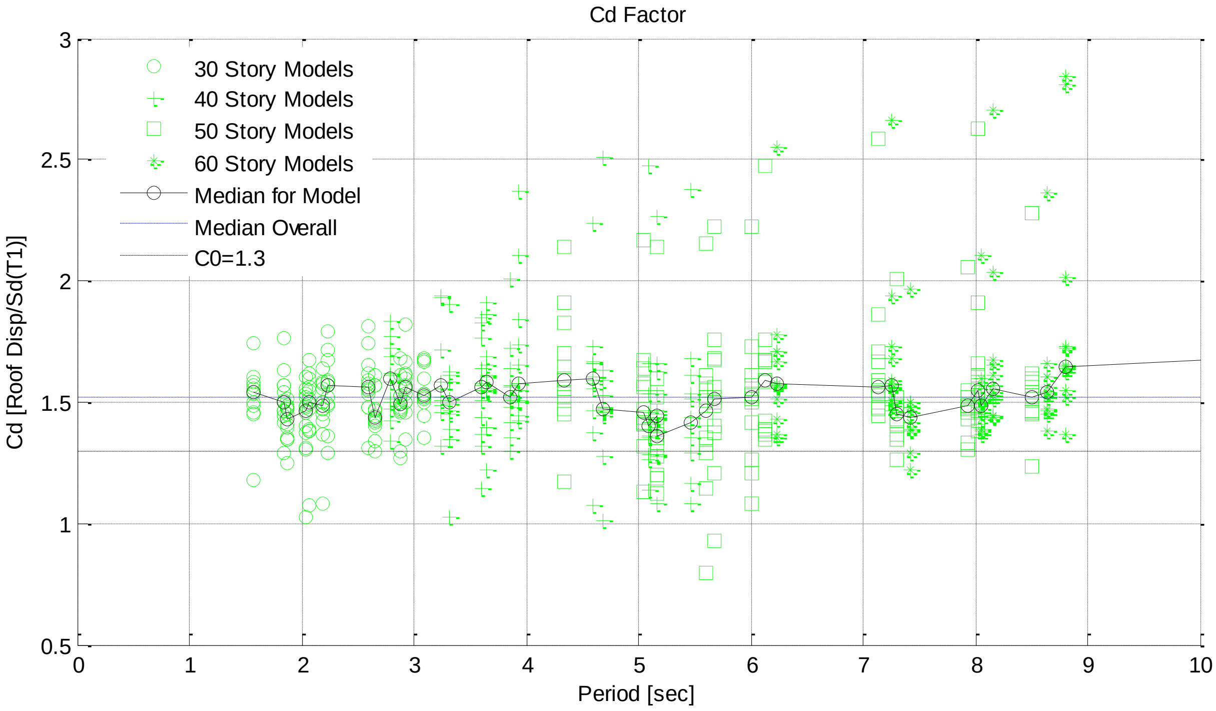

Figure 22: C_0 factors determined from linear analysis of outriggered-walls

For the given modelling parameters, the median value of C_0 was determined to be slightly over 1.5. This closely matches the ASCE-41 recommendation of 1.5 for *Other Buildings* greater than 10 stories. Values as large as 2.8 and as low as 0.7 were observed in a few instances. As the fundamental period increased, the spread of C_0 values from record-to-record generally increased. However, the median for any given model stayed close to 1.5. Based on these results, C_0=1.5 was used for the EEDP procedure.

Immediate Occupancy Performance Objective

The IO performance objective is intended to set the level of shaking for which no damage will occur in the structure. EEDP requires a certain amount of decisions to be made for each intensity. For the IO limit state, the designer can select two of the following four parameters: elastic period, shaking intensity, base shear when fuse yields, roof drift ratio at which fuse yields. Often, much of the design geometry is not governed by the engineer, but rather due to building code restrictions or architectural design considerations. For example, the length of core walls between flanges is typically governed by the number and size of elevators required for that building. As such, a good estimate of the stiffness and the mass can be made before beginning the structural design, and therefore the period is approximately known. Regardless of how this performance objective is set, it should be at least as large as the predicted serviceability demands from wind effects. With the seismic hazard and fundamental period set, the yielding base shear (F_Y) can be determined by Equation 3.6:

$$F_Y = m * S_a(T_1)_{SLE} \qquad [3.6]$$

Rapid Return Performance Objective

At the RR performance objective, the designer selects the plastic roof drift (Δ_p) and the shaking intensity when it would be appropriate for the base of the wall to begin to form the plastic hinge. With these parameters known, the system base shear corresponding to the RR performance objective (F_p) is given by Equation 3.7:

$$F_p = 2 * \frac{\Delta E_{E1}}{\gamma_a(\Delta_P - \Delta_Y)} - F_Y \qquad [3.7]$$

where ΔE_{E1} is the incremental energy from the SLE to DBE hazard and is given by Equation 3.8:

$$\Delta E_{E1} = \frac{W}{2}\left(S_{a_{.SLE}} + S_{a,DBE}\right)\left(C_0 S_{d,DBE} - \Delta_Y\right) \qquad [3.8]$$

and γ_a is an energy modification factor to relate the energy stored by the equivalent linear SDOF system to the energy dissipated by the equivalent nonlinear SDOF system, from the SLE to DBE hazards.

Collapse Prevention Performance Objective

The CP performance objective sets the maximum level of shaking that the structure can withstand without collapse. The primary and secondary systems must possess sufficient ductility to allow the building to reach the ultimate deformations set by this performance objective. The ultimate roof drift ratio (Δ_u) is determined by Equation 3.9:

$$\Delta_U = \frac{\Delta_{E2}}{\gamma_b F_P} + \Delta_P \qquad [3.9]$$

where Δ_{E2} is the incremental energy from the DBE to MCE hazard and is given by Equation 3.10:

$$\Delta E_{E2} = \frac{WC_0}{2}\left(S_{a.MCE} + S_{a,DBE}\right)\left(S_{d,MCE} - S_{d,DBE}\right) \qquad [3.10]$$

and γ_b is an energy modification factor that relates the energy stored by the equivalent elastic SDOF system to the energy dissipated by the equivalent nonlinear SDOF system, from the DBE to MCE hazards.

As per NBC2015, the primary structure must be designed with sufficient ductility for the maximum credible earthquake (MCE). For concrete walls, CSA A23.3-14 expresses this requirement in terms of inelastic rotational capacity and demand. The inelastic rotational capacity is given by Equation 3.11:

$$\theta_{ic} = \left(\phi_c - \phi_y\right) l_p \qquad [3.11]$$

Where the total curvature capacity ϕ_c is equal to:

$$\phi_c = \frac{\epsilon_{cm}}{c} \qquad [3.12]$$

And where ϕ_y is the yield curvature, c is the depth from the extreme compression fiber to the neutral axis and ϵ_{cm} is the maximum allowable concrete compression strain (typically between 0.0035 and 0.014 depending on confinement reinforcing). The plastic hinge can be estimated as $l_p = l_w/2$, therefore, the inelastic rotational capacity can be estimated by:

$$\theta_{ic} = \left(\frac{\epsilon_{cm} l_w}{2c} - 0.002\right) \qquad [3.13]$$

assuming the reinforcing steel yield strain is 0.002. The structure will be required to meet this rotation capacity at the MCE hazard. Therefore, the displacement at the ultimate state is limited by:

$$\Delta_u = \theta_{ic} H + \Delta_y \qquad [3.14]$$

The ultimate displacement is also limited by the applicable drift limit from the building code. For many building codes including NBCC 2015, this limit is around 2.5%.

Distribution of Forces

The proportion of the seismic force that is resisted by the primary and secondary SFRS can be determined using Equations 3.15 and 3.16 from Yang et al. (2017).

$$F_{PR} = F_y \frac{(\mu_p - \lambda)}{(\mu_p - 1)} \qquad [3.15]$$

$$F_{SE} = F_y \mu_p \frac{(\lambda - 1)}{(\mu_p - 1)} \qquad [3.16]$$

where the ductility is $\mu_p = \frac{\Delta p}{\Delta y}$ and the base shear ratio is $\lambda = \frac{Fp}{Fy}$.

The outrigger system is used primarily for tall structures. Per NBCC 2015, buildings greater than 60m in height must be designed with a dynamic method (typically response spectrum analysis). It is possible, but cumbersome, to analyze structures under multiple hazards and with different nonlinear mechanisms occurring at different hazard levels. For this study, however, simplified analysis is used.

Simple rigid-body mechanisms were used to arrive at design forces for the outrigger and wall members. The forces acting on the primary and secondary systems were distributed along the height of the structure using the distribution from Chao et al. (2007) described in Equation 3.17 and 3.18:

$$F_i = \lambda_i V = (\beta_i - \beta_{i+1})V_n \qquad [3.17]$$

Where

$$\beta_i = \left(\frac{V_i}{V_n}\right) = \left(\frac{\sum_{j=i}^{n} w_j h_j}{w_n h_n}\right)^{0.75T^{-0.2}} \qquad [3.18]$$

and i is the level under consideration, F is the story shear, V is the base shear, w is the weight, h is the height. This distribution was selected only for convenience; it is not particularly endorsed as a suitable distribution for outrigger systems or tall buildings in general. A more appropriate distribution of forces for outrigger systems is a potential topic of further study. Using this force distribution, the demand on the outrigger and base of wall can be determined with relatively simple calculation. The remaining structural components are then capacity designed.

The outrigger demand is determined by equating the external and internal work done by the systems. The external work is described by Equation 3.19:

$$W_{ext} = \theta_{base} F_{PR} \sum_{i}^{n} \lambda_i \, h_i \qquad [3.19]$$

while the internal work is equal to Equation 3.20:

$$W_{int} = \theta_{org} F_{org} b \qquad [3.20]$$

Rigid body mechanisms are used for simplicity, and hence $\theta_{org} = \theta_{base}$. Therefore, the outrigger force is determined by simply taking moments about the base. The wall demands can be determined in a similar matter, using the secondary system demands, F_{SE}.

Additional moments will be added to the system through P-delta effects. In tall buildings, these effects become significant and add considerable extra moment to the design forces. These effects were included in the design process of the prototypes by using the same rigid body mechanism and the calculated ultimate roof displacement, Δ_u. The additional P-Delta Moment, M_{PD}, can then be approximated with Equation 3.21:

$$M_{PD} = \frac{\Delta_u}{h_n} \sum_{i}^{n} h_i W_i \qquad [3.21]$$

Capacity Design

The non-yielding elements in the system – in this case the intermediate wall sections, outrigger truss, and mega-columns – need to be capacity designed to enforce the chosen mechanism and prevent undesirable behavior. The mega-columns and outrigger truss are designed for the probable capacity of the outrigger fuses. There could be considerable variation in overstrength depending on the type of fuse used, and an appropriate value should be justified with experimental test data. In this study, a value of 1.3 was assumed to be the ratio between the probable strength and factored design strength of the fuses. Figure 23 shows the forces acting on the intermediate wall sections. The magnified forces in the intermediate wall sections can be determined by doing a static analysis of the final mechanism at probable strength levels, as shown in Equation 3.22:

$$\sum M_{base} = 0 = M_{P,Wall} + M_{P,Org} + \sum_{i=1}^{n} \alpha_i h_i F_L \qquad [3.22]$$

where the third term is the equivalent inertial force necessary for equilibrium in the system. Rearranging for F_L, the force to be designed for in the wall is given by Equations 3.23 and 3.24:

$$F_L = \frac{M_{P,Wall} + M_{P,Org}}{\sum_{i=1}^{n} \alpha_i h_i} \qquad [3.23]$$

where

$$\alpha_i = \frac{\beta_i - \beta_{i+1}}{\sum_{i=1}^{n} (\mathrm{\beta_i} - \beta_{i+1})} \qquad [3.24]$$

and β is the load distribution parameter described previously in Equation 3.18. The probable flexural strength of the concrete wall can be calculated using 1.25 of the specified rebar strength and both material factors (φ_c, φ_s) at unity. The contribution of gravity loads to flexural strength is included by using the seismic load combinations for dead and live load, which is 1.0 and 0.5 respectively in CSA A23.3 (2014).

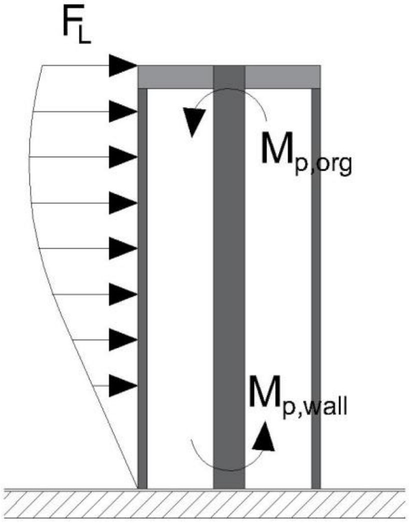

Figure 23: Forces acting on the intermediate wall segment

Chapter 4

Performance Assessment of Outrigger System under Seismic Loads

This chapter presents the results of a seismic performance assessment of prototype outrigger buildings designed using EEDP. The goal of EEDP is to design a structure which achieves multiple performance objectives under different earthquake intensities. Nonlinear time history analysis was used to predict the structure performance. A suite of earthquake records was selected for the design spectrum in Vancouver. The prototype buildings were modelled in OpenSees. Section 4.1 describes the location of the buildings and the seismic hazard. Based on this, ground motions are selected and scaled in Section 4.2. The prototype building geometries and detailing are described in Section 4.3. Section 4.4 describes the nonlinear modeling technique used for all subsequent NLTHA. Section 4.5 summarizes the results of NLTHA. Finally, in Section 4.6, the nonlinear behavior of the prototype buildings are compared to the performance objectives set during the EEDP.

4.1 Seismic Hazard

The building was designed for a hypothetical site located in downtown Vancouver, BC. This region is the third largest population center in Canada, with a regional population of more than 2.1 million people. Since the city's incorporation in 1886, no earthquake event has occurred with sufficient intensity to inflict any serious structural damage to the city's building stock. Despite the lack of damaging earthquakes in the city's short lifetime (short, that is, on a geological timescale), there exists compelling historical and geological evidence that Vancouver has considerable seismic hazard.

The West Coast of Canada is located on the so-called "Pacific Ring of Fire," a region of high seismicity around the Pacific Tectonic Plate. The Geologic Survey of Canada records over 1000 earthquakes in Western Canada every year, though the majority are relatively minor (Geologic Survey of

Canada, 2016). Earthquakes are caused by the movement of tectonic plates along interfaces. The plates in western Canada (Explorer, Juan de Fuca, South Gorda, Pacific, and North American plates) converge, diverge, and slide (transform) relative to each other. These plates produce complex seismicity and three types of earthquakes: subcrustal, crustal, and subduction as shown in Figure 24.

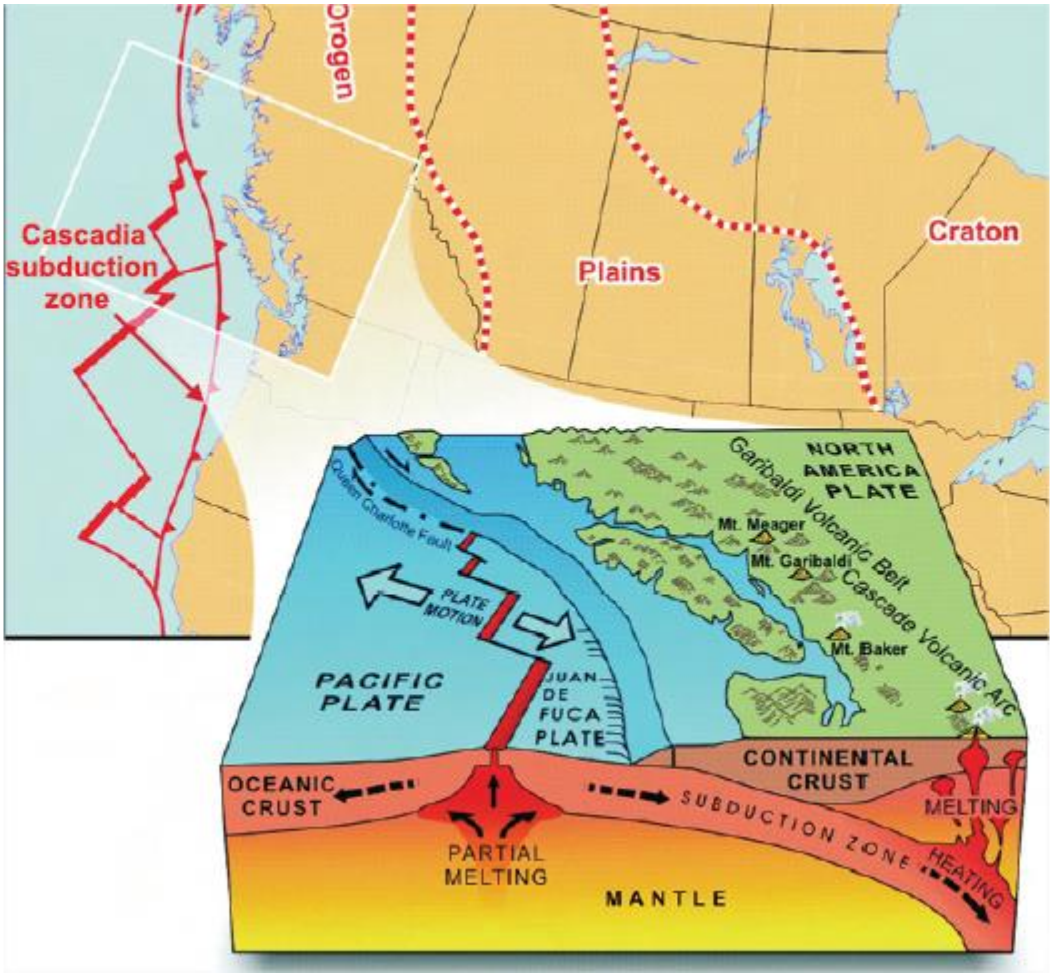
Orogen
Cascadia subduction zone
Plains
Craton
NORTH AMERICA PLATE
Garibaldi Volcanic Belt
Cascade Volcanic Arc
Mt. Meager
Mt. Garibaldi
Mt. Baker
Queen Charlotte Fault
PLATE MOTION
PACIFIC PLATE
JUAN DE FUCA PLATE
CONTINENTAL CRUST
OCEANIC CRUST
SUBDUCTION ZONE
MELTING
HEATING
PARTIAL MELTING
MANTLE

Figure 24: Tectonic setting on the West Coast of BC (Cassidy et al., 2010)

Crustal earthquakes occur in the oceanic and continental crust. The main fault mechanisms are strike-slip and thrust. In the Vancouver region, it is expected that hypocenters are to occur between 0 and 30km deep, and may produce up to magnitude 7.5 earthquakes. Subcrustal earthquakes occur within the

Juan de Fuca plate. They exhibit a normal fault mechanism. In the Vancouver region, it is expected that hypocenters are to occur between 30 and 60 kilometers deep, and produce up to magnitude 7.0 - 7.5 earthquakes. Subduction earthquakes occur well below the earth's surface from the Juan de Fuca plate subducting under the North American plate. A region known as the Cascadia Subduction Zone extends from western Vancouver Island to northern California and is believed to be locked, building strain energy (Geologic Survey of Canada, 2016). At some point, the plates may unlock, releasing the immense energy that is stored in them. These rare events may produce up to a magnitude 9.5 earthquake and rupture zone of 100km or more in length. The epicentral distance is estimated to be about 200km from Vancouver. Geological evidence suggests that a major subduction event reoccurs every 500-600 years.

Seismic sources are generally divided into two categories: Zones (areas) and Faults. Zones are used when there is uncertainty of the source characteristics over a region. When the locations of faults are known, they can be used instead of zones. The seismic parameters of each zone are described by a recurrence relation that relates the frequency and magnitude of earthquakes produced from a zone. In NBCC 2015, this relation is described by the Gutenberg-Richter magnitude-frequency distribution shown in Equation 4.1 (Halchuk et al., 2014):

$$N(M) = N_0 e^{-\beta m}[1 - e^{-\beta(Mmax-m)}] \qquad [4.1]$$

Where:

m is the equivalent to moment magnitude Mw

N is the cumulative number of earthquakes greater than magnitude m

N_0 is the number of earthquakes per year with a magnitude greater or equal to 0

β is the relative number of small-to-large earthquakes where β=b*ln10

Ground motion prediction equations are used to estimate the spectral accelerations at a site from a specific source, based on magnitude, distance to the site, and source type. They are derived by analyzing existing ground motion data from earthquakes around the world. The contribution from different sources are then combined probabilistically

The soil stratigraphy in downtown Vancouver tends to consist of glacial till over bedrock. Site class C was chosen to represent the soil condition at the fictional site, which corresponds to V_{s30} in the range of 300-700 m/s (NRC, 2015). Figure 25 shows the seismic hazard deaggregation for Vancouver at the PGA and periods of 0.2, 1, and 2 seconds. Records were filtered based on the magnitude range 5.5 to 7.5. All fault mechanism types were allowed. The distance range was limited to between 0 to 150 km.

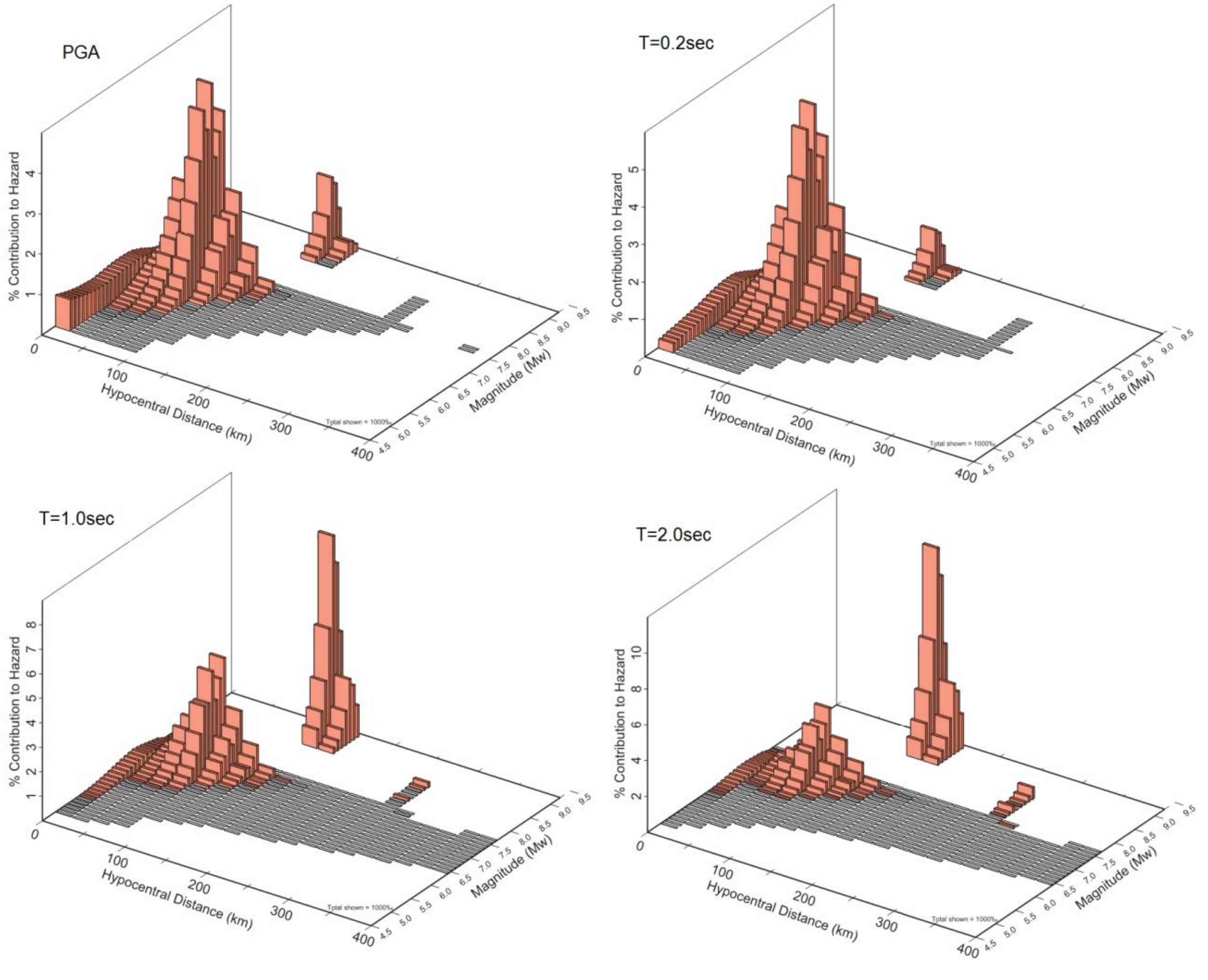

Figure 25: Seismic hazard deaggregation for Vancouver (National Resources Canada, 2016)

4.2 Ground Motion Selection

Using the above information, ground motions records were selected to study the behavior of outriggered-wall structures as summarized in Table 9. The records were amplitude scaled to the target spectrum. This is a simple scaling method where a single scale factor is used to adjust the accelerations for the entire record. A scaling range was defined as [T_{min}, T_{max}] where T_{min} was the lesser of 0.2 seconds and the third modal period, T_3 and T_{max} was the greater of 2 seconds or the first modal period, $T_{1,}$ multiplied by 1.5.

Table 9: Ground motion properties for nonlinear analysis

Ref	NGA	Year	Event	Station	Mechanism	Mw	Vs30 (m/s)	Rjb (km)	Scale Factor		
									SLE	DBE	MCE
GM01	138	1978	Tabas Iran	Boshrooyeh	Reverse	7.35	324.6	24.1	0.25	1.25	2.51
GM02	143	1978	Tabas Iran	Tabas	Reverse	7.35	766.8	1.8	0.05	0.25	0.49
GM03	14	1952	Kern County	Santa Barbara Courthouse	Reverse	7.36	515.0	81.3	0.20	1.01	2.02
GM04	164	1979	Imperial Valley-06	Cerro Prieto	strike slip	6.53	471.5	15.2	0.20	0.98	1.96
GM05	187	1979	Imperial Valley-06	Parachute Test Site	strike slip	6.53	348.7	12.7	0.27	1.36	2.72
GM06	292	1980	Irpinia Italy-01	Sturno (STN)	Normal	6.9	382.0	6.8	0.12	0.61	1.21
GM07	335	1983	Coalinga-01	Parkfield Fault Zone 10	Reverse	6.36	372.7	30.3	0.22	1.10	2.21
GM08	3750	1992	Cape Mendocino	Loleta Fire Station	Reverse	7.01	515.7	23.5	0.12	0.60	1.19
GM09	583	1986	Taiwan SMART1(45)	SMART1 O10	Reverse	7.3	320.1	56.9	0.17	0.83	1.65
GM10	68	1971	San Fernando	LA - Hollywood Stor FF	Reverse	6.61	316.5	22.8	0.17	0.85	1.70
GM11	730	1988	Spitak Armenia	Gukasian	Reverse Oblique	6.77	343.5	24.0	0.20	0.98	1.97
GM12	731	1989	Loma Prieta	APEEL 10 - Skyline	Reverse Oblique	6.93	391.9	41.7	0.24	1.20	2.41
GM13	796	1989	Loma Prieta	SF - Presidio	Reverse Oblique	6.93	594.5	77.3	0.18	0.90	1.81
GM14	827	1992	Cape Mendocino	Fortuna - Fortuna Blvd	Reverse	7.01	457.1	16.0	0.20	0.97	1.95
GM15	832	1992	Landers	Amboy	strike slip	7.28	382.9	69.2	0.23	1.14	2.28

The scaling function minimized the mean square error of each record to the spectrum over the chosen scaling range. It is suggested to use a scaling range to account for higher modal frequencies as well as the effects of stiffness degradation, which will cause the first mode period to increase. In general, it is best to choose ground motions that fit the target spectral shape and hence have scale factors close to unity. However, no suitable records exist for the faults around Vancouver, and hence, records from other sources need to be used. To avoid over-scaling, the scale factors were limited to between 0.5 and 3 for the MCE hazard level. Figure 26 shows the selected ground motions scaled to each of the three hazard levels.

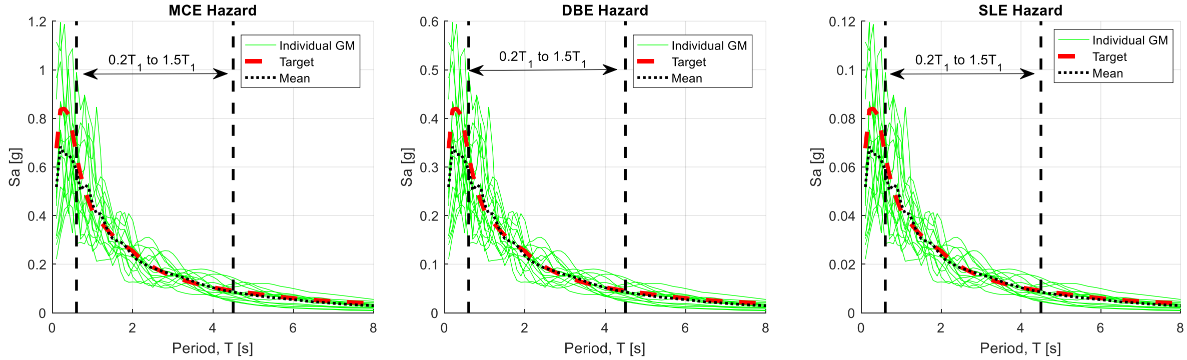

Figure 26: Response spectra of selected ground motions, mean of all motions, and target scaled to each of the three hazard levels

4.3 Prototype Buildings

Three prototype buildings of varying heights were designed using the EEDP methodology described in the previous chapter for a hypothetical site in Vancouver, Canada. The buildings are hereby referred to as Towers A, B, and C respectively. It was decided to use three prototype buildings to get a range of structural responses and help instill confidence in the design procedure. The number of stories in each prototype is 20, 30, and 40. Interstorey floor height is 3.0 meters in all models, resulting in overall heights of 60, 90, and 120 meters as shown in Figure 27.

The buildings utilize two c-shaped reinforced concrete shear walls arranged into a core as shown in Figure 28. The weight of each floor is assumed to be 6675kN, resulting in a seismic weight of 133500, 200200, and 267000 kN for Towers A, B, and C, respectively. The EEDP displacements at each hazard level and the energy modification factors for each prototype buildings are summarized in Table 10. Outriggers were located on the roof of all buildings. It was decided that multiple outriggers or mid height outriggers were not practical because these buildings would typically not have intermediate mechanical floors to accompany the large outrigger members, due to their relatively short heights. The gross concrete wall dimensions for each prototype building are shown in Table 11.

Table 10: EEDP displacements at each hazard and energy modification factors

Building	Outrigger Yielding Displacement, Δ_y [mm]	Wall Yielding Displacement, Δ_p [mm]	Ultimate Displacement, Δ_p [mm]	γ_a [-]	γ_b[-]
Tower A	26	160	394	1.50	2.00
Tower B	39	260	566	1.25	2.00
Tower C	50	400	786	1.00	2.00

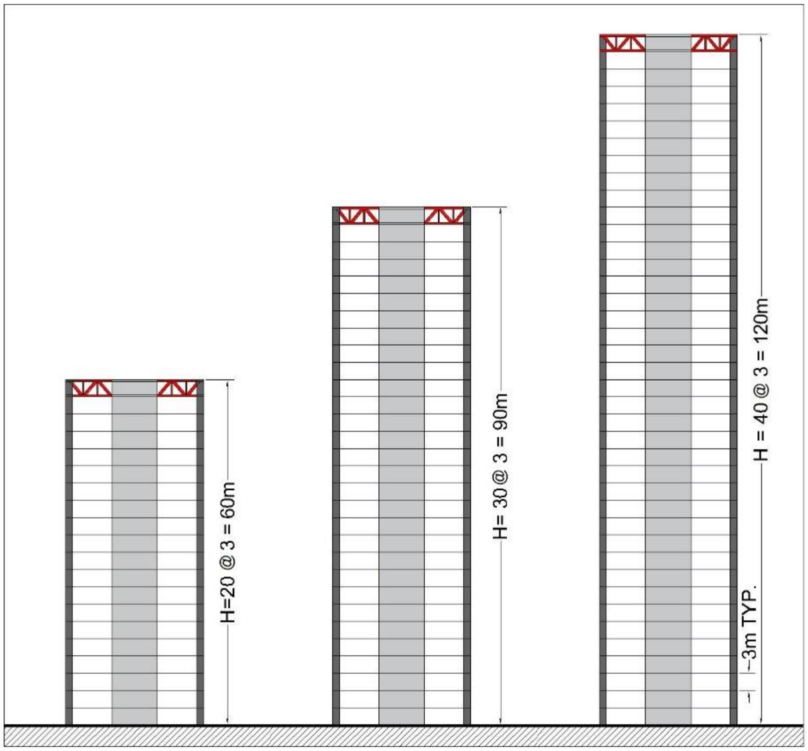

Figure 27: Prototype building elevations (a) Tower A (b) Tower B and (c) Tower C (not to scale).

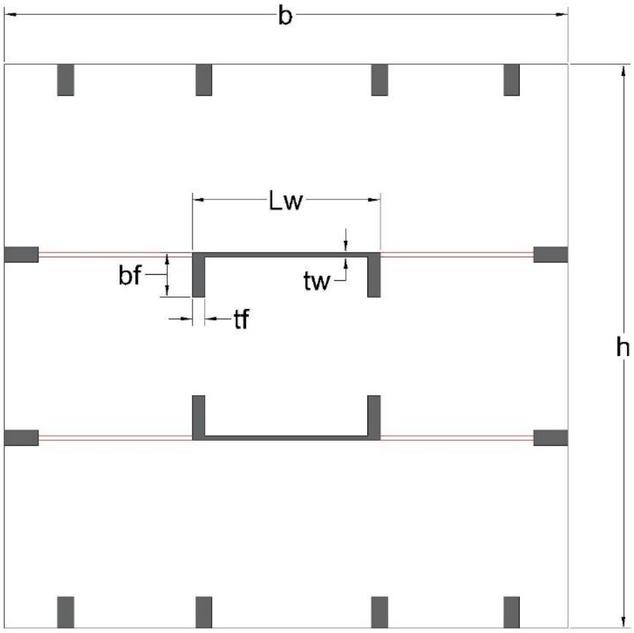

Figure 28: Prototype building floor plan (not to scale)

Table 11: Wall cross-sectional properties for each prototype

Building	Floor length, h [m]	Floor width, b [m]	Wall Length, Lw [mm]	Flange Length, bf [mm]	Web Thickness, tw [mm]	Flange Thickness, tf [mm]	Concrete Strength, f’c [MPa]
Tower A	23.8	23.8	4875	2250	500	600	65
Tower B	23.8	23.8	7315	2250	500	600	65
Tower C	23.8	23.8	9145	2300	600	750	65

Flexural design was completed in MATLAB 2016b (The Mathworks Inc, 2016) using a script to construct the axial-moment interaction curve for a trial section at predefined points, and interpolating for the given axial load. The results were verified at select locations with S-CONCRETE v11.3.7, a commercially-available design tool (S-FRAME Inc, 2016). The reinforcing in the plastic hinge regions was kept constant. Above the plastic hinge, flexural demands were amplified in accordance with the capacity design approach discussed in Chapter 3. Each floor between the outrigger and plastic hinge region was designed for the loads at that floor. In practice, a reinforcing design and layout would be carried through ‘lifts’ of multiple floor for efficiency and constructability. The reinforcing at the base of the wall and at the outrigger level are summarized in Table 12, while the outrigger demand and the chosen fuse size are shown in Table 13.

Table 12: Summary of wall reinforcing at base and below outrigger

Building	**Vertical Distributed Reinforcing**		**Concentrated Reinforcing at base of wall**		**Concentrated Reinforcing at outrigger**	
	Web	Flange	Z1	Z2	Z1	Z2
Tower A	15M@6” VEF	15M@6” VEF	20-35M Verts 10M@6” Ties	20-35M Verts 10M@6” Ties	24-35M Verts 10M@6” Ties	24-35M Verts 10M@6” Ties
Tower B	15M@6” VEF	15M@6” VEF	32-35M Verts 10M@6” Ties	32-35M Verts 10M@6” Ties	28-35M Verts 10M@6” Ties	28-35M Verts 10M@6” Ties
Tower C	15M@6” VEF	15M@6” VEF	28-35M Verts 10M@6” Ties	28-35M Verts 10M@6” Ties	28-35M Verts 10M@6” Ties	28-35M Verts 10M@6” Ties

Table 13: Summary of outrigger fuse and member sizes on each prototype

Building	**Yield Force (kN)**	**Yield Stress (MPa)**	**Fuse Area (mm^2)**	**Chord Area (mm^2)**	**Diagonal Area (mm^2)**
Tower A	7320	350 MPa	20920	663,900	334,700
Tower B	11380	350 MPa	32510	1,031,800	520,100
Tower C	13565	350 MPa	38760	1,246,300	628,200

Figure 29 shows the flexural design of the plastic hinge region of the walls in each of the three towers. Note that the design only considered bending about the Y-Axis. If the walls were designed for the coupled direction, it is likely that they would require additional flexural reinforcement in the web. Additional details of the design of the three towers is included in Appendices A, B, and C.

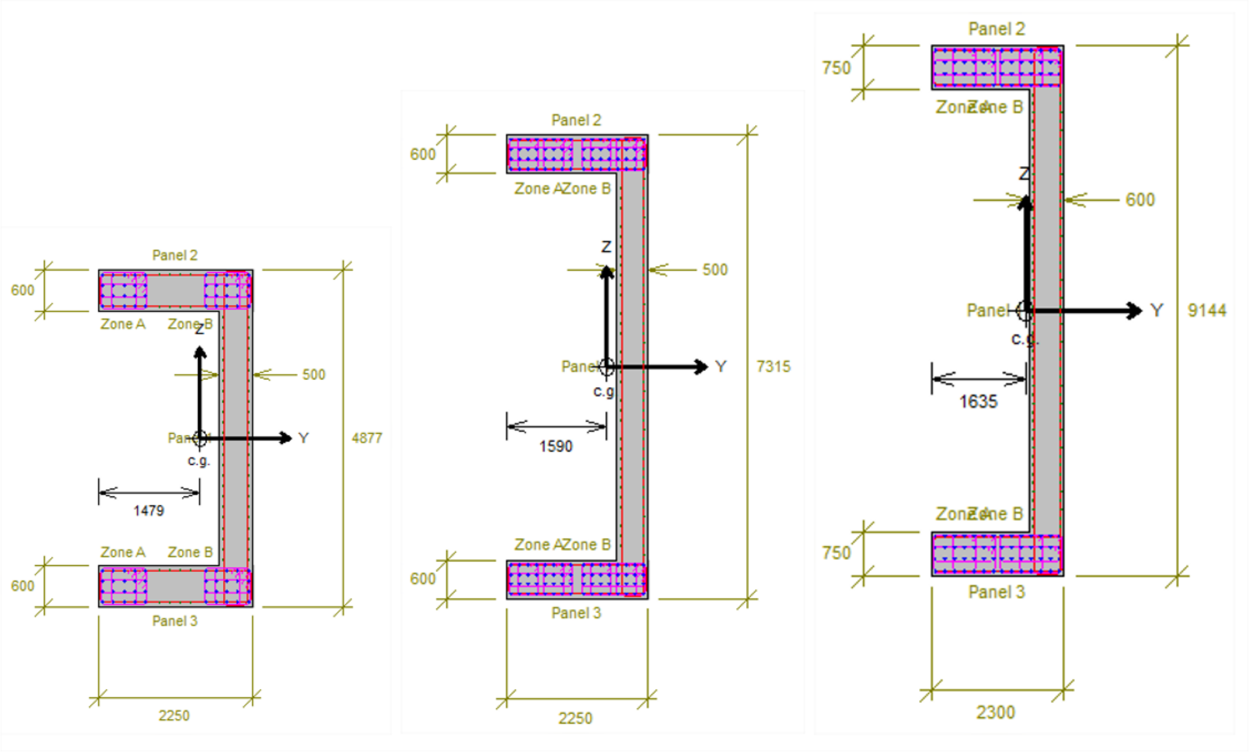
Panel 2
600
Zone A
Zone B
Z
500
Y
4877
c.g.
1479
Zone A
Zone B
600
Panel 3
2250
Panel 2
600
Zone A
Zone B
Z
500
Y
7315
c.g
1590
Zone A
Zone B
600
Panel 3
2250
Panel 2
750
Zone B
Z
600
Y
9144
c.g.
1635
Zone B
750
Panel 3
2300

Figure 29: Flexural design at the base for each of the prototype buildings (a) Tower A, (b) Tower B, and (c) Tower C. Images generated using S-CONCRETE (S-FRAME Inc, 2016)

The first three mode shapes of Tower A are shown in Figure 30 below. Tower B and C had similar mode shapes but different periods. The first three modal periods of each tower are shown in Table 14 below. The eigen analysis was conducted using expected material properties and uncracked sectional properties. The periods below are somewhat lower than would be expected for seismic design with elastic cracked models. The expected material properties and concrete material behavior before cracking is largely responsible for this. After the concrete fibers crack, the system flexibility increases and the effective periods will elongate.

Table 14: Modal periods for the prototype buildings

Building	Mode 1	Mode 2	Mode 3
Tower A	1.41	0.27	0.10
Tower B	2.00	0.37	0.15
Tower C	2.65	0.52	0.22

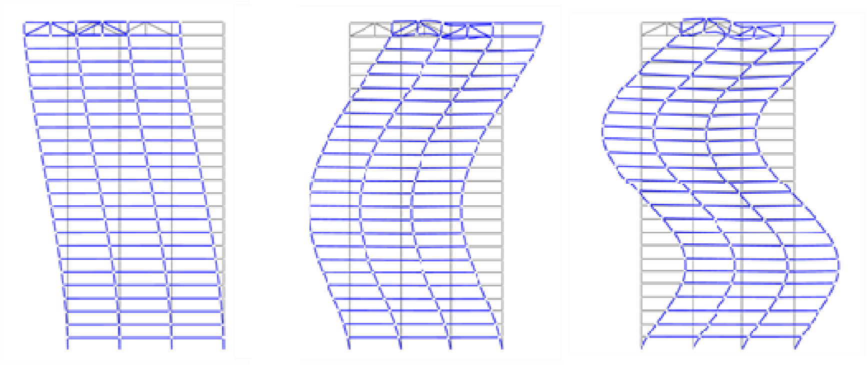

Figure 30: Mode shapes of Tower A prototype (a) T_1=1.41 sec. (b) T_2=0.27 sec. (c) T_3=0.10 sec.

4.4 Nonlinear Modelling Technique

All nonlinear analysis was done using OpenSees (1997) version 2.5.0. OpenSees is an open source analysis framework for earthquake engineering. The modelling intent is to adequately capture the nonlinear response of the SFRS system (wall, coupling beams, and outrigger trusses) so that the design approach can be assessed. If EEDP is working as intended, the target performance objectives used in the design stage should be close to the response of the structure when excited by ground motions scaled to the same hazards.

4.4.1 Modelling Assumptions

The buildings were simulated using a simplified 2D model, as depicted by Figure 31. The walls, outrigger columns, and outrigger truss were modelled explicitly. The remainder of the gravity system was modelled with a leaning column for P-delta effects. The seismic mass was lumped onto wall nodes at every floor. The seismic mass was calculated using the self-weight of the structure, and was the same value used for design and analyses stages. Gravity loads were applied to the mega columns, core wall, and leaning column nodes using tributary area. The gravity load case given by Equation 4.2:

$$P = 1.0D + 0.5L \tag{4.2}$$

was used for analysis, where P is the factored gravity load, D is the dead load and L is the live load. The gravity case was run prior to each time history analysis and held constant for the duration of the analysis. Scaled ground motion accelerograms were applied at the base of the structure, which was assumed to be fully restrained (fixed) at the wall and pinned at the columns.

An important consideration for design and analysis of outriggers is whether the gravity analysis should induce stress in the outrigger system. In reinforced concrete buildings, there are two components of deflection: immediate elastic deflections and long-term deflections (creep). As a building is constructed, floor by floor, the elastic deflections will occur immediately. Immediate deflections should not induce stress in the outrigger, because this would occur prior to installing the outrigger system. On the other hand, long term deflections could induce considerable stress in the outrigger if there is no mitigatory plan in the design. The core walls are generally at a lower axial stress than columns, and thus, differential deflections are expected over time. For this analysis, it was assumed that the outrigger was not stressed during gravity analysis. To implement this assumption, it was necessary for the outrigger columns and walls to deflect equally. The gravity load stress on the columns was therefore made equal to the walls.

It was assumed that there are stiff diaphragms at each floor level from a reinforced concrete slab. It is common to assume that concrete slab floor systems act as ‘rigid diaphragms’ for computational efficiency, due to their high axial stiffness. While this assumption can generally be used on regular buildings without much error, it can cause significant error if used on outrigger floors (Choi et al., 2012). The stiffening effect of rigid diaphragm may overpredict the effectiveness of the outrigger system and under predict forces in chord members (Choi et al., 2012). Slabs were not explicitly modelled for computational efficiency. In the 2D model, the diaphragms were modeled using Multi-Point Constraints (MPCs). For the lateral direction, the *EqualDOF* command in OpenSees was used to slave all nodes on the same horizontal plane to the wall node. On outrigger levels, the MPC was eliminated for nodes connected to the outrigger truss chord. This was done to avoid affecting the outrigger stiffness. A MPC was still used to constrain the P-delta column to the wall.

A P-Delta leaning column was used to capture P-Delta effects from the remainder of the gravity system (which was not modelled explicitly). In this approach, the axial load that is tributary to that portion of the gravity system is placed on a column with a P-delta transformation. It was assumed that the remaining gravity-resisting elements contributed very little to the lateral stiffness and strength, and so the P-delta column was modelled as an elastic beam column element with very low moment of inertia (effectively making it pinned in between stories). When the building deflects laterally, the diaphragms force compatible deflections of the column and wall. The axial load on the leaning column then induces additional overturning moment that must be resisted by the SFRS (because the column itself has effectively no lateral strength or stiffness). Modelling P-delta effects is an important consideration in assessing collapse prevention limit states because system instability may result.

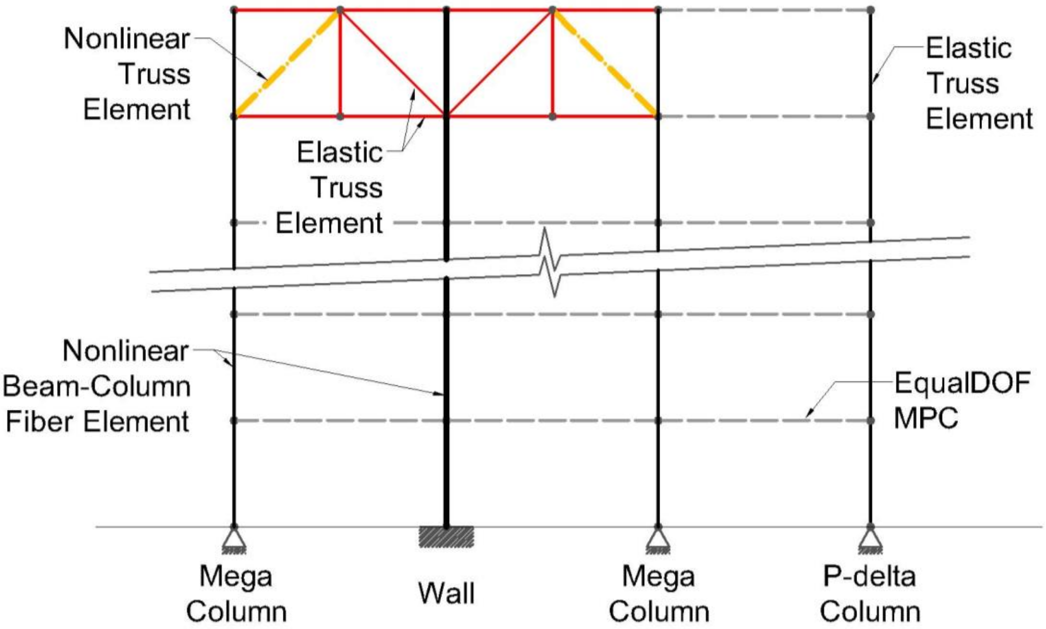
Nonlinear Truss Element
Elastic Truss Element
Elastic Truss Element
Nonlinear Beam-Column Fiber Element
EqualDOF MPC
Mega Column
Wall
Mega Column
P-delta Column

Figure 31: Conceptual configuration of nonlinear model

4.4.2 Materials

Linear and nonlinear material properties were included in the analysis using the built-in material models in OpenSees. This analysis series required nonlinear material behavior for concrete, reinforcing steel, structural steel, and linear material for the wall shear behavior and outrigger trusses.

Concrete was modelled using the Concrete02 material in OpenSees. Concrete02 is a nonlinear concrete material model which includes tensile strength and linear softening of the tensile strength. Figure 32 shows the behavior of Concrete02 material. The initial stiffness in this model is equal to 2 $fpc/$epsc0. Table 15 shows the value of the Concrete02 parameters used in this study.

Table 15: Summary of concrete material properties for analysis

Name	$fpc (MPa)	$epsc0	$fpcU (MPa)	$epsU	$lambda	$ft (MPa)	$Ets (MPa)
Confined	97	-0.0035	10.8	-0.014	0.1	2.42	1935
Unconfined	65	-0.0020	3.25	-0.008	0.1	2.42	1935

$fpc	concrete compressive strength at 28 days
$epsc0	concrete strain at maximum strength
$fpcu	concrete crushing strength
$epsU	concrete strain at crushing strength
$lambda	ratio between unloading slope at $epscu and the initial slope
$ft	tensile strength
$Ets	tension softening stiffness (absolute value) (slope of the linear tension softening branch)

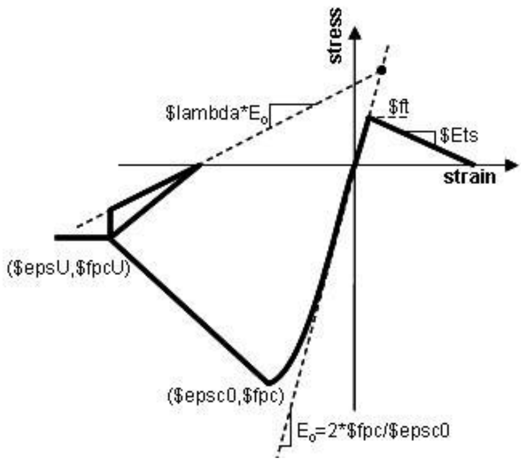

Figure 32: Concrete02 material behavior (Filippou & Mazzoni, 2009a)

The shear and flexural response of walls was assumed to be uncoupled, as is commonly assumed in commercially-available structural analysis software. The shear material is aggregated with the axial-flexural behavior using a section aggregator in OpenSees. Shear response was assumed to be elastic, as capacity design will provide adequate strength to limit the inelastic action of this failure mode. Shear demand is then checked to ensure the assumption is valid. In all analysis cases, no shear yielded was observed, so the results were not affected.

The uniaxial steel behavior was modelled with the Steel02 material in OpenSees. Steel02 is based on the Giuffree-Menegotto-Pinto steel relation which includes isotropic strain hardening.

$Fy	yield strength	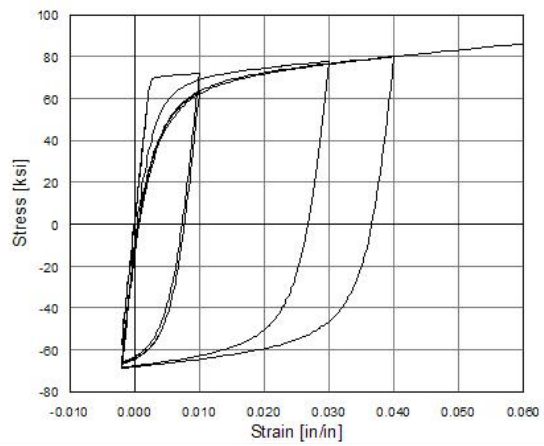
$E0	initial elastic tangent	
$b	strain-hardening ratio	
$R0 $CR1 $CR2	elastic-plastic transition parameters	
$a1	isotropic hardening parameter	
$a2	isotropic hardening parameter	
$a3	isotropic hardening parameter	
$a4	isotropic hardening parameter	

Figure 33 summarizes the Steel material model properties. A separate material was made for the reinforcing steel in fibers and the structural steel used in the outriggers. Table 16 summarizes the parameters of the steel materials used in this study

Table 16: Summary of steel material properties for analysis

Name	$Fy (MPa)	$E0 (GPa)	$b	$R0	$CR1	$CR2	$a1	$a1	$a3	$a4
Structural Steel	350	200	0.001	18	0.925	0.15	0	1	0	1
Reinforcing Steel	400	200	0.001	18	0.925	0.15	0	1	0	1

$Fy	yield strength
$E0	initial elastic tangent
$b	strain-hardening ratio
$R0 $CR1 $CR2	elastic-plastic transition parameters
$a1	isotropic hardening parameter
$a2	isotropic hardening parameter
$a3	isotropic hardening parameter

$a4	isotropic hardening parameter	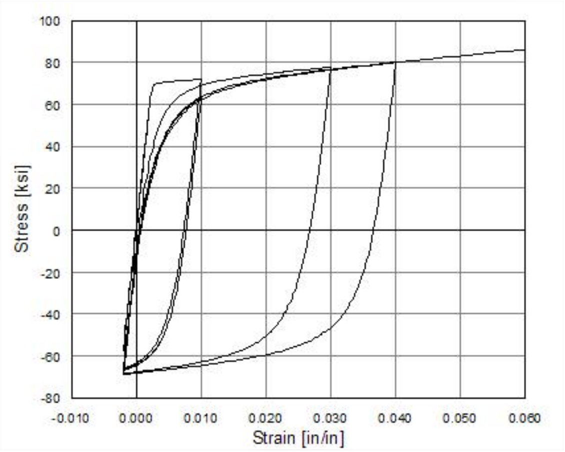

Figure 33: Steel02 material behavior (Filippou & Mazzoni, 2009b)

4.4.3 Elements

The design of shear walls is typically accomplished using a linear analysis with cracked section properties. Unlike design, however, more accurate prediction of response parameters is required when assessing the seismic performance of shear wall buildings, and this can be accomplished using nonlinear analysis. Shear walls may behave differently depending on the thickness, aspect ratio, and level of reinforcing present (Orakcal & Wallace, 2004). The nonlinear behavior of reinforced concrete walls is also complex. Multiple sources of nonlinearity are present in most walls, including the nonlinear behavior of the steel and concrete materials, and various nonlinear interaction between the materials, such as the imperfect bond between the steel and concrete. The nonlinearity may also occur at localized regions, such as concrete crushing at wall end or strain hardening and bar rupture of rebar in tension. In this study, shear wall elements were modeled as nonlinear beam-columns with a force-based element formulation. Axial and flexural behavior is captured using a fiber section, while shear behavior is defined using an aggregated material behavior. A fiber section of reinforcing steel, confined concrete, and unconfined concrete was created for the core walls using materials Steel02 and Concrete02. An elastic shear material was aggregated onto the element, corresponding to its calculated shear stiffness.

To verify the prediction capability of the modelling approach, a well-documented shear wall experiment was modelled using the elements in OpenSees. The experiment was conducted by Thomsen and Wallace at Clarkson University (1995). Figure 34 below shows the specimen geometry and reinforcement detailing. The wall aspect ratio (h_w/l_w) was equal to 3. The top of the specimen was connected to a loading beam and actuator. Braces restrained the top of the wall from significant out-of-plane movement. Axial loads equal to approximately $0.1A_g f'_c$ were applied to the wall through the loading beam. The material properties of the specimen were determined by experimental testing, and are summarized in Table 17.

Table 17: Material properties from wall test (Thomsen & Wallace, 1995)

Concrete:	**f'c (MPa)**	**e'c**	**Ec (GPa)**	**ecr**	**ft (MPa)**	**et**
Confined	47.6	0.0033	31.03	0.0037	2.03	0.00008
Unconfined	42.8	0.0021	31.03	0.0022	2.03	0.00008
Steel:	**Fy (MPa)**	**Es (MPa)**	**b**			
Rebar	434	200000	0.02			

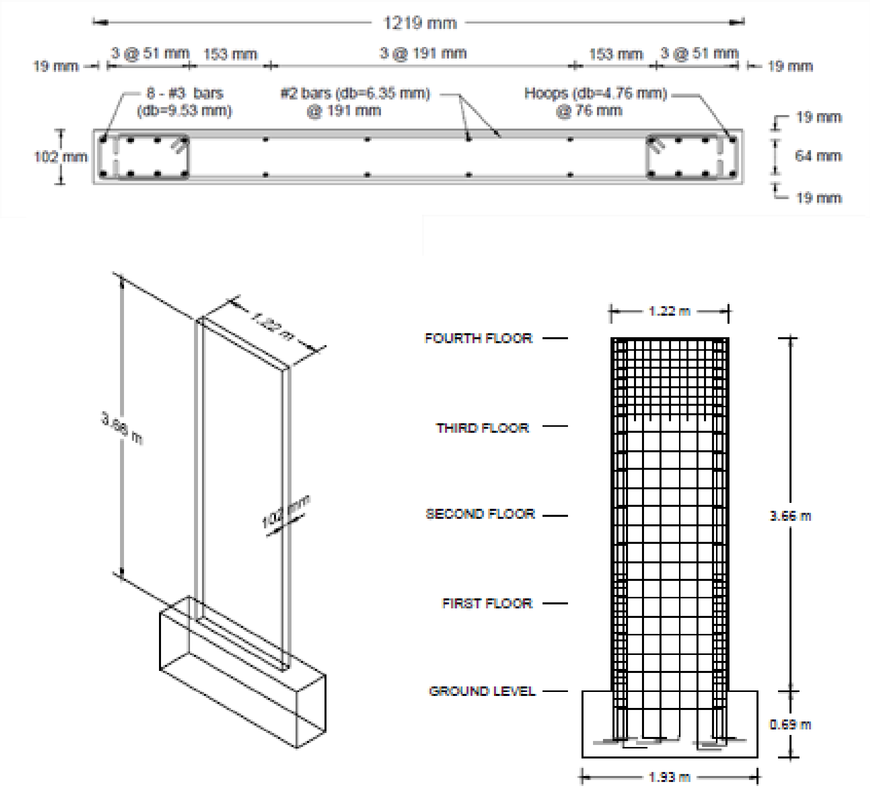
1219 mm
19 mm
3 @ 51 mm
153 mm
3 @ 191 mm
153 mm
3 @ 51 mm
19 mm
8 - #3 bars (db=9.53 mm)
#2 bars (db=6.35 mm) @ 191 mm
Hoops (db=4.76 mm) @ 76 mm
102 mm
19 mm
64 mm
19 mm
1.22 m
3.66 m
102 mm
FOURTH FLOOR
THIRD FLOOR
SECOND FLOOR
FIRST FLOOR
GROUND LEVEL
1.22 m
3.66 m
0.69 m
1.93 m

Figure 34: Shear wall specimen RW1 (a) cross-section (b) isotropic view, and (c) elevation view (Thomsen & Wallace, 1995)

The wall specimen was loaded according to the quasi-static load protocol shown in Figure 35. The load protocol consisted of two reverse cycles of displacement to each of the following drifts: 0.1%, 0.25%, 0.5%, 0.75%, 1.0%, 1.5%, 2.0%, and 2.5%.

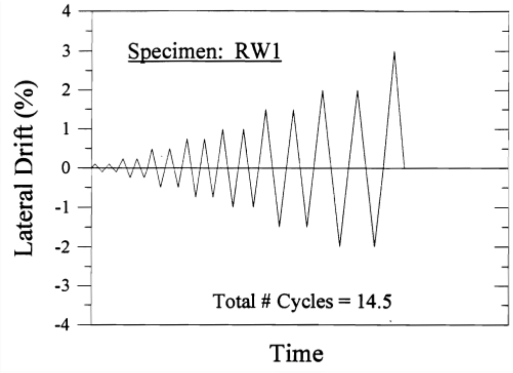

Figure 35: Loading protocol for test specimen RW1 (Thomsen and Wallace, 1995)

The results of the chosen modelling technique are plotted in Figure 36 alongside the experiment result. The model exhibits many of the same characteristics as the experiment. The overal shape of the hysteretic loops are similar. Stiffness degredation and pinching behavior is similar to the experiment, though the model tends to have a more pronounced pinching behavior. Nevertheless, the wall model is sufficiently good for the purposes of this thesis, where overall building behavior is desired.

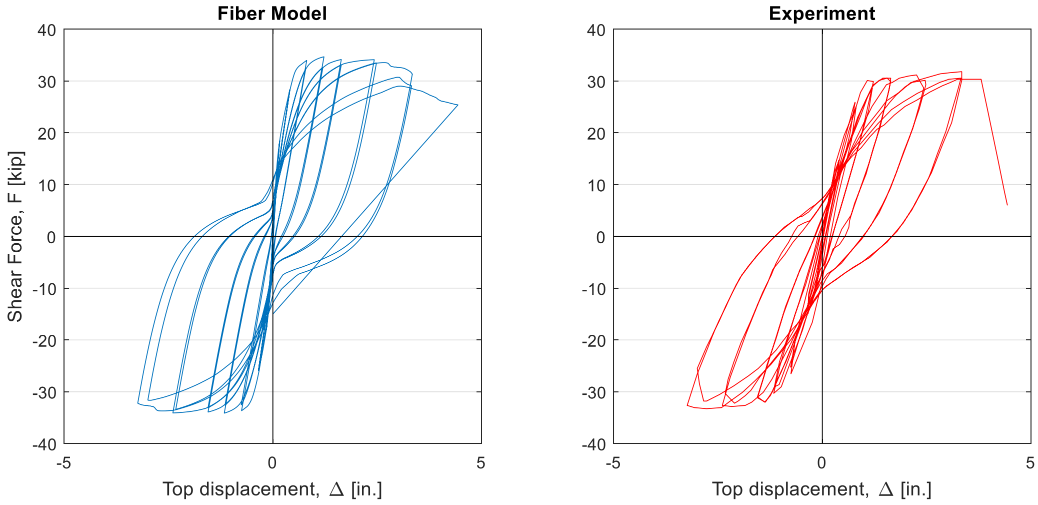

Figure 36: Comparison of (a) modeling technique used in this study and (b) experimental result of wall test RW1 by Thomsen and Wallace (1995)

Fuse elements are used to limit the force delivery of the outrigger system, protect the wall from being overloaded, and provide stable energy dissipation. Buckling restrained braces (BRBs) were modelled using OpenSees material Steel02, which is a Giuffre-Menegotto-Pinto steel material with isotropic strain hardening. All other outrigger truss members were modelled elastically, as they are capacity designed to the probable strength of the buckling-restrained braces. Figure 37 shows the BRB model compared to an experiment by Black et al. (2004).

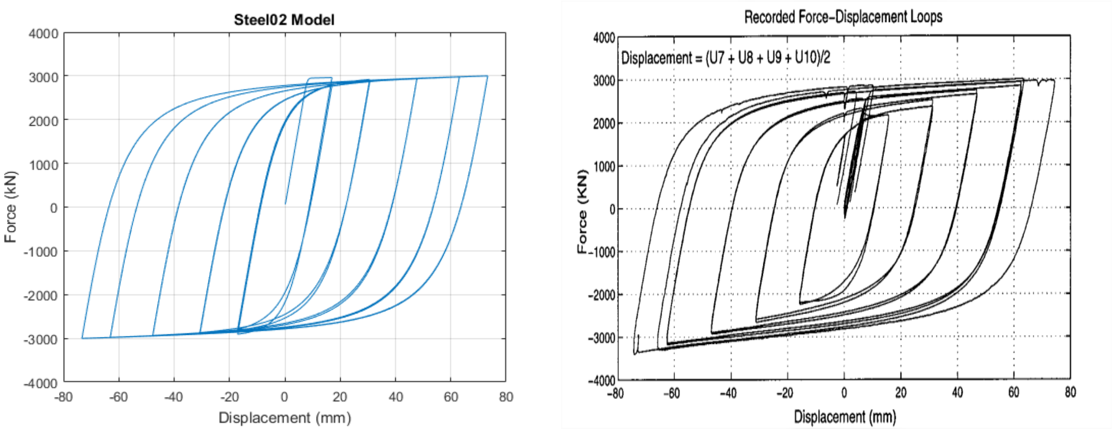

Figure 37: Comparison of (a) modeling technique used in this study and (b) experimental result of a BRB test (Black et al., 2004)

The mega-columns that are part of the outrigger system were modeled using nonlinear fiber elements. The net steel and concrete areas were lumped into fibers located close to the centroid of the section to avoid attracting large moments and shears into these elements. The bases of the mega-columns were pinned.

The P-Delta column elements were modelled using elastic beam column elements. A large stiffness reduction factor was applied to the moment of inertia of these elements to prevent it from contributing to the lateral stiffness of the building. The base of the P-Delta column was pinned.

4.5 Nonlinear Time-History Analysis Results

In this section, the results of nonlinear time-history analysis are shown for the three prototype buildings using the ground motions from Section 4.2. Section 4.5.1 presents the results for Tower A (20-story building), Section 4.5.2 presents the results for Tower B (30-story building), and Section 4.5.3 present the results for Tower C (40-story building).

4.5.1 Results for Tower A

This section presents the results of nonlinear analysis on a 20-story building designed using EEDP. Figure 38 shows the maximum wall moments along the height of the wall for each of the three hazard levels. The moment envelope generally peaks at the base of the wall and decreases to a minimum at around 50-60% of the height. Moments then increase further up the wall due to the outrigger, which was located at the roof level. The mean peak wall moments at the SLE, DBE, and MCE hazard levels were 115 MN-m, 283 MN-m, and 345 MN-m respectively. There was generally a larger dispersion of moments from record-to-record as the hazard level increased. This was not due to record variability, as the ratio between record scale factors at each hazard level was unchanged. Instead, the increased variability comes from the increased nonlinearity in the model behavior.

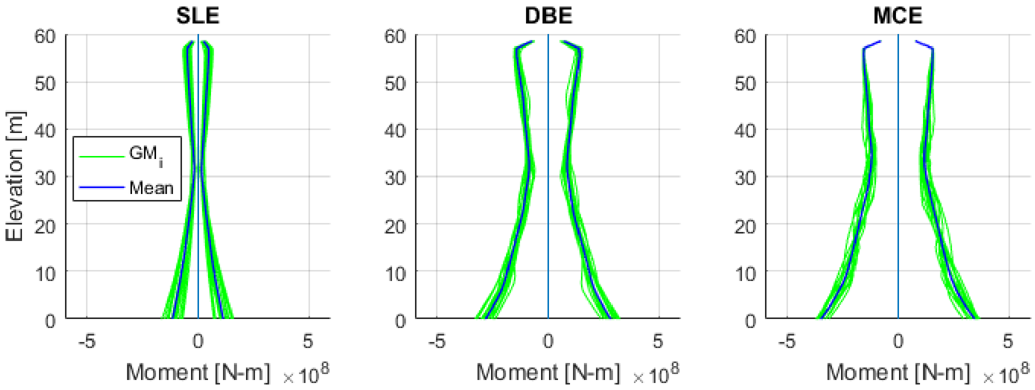

Figure 38: Peak moment vs height in Tower A wall for all GMs and hazards

Figure 39 presents the peak wall shears along the height of the wall for each of the three hazard levels. The shear envelope is generally largest at the base and decreases around 40-50% of the height. Higher mode effects then cause shears to increase further up the building. The peak mean base shears at the SLE, DBE, and MCE hazards were 4610 kN, 15800 kN, and 24010 kN respectively.

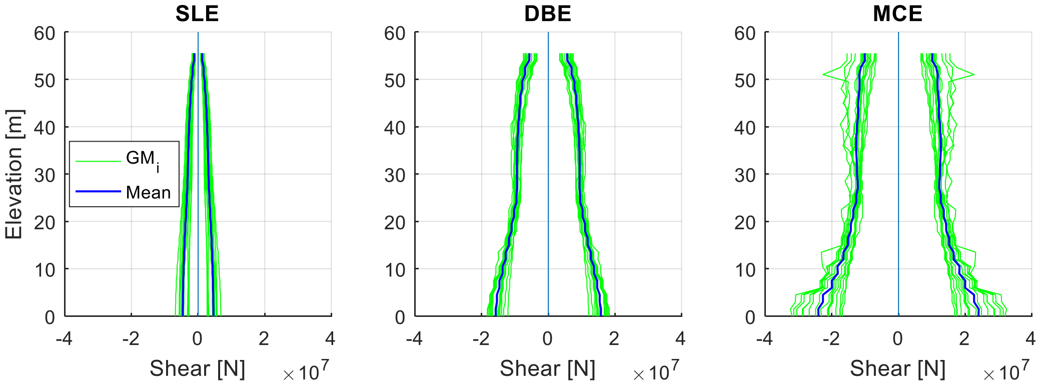

Figure 39: Peak shear force vs height in Tower A wall for all GMs and hazards

Figure 40 presents the peak displacement envelopes over the height of the building for the three hazard levels. The mean roof displacement at each hazard level was approximately 28mm, 177mm, and 328mm, respectively. At the MCE hazard level, roof displacements varied from 152 – 469mm.

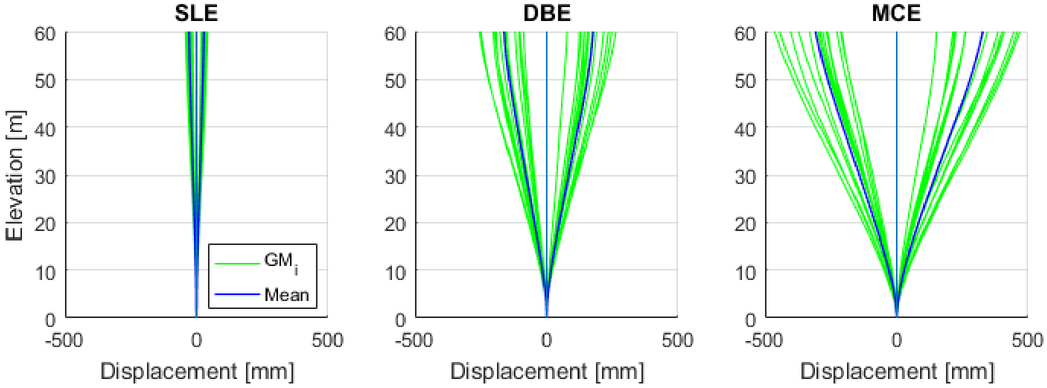

Figure 40: Peak and mean story displacements in Tower A for each hazard level

Figure 41 presents the peak interstory drift envelopes over the height of the building for each hazard level. The mean interstory drifts were maximum at 50-60% of the building height, which is consistent with the first mode shape of the structure. These maxima were 0.064%, 0.42%, and 0.75% at each hazard level, respectively.

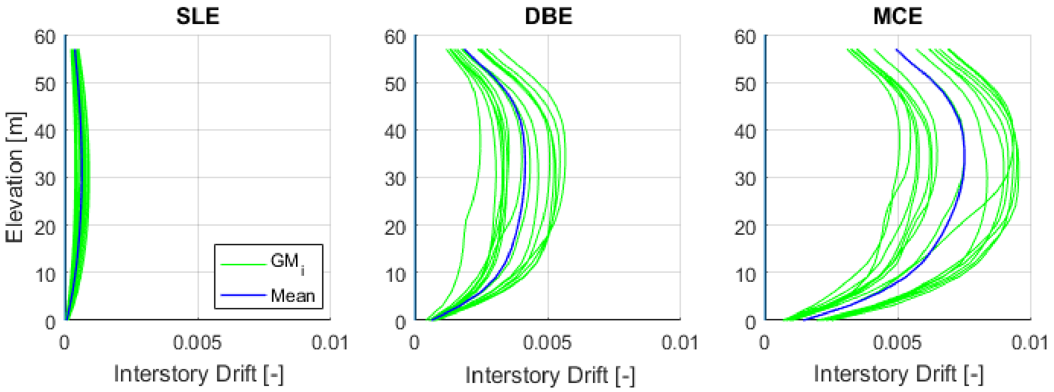

Figure 41: Peak and mean interstory drifts in Tower A for each hazard level

Figure 42 presents the moment curvature response of the shear wall for GM01 and GM15 scaled to each hazard level. At the SLE hazard level, the walls remain elastic. At the DBE, some nonlinear behavior is observed but hysteresis loops are generally small, which is characteristic of heavily axially-loaded shear walls. At the MCE hazard level, larger hysteretic loops were observed in most ground motions.

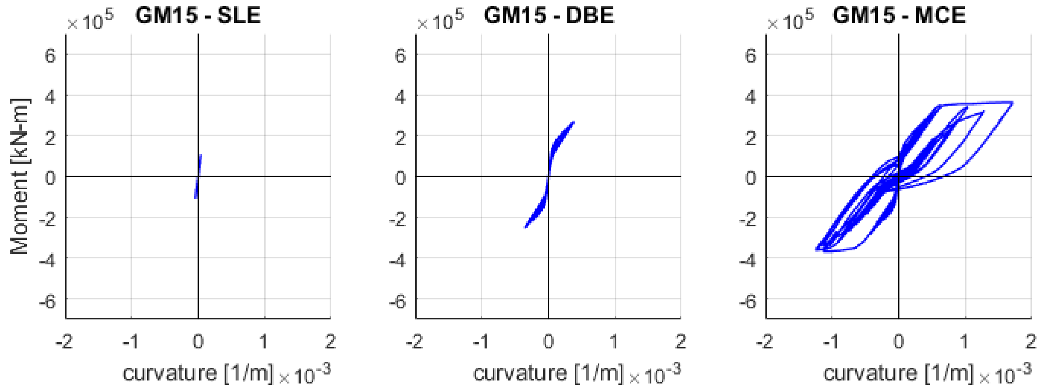

Figure 42: Sample moment-curvature plot at base of Tower A wall

Figure 43 presents the moment-curvature response of the wall immediately below the outrigger for the same two ground motions. At the SLE hazard level, the wall at this location also remains elastic. At the DBE and MCE hazards, nonlinear behavior is observed. Despite the reinforcing at these two locations being quite similar, the behavior of the wall here is noticeably different from the base due to the drastically different axial load (approximately a factor of 10). For the base wall, the unloading path tends to follow the loading path when demands are not too large. The wall at the roof, however, does not exhibit this behavior. The unloading path tends to be linear through the origin.

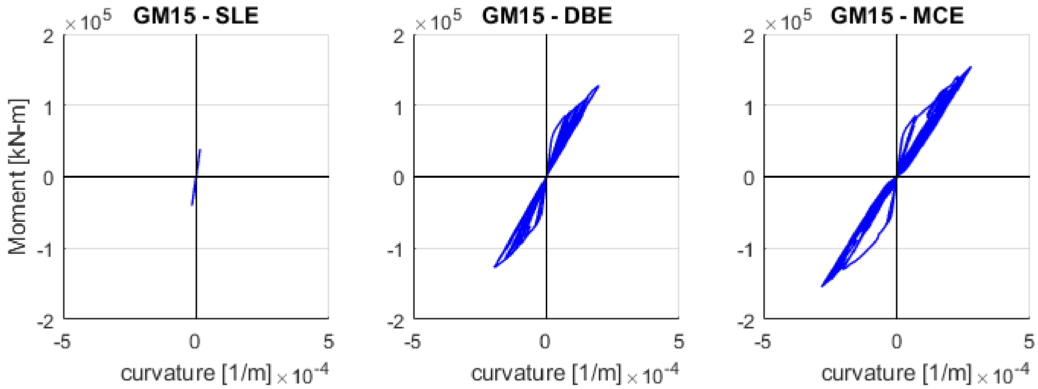

Figure 43: Sample moment-curvature plot of Tower A wall at outrigger

The force-deformation response of the outrigger fuses for GM01 and GM02 scaled to each hazard level are presented in Figure 44. At the SLE hazard level, the fuses did not reach their yield force. For all but two ground motions, the fuses did yield at the DBE hazard level. All MCE-level ground motion caused fuse yielding and significant hysteretic energy dissipation.

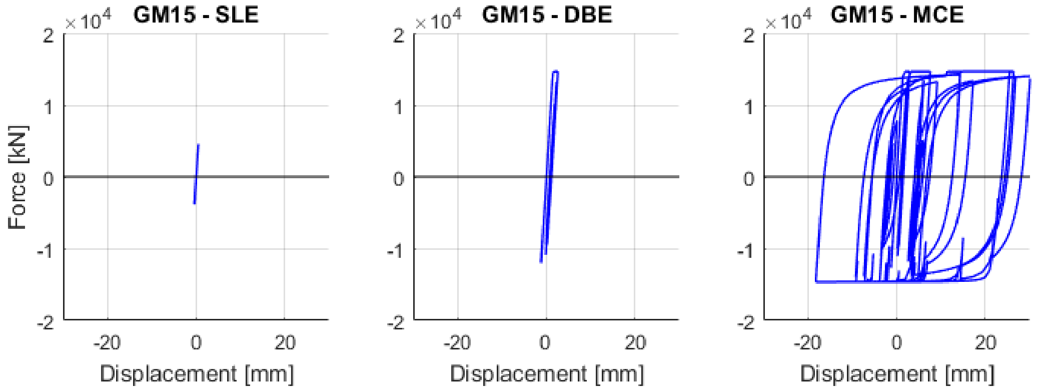

Figure 44: Sample force-deformation response of outrigger fuses in Tower A

Comparison of these results to the intended performance objectives is presented in Section 4.6

4.5.2 Results for Tower B

This section presents the results of nonlinear analysis on a 30-story building designed using EEDP. Figure 45 presents the peak wall moments along the height of the wall for each of the three hazard levels. The moment envelope generally peaks at the base of the wall and decreases to a minimum at around 50-60% of the height. Moments then increase further up the wall due to the outrigger, which was located at the roof level. The mean peak wall moments at the SLE, DBE, and MCE hazard levels were 205 MN-m, 536 MN-m, and 709 MN-m respectively. There was generally a larger dispersion of moments from record-to-record as the hazard level increased. This was not due to record variability, as the ratio between scale factors at each hazard level was unchanged. Instead, the increased variability comes from the model behavior.

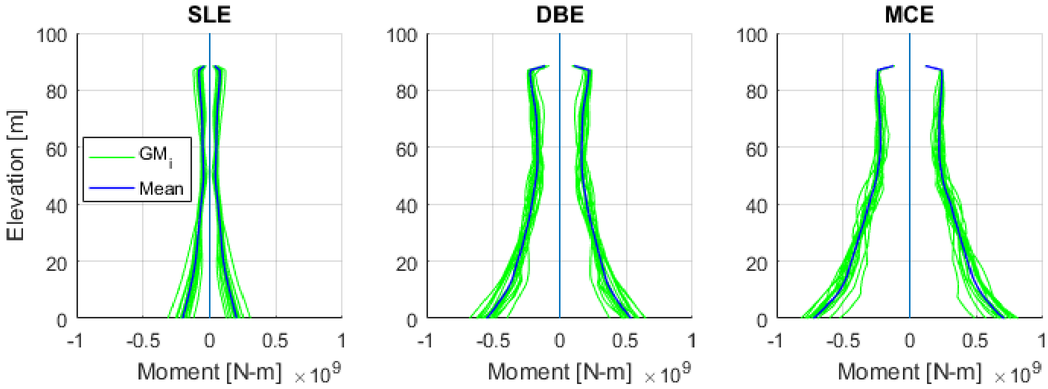

Figure 45: Peak moment vs height in Tower B wall for all GMs and hazards

Figure 46 presents the peak wall shears along the height of the wall for each of the three hazard levels. The shear envelope is generally largest at the base and decreases around 40-50% of the height. Higher mode effects then cause shears to increase further up the building. The peak mean base shears at the SLE, DBE, and MCE hazards were 6260 kN, 20860 kN, and 31430 kN respectively.

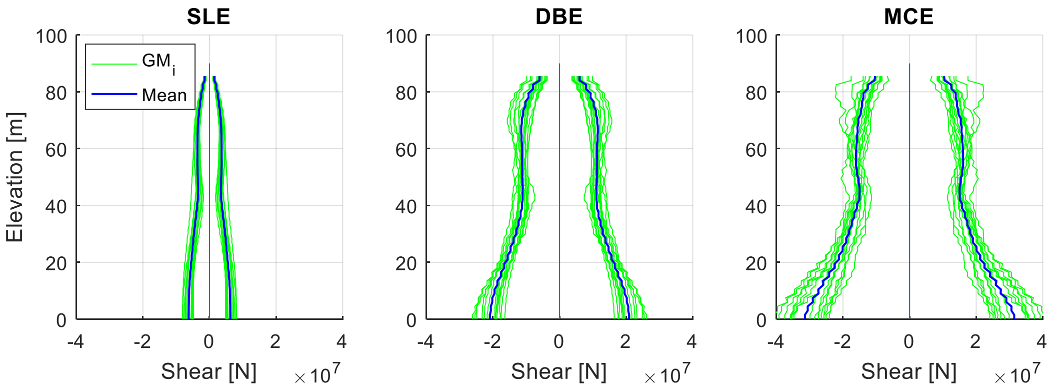

Figure 46: Peak shear force vs height in Tower B wall for all GMs and hazards

Figure 47 presents the peak displacement envelopes over the height of the building for the three hazard levels. The mean roof displacement at each hazard level was approximately 41mm, 213mm, and 431mm, respectively. At the MCE hazard level, record-to-record roof displacements varied from 172 – 632mm.

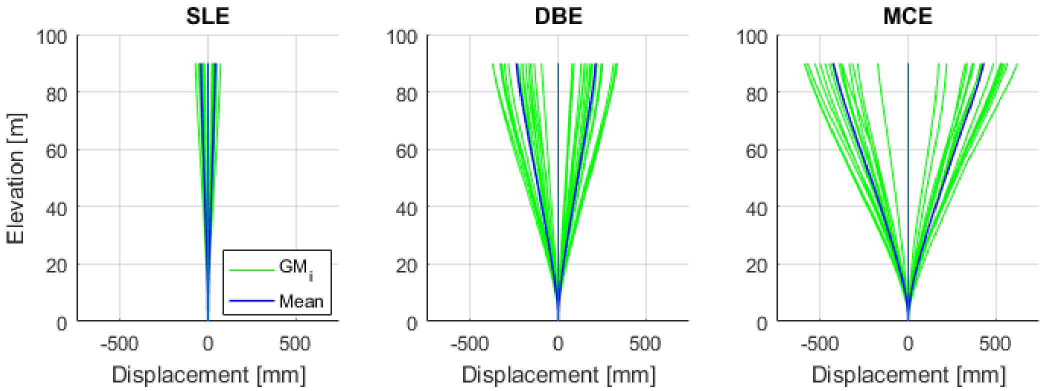

Figure 47: Peak floor displacements in Tower B for each hazard level

Figure 48 presents the peak interstory drift envelopes over the height of the building for each hazard level. The mean interstory drifts were maximum at approximately 60 - 70% of the building height, which is consistent with the first mode shape of the structure. These maxima were 0.064%, 0.35%, and 0.70% at each hazard level, respectively.

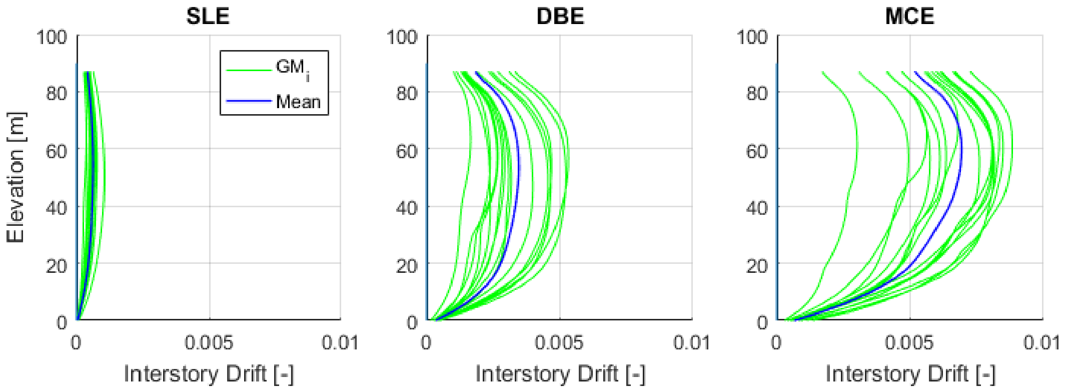

Figure 48: Peak interstory drifts in Tower B for each hazard level

Figure 49 presents a sample moment curvature response of the shear wall for GM15 at each hazard level. At the SLE hazard level, the walls remain elastic. At the DBE, demands exceed the cracking moment and some nonlinear behavior is observed but hysteresis loops are generally small, which is characteristic of heavily axially-loaded shear walls. At the MCE hazard level, larger hysteretic loops were observed in some but not all ground motions.

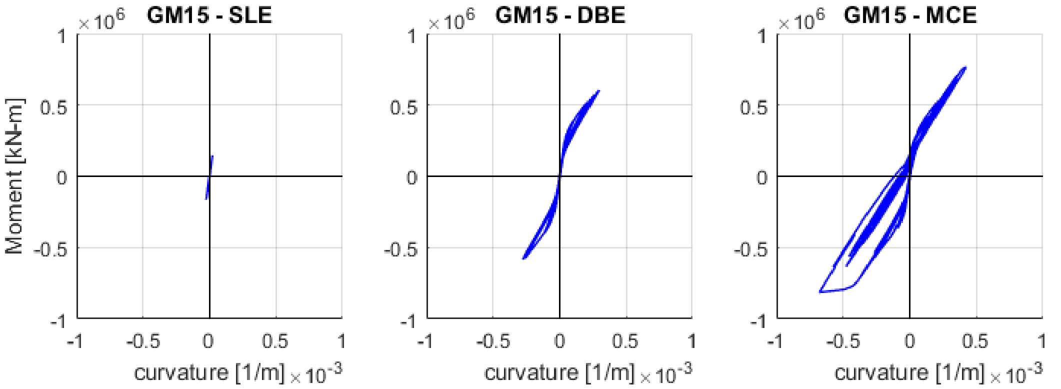

Figure 49: Sample moment-curvature plot at base of Tower B wall

Figure 50 presents a sample moment-curvature response of the wall immediately below the outrigger for the same ground motions. At the SLE hazard level, the wall at this location also remains elastic. At the DBE and MCE hazards, nonlinear behavior is observed. Despite the reinforcing at these two locations being quite similar, the behavior of the wall here is noticeably different from the base due to the drastically different axial load (approximately a factor of 20). For the base wall, the unloading path tends to follow the loading path when demands are not too large. The wall at the roof, however, does not exhibit this behavior. The unloading path tends to be linear through the origin.

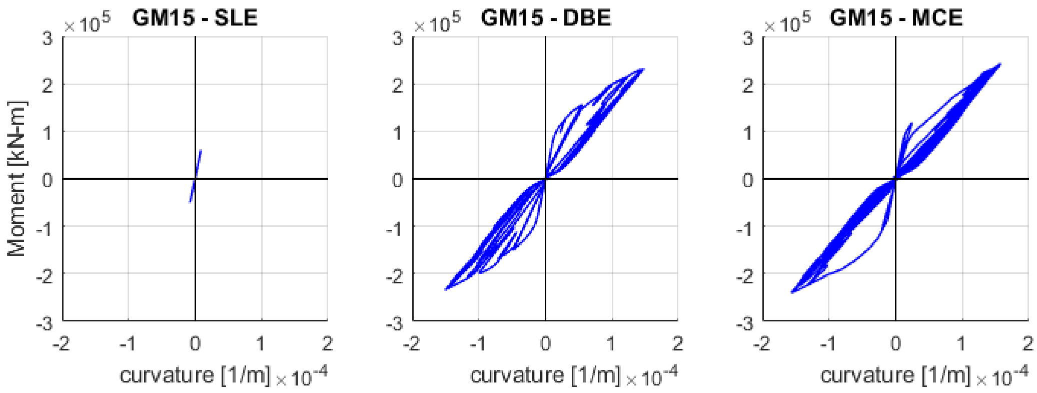

Figure 50: Sample moment-curvature plot of Tower B wall at outrigger

A sample force-deformation response of the outrigger fuses at each hazard level are presented in Figure 51. At the SLE hazard level, the fuses did not reach their yield force. For all but two ground motions, the fuses did yield at the DBE hazard level. All MCE-level ground motion caused fuse yielding and significant hysteretic energy dissipation.

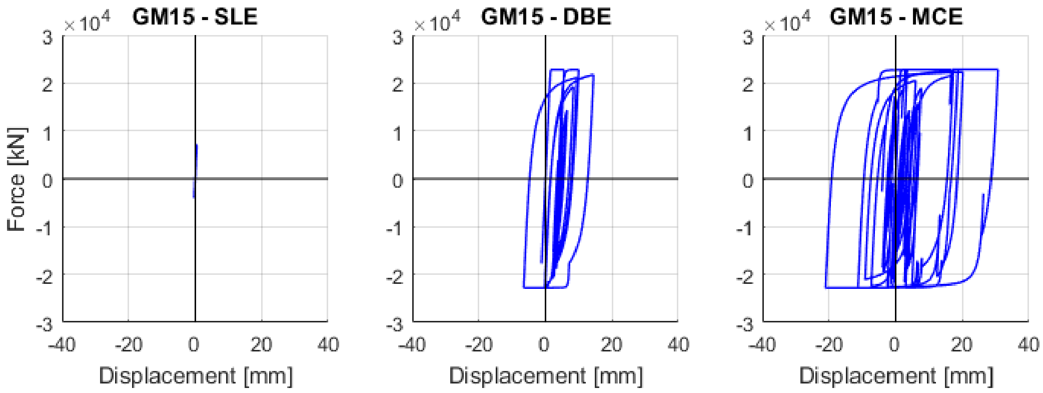

Figure 51: Sample force-deformation response of outrigger fuses in Tower B

Comparison of these results to the intended performance objectives is presented in Section 4.6.

4.5.3 Results for Tower C

This section presents the results of nonlinear analysis on a 40-story building designed using EEDP. Figure 52 presents the peak wall moments along the height of the wall for each of the three hazard levels. The moment envelope generally peaks at the base of the wall and decreases to a minimum at around 50-60% of the height. Moments then increase further up the wall due to the outrigger, which was located at the roof level. The mean peak wall moments at the SLE, DBE, and MCE hazard levels were 315 MN-m, 691 MN-m, and 802 MN-m respectively. There was generally a larger dispersion of moments from record-to-record as the hazard level increased. This was not due to record variability, as the ratio between scale factors at each hazard level was unchanged. Instead, the increased variability comes from the model behavior.

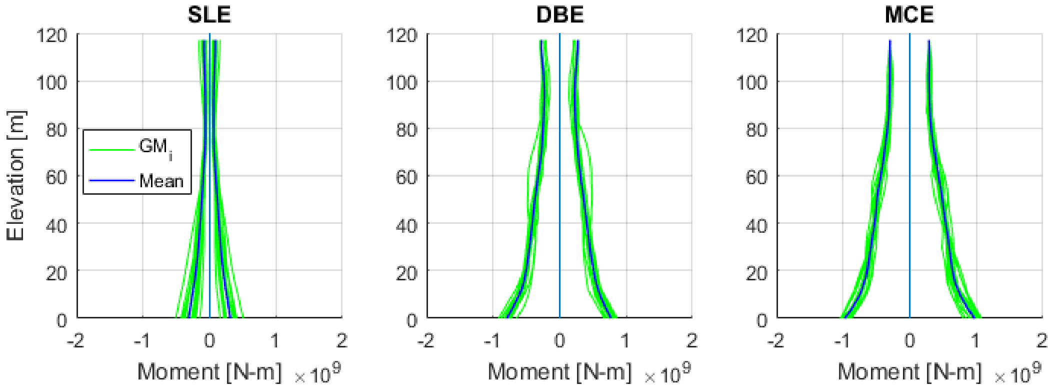

Figure 52: Peak moment vs height in wall of Tower C for all GMs and hazards

Figure 53 presents the peak wall shears along the height of the wall for each of the three hazard levels. The shear envelope is generally largest at the base and decreases around 40-50% of the height. Higher mode effects then cause shears to increase further up the building. The peak mean base shears at the SLE, DBE, and MCE hazards were 6260 kN, 20860 kN, and 31430 kN respectively.

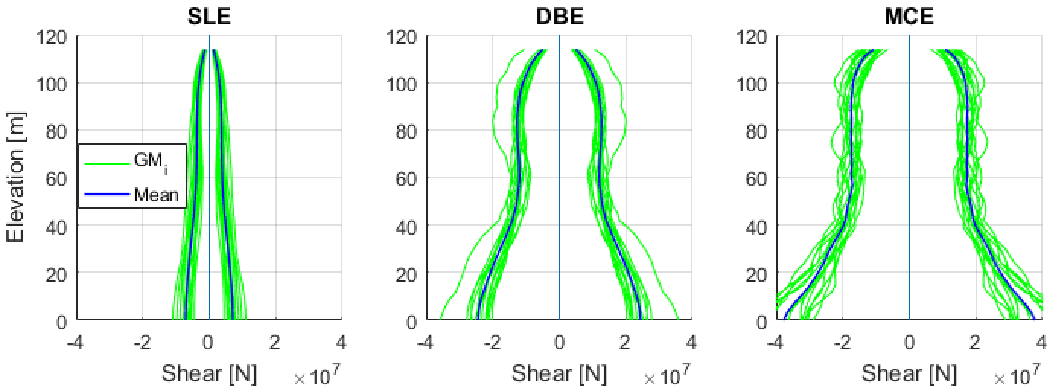

Figure 53: Peak shear force vs height in Tower C wall for all GMs and hazards

Figure 54 presents the peak displacement envelopes over the height of the building for the three hazard levels. The mean roof displacement at each hazard level was approximately 60mm, 267mm, and 544mm, respectively. At the MCE hazard level, roof displacements varied from 248 – 826mm.

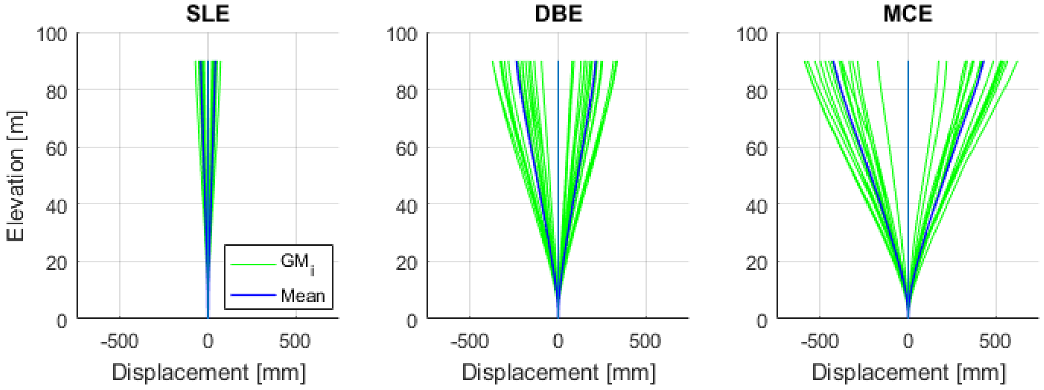

Figure 54: Peak floor displacements in Tower C for each hazard level

Figure 55 presents the peak interstory drift envelopes over the height of the building for each hazard level. The mean interstory drifts were maximum at 50-60% of the building height, which is consistent with the first mode shape of the structure. These maxima were 0.069%, 0.32%, and 0.61% at each hazard level, respectively.

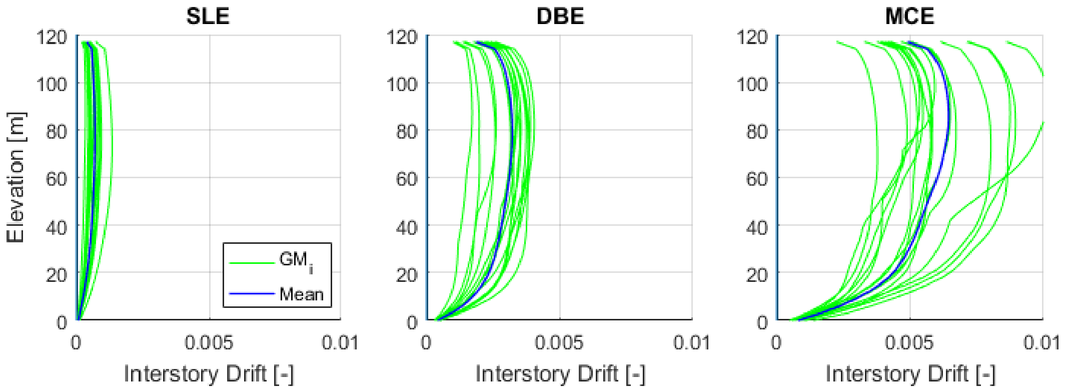

Figure 55: Peak interstory drifts in Tower C for each hazard level

Figure 56 presents a sample moment curvature response of the shear wall for GM15 scaled to each hazard level. At the SLE hazard level, the walls remain elastic. At the DBE, demands exceed the cracking moment and some nonlinear behavior is observed but hysteresis loops are generally small, which is characteristic of heavily axially-loaded shear walls. At the MCE hazard level, larger hysteretic loops were observed in some - but not all - ground motions.

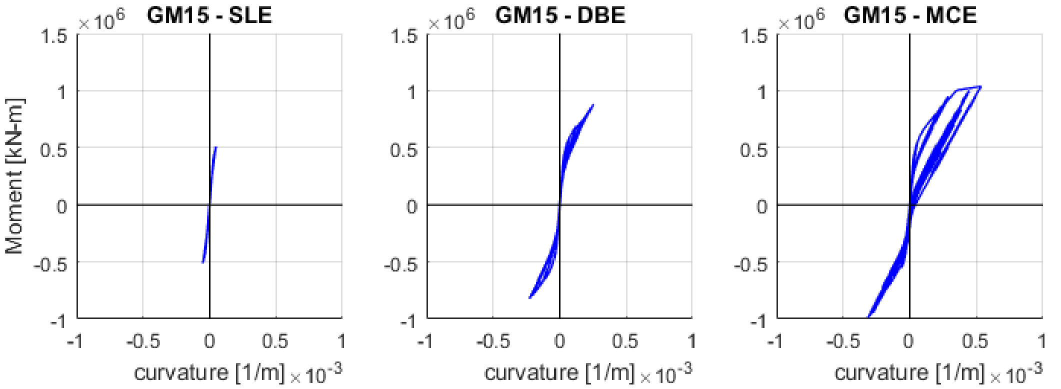

Figure 56: Sample moment-curvature plot at base of Tower C wall

Figure 57 presents the moment-curvature response of the wall immediately below the outrigger for the same ground motion. At the SLE hazard level, the wall at this location also remains elastic. At the DBE and MCE hazards, nonlinear behavior is observed. Despite the reinforcing at these two locations being quite similar, the behavior of the wall here is noticeably different from the base due to the drastically different axial load (approximately a factor of 40). For the base wall, the unloading path tends to follow the loading path when demands are not too large. The wall at the roof, however, does not exhibit this behavior. The unloading path tends to be linear through the origin.

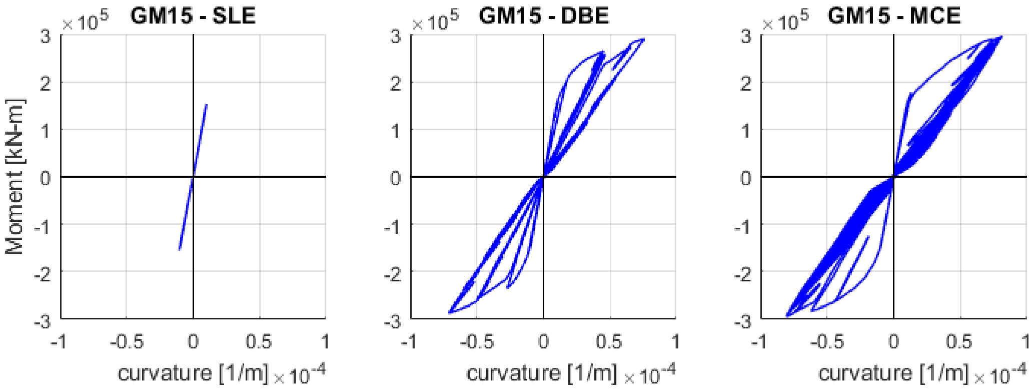

Figure 57: Sample moment-curvature plot at outrigger for Tower C wall

A sample force-deformation response of the outrigger fuses for GM15 scaled to each hazard level are presented in Figure 58. At the SLE hazard level, the fuses did not reach their yield force. For all but two ground motions, the fuses did yield at the DBE hazard level, but the ductility demands were generally small. All MCE-level ground motion caused fuse yielding and significant hysteretic energy dissipation.

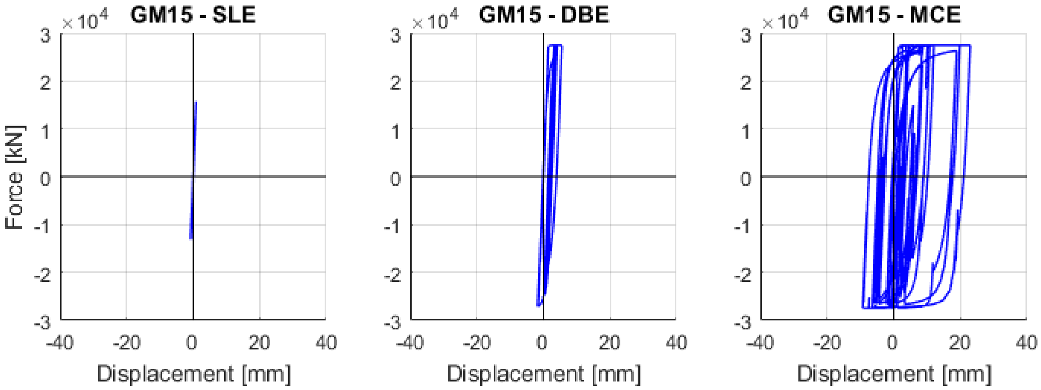

Figure 58: Sample force-deformation response of outrigger fuses in Tower C

Comparison of these results to the intended performance objectives is presented in Section 4.6.

4.6 Comparison to Performance Objectives

In designing the prototype buildings with EEDP, certain assumptions and objectives were made to calculate a rational set of demands for the system. This section analyzes these design assumptions with respect to the NLTHA results gathered in Section 4.5. Results for roof displacements, wall moments, and fuse forces are presented as boxplots. The red band within the box represents the median result. The blue box represents the interquartile range, which is where 50% of the data points nearest to the median reside. The whiskers on either side of the interquartile range show the range of all ground motions not considered outliers, while the plus (+) symbol shows outlier data points.

Target roof displacements corresponding to the different hazard levels (Δ_y, Δ_p, Δ_u) were set during the design process. Figure 59 shows the roof displacement for each building and hazard level normalized to the corresponding EEDP target displacement. The median response of all buildings was reasonably on-target at the SLE hazard level. At the DBE hazard level, Tower A and C experienced approximately 125% of the predicted displacement, while Tower B was on-target. Finally, at the MCE hazard level, displacements were about 130% of the target for Tower A, but reasonably on-target for Towers B and C.

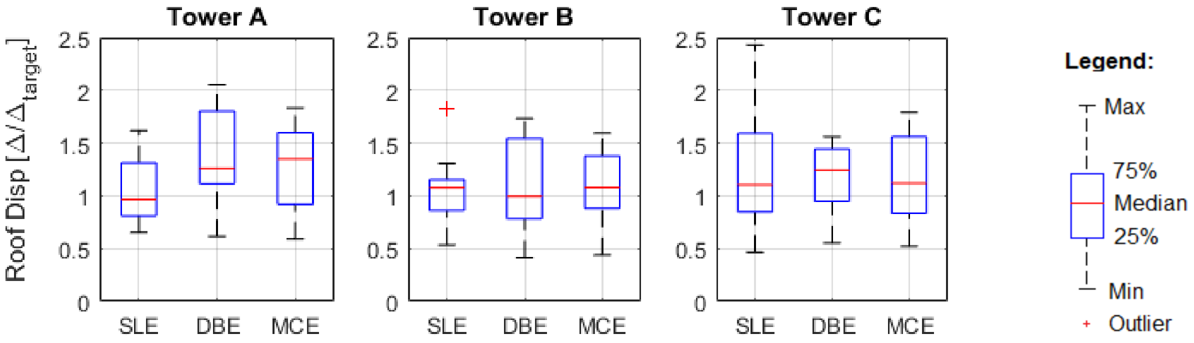

Figure 59: Roof displacements normalized to EEDP targets for each tower and hazard level

Fuse forces at the SLE hazard were generally lower than the design prediction for all three buildings. Figure 60 shows that the mean normalized force varied from 35-40% of the yield force for which the fuse was designed. The flexibility of the system was not accounted for in the simplified design procedure, to facilitate calculations. Accounting for the relative stiffness of the outrigger and wall would likely bring the mean fuse forces closer to yield at the SLE hazard level. At the DBE hazard, most records caused fuse yielding; only two out of fifteen records did not cause yielding in any of the prototype buildings. As expected, all buildings had their outrigger fuses yield at all the MCE-level ground motions.

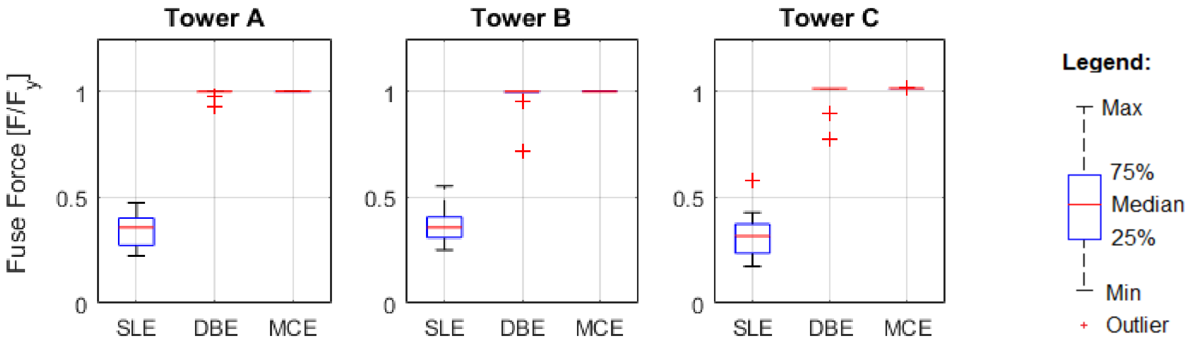

Figure 60: Outrigger fuse force for each tower and hazard

Peak moment at base of wall was determined with simple statics during the design process. The wall was designed to remain essentially-elastic below the DBE hazard level. As shown in Figure 61, the wall DCR was around 50% at the SLE hazard level for all towers, between 100-120% at the DBE hazard level, and around 140-150% at the MCE hazard level. The flexural demand in NLTHA can exceed the design moment because of several factors, including (a) imperfect design, where the wall detailing ends up with slightly more reinforcing steel than strictly required; (b) going from factored capacity for design to probable strength for analysis, (c) strain hardening, which allows the reinforcing steel to resist forces beyond the probable strength. Accounting for the material factor and probable strength of steel results in an apparent increase of 1.17/0.85=1.38 over the factored capacity.

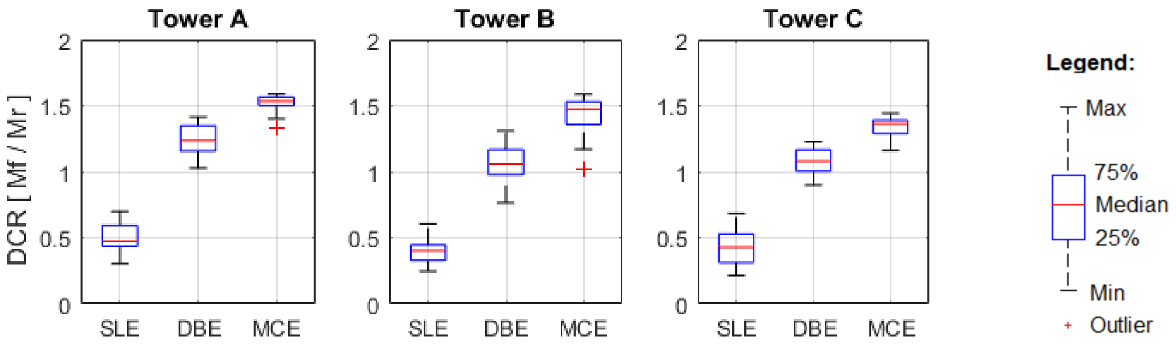

Figure 61: Maximum wall base moment normalized to the design moment for each tower and hazard level

The other critical wall section for flexural design occurs at the outrigger location. In the design procedure, this section was capacity designed to the probable strength of the outrigger system, which was assumed to be 1.3 times the design strength for the purposes of this research. The DBE and MCE flexural demands for all towers did not reach the design strength of the wall at the outrigger location. The fuse effectively limited the force delivery to the wall as intended. Theoretically, the demands should have been closer to 1/1.3 = 77%. However, the simplified static analysis used in design overestimated the outrigger participation.

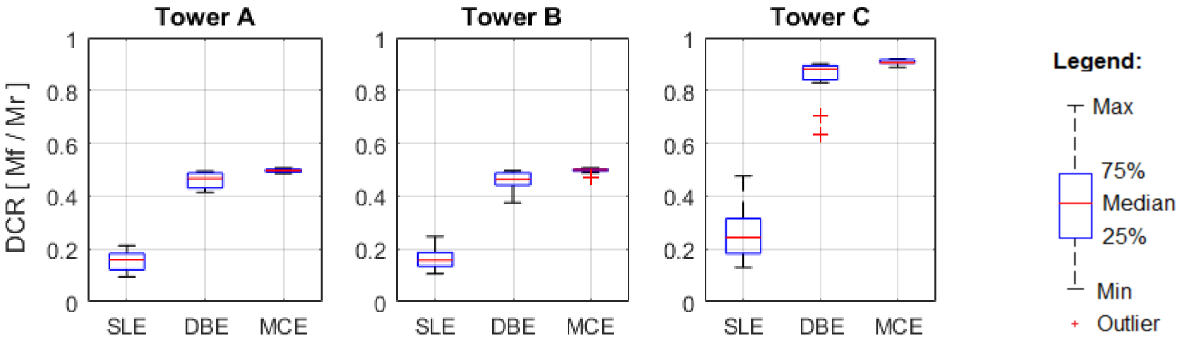

Figure 62: Maximum wall moment at outrigger normalized to the design moment for each tower and hazard level

Through the capacity design procedure, the ductility demands in the wall above the plastic hinge region should be small. This was checked by looking at the tension and compression strains at the extreme fibers of the wall cross section. Figure 63 shows the wall strains over the height of the wall normalized to the yield strain ($\varepsilon_y = 0.002$) in tension and normalized to the concrete crushing strain ($\varepsilon_{cu} = -0.0035$) in compression. Positive values indicate tensile strain.

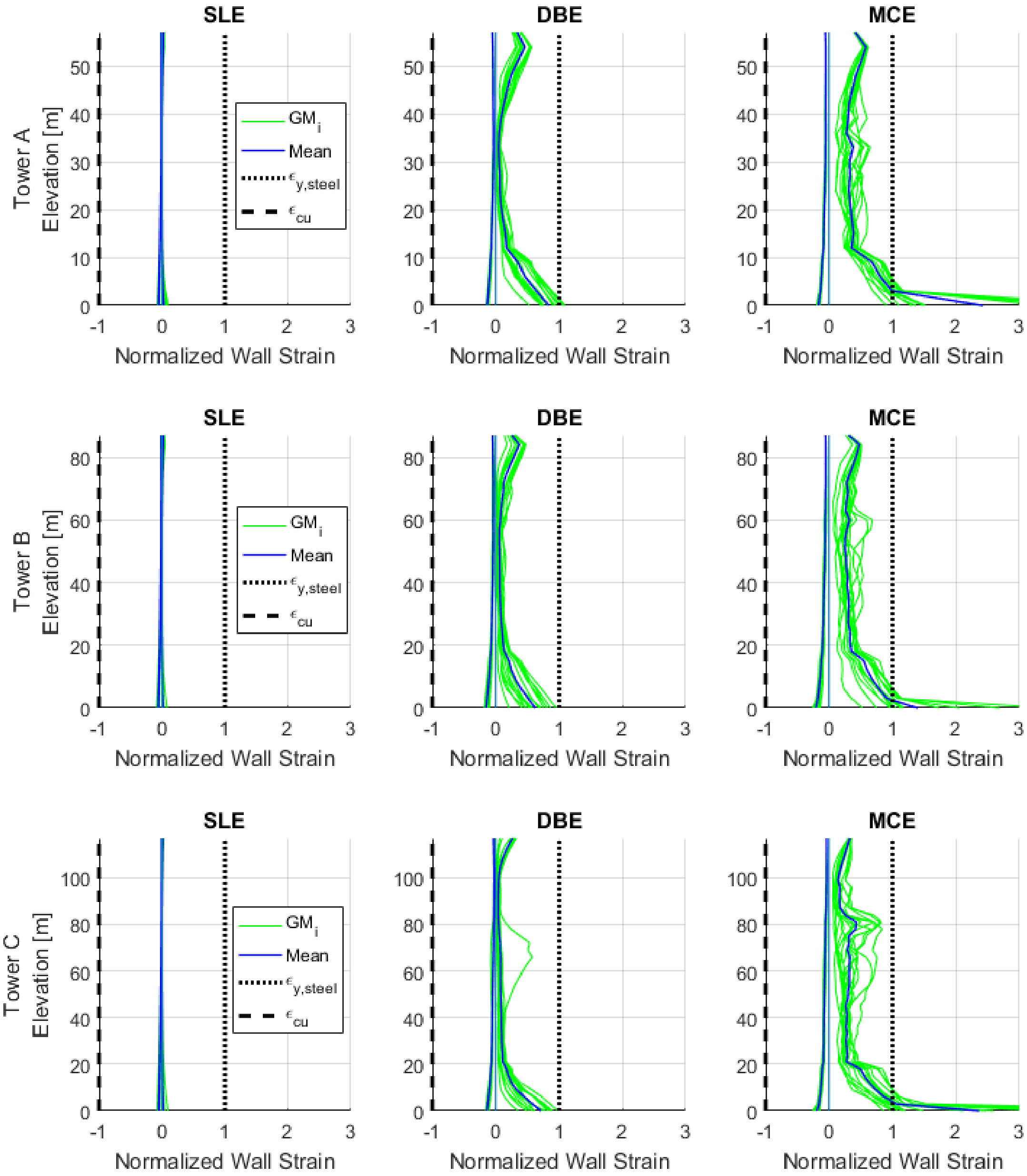

Figure 63: Normalized wall strains over the height of each tower for each hazard level

The results show that the compression strains were well below the concrete crushing strain at all hazard levels. The flanged walls in the prototype buildings provide a large compression block area which helps keep these strains low. At their largest, compression strains were on the order of 0.25 ε_{cu} at the MCE hazard. Likewise, mean tensile strains were below the yield strain for the SLE and DBE hazard levels, indicating that the walls would not experience significant yielding at these hazards. Small flexural cracks might be visible, as the cracking moment was exceeded in many GMs, however the large axial load on these walls would cause the cracks to close at the end of the earthquake. At the MCE hazard, yielding is observed at the base of wall. Tensile strain demands are reasonably low and within acceptable limits. No yielding is detected at the outrigger, as the capacity design procedure limited the amount of moment that the outrigger could deliver to the wall.

Chapter 5

Verification of Design Procedure for Outrigger Systems

In this chapter, 2-dimensional nonlinear models used to verify the designs meet a minimum level of safety. FEMA P695 is a procedure developed to determine the margin of safety against collapse of structural systems. The full FEMA P695 procedure is an extensive undertaking and requires many different archetype systems, because the objective is to qualify a building system to be included in building codes. Such an extensive study is outside of the scope of this thesis. Instead, the P695 theory is applied to three prototype buildings, and used to show that the design methodology works for these systems. Section 5.1 presents an overview of the P695 methodology. Section 5.2 presents the results of the methodology applied to the two prototype buildings.

5.1 Overview of FEMA P695 Methodology

FEMA P695 was developed by the Applied Technology Council (ATC) under contract from the Federal Emergency Management Agency (FEMA). The objective of this document is to provide a rational procedure to quantify the seismic performance of structures, and to assess whether the seismic design parameters (response modification factor, R; system overstrength factor, Ω; deflection amplification factor, C_d) are sufficient to ensure a low probability of collapse under MCE ground motions. The relation between the seismic design parameters, hazard curves, and collapse margin ratio are illustrated in Figure 64. These seismic design parameters are used for conventional design procedure in US building codes. However, the methodology can also be used to assess the collapse safety of structures designed using other methods, with some small modifications.

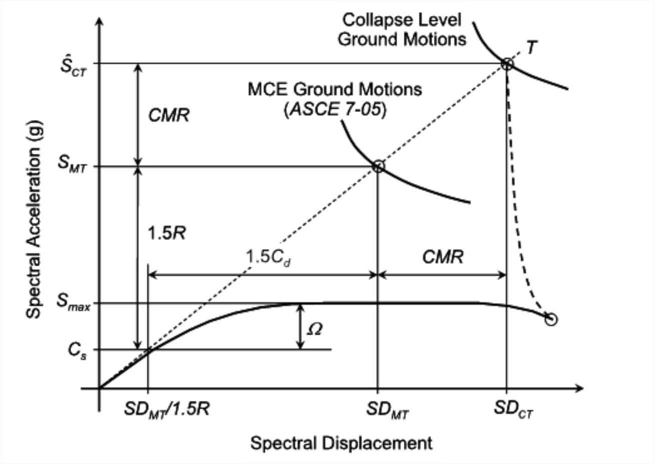
Collapse Level
Ground Motions
T
$\hat{S}_{CT}$
CMR
MCE Ground Motions
(ASCE 7-05)
S_{MT}
1.5R
$1.5C_d$
CMR
Spectral Acceleration (g)
S_{max}
Ω
C_s
$SD_{MT}/1.5R$
SD_{MT}
SD_{CT}
Spectral Displacement

Figure 64: FEMA P695 definition of seismic performance factors (2009)

The methodology is divided into several steps (ATC, 2009):

a) **Develop system concept**: The proposed SFRS is thoroughly defined, including materials, mechanisms of energy dissipation, applicable range and limits of application

b) **Design provisions**: The rules used to design the system are explicitly stated along with theoretical or experimental evidence. This includes provisions from any applicable building and material codes, experimental test data on materials and components.

c) **Characterize Behavior:** The intended and unintended collapse mechanisms are identified, and the range of structural configurations of the SFRS are captured using archetype structures. Archetypes are intended to cover all possible or allowable configurations of the SFRS which may alter the seismic performance.

d) **Develop Models:** Nonlinear models of the archetypes from step c) are developed to capture all or as many as possible of the expected collapse mechanisms and failure modes. The models only include the components that make up the SFRS. Any non-simulated collapse modes must be checked in the assessment stage.

e) **Analyze Models:** The models are subjected to incremental dynamic analysis (IDA) from a suite of preselected ground motions. FEMA P695 specifies two suites of ground motions: Near-Field Record

Set and Far-Field Record Set. Only the far-field set is required for most applications, and therefore the Near-Field Record set was not included in this study. The Far-field record set is summarized in Table 18.

Table 18: Ground motions from the FEMA P695 far-field record set (2009)

ID	PEER NGA Record Information				PGA (g)	PGV (cm/s)
	NGA No.	Lowest Freq. (Hz)	File Names			
			H1	H2		
1	953	0.25	NORTHR/MUL009	NORTHR/MUL279	0.52	63
2	960	0.13	NORTHR/LOS000	NORTHR/LOS270	0.48	45
3	1602	0.06	DUZCE/BOL000	DUZCE/BOL090	0.82	62
4	1787	0.04	HECTOR/HEC000	HECTOR/HEC090	0.34	42
5	169	0.06	IMPVALL/H-DLT262	IMPVALL/H-DLT352	0.35	33
6	174	0.25	IMPVALL/H-E11140	IMPVALL/H-E11230	0.38	42
7	1111	0.13	KOBE/NIS000	KOBE/NIS090	0.51	37
8	1116	0.13	KOBE/SHI000	KOBE/SHI090	0.24	38
9	1158	0.24	KOCAELI/DZC180	KOCAELI/DZC270	0.36	59
10	1148	0.09	KOCAELI/ARC000	KOCAELI/ARC090	0.22	40
11	900	0.07	LANDERS/YER270	LANDERS/YER360	0.24	52
12	848	0.13	LANDERS/CLW-LN	LANDERS/CLW-TR	0.42	42
13	752	0.13	LOMAP/CAP000	LOMAP/CAP090	0.53	35
14	767	0.13	LOMAP/G03000	LOMAP/G03090	0.56	45
15	1633	0.13	MANJIL/ABBAR--L	MANJIL/ABBAR--T	0.51	54
16	721	0.13	SUPERST/B-ICC000	SUPERST/B-ICC090	0.36	46
17	725	0.25	SUPERST/B-POE270	SUPERST/B-POE360	0.45	36
18	829	0.07	CAPEMEND/RIO270	CAPEMEND/RIO360	0.55	44
19	1244	0.05	CHICHI/CHY101-E	CHICHI/CHY101-N	0.44	115
20	1485	0.05	CHICHI/TCU045-E	CHICHI/TCU045-N	0.51	39
21	68	0.25	SFERN/PEL090	SFERN/PEL180	0.21	19
22	125	0.13	FRIULI/A-TMZ000	FRIULI/A-TMZ270	0.35	31

The ground motions were first anchored to the MCE spectral acceleration at the fundamental period of the structure, S_{MT}. This was done by scaling the suite of 44 motions so that the median spectral acceleration of the suite calculated at T_1, S_{NRT}, equals S_{MT}. Figure 65 shows the response spectra of the 44 ground motions scaled in this manner, along with the median and MCE design spectrum for the Tower C prototype. Unless the target and mean spectra have similar shapes, anchoring the mean spectra to a single period results in varying error at other periods. The spectra shape of the motions generally match the target spectrum for periods larger than 1.7 seconds. In the short period range, however, the spectra values are much higher than the target. The peak error, at about 0.4 seconds, is a difference of 0.62g or 70% over the target. Anchoring to lower periods for Tower A and B will reduce this peak error but introduce more error at other periods.

After anchoring the motions, the IDA procedure was carried out by applying increasingly larger scale factors to the suite of motions until collapse was detected. To fully develop the IDA curves, the factors for Tower A and B ranged from 0.5 to 6.0 in increments of 0.5. The factors for Tower C ranged from 0.2 to 3.0 in increments of 0.2. This was not strictly necessary for implementing the P695 methodology; a few points near the collapse intensity would have sufficed.

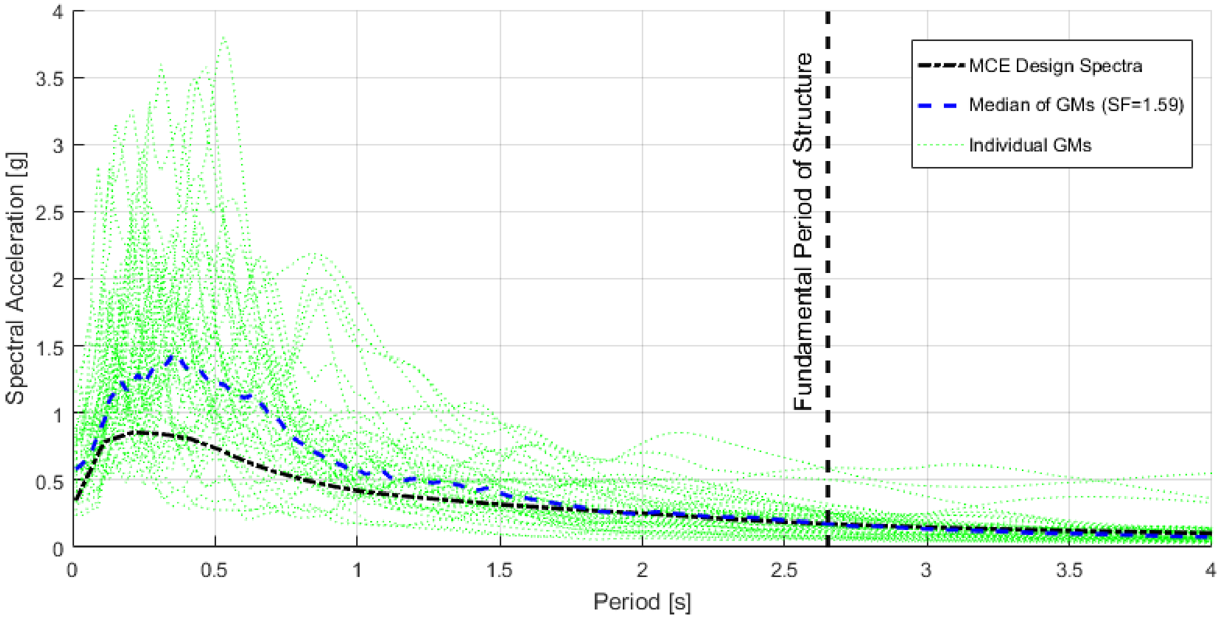

Figure 65: Individual P695 acceleration response spectra and median spectrum anchored to the MCE spectrum for Tower C

f) **Evaluate Performance:** FEMA P695 defines collapse as the intensity at which 50% of the ground motions cause collapse. In this context, collapse could be through side sway or any other limit state suitable for the structural system.

   a. The Collapse Margin Ratio (CMR) is defined as the ratio of the median spectral acceleration which causes collapse (S_{CT}) to the MCE spectral acceleration S_{MT} at the first-mode period of the structure.
   b. The CMR is adjusted to account for the spectral shape.
   c. The total system collapse uncertainty is estimated.
   d. The Adjusted CMR is compared to acceptable values, based on the total uncertainty.

g) **Document and Peer review:** Peer review of all aspects of the methodology is required for formal evaluation of new building systems. This step was not included in the present study.

5.2 Application to Prototype Outrigger Buildings

The concepts from FEMA P695 are implemented on the three prototype outrigger buildings designed in the previous section. To fully develop and characterize the structural system in accordance with P695, a much larger variety of archetype designs would be required. The three buildings are subjected to an incremental dynamic analysis using the P695 far-field ground motions. The performance of the buildings is evaluated by calculating the adjusted collapse margin ratio and comparing to acceptable values.

The possible failure modes of the system include: (1) sidesway collapse from global instability, (2) fracture of reinforcing steel, (3) crushing of concrete in the toe of the wall, (4) shear failure in the walls. The analysis model did not explicitly include items (2) through (4). These items were checked during the post-processing of results. If any of these non-simulated failure modes were detected, the drift for that ground motion intensity was set to 10%, as a proxy for collapse.

Wall strains were limited to the fracture strain of rebar in tension, and the concrete crushing strain in compression. The fracture strain for Grade 400W rebar was assumed to be 0.15. A large value was used because only the extreme fiber strain was used to check this failure mode. This mode of wall failure would require a large amount of the interior rebar to fracture as well, rather than simply the extreme fiber, and this interior reinforcing steel experiences lower strains than the extreme fiber. The maximum compressive strain for the 65MPa concrete in the walls was assumed to be 0.007. The design process assumes a concrete compressive strain of 0.0035 for flexural design calculations, however, with closely spaced ties in the zones, the maximum strain that can be sustained is generally higher than this value. CSA A23.3 limits the maximum confined strain in walls to 0.014, and so the limit of 0.007 is deemed a realistic value for well-detailed walls. Bar buckling was not considered, because of the buckling prevention ties required by code.

Wall shear was limited to the shear which would cause diagonal compression failure, using probable material strengths. A23.3 specifies this limiting shear, V_{rmax}, as:

$$V_{r,max} = 0.25\,\phi_c\, f_c\, b_w d_v \qquad [5.1]$$

where, for this collapse assessment, the material factor ϕ_c was taken as 1.0 and the effective concrete strength f_c was 1.3 times the specified strength (CSA, 2004).

Nonlinear Pushover Results

Nonlinear pushover analysis is necessary for quantifying the prototype-specific metric used to calculate the SSF, namely the period-based ductility, μ_T. In addition, the overstrength factor Ω can be evaluated for use in conventional design provisions. With respect to Figure 66, the overstrength factor is calculated as:

$$\Omega = \frac{V_{max}}{V} \qquad [5.2]$$

and the period-based ductility is:

$$\mu_T = \frac{\delta_u}{\delta_{y,eff}} \qquad [5.3]$$

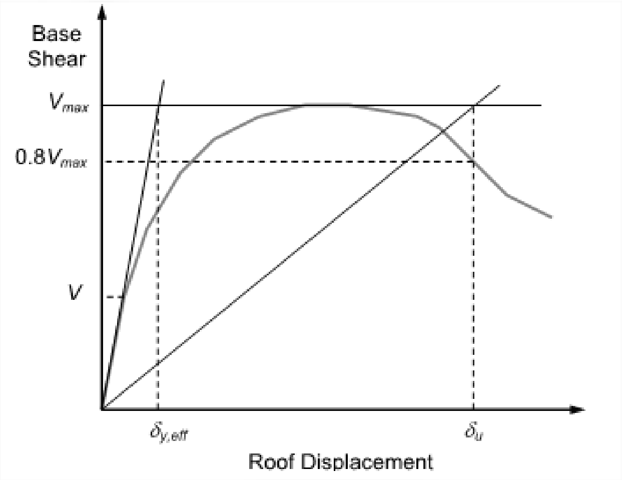

Figure 66: Generic pushover curve showing the various parameters needed from the pushover analysis (ATC, 2009)

The pushover analysis for each prototype was conducted by applying the same lateral load pattern that was used in the design stage until the system became unstable or significant degradation was observed. Figure 67 shows the pushover curves for each of the three prototype buildings. The pushover curves use the roof drift ratio as the x ordinate, which is equal to the roof displacement divided by the height of the building. The base shear normalized to the total seismic weight of the structure was used as the y ordinate. As the building height increased, the roof drift ratio and the base shear at which failure occurred generally decreased. Put another way, the taller buildings could withstand a smaller proportion of their total weight applied as a lateral load. Table 19 summarizes the results of the pushover analysis.

Table 19: Summary of key parameters from pushover analysis of each prototype building

Prototype	**V/W [-]**	**V_{max}/W [-]**	**δ_{yeff} [%]**	**δ_u [%]**	**Ω [-]**	**M [-]**
Tower A	0.0672	0.0847	0.154	4.553	**1.26**	**29.6**
Tower B	0.0570	0.0734	0.189	3.151	**1.29**	**16.7**
Tower C	0.0405	0.0521	0.141	1.465	**1.29**	**10.4**

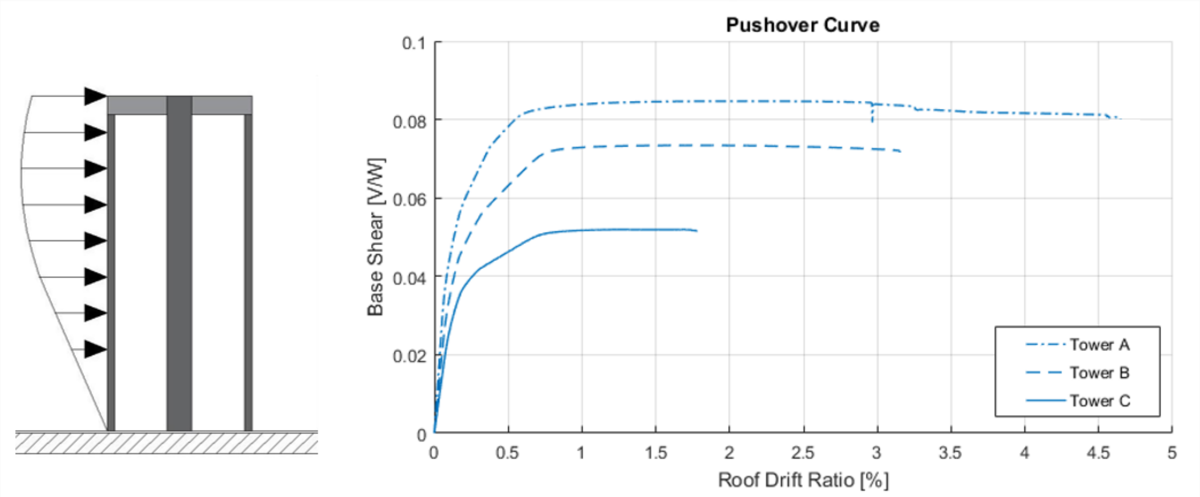

Figure 67: Pushover curves for the three prototype outrigger buildings

Incremental Dynamic Analysis Results

The IDA curves for Tower A subjected to all 44 of the far-field ground motions, along with the median response and MCE spectral acceleration are shown on Figure 68. The intensity measure was chosen to be the spectral acceleration of the ground motion at the fundamental period of the structure. Maximum interstory drift is used as the demand measure. The median collapse intensity and MCE intensity are 1.447g and 0.335g, respectively. This results in a CMR for Tower A of 4.32. The IDA curves for Tower B subjected to all 44 of the far-field ground motions, along with the median response and MCE spectral acceleration are shown on Figure 69. The median collapse intensity and MCE intensity are 0.885g and 0.254g, respectively. This results in a CMR for Tower B of 3.49. The IDA curves for Tower C subjected to all 44 of the far-field ground motions, along with the median response and MCE spectral acceleration are shown on Figure 70. The median collapse intensity and MCE intensity are 0.219g and 0.155g, respectively. This results in a CMR for Tower C of 1.41.

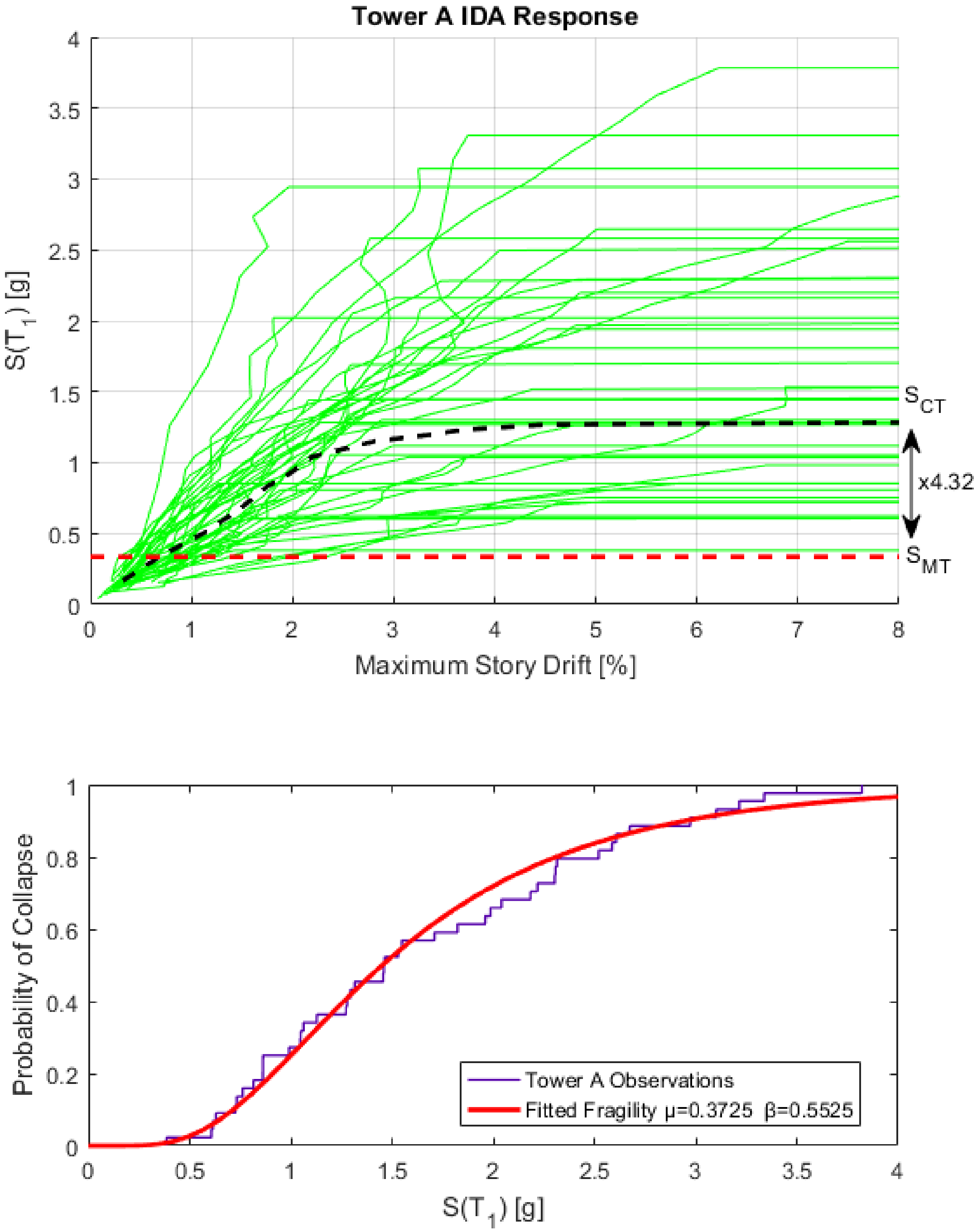

Figure 68: IDA response of Tower A

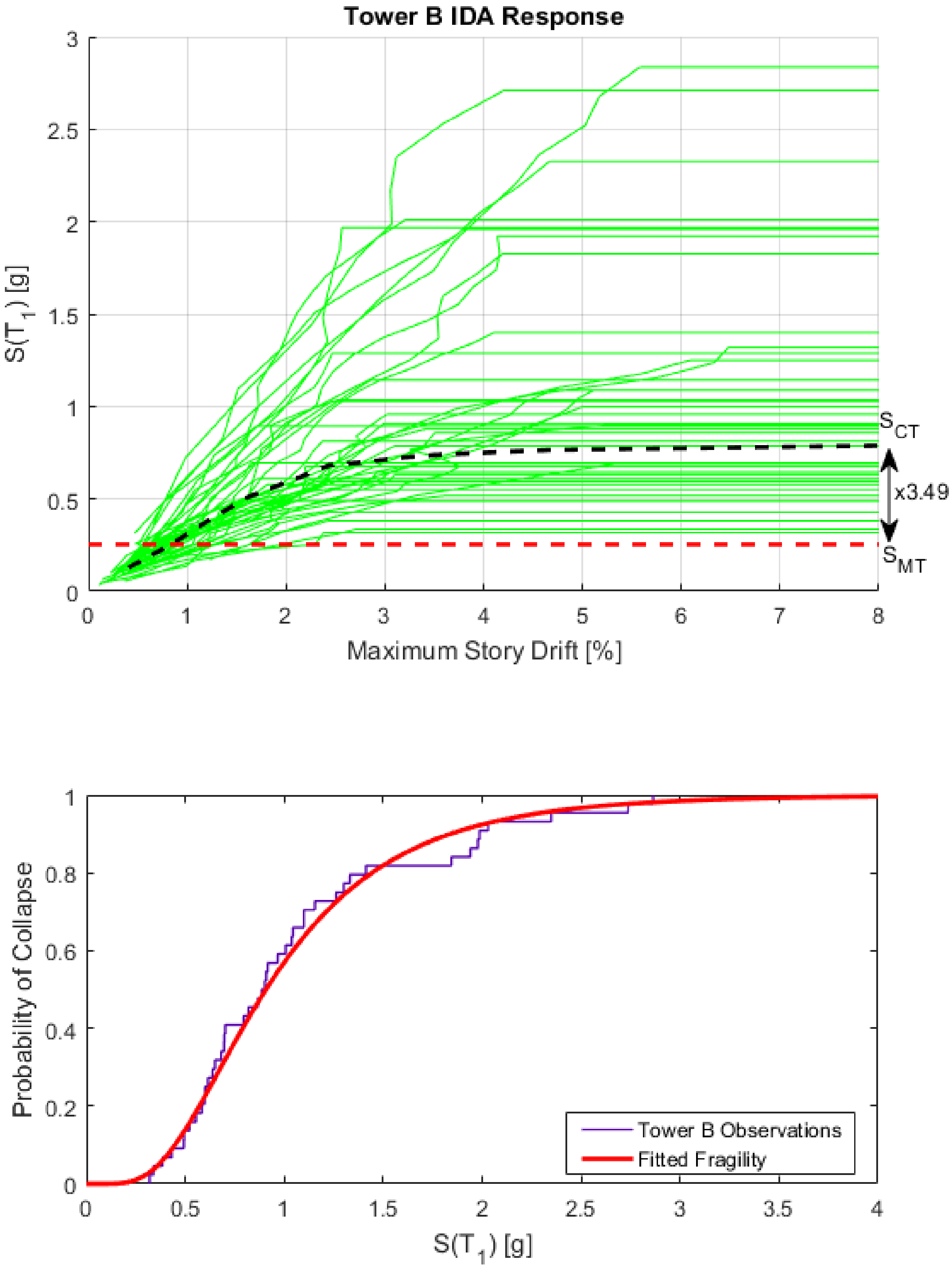

Figure 69: IDA response of Tower B

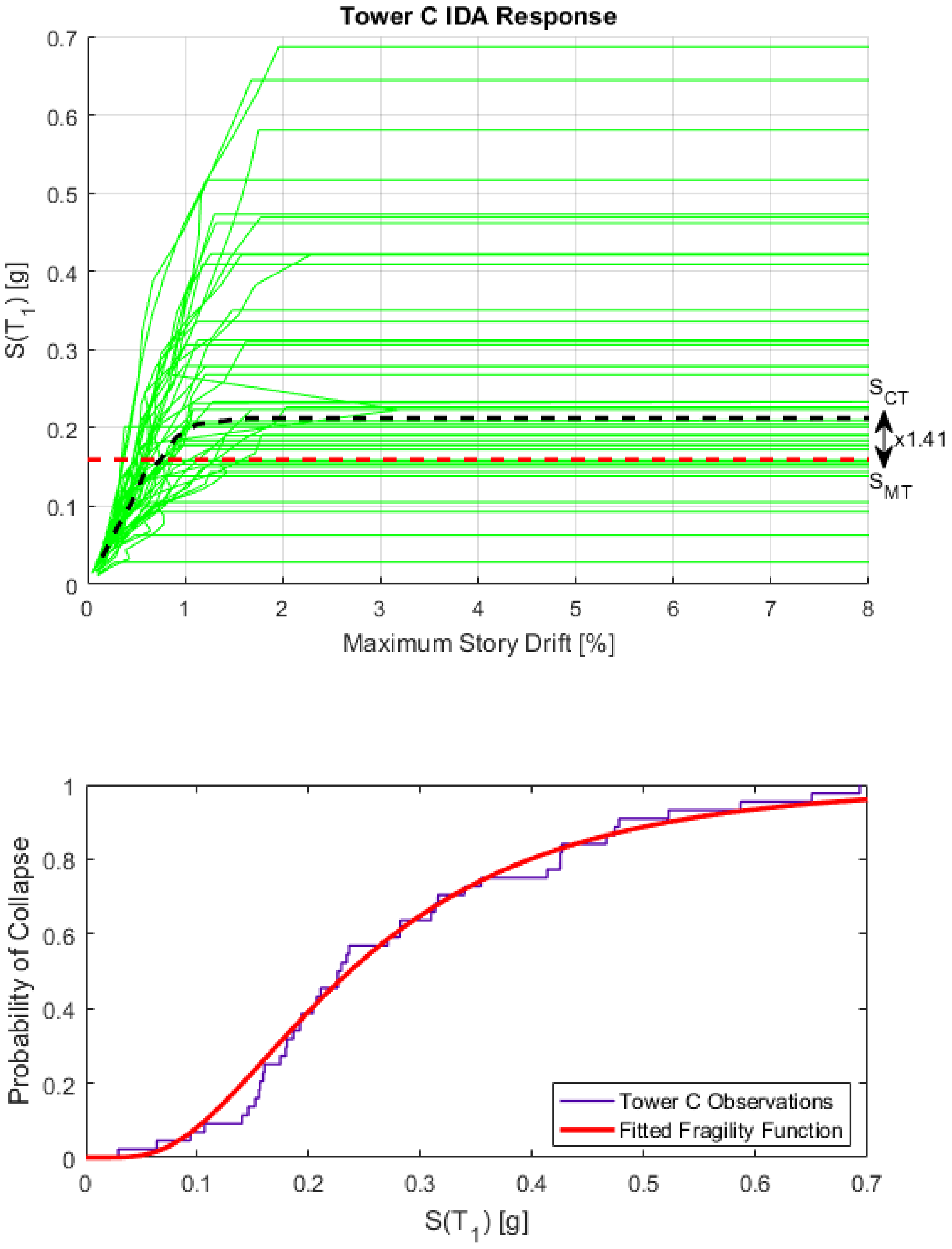

Figure 70: IDA response of Tower C

The Adjusted Collapse Margin Ratio (ACMR) is used to account for the effects of spectral shape of the P695 ground motions record set. The ACMR is calculated by multiplying the CMR by a Spectral Shape Factor (SSF) as shown in Equation 5.4. The SSF is a function of the seismic design category, first-mode period of the structure, and period-based ductility (FEMA, 2009):

$$ACMR = SSF \times CMR \qquad [5.4]$$

The fundamental period, period-based ductility, and resulting SSF for each prototype are shown in Table 20. FEMA P695 simplifies the determination of the SSF by using a lookup table, and for this study the SSFs ranged from 1.35-1.37.

The ACMR of each prototype must be larger than the Acceptable $\text{ACMR}_{10\%}$. For the purposes of determining the value of Acceptable $\text{ACMR}_{10\%}$, the total system collapse uncertainty must be estimated. Total collapse uncertainty is a function of the record-to-record uncertainty (β_{RTR}), quality of design requirements (β_{DR}), quality of test data (β_{TD}), and sophistication of modelling techniques (β_{MDL}) as shown in Equation 5.5.

$$\beta_{TOT} = \sqrt{\beta_{RTR}^2 + \beta_{DR}^2 + \beta_{TD}^2 + \beta_{MDL}^2} \qquad [5.5]$$

The record-to-record uncertainty accounts for the variation of structural responses from the different ground motions. For buildings with significant period elongation (and hence large ductility) the record-to-record variability has been shown to remain constant over a range of building types (FEMA, 2009). The period-based ductility was greater than 3 for all prototypes and therefore the record-to-record uncertainty can be assumed to be 0.4.

The uncertainty from design requirements accounts for how robust the requirements are for ensuring the desired system mechanism is achieved and undesired mechanisms are avoided. This source of uncertainty was assigned to the *(B) Good* category and β_{DR} is given a value of 0.2. Capacity design procedures were employed to prevent overloading of the outrigger columns, shear failure in the wall, and yielding outside of specially-detailed plastic hinge regions of the wall.

The uncertainty from test data accounts for the completeness of test data for the system. Seismic detailing of ductile walls is quite mature and well-researched. This source of uncertainty was assigned to the (A) Superior category and β_{MDL} is given a value of 0.1

Modelling uncertainty accounts for the sophistication of the modelling technique and how thoroughly the prototypes cover the design space. In this study, the main failure modes were either directly simulated or checked during the post-processing of nonlinear results. Therefore, this source of uncertainty was assigned to the (B) Good category and β_{MDL} is given a value of 0.2

Using Equation 5.5 for total uncertainty, the total system collapse uncertainty is determined to be 0.5. From Table 7-3 of P695, the Acceptable $ACMR_{10\%}$ for this level of uncertainty is 1.90 (2009). As summarized in Table 20, the three prototype buildings had ACMR values ranging from 5.83 for Tower A to 1.93 for Tower C. It is therefore shown that these three prototypes achieve acceptable collapse performance when designed using the EEDP design procedure.

Table 20: Comparison of ACMR to acceptable values for each prototype building

Prototype	**Period T_1 (sec)**	**Ductility μ_T**	**Median Collapse Intensity S_{CT} (g)**	**MCE Hazard S_{MT} (g)**	**CMR**	**SSF**	**ACMR**	**Acceptable ACMR10%**
Tower A	1.41	29.6	1.447	0.335	4.32	1.35	5.83	1.90
Tower B	2.00	16.7	0.885	0.254	3.49	1.37	4.78	1.90
Tower C	2.61	10.4	0.219	0.155	1.41	1.37	1.93	1.90

Chapter 6

Conclusion

In this thesis, the seismic design and performance of outrigger systems was investigated. There were four primary aspects to this work and they are summarized below:

Simplified models were derived to examine the static and dynamic behavior of outriggered-wall systems. The simplified models were used to develop relations between deflection, moment, shear, and period. These relations can be used by the designer in the preliminary stage to assess the effectiveness of using outriggers as part of the SFRS.

A design procedure was developed for outrigger systems. The procedure uses Equivalent Energy-based Design Procedure (EEDP) to explicitly account for multiple performance objectives at different seismic hazard levels. The result is a more resilient structure that goes beyond current building code requirements.

The design procedure was validated using advanced analysis techniques. Three prototype buildings were designed using the EEDP procedure. Advanced finite element models were created for each building to capture the linear and nonlinear response of the system under earthquake excitation. The analysis results showed that the design procedure generally results in a structure that meets the intended performance objectives.

The design procedure was shown to provide sufficient margin of safety against collapse. Incremental dynamic analysis using FEMA P695 methodology was employed to assess the collapse safety of the three prototype buildings under extreme earthquake loading. It was shown that the EEDP procedure resulted in designs which meet current code requirements for collapse safety, namely that the probability of collapse at the MCE earthquake hazard is less than 10%.

6.1 Conclusions and Significance

Outrigger systems are an effective structural scheme that is commonly used in high-rise construction to add lateral stiffness and distribute the moment demand within the core to the exterior columns. At the time of writing, very little research has been conducted on the seismic design and performance of outriggered wall systems. Additionally, current prescriptive building codes in Canada and the United States do not provide a straightforward design procedure that considers multiple performance objectives. This work shows that an alternative design method, called Equivalent Energy-based Design Procedure (EEDP), can be used to effectively design outriggered wall systems for multiple performance objectives at different hazard levels. Three buildings designed using EEDP were shown to behave as predicted at the three hazard levels considered. The designs also have sufficient margin of safety against collapse at the MCE hazard level to satisfy the intent of US and Canadian building codes. The outrigger system is therefore shown to be a safe choice of SFRS that can successfully be designed using EEDP.

6.2 Future Research

There are multiple issues that were identified during this course of study which require additional investigation but were outside of the scope of this thesis. Further research into these areas would help further develop the outriggered-wall system as an efficient choice of SFRS for tall buildings. These issues are briefly summarized here.

a) The development of outrigger systems would benefit from detailed investigation of different connections for the interface between outrigger and wall. There are a variety of connection designs that have been used on existing outrigger buildings. These include attaching to previously cast embed plates, using a continuous truss cast into the wall, and embedding truss members into the wall. The benefits and disadvantages of different connections should be investigated for their ease of construction, cost, effectiveness and performance under wind and earthquake loading.

b) The effects of overstrength and strain hardening in the capacity design procedure can be studied. In this thesis, an assumed outrigger overstrength of 1.3 was used to design the wall below the outrigger, but strain hardening was kept small in the BRB model. Different overstrength and strain hardening behaviors may affect the wall performance.

c) A complete implementation of FEMA P695 can be carried out to provide designers with conventional seismic design parameters (Rd and Ro in NBCC 2015). Outrigger systems may combine SFRS components that have different seismic design parameters (R_d R_o); for example, a ductile shear wall with steel outrigger truss and buckling restrained brace fuses. It is therefore unclear what is the appropriate parameters to use in the conventional design procedure. FEMA P695 could be used to propose parameters specifically for outriggered wall buildings.

d) A comparison of conventional and outrigger buildings based on capital and future costs, including downtime and probable repair costs in the event of an earthquake would be a useful study to assess whether outriggers are worth the cost and complexity.

e) Consideration of wind demands and wind performance objectives will complicate the EEDP design methodology, and therefore a study in which wind effects are included would be useful. As building height increases, the wind demands grow larger than the seismic demands, and govern the design. It is likely that these wind performance objectives will require a strong and stiff outrigger, resulting in larger seismic overstrength for the wall design.

Bibliography

Ali, M. M., & Moon, K. S. (2007). Structural Developments in Tall Buildings: Current Trends and Future Prospects. *Architectural Science Review*, *50*(3), 205–223. https://doi.org/10.3763/asre.2007.5027

ASCE/SEI. (2014). *Seismic Evaluation and Retrofit of Existing Buildings*. Reston, VA: American Society of Civil Engineers. https://doi.org/10.1061/9780784412855

ATC. (2009). *Quantification of building seismic performance factors*. *FEMA P695*.

Black, C. J., Makris, N., & Aiken, I. D. (2004). Component Testing, Seismic Evaluation and Characterization of Buckling-Restrained Braces. *Journal of Structural Engineering*, *130*(6), 880–894. https://doi.org/10.1061/(ASCE)0733-9445(2004)130:6(880)

Bruneau, M., Uang, C.-M., & Sabelli, R. (2011). *Ductile design of steel structures* (Vol. 2nd). New York: McGraw-Hill.

Cassidy, J., Rogers, G., Lamontagne, M., Halchuk, S., & Adams, J. (2010). Canada's Earthquakes: The Good, the Bad, and the Ugly. *Geoscience Canada*, *37*(1). Retrieved from https://journals.lib.unb.ca/index.php/GC/article/view/15300

Chao, S.-H., Goel, S. C., & Lee, S.-S. (2007). A Seismic Design Lateral Force Distribution Based on Inelastic State of Structures. *Earthquake Spectra*, *23*(3), 547–569. https://doi.org/10.1193/1.2753549

Choi, H. S., & Joseph, L. (2012). Outrigger System Design Considerations High-Rise Buildings Outrigger System Design Considerations. *International Journal of High-Rise Buildings*, *1*(3), 237–246. Retrieved from www.ctbuh.org

Council on Tall Buildings and Urban Habitat. (2012). *Outrigger design for high-rise buildings: an output of the CTBUH Outrigger Working Group*. Chicago, IL: CTBUH in conjunction with IIT.

CSA. (2004). *Design of concrete structures* (A23.3-04). Mississauga, Ont: Canadian Standard Association.

Deng, K., Pan, P., Lam, A., & Xue, Y. (2014). A simplified model for analysis of high-rise buildings equipped with hysteresis damped outriggers. *The Structural Design of Tall and Special Buildings*, *23*(15), 1158–1170. https://doi.org/10.1002/tal.1113

Filippou, F., & Mazzoni, S. (2009a). Concrete02 Material -- Linear Tension Softening - OpenSeesWiki. Retrieved March 1, 2017, from http://opensees.berkeley.edu/wiki/index.php/Concrete02_Material_--_Linear_Tension_Softening

Filippou, F., & Mazzoni, S. (2009b). Steel02 Material -- Giuffré-Menegotto-Pinto Model with Isotropic Strain Hardening - OpenSeesWiki. Retrieved March 1, 2017, from http://opensees.berkeley.edu/wiki/index.php/Steel02_Material_--_Giuffré-Menegotto-Pinto_Model_with_Isotropic_Strain_Hardening

Groupe Petra. (2017). Place Victoria. Retrieved February 19, 2017, from http://www.groupepetra.com/eng/properties/view?id=41

Halchuk, S., Allen, T. I., Adams, J., & Rogers, G. C. (2014). *Fifth Generation Seismic Hazard Model Input Files as Proposed to Produce Values for the 2015 National Building Code of Canada*. https://doi.org/10.4095/293907

McKenna, F., & Fenves, G. (1997). OpenSees. The Regents of the University of California. Retrieved from http://opensees.berkeley.edu/

Moudarres, F. R. (1984). Outrigger-Braced Coupled Shear Walls. *Journal of Structural Engineering*, *110*(12), 2876–2890. https://doi.org/10.1061/(ASCE)0733-9445(1984)110:12(2876)

National Research Council of Canada. (2015). *National Building Code of Canada, 2015* (14th ed.). Ottawa: National Research Council of Canada.

National Resources Canada. (2016). Seismic zones in Western Canada. Retrieved February 18, 2017, from http://www.earthquakescanada.nrcan.gc.ca/zones/westcan-en.php#Cascadia

Nieblas, G. M. (2017, February). West Coast Boast. *Modern Steel Construction*, 36–40.

Orakcal, K., & Wallace, J. W. (2004). Flexural Modeling of Reinforced Concrete Walls - Experimental Verification. *ACI Structural Journal*, *103*(2), 196–206. https://doi.org/10.14359/15177

Pacific Earthquake Engineering Research Center (PEER). (2010). *Guidelines for Performance-Based*

Seismic Design of Tall Buildings.

RJC Engineers. (2016). MNP Tower. Retrieved February 18, 2017, from https://www.rjc.ca/projects/projects-detail/mnp-tower

S-FRAME Inc. (2016). S-CONCRETE.

Smith, B. S., & Salim, I. (1983). Formulae for optimum drift resistance of outrigger braced tall building structures. *Computers & Structures*, *17*(1), 45–50. https://doi.org/10.1016/0045-7949(83)90027-5

Smith, R. J., & Willford, M. R. (2007). The damped outrigger concept for tall buildings. *The Structural Design of Tall and Special Buildings*, *16*(4), 501–517. https://doi.org/10.1002/tal.413

The Mathworks Inc. (2016). MATLAB. Natick, Massachusetts.

Thomsen IV, J. H., & Wallace, J. W. (1995). Displacement−Based Design of Reinforced Concrete Structural Walls: An Experimental Investigation of Walls with Rectangular and T-Shaped Cross-Sections. Retrieved from http://nisee.berkeley.edu/elibrary/Text/200606122

Tsai, K.-C., & Hsiao, P.-C. (2008). Pseudo-dynamic test of a full-scale CFT/BRB frame—Part II: Seismic performance of buckling-restrained braces and connections. *Earthquake Engineering & Structural Dynamics*, *37*(7), 1099–1115. https://doi.org/10.1002/eqe.803

Yang, T. Y., Tung, D. P., & Li, Y. (2017). Equivalent energy-based design procedure for innovative earthquake resilient structures. *Earthquake Engineering & Structural Dynamics*, (Under Review).

Appendices

Appendix A: Design Calculations for 20-Story Prototype Building

This appendix shows the detailed calculations for the design of a 20-story prototype building using EEDP. For an overview of EEDP, refer to Section 3.2. The prototype building consists of a reinforced concrete core wall with steel outrigger truss at the roof level. The building properties are summarized below:

Parameter	Value	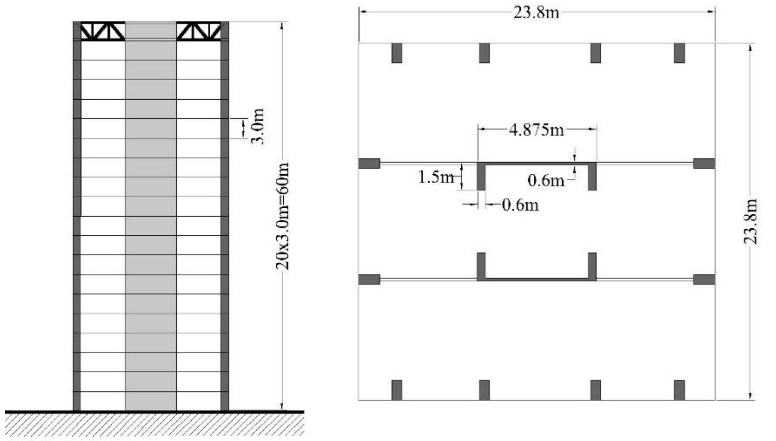 3.0m 20x3.0m=60m 23.8m 4.875m 1.5m 0.6m 0.6m 23.8m
Number of stories	20	
Floor height	3.0m	
Wall length	4.877m	
Outrigger length	23.774m	
Floor weight	6550 kN	
Building Period	1.45sec	

The prototype building is located on Site Class C in Vancouver, BC. For simplicity, a scale factor was applied to the MCE hazard spectrum (2% in 50-year probability of exceedance) to produce spectrums for a DBE and SLE hazard. This was only done for convenience in the NLTHA ground motion selection; actual spectra corresponding to lower hazards (e.g. 10% and 50% probability of exceedance in 50 years) of could have been used instead with appropriately selected and scaled ground motions. The scale factors for the DBE and SLE spectra were 0.5 and 0.1, respectively.

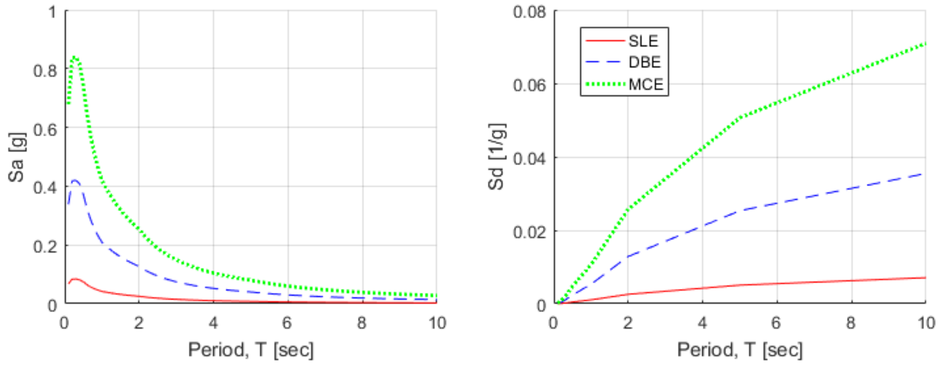

Desired Mechanism

The objective is to design the building such that the outrigger system will yield at the SLE hazard level, the wall will yield at the DBE hazard level, and the system will avoid collapse at the MCE hazard.

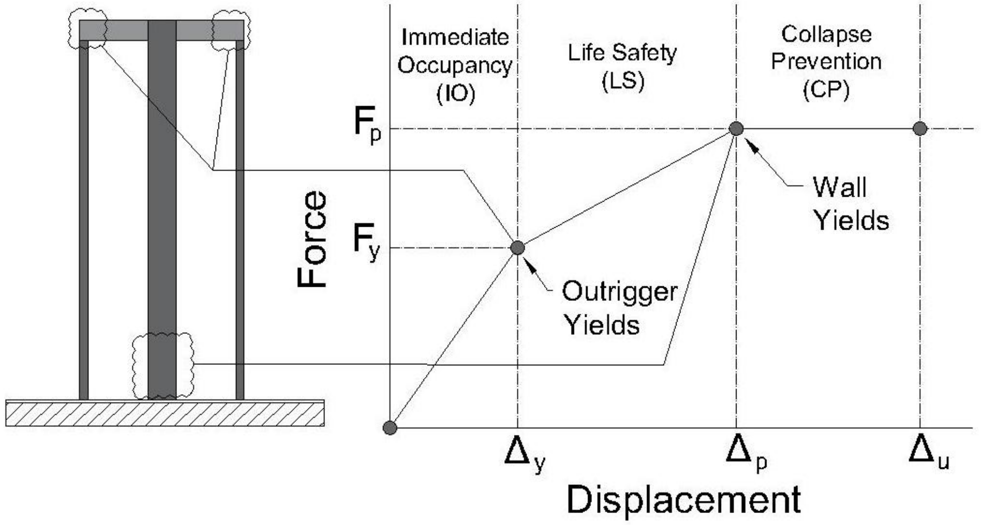
Immediate Occupancy (IO)
Life Safety (LS)
Collapse Prevention (CP)
F_p
F_y
Force
Wall Yields
Outrigger Yields
Δ_y
Δ_p
Δ_u
Displacement

Select Yield Displacement and Period to Compute Fy

From preliminary modelling, the period of the structure is around 1.45 seconds. The value of C0 can be taken as 1.5, based on the results from Chapter 3. Therefore, the yield displacement is:

$$\Delta_y = C_0 \, g \, S_{d,SLE} = (1.5)(0.0017)(9.81) = 0.026 \, m$$

And the SLE-level base shear is:

$$F_y = S_a(T_1)\,W = (0.0327)(133\,447kN) = 4367\,kN$$

Alternatively, a target displacement could have been selected, and the required period and member sizing back-calculated.

Select Yield Displacement of Secondary System

Based on the chosen elastic period, the displacement target for yielding of the secondary system, Δ_p, could range from 0.128m (system essentially continues to be elastic) to 0.393m (wall yields at same time as outrigger). The parameter Δ_p was chosen to be 0.160m. The ductility is $\mu = \Delta_p/\Delta y = 6.15$. The energy modification factors γ_a and γ_b were 1.5 and 2.0.

The base shear of the elastic system at the SLE hazard is:

$$F_Y = m * S_{a,SLE} = (133\,447kN)(0.0327) = 4367kN$$

The incremental energy from the SLE to DBE hazard is:

$$\Delta E_{E1} = \frac{W}{2}\left(S_{a.SLE} + S_{a,DBE}\right)\left(C_0 S_{d,DBE} - \Delta_Y\right)$$

$$\Delta E_{E1} = \frac{(133\,447kN)}{2}(0.0327 + 0.1636)(1.5 * 0.0087 * 9.81 - 0.026m)$$

$$\Delta E_{E1} = 1343kNm$$

The base shear of the nonlinear system at the DBE hazard is:

$$F_p = 2 * \frac{\Delta E_{E1}}{\gamma_a(\Delta_P - \Delta_Y)} - F_Y = \frac{(2)(1343kNm)}{(1.5)(0.160m - 0.026m)} - 4367kN = 8961\text{kN}$$

The incremental energy from the DBE to MCE hazard is:

$$\Delta E_{E2} = \frac{WC_0}{2}\left(S_{a.MCE} + S_{a,DBE}\right)\left(S_{d,MCE} - S_{d,DBE}\right)$$

$$\Delta E_{E2} = \frac{(133\,447kN)(1.5)}{2}(0.3273 + 0.1636)(0.171m - 0.0854m)$$

$$\Delta E_{E2} = 4198kNm$$

The ultimate displacement is determined as:

$$\Delta_U = \frac{\Delta_{E2}}{\gamma_b F_P} + \Delta_P = \frac{(4198kNm)}{(2)(8961kN)} + (0.160m) = 0.394m$$

Distribute the Base Shear to the Primary and Secondary Systems

The ductility is $\mu = \frac{\Delta p}{\Delta y} = \frac{0.160m}{0.026m} = 6.15$

The base shear ratio is $\lambda = \frac{Fp}{Fy} = \frac{8961kN}{4367kN} = 2.05$

The primary (outrigger) system portion is:

$$F_{PR} = F_y \frac{(\mu_p - \lambda)}{(\mu_p - 1)} = (4367kN)\frac{(6.15 - 2.05)}{(6.15 - 1)} = 3491kN$$

The secondary (wall) portion is:

$$F_{SE} = F_y \mu_p \frac{(\lambda - 1)}{(\mu_p - 1)} = (4367kN)(6.15)\frac{(2.05 - 1)}{(6.15 - 1)} = 5471kN$$

The trilinear system curves are shown below for (1) Flexure and (2) Shear

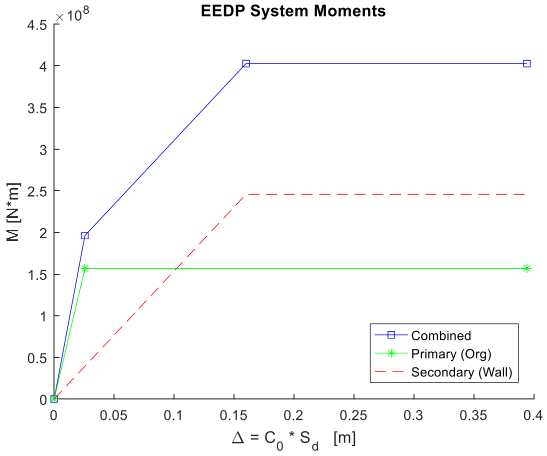

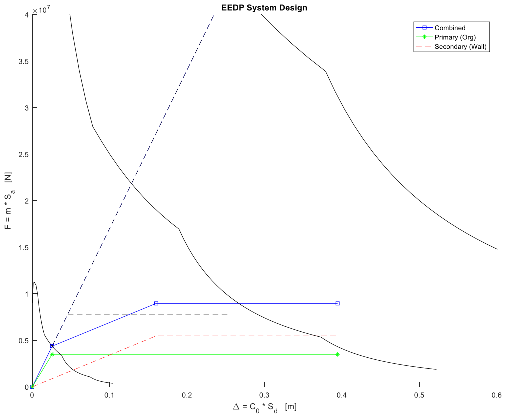

Distribute the Primary and Secondary Forces to their Respective Systems

The forces will be distributed along the height of the structure using the following distribution from Chao et al (2007). This distribution was selected only for convenience; more appropriate distribution of forces for outrigger systems is a topic of further study.

$$F_i = \lambda_i V = (\beta_i - \beta_{i+1})V_n$$

Where

$$\beta_i = \left(\frac{V_i}{V_n}\right) = \left(\frac{\sum_{j=i}^{n} w_j h_j}{w_n h_n}\right)^{0.75T^{-0.2}}$$

Design Yielding Elements

External work equals internal work:

$$W_{ext} = W_{int}$$

For the primary system:

$$\sum_{i=1}^{n} F_{,PR_i} * h_i * \frac{\Delta_{roof}}{h_{total}} = \frac{\Delta_{roof}}{h_{total}} * b * F_{BRB}$$

$$F_{BRB} = \frac{\sum_{i=1}^{n} F * h_i}{b}$$

For the secondary system:

$$W_{ext} = W_{int}$$

$$\sum_{i=1}^{n} F_{SE_i} * h_i * \frac{\Delta_{roof}}{h_{total}} = \frac{\Delta_{roof}}{h_{total}} * My_{wall}$$

$$My_{wall} = \sum_{i=1}^{n} F_{SE_i} * h_i$$

The outrigger system needs to resist a moment of 156850 kNm, and the wall resists 245830 kNm.

Appendix B: Design Calculations for 30-Story Prototype Building

This appendix shows the detailed calculations for the design of a 30-story prototype building using EEDP. For an overview of EEDP, refer to Section 3.2. The prototype building consists of a reinforced concrete core wall with steel outrigger truss at the roof level. The building properties are summarized below:

Parameter	Value
Number of stories	30
Floor height	3.0m
Wall length	7.32m
Outrigger length	23.8m
Floor weight	6550 kN
Building Period	2.1

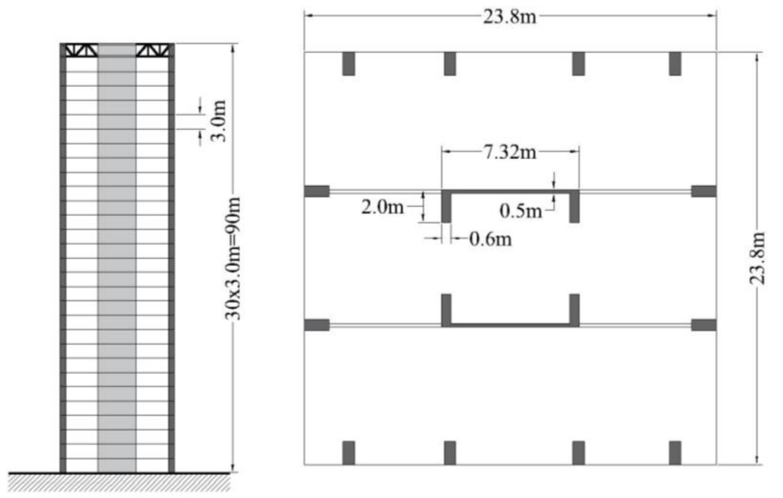

The prototype building is located on Site Class C in Vancouver, BC. For simplicity, a scale factor was applied to the MCE hazard spectrum (2% in 50-year probability of exceedance) to produce spectrums for a DBE and SLE hazard. This was only done for convenience in the NLTHA ground motion selection; actual spectra corresponding to lower hazards (e.g. 10% and 50% probability of exceedance in 50 years) of could have been used instead with appropriately selected and scaled ground motions. The scale factors for the DBE and SLE spectra were 0.5 and 0.1, respectively.

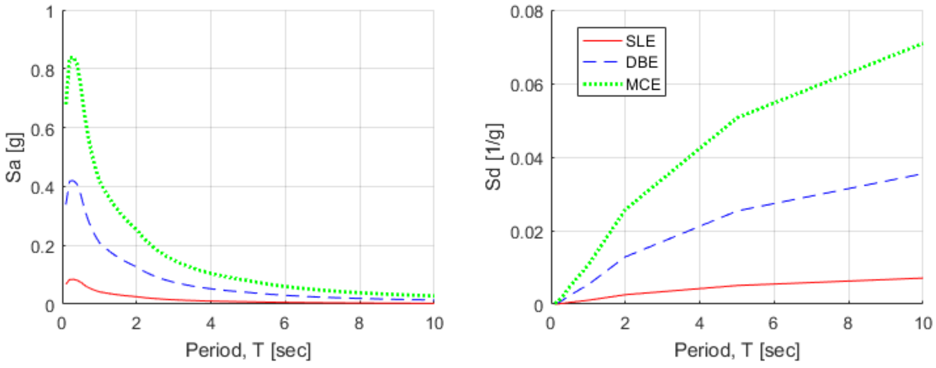

Desired Mechanism

The objective is to design the building such that the outrigger system will yield at the SLE hazard level, the wall will yield at the DBE hazard level, and the system will avoid collapse at the MCE hazard.

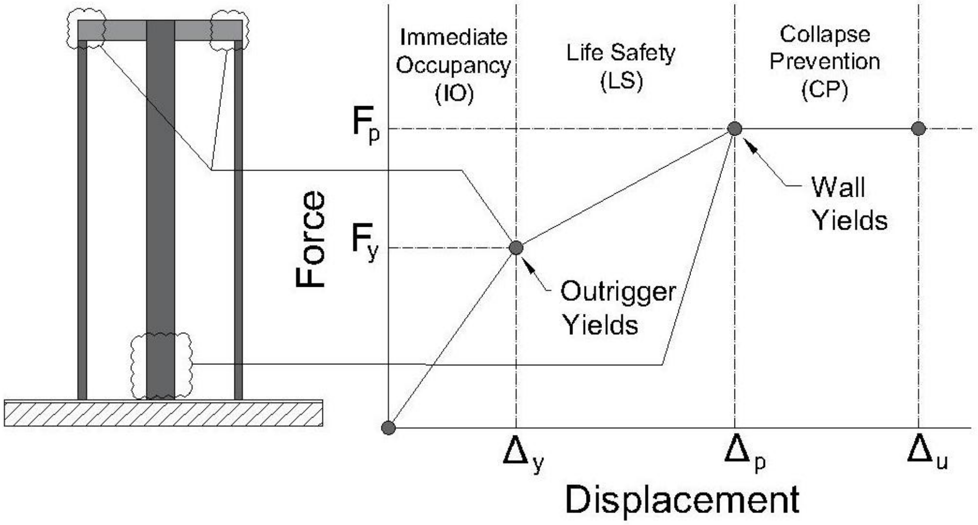
Immediate Occupancy (IO)
Life Safety (LS)
Collapse Prevention (CP)
F_p
Force
F_y
Wall Yields
Outrigger Yields
Δ_y
Δ_p
Δ_u
Displacement

Select Yield Displacement and Period to Compute Fy

From preliminary modelling, the period of the structure is around 2.1 seconds. The value of C0 can be taken as 1.5, based on the results from Chapter 3. Therefore, the yield displacement is:

$$\Delta_y = C_0\, S_{d,SLE} = (1.5)(0.0027)(9.81) = 0.039\, m$$

And the SLE-level base shear is:

$$F_y = S_a(T_1)\, W = (0.0238)(200\,170 kN) = 4761\, kN$$

Alternatively, a target displacement could have been selected, and the required period and member sizing back-calculated.

Select Yield Displacement of Secondary System

Based on the chosen elastic period, the displacement target for yielding of the secondary system, Δ_p, could range from 0.195m (system essentially continues to be elastic) to 0.432m (wall yields at same time as outrigger). The parameter Δ_p was chosen to be 0.260m. The ductility is $\mu = \Delta_p/\Delta y = 6.65$. The energy modification factors γ_a and γ_b were 1.25 and 2.0.

The incremental energy from the SLE to DBE hazard is:

$$\Delta E_{E1} = \frac{W}{2}\left(S_{a.SLE} + S_{a,DBE}\right)\left(C_0 S_{d,DBE} - \Delta_Y\right)$$

$$\Delta E_{E1} = \frac{(200\ 170kN)}{2}(0.0238 + 0.1189)(1.5 * 0.130m - 0.039m)$$

$$\Delta E_{E1} = 2233kNm$$

The base shear of the nonlinear system at the DBE hazard is:

$$F_p = 2 * \frac{\Delta E_{E1}}{\gamma_a(\Delta_P - \Delta_Y)} - F_Y = \frac{(2)(2233kNm)}{(1.25)(0.260m - 0.039m)} - 4761kN = 11414\text{kN}$$

The incremental energy from the DBE to MCE hazard is:

$$\Delta E_{E2} = \frac{WC_0}{2}\left(S_{a.MCE} + S_{a,DBE}\right)\left(S_{d,MCE} - S_{d,DBE}\right)$$

$$\Delta E_{E2} = \frac{(200\ 170kN)(1.5)}{2}(0.2378 + 0.1189)(0.261m - 0.130m)$$

$$\Delta E_{E2} = 6979kNm$$

The ultimate displacement is determined as:

$$\Delta_U = \frac{\Delta_{E2}}{\gamma_b F_P} + \Delta_P = \frac{(6979kNm)}{(2)(11414kN)} + (0.260m) = 0.566m$$

Distribute the Base Shear to the Primary and Secondary Systems

The ductility is $\mu = \frac{\Delta p}{\Delta y} = \frac{0.260m}{0.039m} = 6.65$

The base shear ratio is $\lambda = \frac{Fp}{Fy} = \frac{11414kN}{4761kN} = 2.4$

The primary (outrigger) system portion is:

$$F_{PR} = F_y \frac{(\mu_p - \lambda)}{(\mu_p - 1)} = (4367kN)\frac{(6.65 - 2.4)}{(6.65 - 1)} = 3583kN$$

The secondary (wall) portion is:

$$F_{SE} = F_y \mu_p \frac{(\lambda - 1)}{(\mu_p - 1)} = (4367kN)(6.65)\frac{(2.4 - 1)}{(6.65 - 1)} = 7831kN$$

The trilinear system curves are shown below for (1) Flexure and (2) Shear

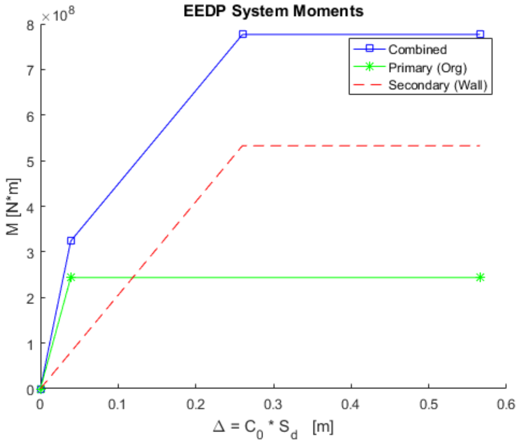

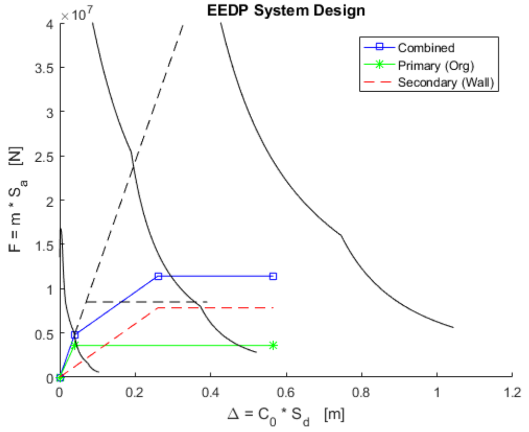

Distribute the Primary and Secondary Forces to their Respective Systems

The forces will be distributed along the height of the structure using the following distribution from Chao et al (2007). This distribution was selected only for convenience; more appropriate distribution of forces for outrigger systems is a topic of further study.

$$F_i = \lambda_i V = (\beta_i - \beta_{i+1})V_n$$

Where

$$\beta_i = \left(\frac{V_i}{V_n}\right) = \left(\frac{\sum_{j=i}^{n} w_j h_j}{w_n h_n}\right)^{0.75T^{-0.2}}$$

Design Yielding Elements

External work equals internal work:

$$W_{ext} = W_{int}$$

For the primary system:

$$\sum_{i=1}^{n} F_{,PR_i} * h_i * \frac{\Delta_{roof}}{h_{total}} = \frac{\Delta_{roof}}{h_{total}} * b * F_{BRB}$$

$$F_{BRB} = \frac{\sum_{i=1}^{n} F * h_i}{b}$$

For the secondary system:

$$W_{ext} = W_{int}$$

$$\sum_{i=1}^{n} F_{SE_i} * h_i * \frac{\Delta_{roof}}{h_{total}} = \frac{\Delta_{roof}}{h_{total}} * My_{wall}$$

$$My_{wall} = \sum_{i=1}^{n} F_{SE_i} * h_i$$

The outrigger system needs to resist a moment of 243,770 kNm, and the wall resists 532,790 kNm.

Appendix C: Design Calculations for 40-Story Prototype Building

This appendix shows the detailed calculations for the design of a 40-story prototype building using EEDP. For an overview of EEDP, refer to Section 3.2. The prototype building consists of a reinforced concrete core wall with steel outrigger truss at the roof level. The building properties are summarized below:

Parameter	**Value**	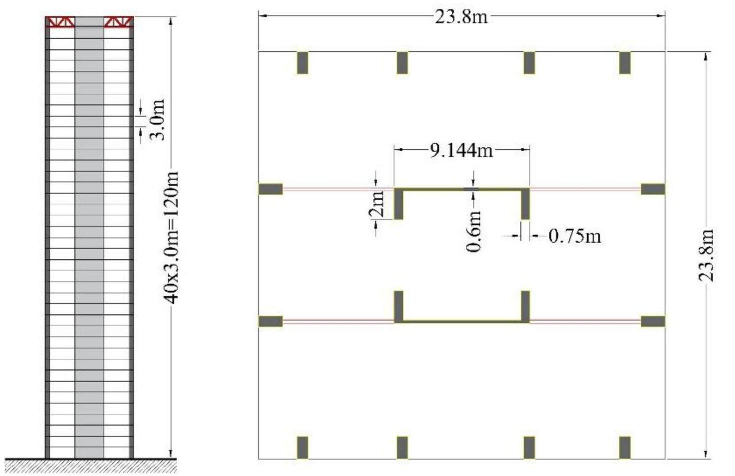 3.0m 40x3.0m=120m 23.8m 9.144m 2m 0.6m 0.75m 23.8m
Number of stories	40	
Floor height	3.0m	
Wall length	9.15m	
Outrigger length	23.8m	
Floor weight	6550 kN	
Building Period	3.0	

The prototype building is located on Site Class C in Vancouver, BC. For simplicity, a scale factor was applied to the MCE hazard spectrum (2% in 50-year probability of exceedance) to produce spectrums for a DBE and SLE hazard. This was only done for convenience in the NLTHA ground motion selection; actual spectra corresponding to lower hazards (e.g. 10% and 50% probability of exceedance in 50 years) of could have been used instead with appropriately selected and scaled ground motions. The scale factors for the DBE and SLE spectra were 0.5 and 0.1, respectively.

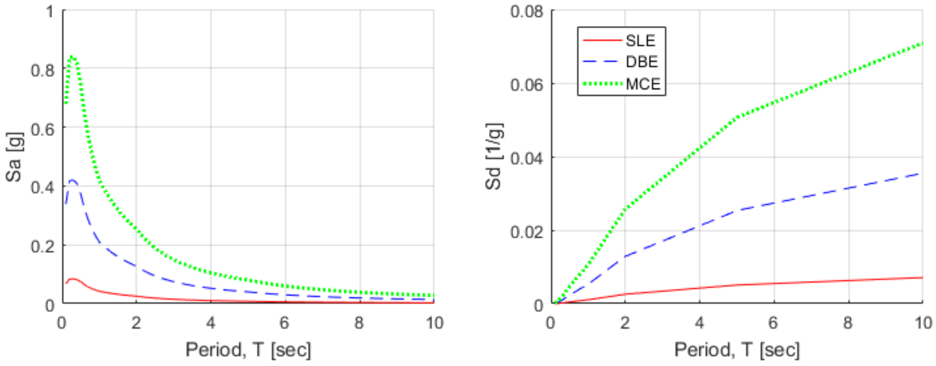

Desired Mechanism

The objective is to design the building such that the outrigger system will yield at the SLE hazard level, the wall will yield at the DBE hazard level, and the system will avoid collapse at the MCE hazard.

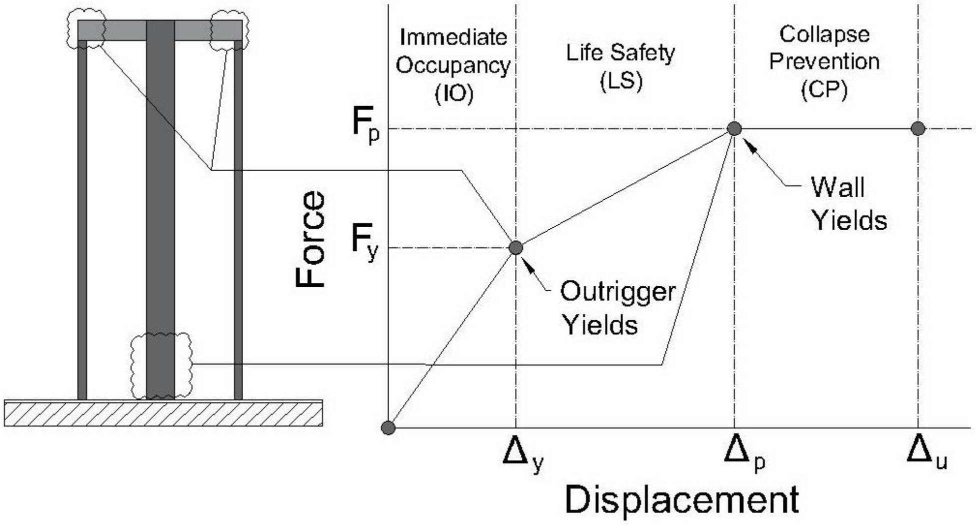
Immediate Occupancy (IO)
Life Safety (LS)
Collapse Prevention (CP)
F_p
F_y
Force
Wall Yields
Outrigger Yields
Δ_y
Δ_p
Δ_u
Displacement

Select Yield Displacement and Period to Compute Fy

From preliminary modelling, the period of the structure is around 1.45 seconds. The value of C0 can be taken as 1.5, based on the results from Chapter 3. Therefore, the yield displacement is:

$$\Delta_y = C_0 \, g \, S_{d,SLE} = (1.5)(0.0034)(9.81) = 0.050 \, m$$

And the SLE-level base shear is:

$$F_y = S_a(T_1) \, W = (0.015)(266\,893 kN) = 3986 \, kN$$

Alternatively, a target displacement could have been selected, and the required period and member sizing back-calculated.

Select Yield Displacement of Secondary System

Based on the chosen elastic period, the displacement target for yielding of the secondary system, Δ_p, could range from 0.250m (system essentially continues to be elastic) to 0.509m (wall yields at same time as outrigger). The parameter Δ_p was chosen to be 0.400m. The ductility is $\mu = \Delta_p/\Delta y = 7.98$. The energy modification factors γ_a and γ_b were 1.0 and 2.0.

The incremental energy from the SLE to DBE hazard is:

$$\Delta E_{E1} = \frac{W}{2}\left(S_{a.SLE} + S_{a,DBE}\right)\left(C_0 S_{d,DBE} - \Delta_Y\right)$$

$$\Delta E_{E1} = \frac{(266\,893kN)}{2}(0.0149 + 0.0747)(1.5 * 0.017 * 9.81 - 0.050m)$$

$$\Delta E_{E1} = 2396kNm$$

The base shear of the nonlinear system at the DBE hazard is:

$$F_p = 2 * \frac{\Delta E_{E1}}{\gamma_a(\Delta_P - \Delta_Y)} - F_Y = \frac{(2)(2396kNm)}{(1.0)(0.400m - 0.050m)} - 3986kN = 9709\text{kN}$$

The incremental energy from the DBE to MCE hazard is:

$$\Delta E_{E2} = \frac{WC_0}{2}\left(S_{a.MCE} + S_{a,DBE}\right)\left(S_{d,MCE} - S_{d,DBE}\right)$$

$$\Delta E_{E2} = \frac{(266\,893kN)(1.5)}{2}(0.1493 + 0.0747)(0.334m - 0.167m)$$

$$\Delta E_{E2} = 7487kNm$$

The ultimate displacement is determined as:

$$\Delta_U = \frac{\Delta_{E2}}{\gamma_b F_P} + \Delta_P = \frac{(7487kNm)}{(2)(9709kN)} + (0.400m) = 0.786m$$

Distribute the Base Shear to the Primary and Secondary Systems

The ductility is $\mu = \frac{\Delta p}{\Delta y} = \frac{0.400m}{0.050m} = 7.98$

The base shear ratio is $\lambda = \frac{Fp}{Fy} = \frac{9709kN}{3986\,kN} = 2.44$

The primary (outrigger) system portion is:

$$F_{PR} = F_y \frac{\left(\mu_p - \lambda\right)}{\left(\mu_p - 1\right)} = (3986kN)\frac{(7.98 - 2.44)}{(7.98 - 1)} = 3166kN$$

The secondary (wall) portion is:

$$F_{SE} = F_y \mu_p \frac{(\lambda - 1)}{(\mu_p - 1)} = (3986kN)(7.98)\frac{(2.44 - 1)}{(7.98 - 1)} = \ 6543kN$$

The trilinear system curves are shown below for (1) Flexure and (2) Shear

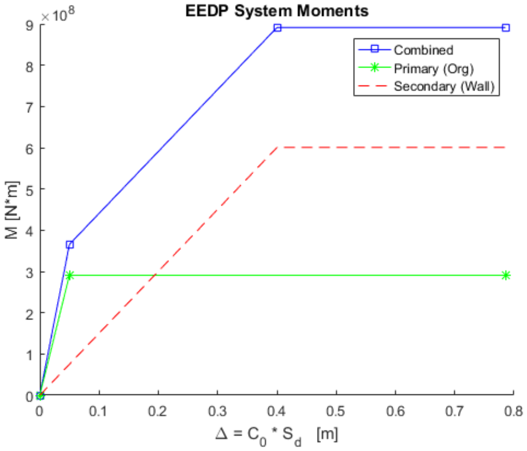

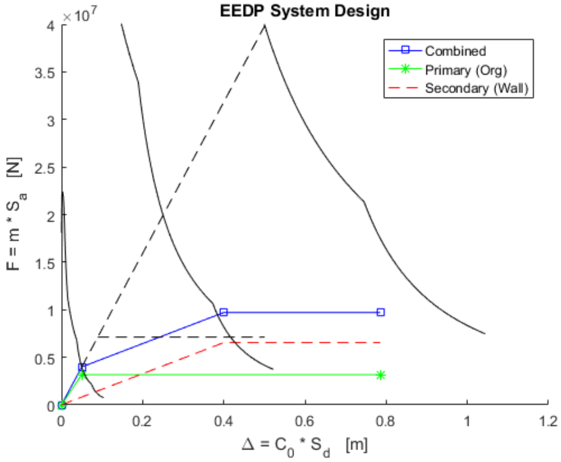

Distribute the Primary and Secondary Forces to their Respective Systems

The forces will be distributed along the height of the structure using the following distribution from Chao et al (2007). This distribution was selected only for convenience; more appropriate distribution of forces for outrigger systems is a topic of further study.

$$F_i = \lambda_i V = (\beta_i - \beta_{i+1})V_n$$

Where

$$\beta_i = \left(\frac{V_i}{V_n}\right) = \left(\frac{\sum_{j=i}^{n} w_j h_j}{w_n h_n}\right)^{0.75T^{-0.2}}$$

Design Yielding Elements

External work equals internal work:

$$W_{ext} = W_{int}$$

For the primary system:

$$\sum_{i=1}^{n} F_{,PR_i} * h_i * \frac{\Delta_{roof}}{h_{total}} = \frac{\Delta_{roof}}{h_{total}} * b * F_{BRB}$$

$$F_{BRB} = \frac{\sum_{i=1}^{n} F * h_i}{b}$$

For the secondary system:

$$W_{ext} = W_{int}$$

$$\sum_{i=1}^{n} F_{SE_i} * h_i * \frac{\Delta_{roof}}{h_{total}} = \frac{\Delta_{roof}}{h_{total}} * My_{wall}$$

$$My_{wall} = \sum_{i=1}^{n} F_{SE_i} * h_i$$

The outrigger system needs to resist a moment of 290,630 kNm, and the walls resists 600,600 kNm.

Appendix D: Reinforcing Schedule for Prototype Buildings

SHEARWALL SCHEDULES

FLOOR	TOWER A				TOWER B				TOWER C				f'c
	WALLS		ZONES		WALLS		ZONES		WALLS		ZONES		
	W2	W1	Z2	Z1	W2	W1	Z2	Z1	W2	W1	Z2	Z1	
L40	▨	▨	▨	▨	▨	▨	▨	▨	↑	↑	↑	↑	↑
L39	▨	▨	▨	▨	▨	▨	▨	▨					
L38	▨	▨	▨	▨	▨	▨	▨	▨					
L37	▨	▨	▨	▨	▨	▨	▨	▨					
L36	▨	▨	▨	▨	▨	▨	▨	▨					
L35	▨	▨	▨	▨	▨	▨	▨	▨					
L34	▨	▨	▨	▨	▨	▨	▨	▨			28-35M V 10M@6" T	28-35M V 10M@6" T	
L33	▨	▨	▨	▨	▨	▨	▨	▨			20-35M V 10M@8" T	20-35M V 10M@8" T	
L32	▨	▨	▨	▨	▨	▨	▨	▨			18-35M V 10M@8" T	18-35M V 10M@8" T	
L31	▨	▨	▨	▨	▨	▨	▨	▨			22-30M 10M@8" T	22-30M 10M@8" T	
L30	▨	▨	▨	▨	↑	↑	↑	↑			14-35M 10M@8" T	14-35M 10M@8" T	
L29	▨	▨	▨	▨							16-30M 10M@8" T	16-30M 10M@8" T	
L28	▨	▨	▨	▨							10-35M 10M@8" T	10-35M 10M@8" T	
L27	▨	▨	▨	▨							16-30M 10M@8" T	16-30M 10M@8" T	
L26	▨	▨	▨	▨							14-35M 10M@8" T	14-35M 10M@8" T	
L25	▨	▨	▨	▨			28-35M V 10M@6" T	28-35M V 10M@6" T			20-30M 10M@8" T	20-30M 10M@8" T	
L24	▨	▨	▨	▨			22-35M V 10M@8" T	22-35M V 10M@8" T			18-35M 10M@8" T	18-35M 10M@8" T	
L23	▨	▨	▨	▨			20-35M V 10M@8" T	20-35M V 10M@8" T			18-35M 10M@8" T	18-35M 10M@8" T	
L22	▨	▨	▨	▨			18-35M V 10M@8" T	18-35M V 10M@8" T			20-35M 10M@8" T	20-35M 10M@8" T	
L21	▨	▨	▨	▨			14-35M V 10M@8" T	14-35M V 10M@8" T			22-35M 10M@8" T	22-35M 10M@8" T	
L20	↑	↑	↑	↑			16-30M V 10M@8" T	16-30M V 10M@8" T			24-35M 10M@8" T	24-35M 10M@8" T	65 MPA U.N.O.
L19							18-35M V 10M@8" T	18-35M V 10M@8" T			26-35M 10M@8" T	26-35M 10M@8" T	
L18							20-35M V 10M@8" T	20-35M V 10M@8" T			↑	↑	
L17			24-35M 10M@6" T	24-35M 10M@6" T			22-35M V 10M@8" T	22-35M V 10M@8" T					
L16			22-35M 10M@8" T	22-35M 10M@8" T			26-35M V 10M@8" T	26-35M V 10M@8" T					
L15			20-35M 10M@8" T	20-35M 10M@8" T			28-35M V 10M@8" T	28-35M V 10M@8" T					
L14			16-35M 10M@8" T	16-35M 10M@8" T			↑	↑					
L13			14-35M 10M@8" T	14-35M 10M@8" T									
L12			16-30M 10M@7" T	16-30M 10M@7" T									
L11			14-35M 10M@8" T	14-35M 10M@8" T									
L10			16-35M 10M@8" T	16-35M 10M@8" T									
L09			↑	↑									
L08											28-35M V 10M@8" T	28-35M V 10M@8" T	
L07							32-35M V 10M@8" T	32-35M V 10M@8" T			↑	↑	
L06			20-35M V 10M@8" T	20-35M V 10M@8" T			↑	↑					
L05			↑	↑									
L04													
L03													
L02													
L01	20" Wall 15M@6" VE 20M@4" HE	24" Wall 15M@6" VE 20M@4" HEF	20-35M V 10M@6" T	20-35M V 10M@6" T	20" Wall 15M@6" VE 20M@4" HE	24" Wall 15M@6" VE 20M@4" HEF	32-35M V 10M@6" T	32-35M V 10M@6" T	20" Wall 15M@6" VE 20M@4" HE	24" Wall 15M@6" VE 20M@4" HEF	28-35M V 10M@6" T	28-35M V 10M@6" T	↓
	W2	W1	Z2	Z1	W2	W1	Z2	Z1	W2	W1	Z2	Z1	f'c

Appendix E: Additional Results from Seismic Performance Assessment

E.1 Tower A

Moment-curvature response of wall base from Tower A:

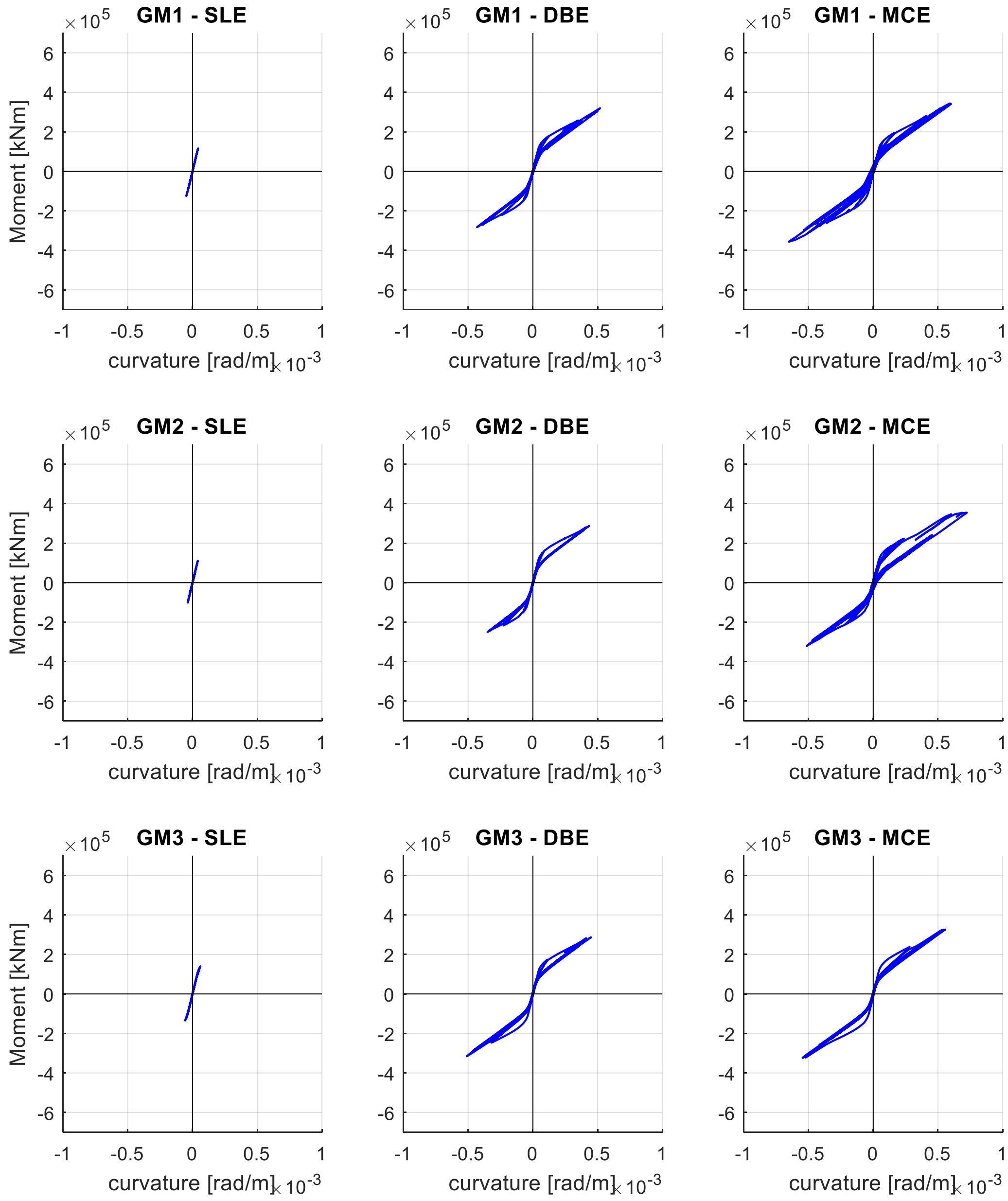

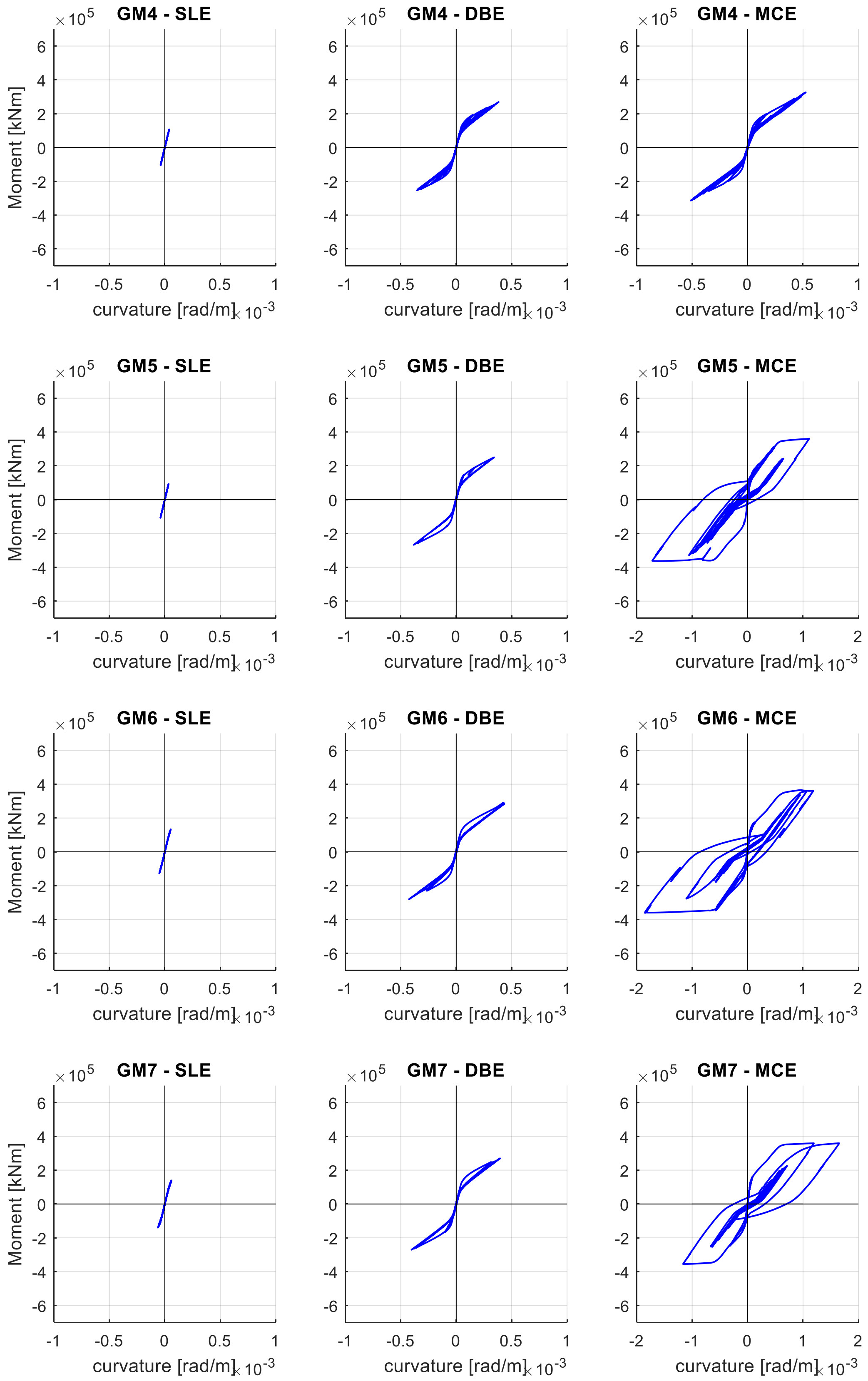
GM4 - SLE
GM4 - DBE
GM4 - MCE
GM5 - SLE
GM5 - DBE
GM5 - MCE
GM6 - SLE
GM6 - DBE
GM6 - MCE
GM7 - SLE
GM7 - DBE
GM7 - MCE
Moment [kNm]
$\times 10^5$
6
4
2
0
-2
-4
-6
curvature [rad/m]
$\times 10^{-3}$
-1
-0.5
0
0.5
1
-2
-1
0
1
2

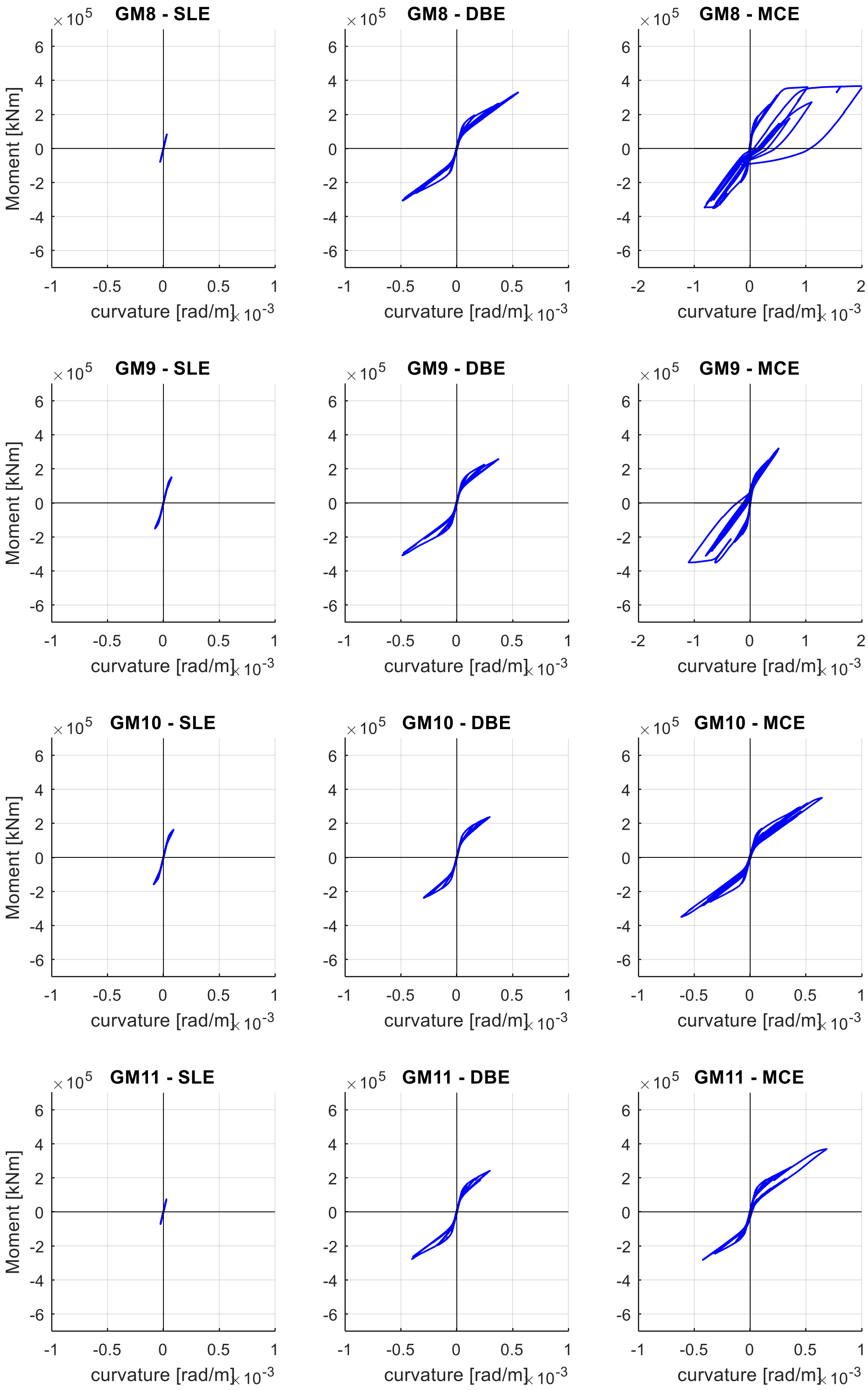
GM8 - SLE
GM8 - DBE
GM8 - MCE
GM9 - SLE
GM9 - DBE
GM9 - MCE
GM10 - SLE
GM10 - DBE
GM10 - MCE
GM11 - SLE
GM11 - DBE
GM11 - MCE
×10^5
Moment [kNm]
6
4
2
0
-2
-4
-6
curvature [rad/m]
×10^-3
-1
-0.5
0
0.5
1
-2
-1
0
1
2

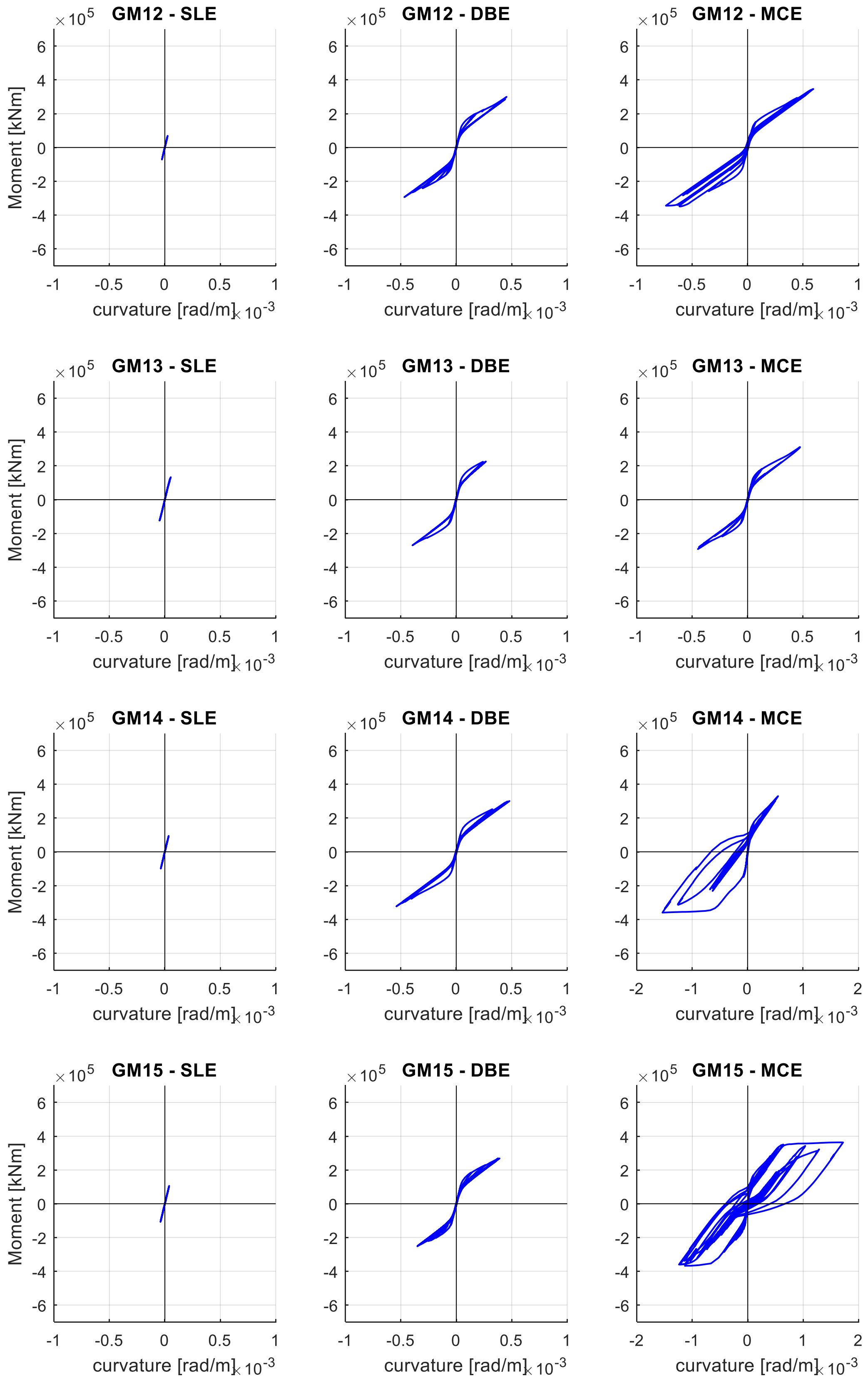
GM12 - SLE
GM12 - DBE
GM12 - MCE
GM13 - SLE
GM13 - DBE
GM13 - MCE
GM14 - SLE
GM14 - DBE
GM14 - MCE
GM15 - SLE
GM15 - DBE
GM15 - MCE
Moment [kNm]
× 10^5
6
4
2
0
-2
-4
-6
curvature [rad/m]
× 10^-3
-1
-0.5
0
0.5
1
-2
-1
0
1
2

Moment-curvature response of wall at outrigger from Tower A:

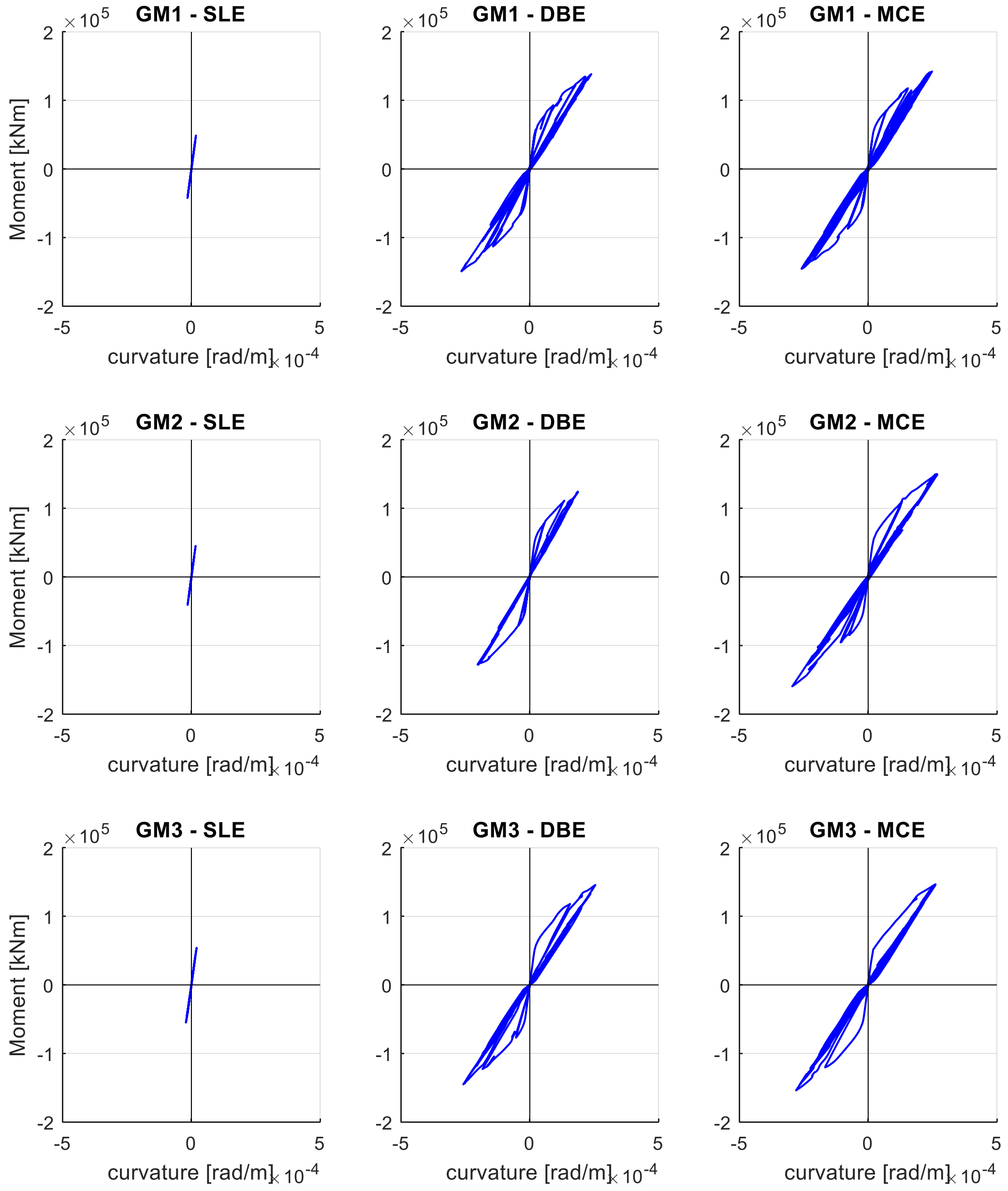

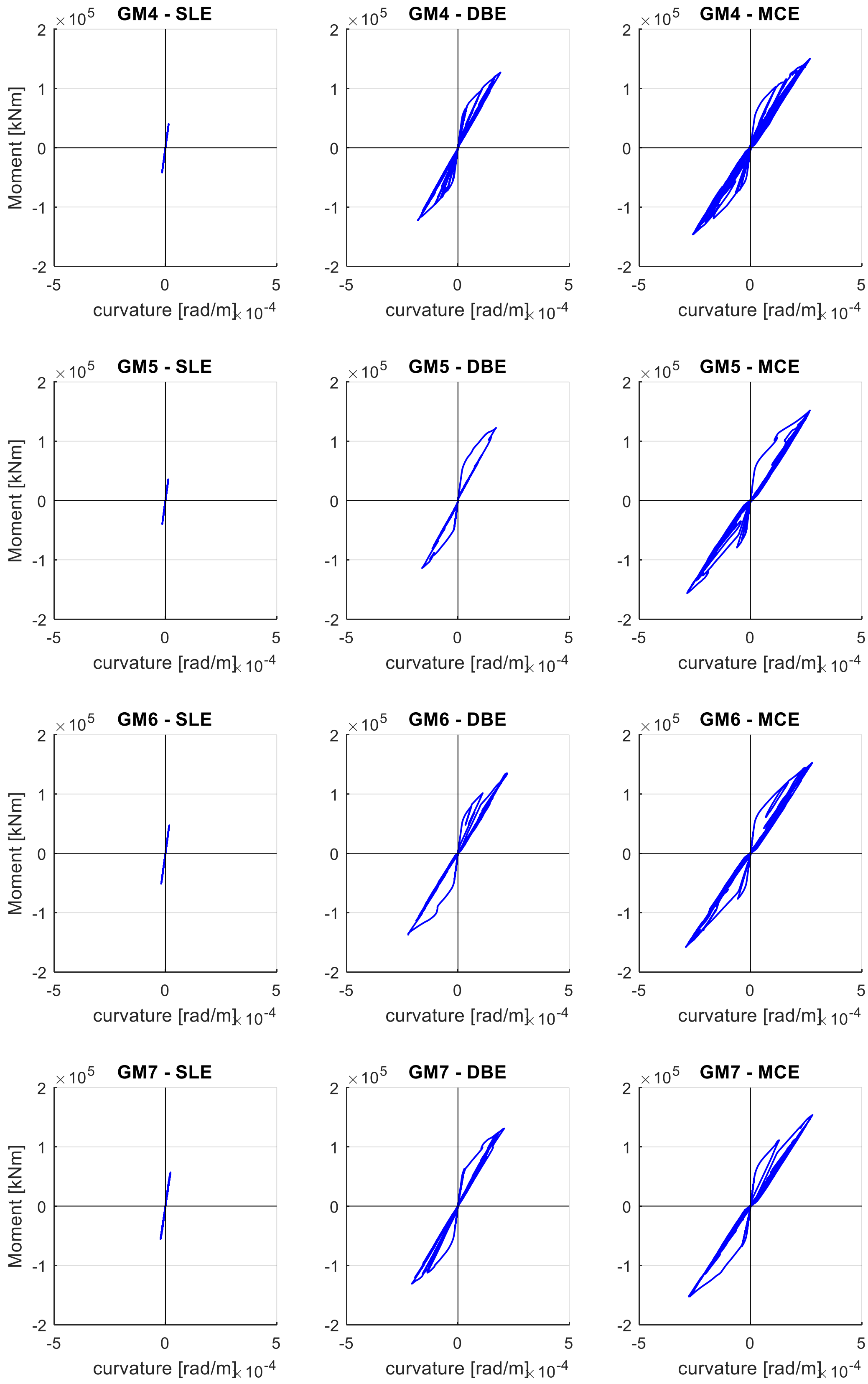
GM4 - SLE
GM4 - DBE
GM4 - MCE
GM5 - SLE
GM5 - DBE
GM5 - MCE
GM6 - SLE
GM6 - DBE
GM6 - MCE
GM7 - SLE
GM7 - DBE
GM7 - MCE
Moment [kNm]
×10^5
2
1
0
-1
-2
curvature [rad/m]
×10^-4
-5
0
5

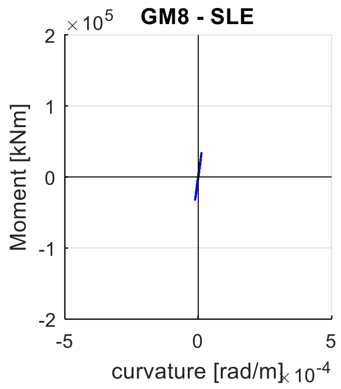
GM8 - SLE

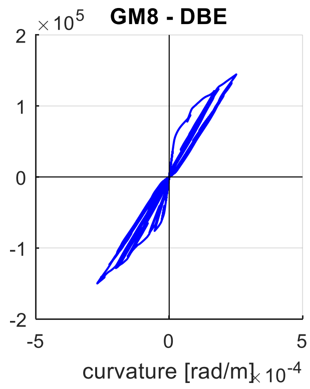
GM8 - DBE

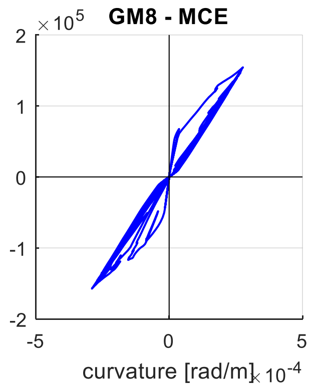
GM8 - MCE

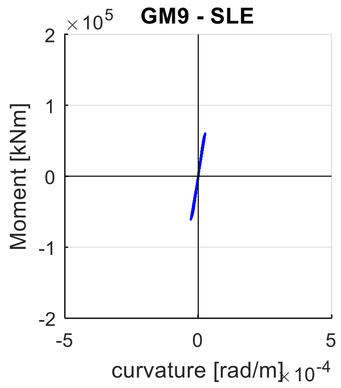
GM9 - SLE

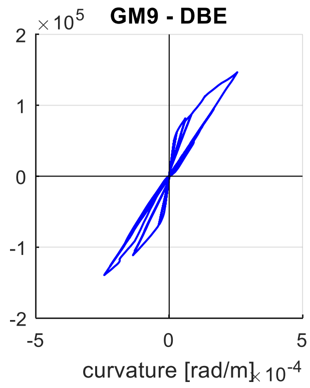
GM9 - DBE

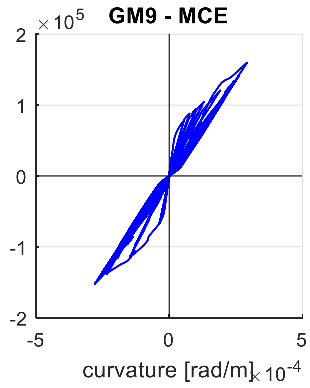
GM9 - MCE

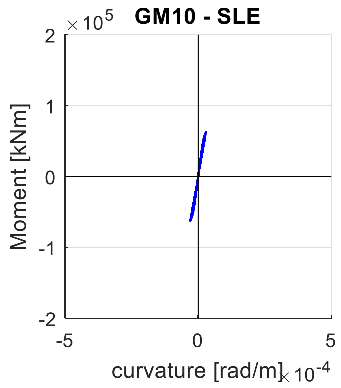
GM10 - SLE

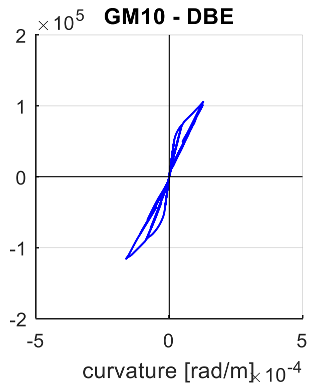
GM10 - DBE

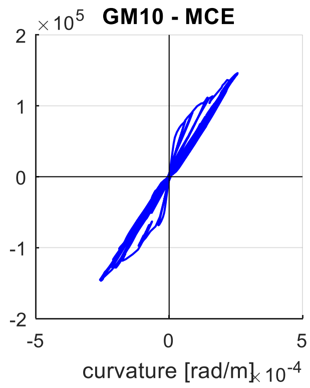
GM10 - MCE

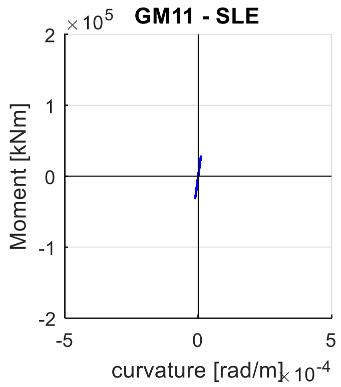
GM11 - SLE

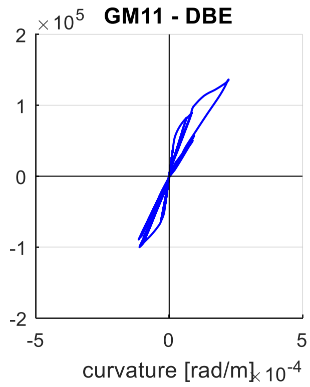
GM11 - DBE

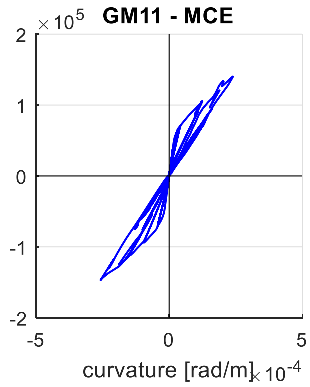
GM11 - MCE

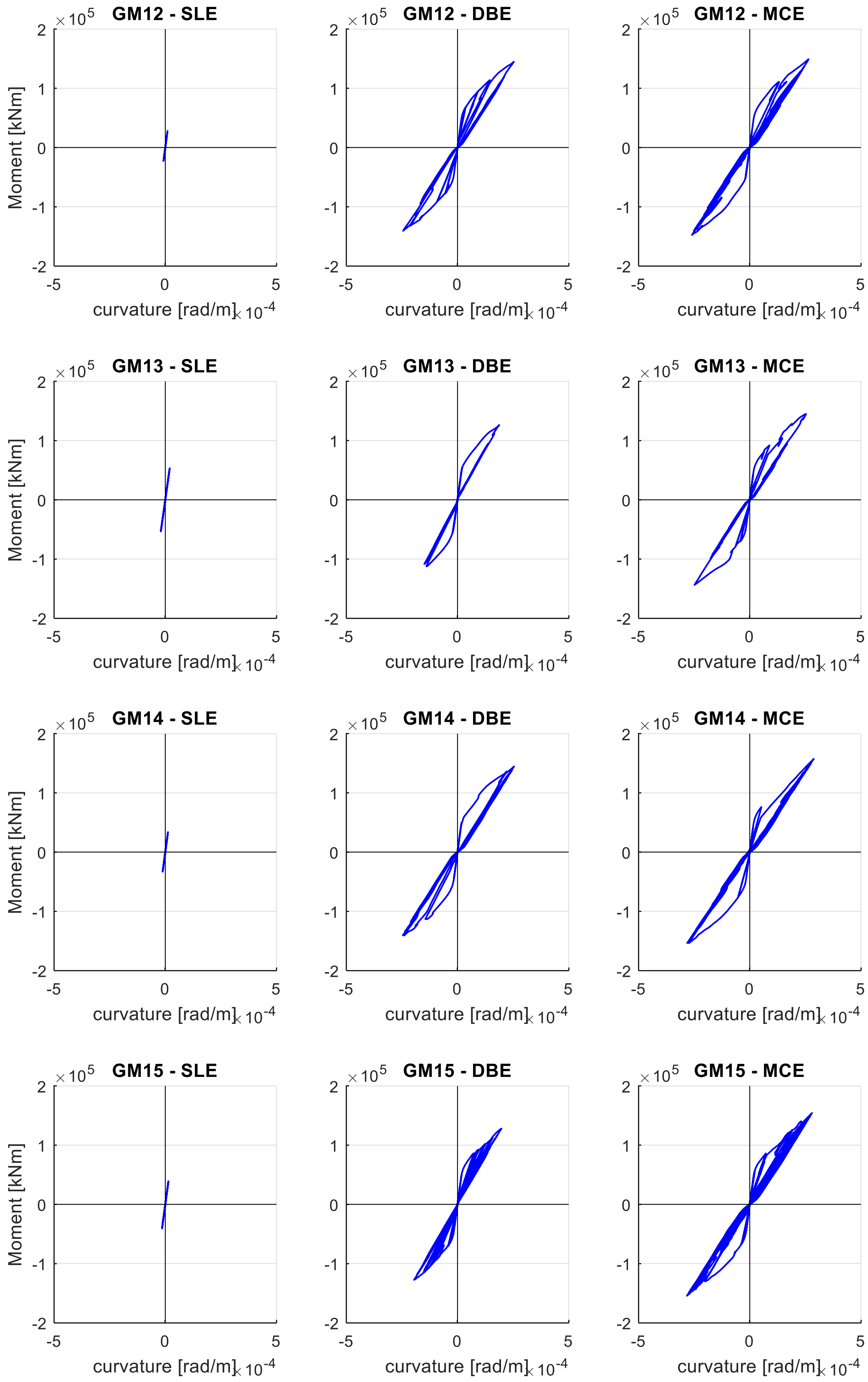
GM12 - SLE
GM12 - DBE
GM12 - MCE
GM13 - SLE
GM13 - DBE
GM13 - MCE
GM14 - SLE
GM14 - DBE
GM14 - MCE
GM15 - SLE
GM15 - DBE
GM15 - MCE
Moment [kNm]
× 10^5
2
1
0
-1
-2
curvature [rad/m]
× 10^-4
-5
0
5

Outrigger Fuse Hysteresis from Tower A:

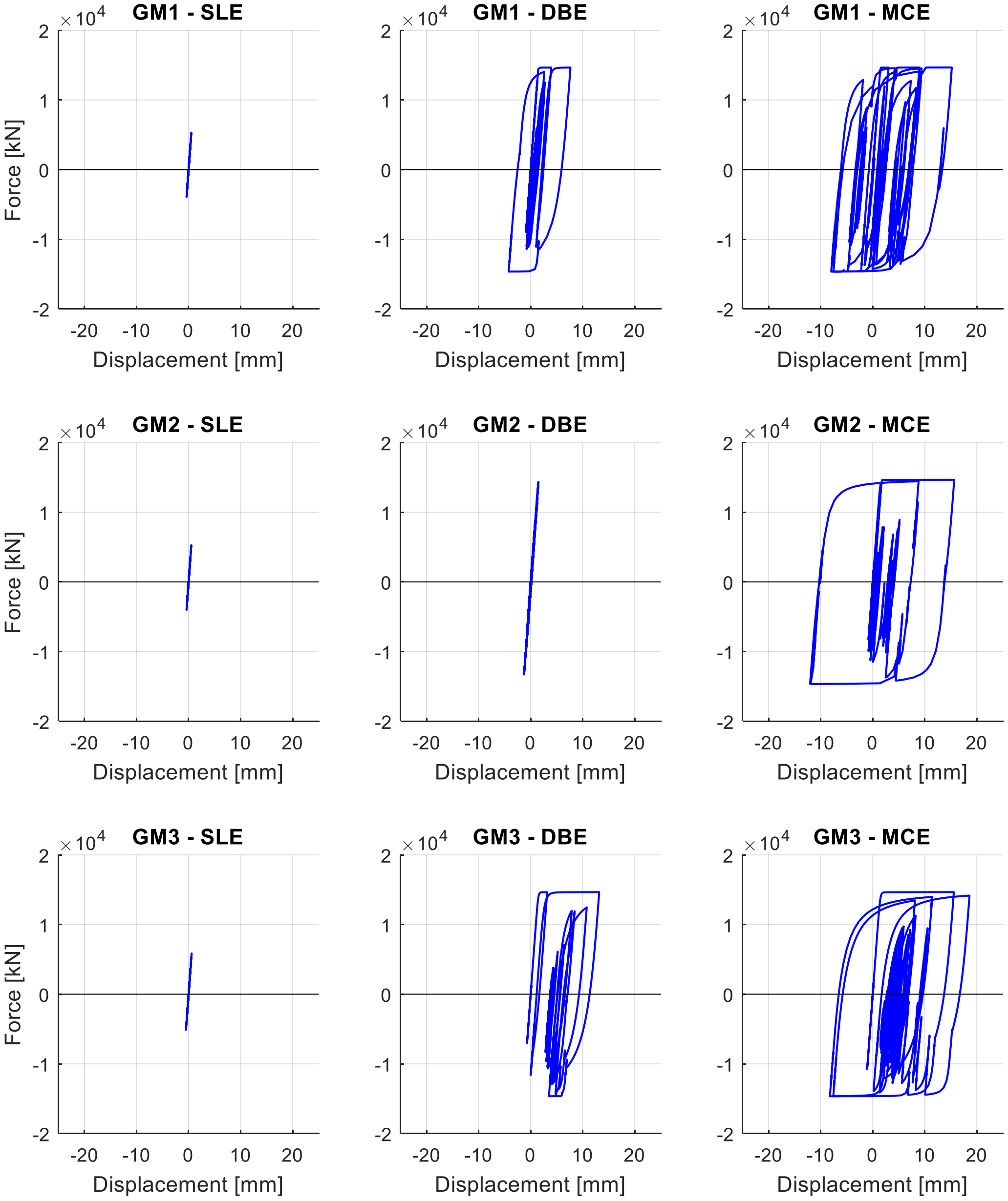

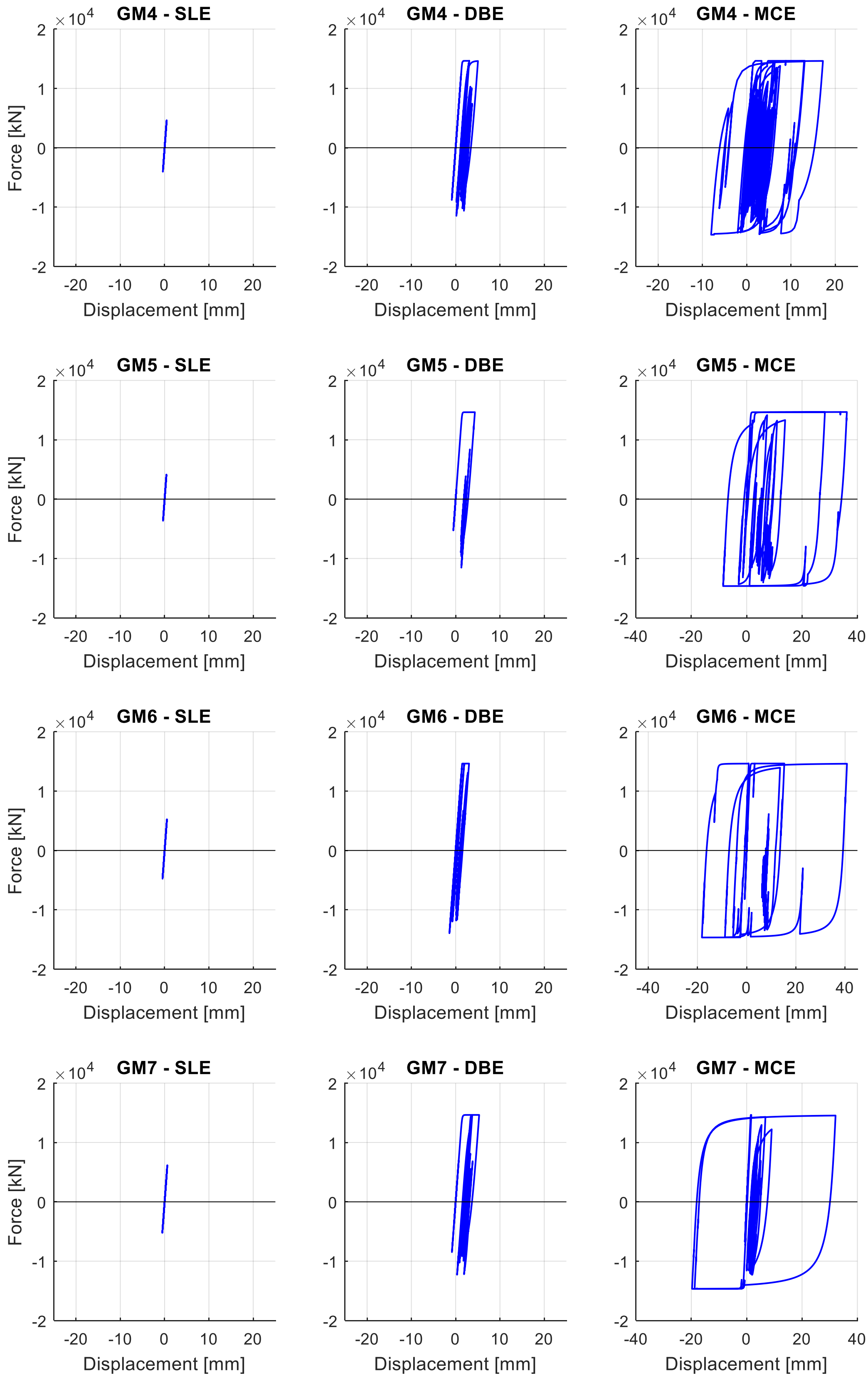
GM4 - SLE
GM4 - DBE
GM4 - MCE
GM5 - SLE
GM5 - DBE
GM5 - MCE
GM6 - SLE
GM6 - DBE
GM6 - MCE
GM7 - SLE
GM7 - DBE
GM7 - MCE
×10^4
Force [kN]
2
1
0
-1
-2
Displacement [mm]
-20
-10
0
10
20
-40
-20
0
20
40

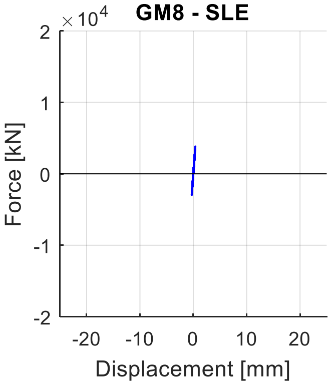
GM8 - SLE
×10^4
2
1
0
-1
-2
Force [kN]
-20
-10
0
10
20
Displacement [mm]

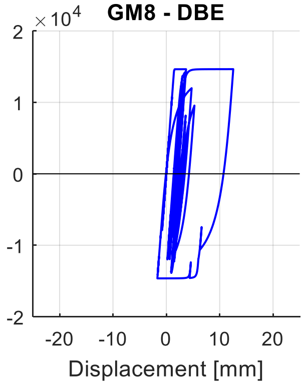
GM8 - DBE
×10^4
2
1
0
-1
-2
-20
-10
0
10
20
Displacement [mm]

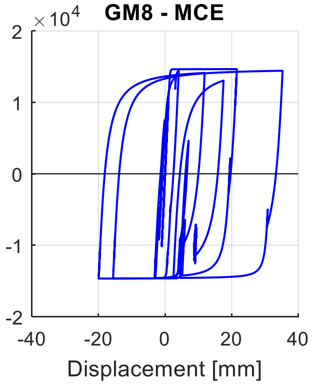
GM8 - MCE
×10^4
2
1
0
-1
-2
-40
-20
0
20
40
Displacement [mm]

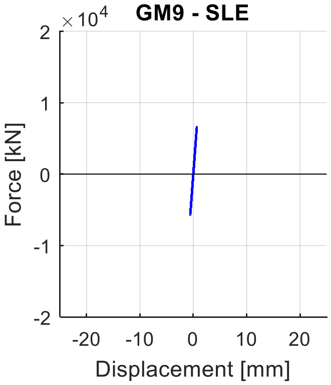
GM9 - SLE
×10^4
2
1
0
-1
-2
Force [kN]
-20
-10
0
10
20
Displacement [mm]

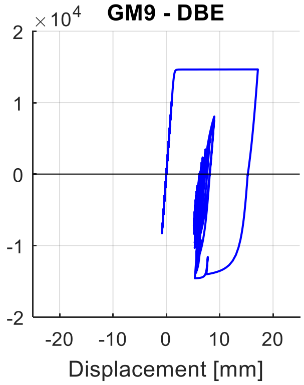
GM9 - DBE
×10^4
2
1
0
-1
-2
-20
-10
0
10
20
Displacement [mm]

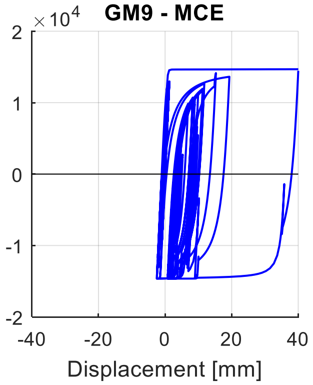
GM9 - MCE
×10^4
2
1
0
-1
-2
-40
-20
0
20
40
Displacement [mm]

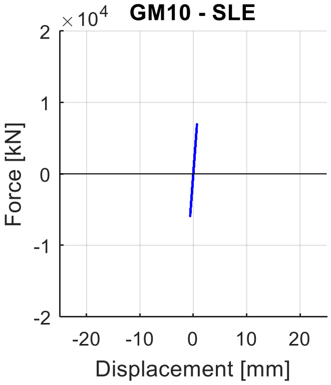
GM10 - SLE
×10^4
2
1
0
-1
-2
Force [kN]
-20
-10
0
10
20
Displacement [mm]

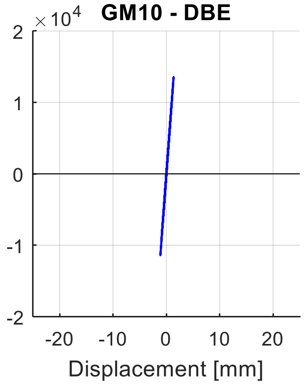
GM10 - DBE
×10^4
2
1
0
-1
-2
-20
-10
0
10
20
Displacement [mm]

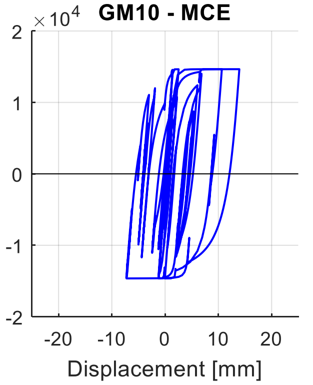
GM10 - MCE
×10^4
2
1
0
-1
-2
-20
-10
0
10
20
Displacement [mm]

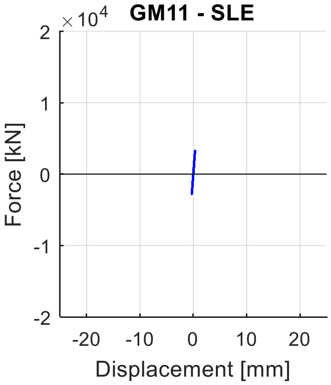
GM11 - SLE
×10^4
2
1
0
-1
-2
Force [kN]
-20
-10
0
10
20
Displacement [mm]

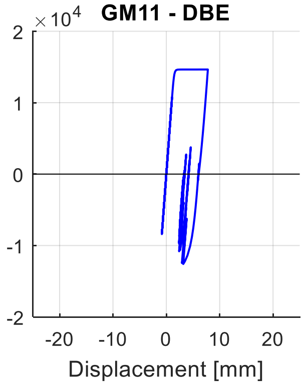
GM11 - DBE
×10^4
2
1
0
-1
-2
-20
-10
0
10
20
Displacement [mm]

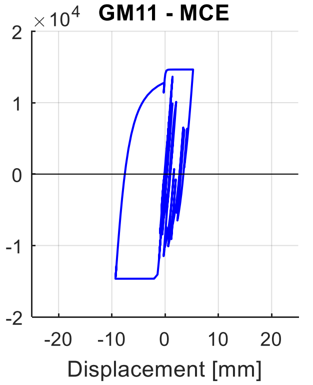
GM11 - MCE
×10^4
2
1
0
-1
-2
-20
-10
0
10
20
Displacement [mm]

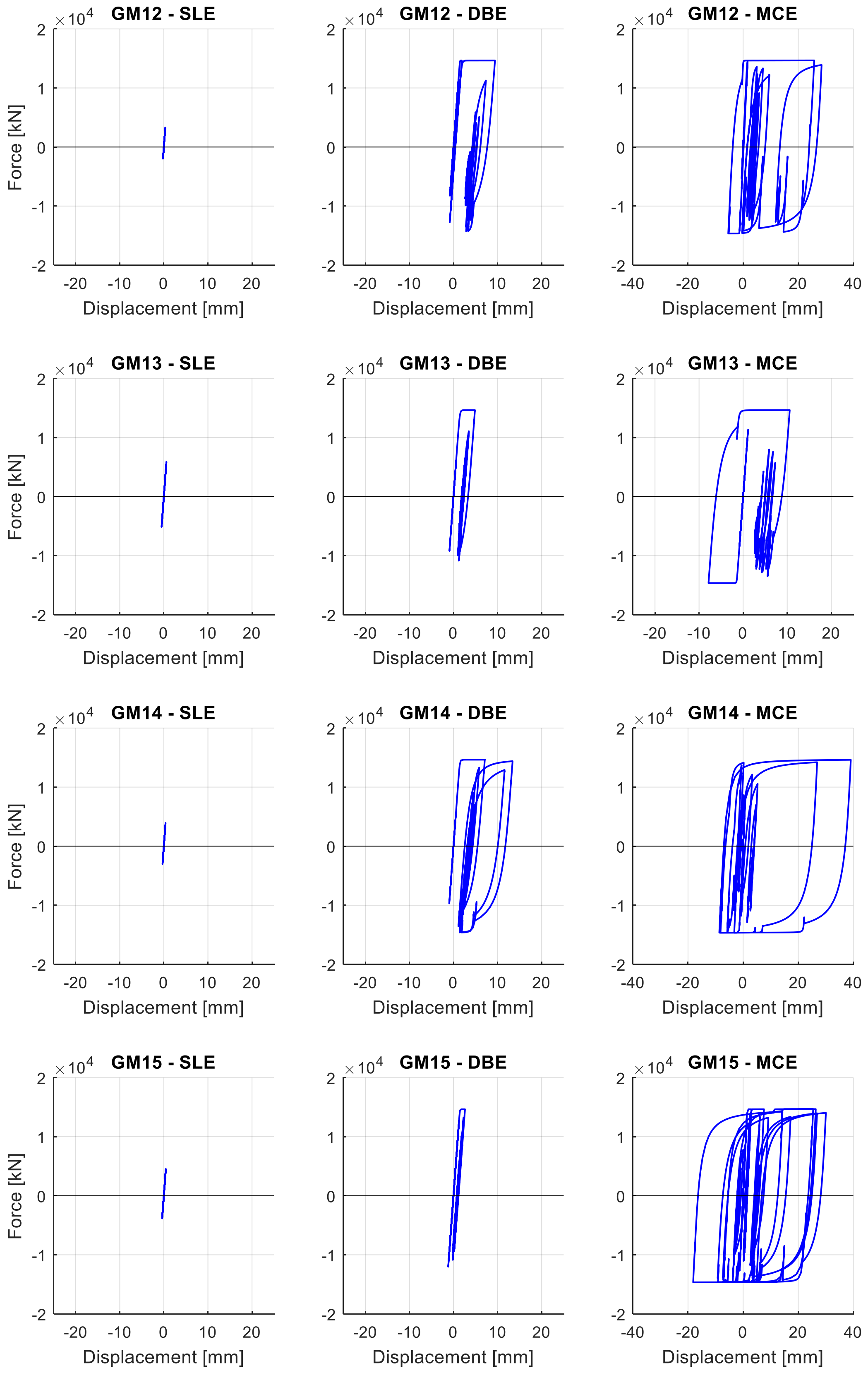
GM12 - SLE
GM12 - DBE
GM12 - MCE
GM13 - SLE
GM13 - DBE
GM13 - MCE
GM14 - SLE
GM14 - DBE
GM14 - MCE
GM15 - SLE
GM15 - DBE
GM15 - MCE
$\times 10^4$
Force [kN]
Displacement [mm]
2
1
0
-1
-2
-20
-10
0
10
20
-40
40

E.2 Tower B

Moment-curvature response of wall base from Tower B:

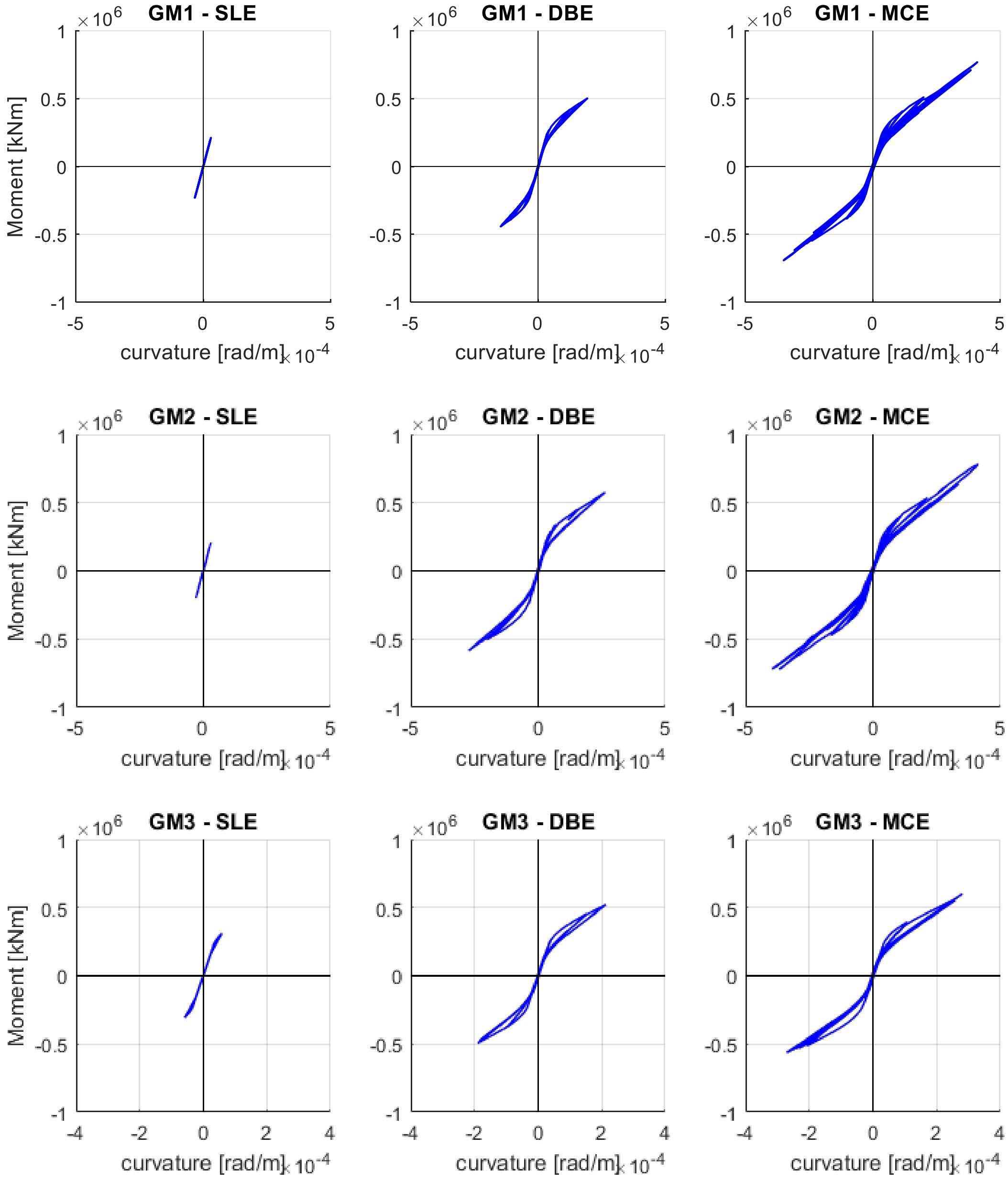

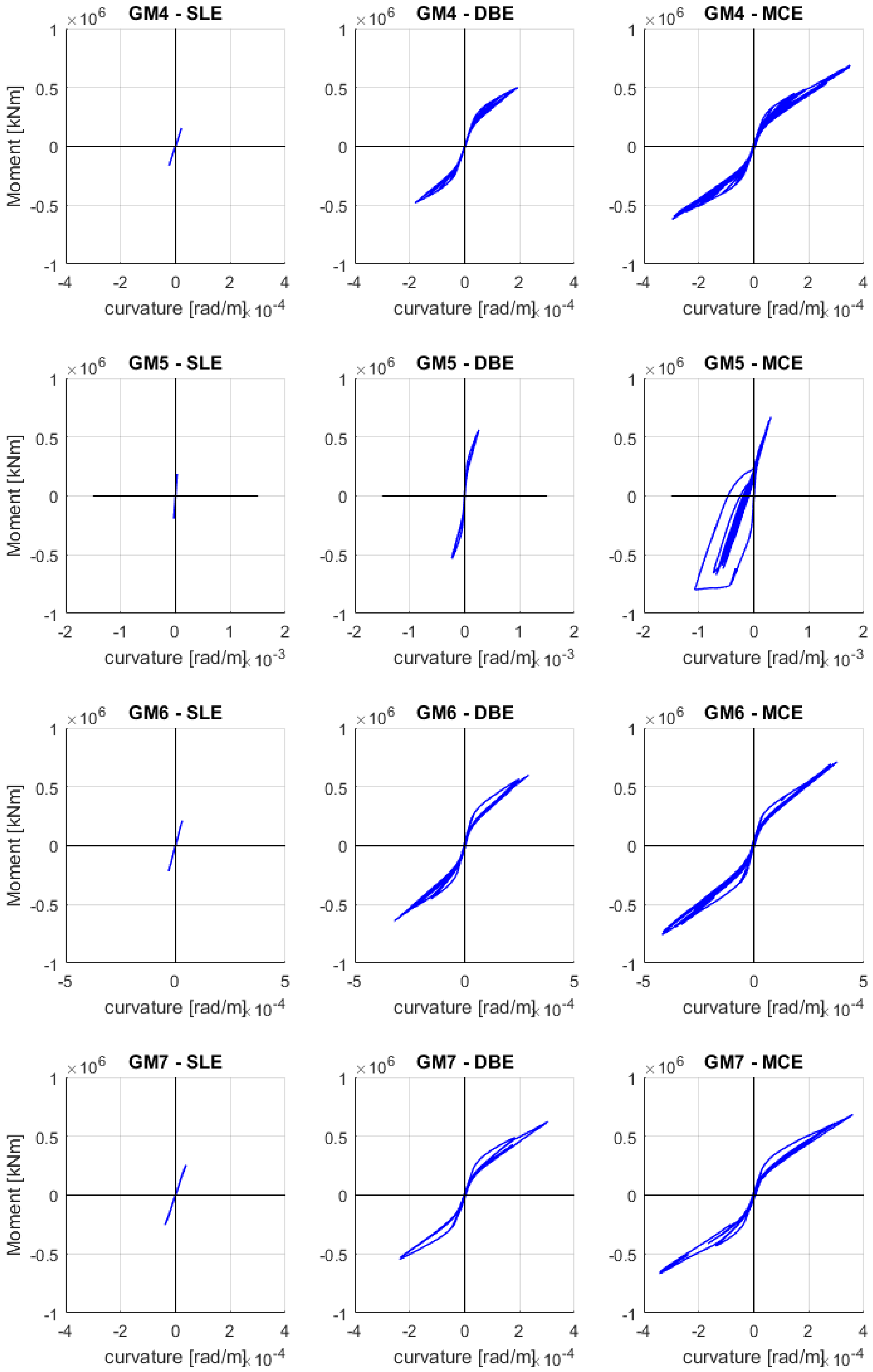
GM4 - SLE
GM4 - DBE
GM4 - MCE
GM5 - SLE
GM5 - DBE
GM5 - MCE
GM6 - SLE
GM6 - DBE
GM6 - MCE
GM7 - SLE
GM7 - DBE
GM7 - MCE
Moment [kNm]
$\times 10^6$
1
0.5
0
-0.5
-1
curvature [rad/m]
$\times 10^{-4}$
$\times 10^{-3}$
-4
-2
0
2
4
-5
5
-1
1

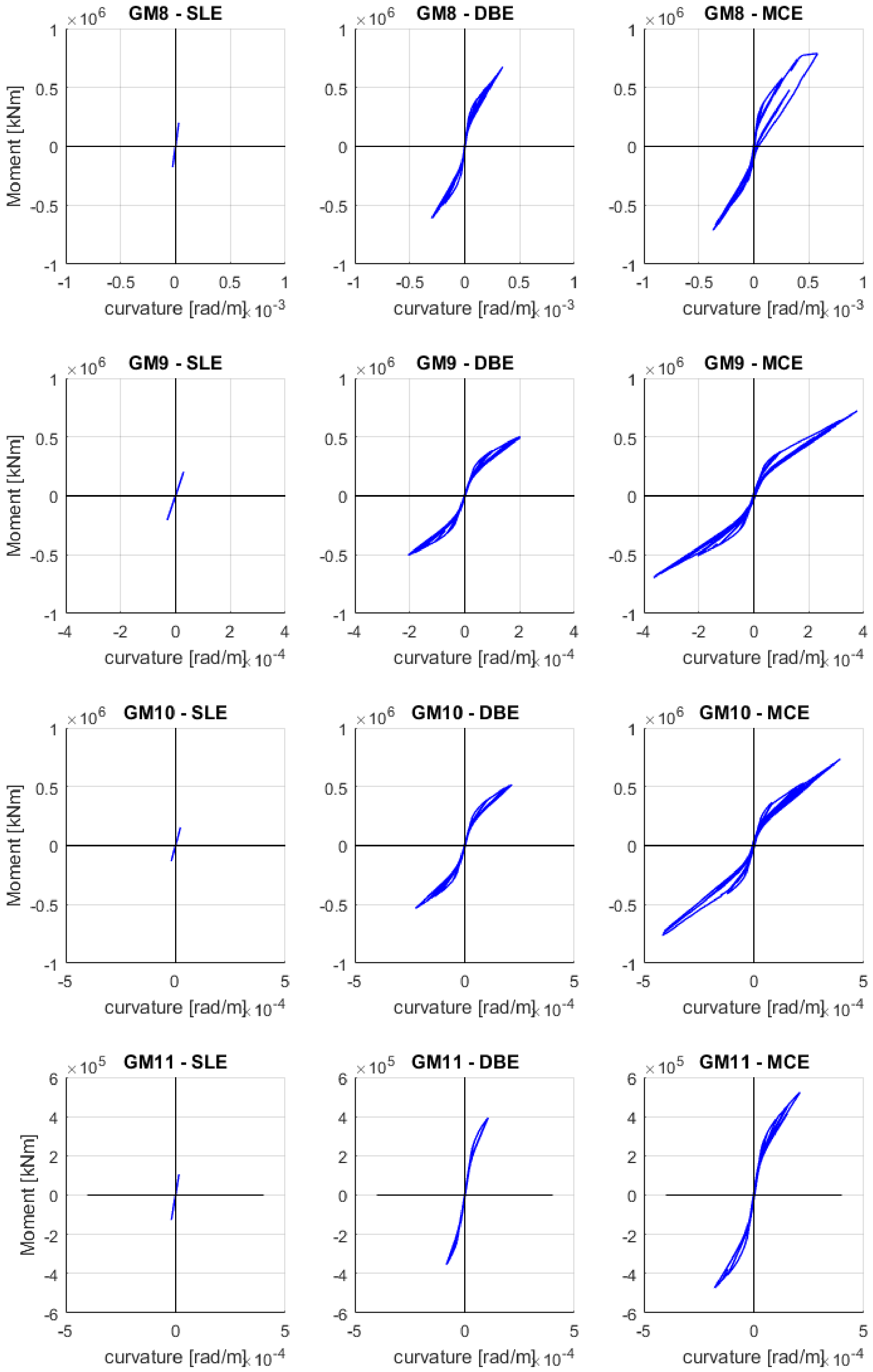
GM8 - SLE
GM8 - DBE
GM8 - MCE
×10^6
Moment [kNm]
1
0.5
0
-0.5
-1
-1
-0.5
0
0.5
1
curvature [rad/m]
×10^-3
GM9 - SLE
GM9 - DBE
GM9 - MCE
×10^6
Moment [kNm]
-4
-2
0
2
4
curvature [rad/m]
×10^-4
GM10 - SLE
GM10 - DBE
GM10 - MCE
×10^6
Moment [kNm]
-5
0
5
curvature [rad/m]
×10^-4
GM11 - SLE
GM11 - DBE
GM11 - MCE
×10^5
Moment [kNm]
6
4
2
0
-2
-4
-6
-5
0
5
curvature [rad/m]
×10^-4

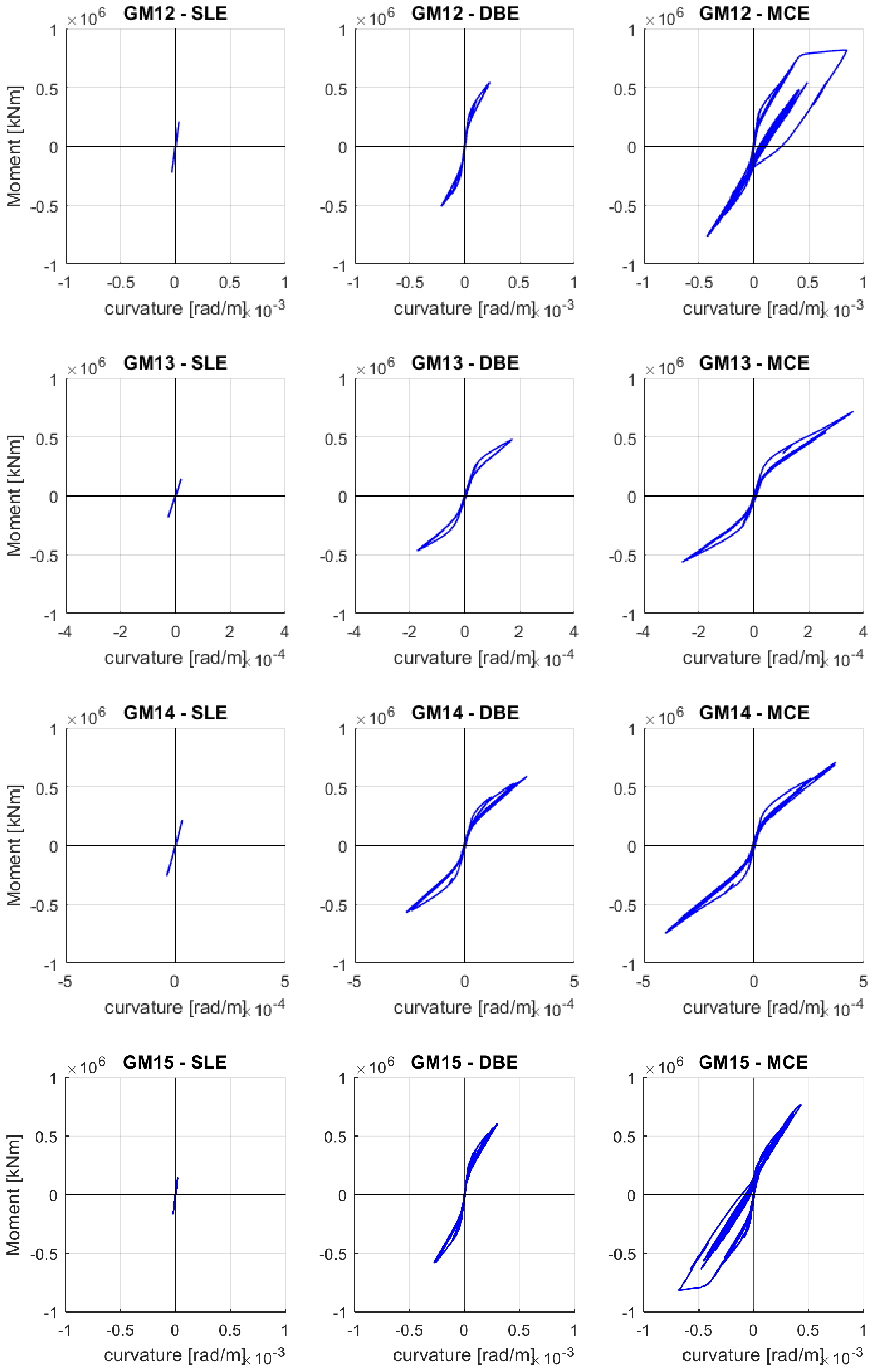
GM12 - SLE
GM12 - DBE
GM12 - MCE
GM13 - SLE
GM13 - DBE
GM13 - MCE
GM14 - SLE
GM14 - DBE
GM14 - MCE
GM15 - SLE
GM15 - DBE
GM15 - MCE
Moment [kNm]
× 10^6
curvature [rad/m]
× 10^-3
× 10^-4
1
0.5
0
-0.5
-1
-4
-2
2
4
-5
5

Moment-curvature response of wall at outrigger from Tower B:

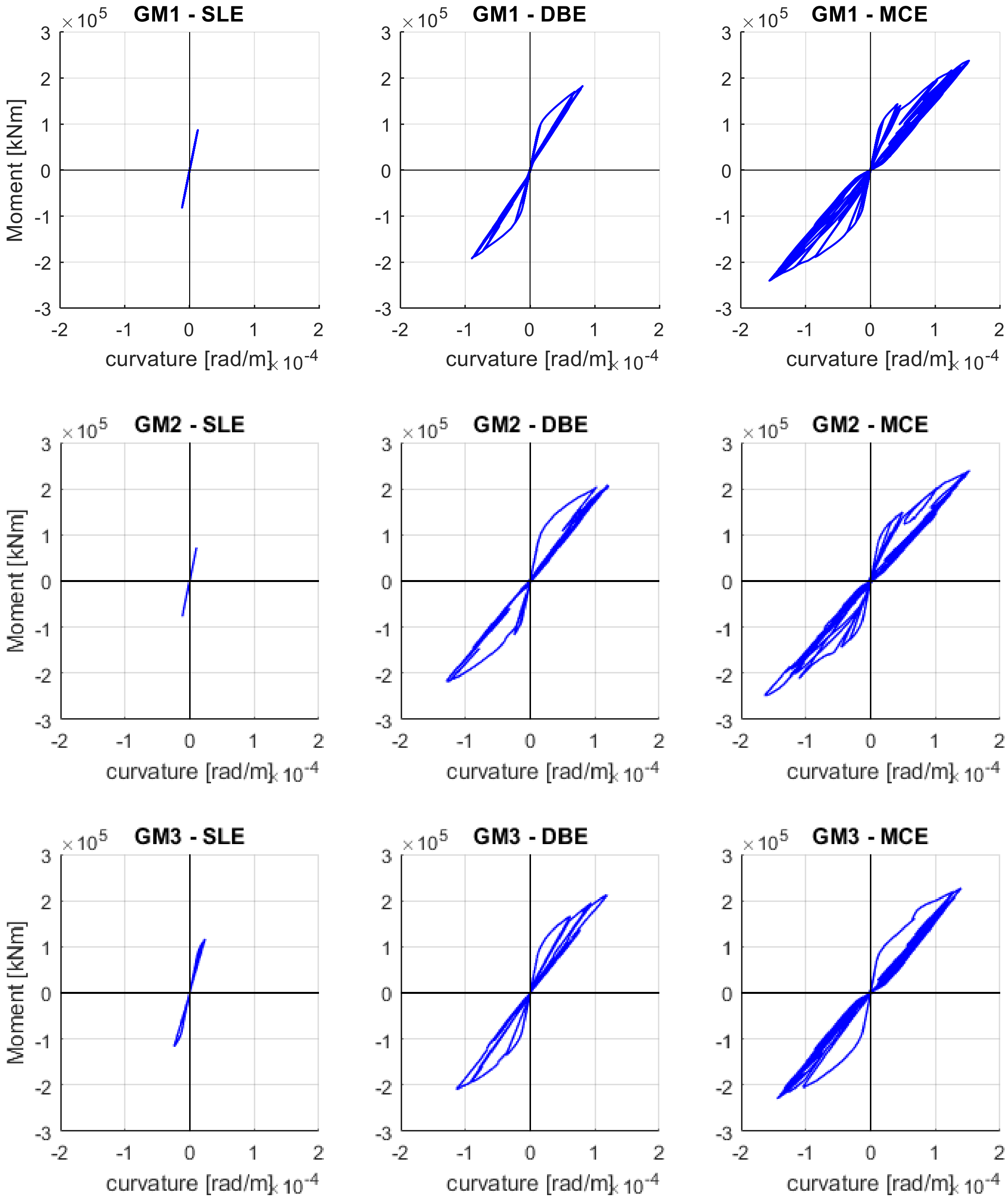

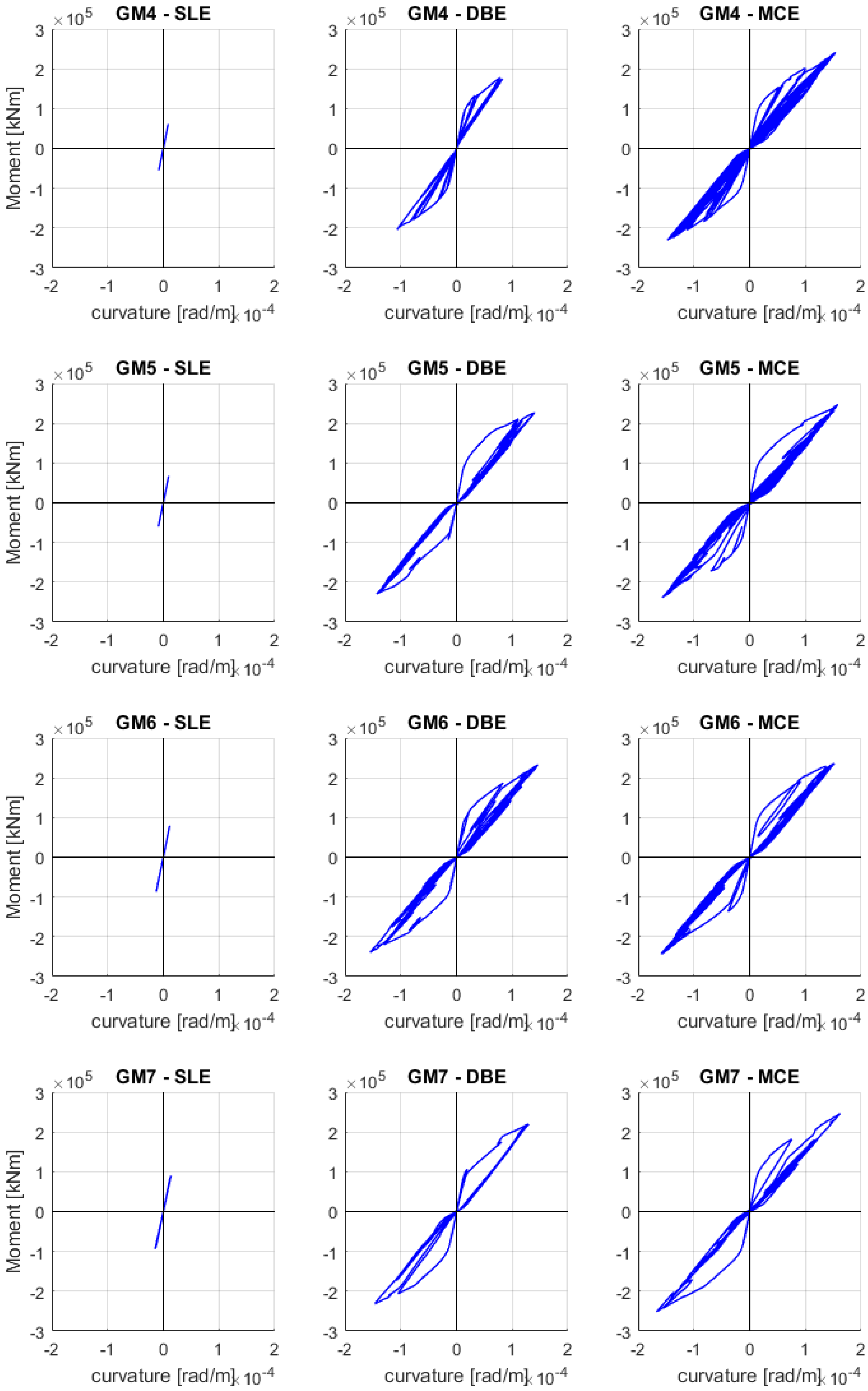
GM4 - SLE
GM4 - DBE
GM4 - MCE
GM5 - SLE
GM5 - DBE
GM5 - MCE
GM6 - SLE
GM6 - DBE
GM6 - MCE
GM7 - SLE
GM7 - DBE
GM7 - MCE
Moment [kNm]
× 10^5
3
2
1
0
-1
-2
-3
curvature [rad/m]
× 10^-4
-2
-1
0
1
2

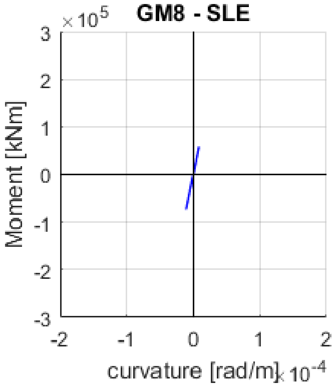
GM8 - SLE
×10^5
3
2
1
0
-1
-2
-3
Moment [kNm]
-2
-1
0
1
2
curvature [rad/m]
×10^-4

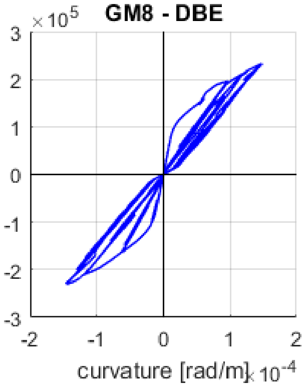
GM8 - DBE
×10^5
3
2
1
0
-1
-2
-3
-2
-1
0
1
2
curvature [rad/m]
×10^-4

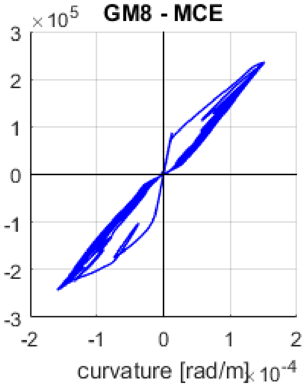
GM8 - MCE
×10^5
3
2
1
0
-1
-2
-3
-2
-1
0
1
2
curvature [rad/m]
×10^-4

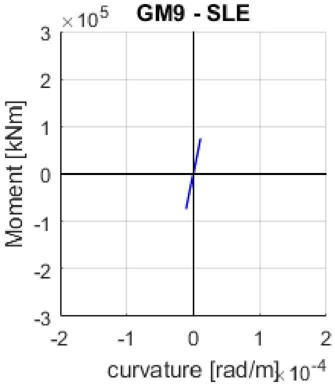
GM9 - SLE
×10^5
3
2
1
0
-1
-2
-3
Moment [kNm]
-2
-1
0
1
2
curvature [rad/m]
×10^-4

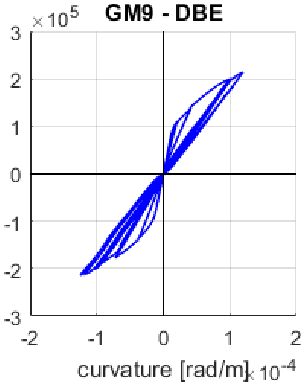
GM9 - DBE
×10^5
3
2
1
0
-1
-2
-3
-2
-1
0
1
2
curvature [rad/m]
×10^-4

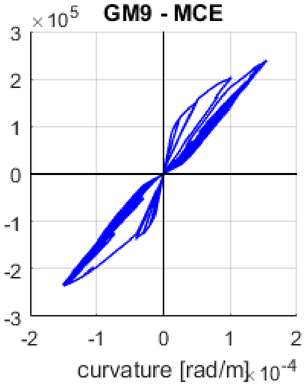
GM9 - MCE
×10^5
3
2
1
0
-1
-2
-3
-2
-1
0
1
2
curvature [rad/m]
×10^-4

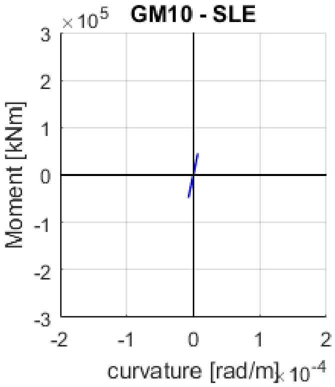
GM10 - SLE
×10^5
3
2
1
0
-1
-2
-3
Moment [kNm]
-2
-1
0
1
2
curvature [rad/m]
×10^-4

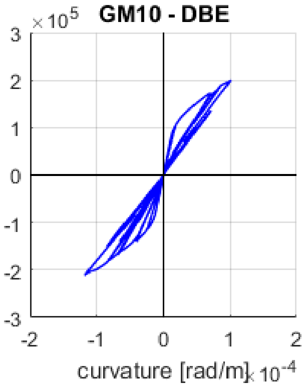
GM10 - DBE
×10^5
3
2
1
0
-1
-2
-3
-2
-1
0
1
2
curvature [rad/m]
×10^-4

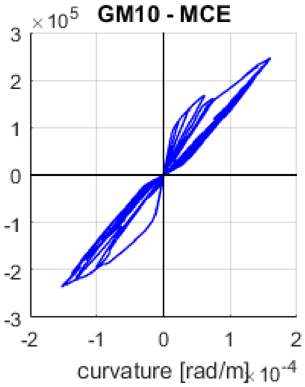
GM10 - MCE
×10^5
3
2
1
0
-1
-2
-3
-2
-1
0
1
2
curvature [rad/m]
×10^-4

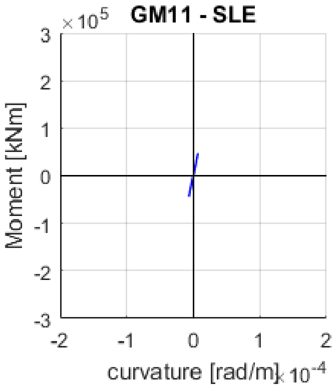
GM11 - SLE
×10^5
3
2
1
0
-1
-2
-3
Moment [kNm]
-2
-1
0
1
2
curvature [rad/m]
×10^-4

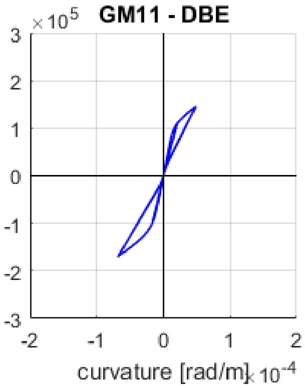
GM11 - DBE
×10^5
3
2
1
0
-1
-2
-3
-2
-1
0
1
2
curvature [rad/m]
×10^-4

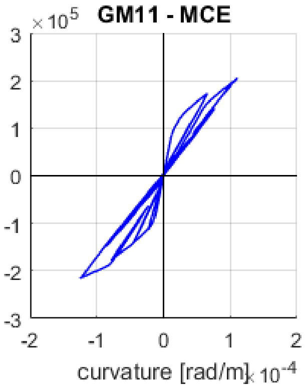
GM11 - MCE
×10^5
3
2
1
0
-1
-2
-3
-2
-1
0
1
2
curvature [rad/m]
×10^-4

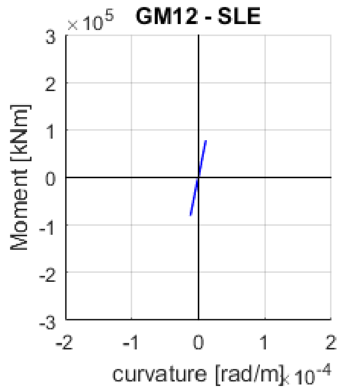
GM12 - SLE
×10^5
Moment [kNm]
curvature [rad/m]
×10^-4
3
2
1
0
-1
-2
-3
-2
-1
0
1
2

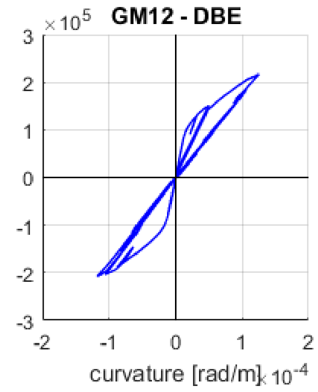
GM12 - DBE
×10^5
curvature [rad/m]
×10^-4
3
2
1
0
-1
-2
-3
-2
-1
0
1
2

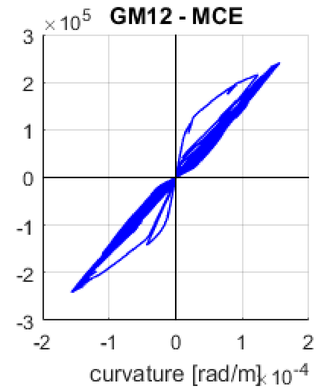
GM12 - MCE
×10^5
curvature [rad/m]
×10^-4
3
2
1
0
-1
-2
-3
-2
-1
0
1
2

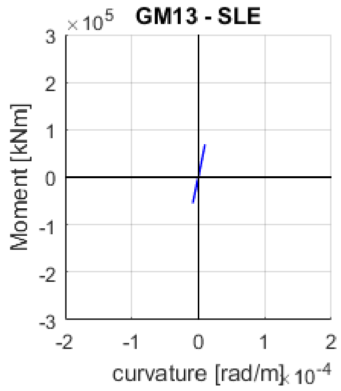
GM13 - SLE
×10^5
Moment [kNm]
curvature [rad/m]
×10^-4
3
2
1
0
-1
-2
-3
-2
-1
0
1
2

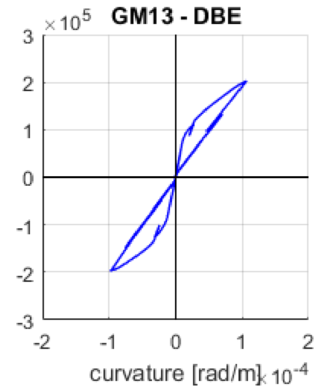
GM13 - DBE
×10^5
curvature [rad/m]
×10^-4
3
2
1
0
-1
-2
-3
-2
-1
0
1
2

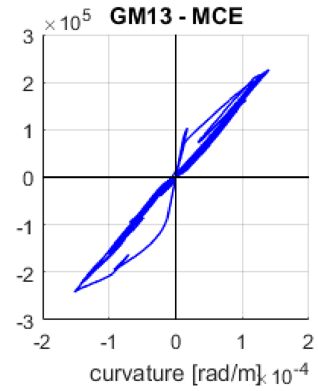
GM13 - MCE
×10^5
curvature [rad/m]
×10^-4
3
2
1
0
-1
-2
-3
-2
-1
0
1
2

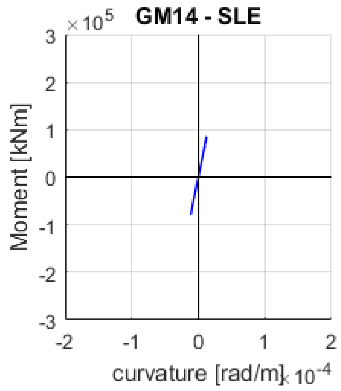
GM14 - SLE
×10^5
Moment [kNm]
curvature [rad/m]
×10^-4
3
2
1
0
-1
-2
-3
-2
-1
0
1
2

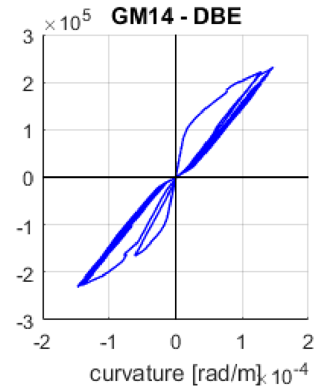
GM14 - DBE
×10^5
curvature [rad/m]
×10^-4
3
2
1
0
-1
-2
-3
-2
-1
0
1
2

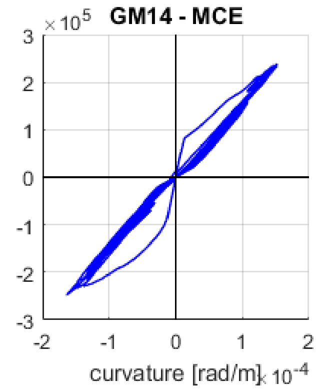
GM14 - MCE
×10^5
curvature [rad/m]
×10^-4
3
2
1
0
-1
-2
-3
-2
-1
0
1
2

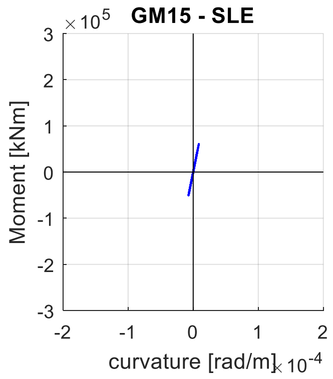
GM15 - SLE
×10^5
Moment [kNm]
curvature [rad/m]
×10^-4
3
2
1
0
-1
-2
-3
-2
-1
0
1
2

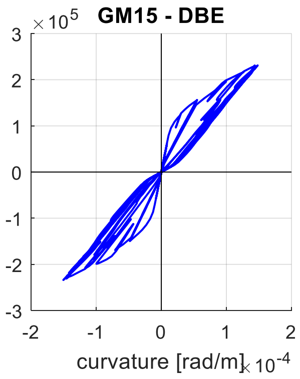
GM15 - DBE
×10^5
curvature [rad/m]
×10^-4
3
2
1
0
-1
-2
-3
-2
-1
0
1
2

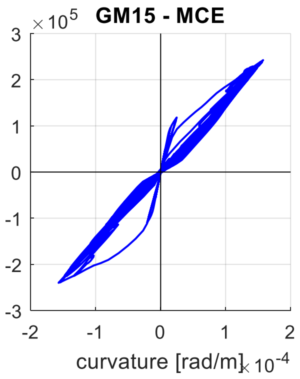
GM15 - MCE
×10^5
curvature [rad/m]
×10^-4
3
2
1
0
-1
-2
-3
-2
-1
0
1
2

Outrigger Fuse Hysteresis from Tower B:

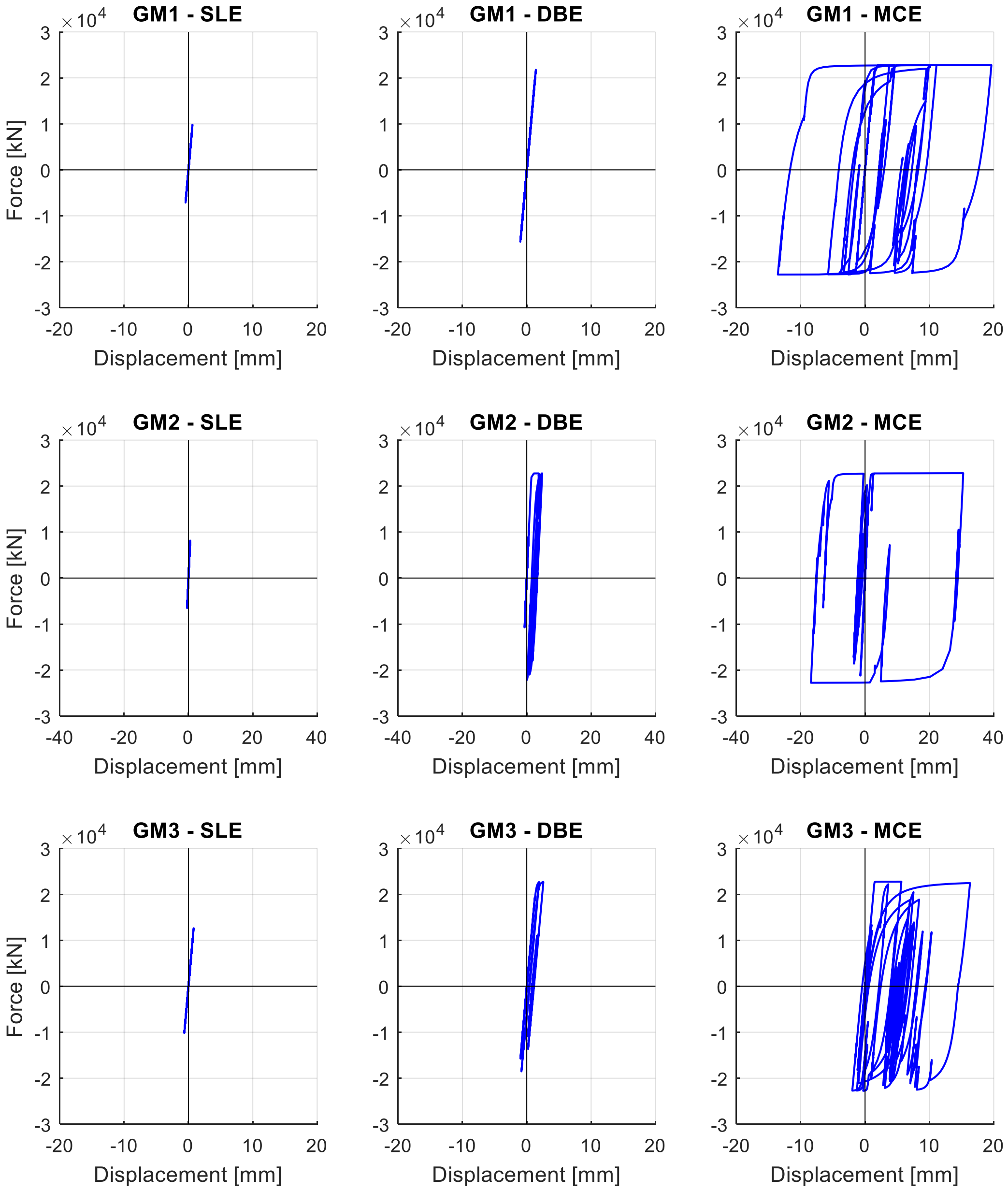

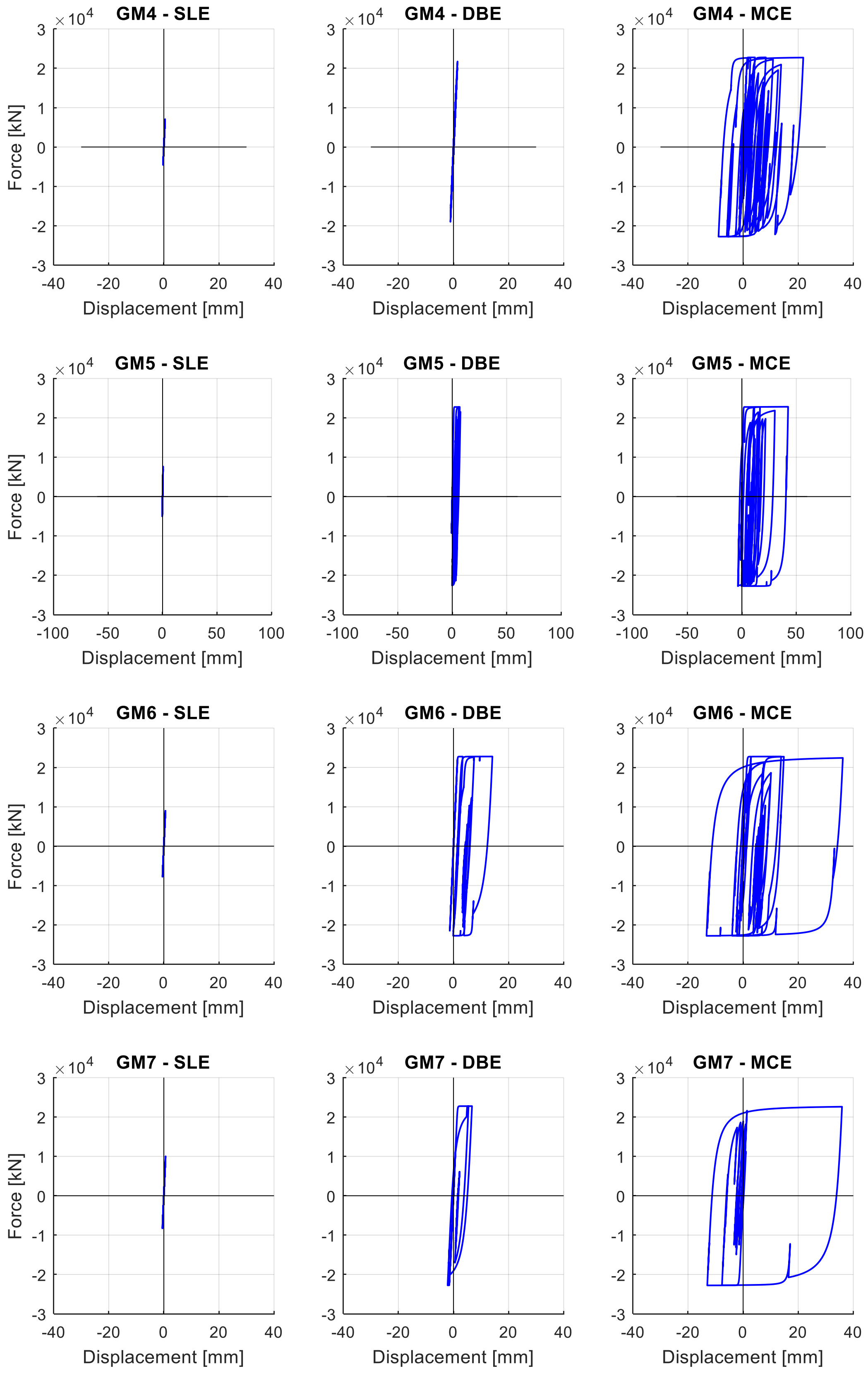
GM4 - SLE
GM4 - DBE
GM4 - MCE
GM5 - SLE
GM5 - DBE
GM5 - MCE
GM6 - SLE
GM6 - DBE
GM6 - MCE
GM7 - SLE
GM7 - DBE
GM7 - MCE
Force [kN]
$\times 10^4$
3
2
1
0
-1
-2
-3
Displacement [mm]
-40
-20
0
20
40
-100
-50
0
50
100

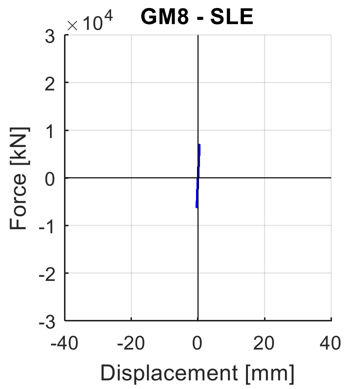
GM8 - SLE
×10^4
3
2
1
0
-1
-2
-3
Force [kN]
-40
-20
0
20
40
Displacement [mm]

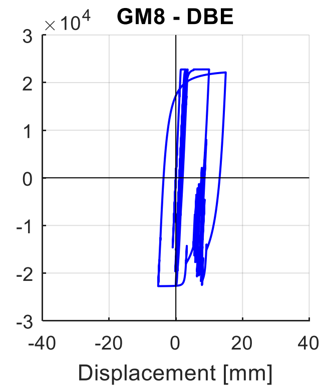
GM8 - DBE
×10^4
3
2
1
0
-1
-2
-3
-40
-20
0
20
40
Displacement [mm]

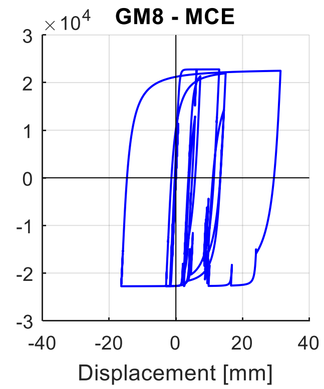
GM8 - MCE
×10^4
3
2
1
0
-1
-2
-3
-40
-20
0
20
40
Displacement [mm]

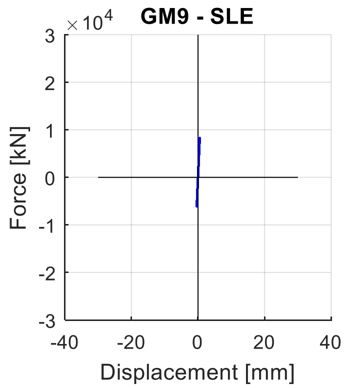
GM9 - SLE
×10^4
3
2
1
0
-1
-2
-3
Force [kN]
-40
-20
0
20
40
Displacement [mm]

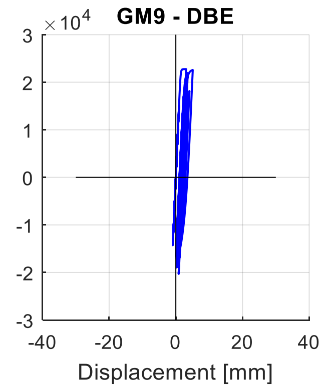
GM9 - DBE
×10^4
3
2
1
0
-1
-2
-3
-40
-20
0
20
40
Displacement [mm]

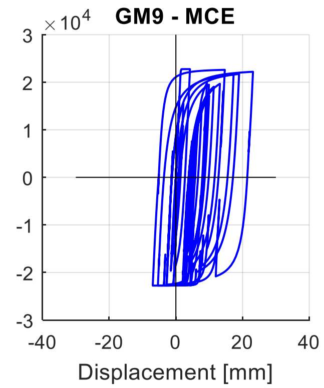
GM9 - MCE
×10^4
3
2
1
0
-1
-2
-3
-40
-20
0
20
40
Displacement [mm]

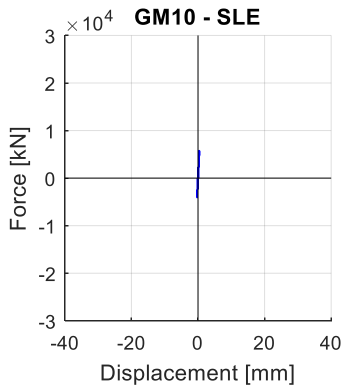
GM10 - SLE
×10^4
3
2
1
0
-1
-2
-3
Force [kN]
-40
-20
0
20
40
Displacement [mm]

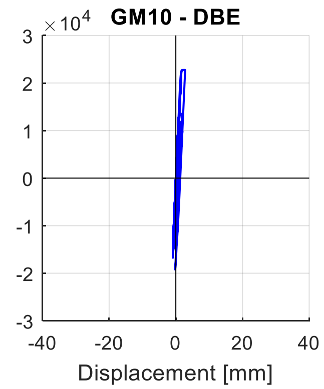
GM10 - DBE
×10^4
3
2
1
0
-1
-2
-3
-40
-20
0
20
40
Displacement [mm]

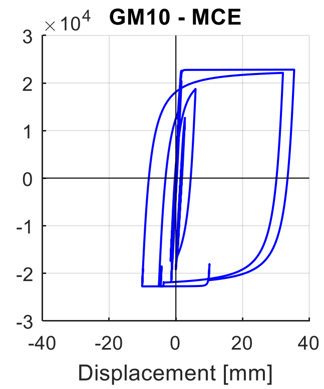
GM10 - MCE
×10^4
3
2
1
0
-1
-2
-3
-40
-20
0
20
40
Displacement [mm]

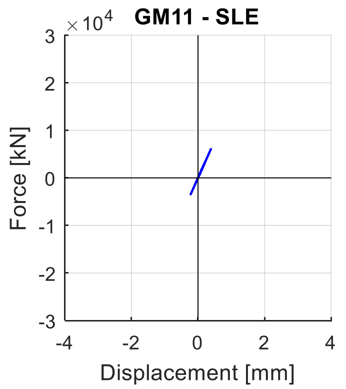
GM11 - SLE
×10^4
3
2
1
0
-1
-2
-3
Force [kN]
-4
-2
0
2
4
Displacement [mm]

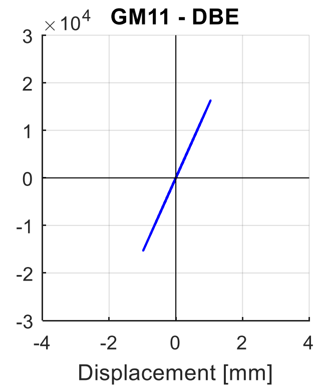
GM11 - DBE
×10^4
3
2
1
0
-1
-2
-3
-4
-2
0
2
4
Displacement [mm]

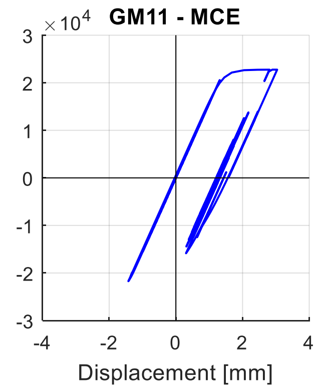
GM11 - MCE
×10^4
3
2
1
0
-1
-2
-3
-4
-2
0
2
4
Displacement [mm]

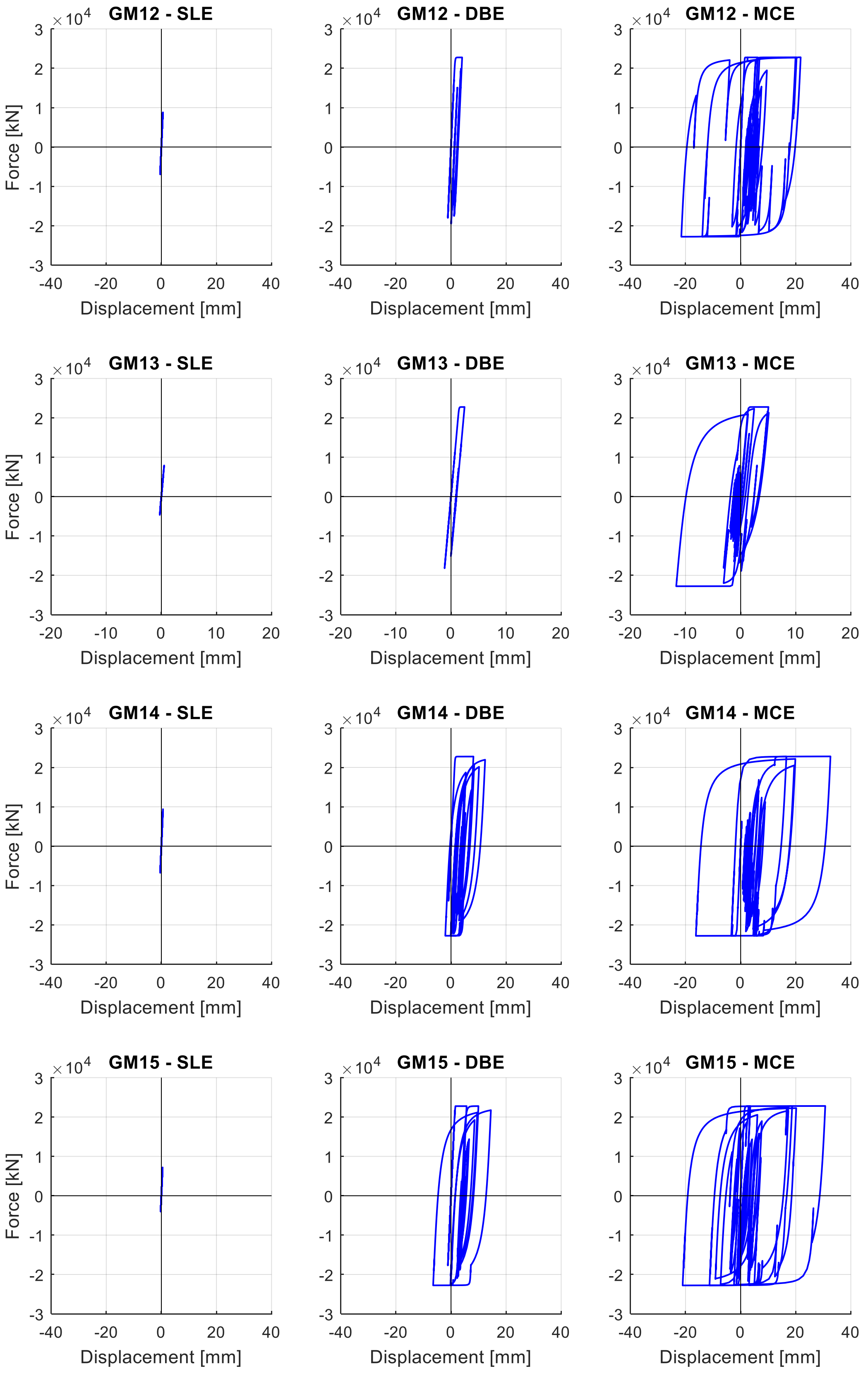
GM12 - SLE
GM12 - DBE
GM12 - MCE
GM13 - SLE
GM13 - DBE
GM13 - MCE
GM14 - SLE
GM14 - DBE
GM14 - MCE
GM15 - SLE
GM15 - DBE
GM15 - MCE
×10^4
Force [kN]
Displacement [mm]
3
2
1
0
-1
-2
-3
-40
-20
0
20
40
-20
-10
0
10
20

E.3 Tower C

Moment-curvature response of wall base from Tower C:

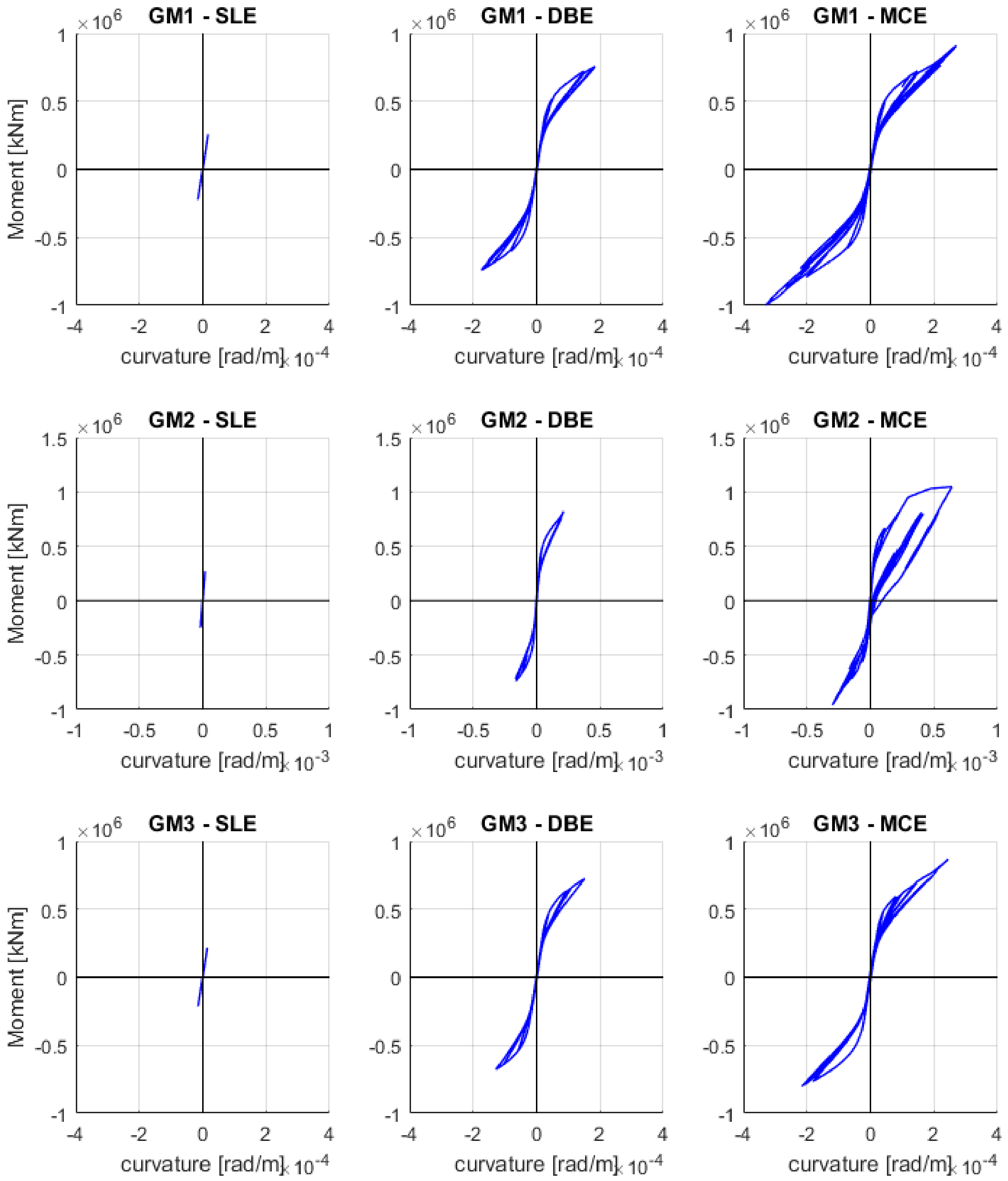

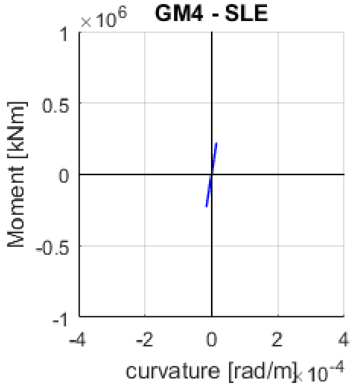

GM4 - SLE

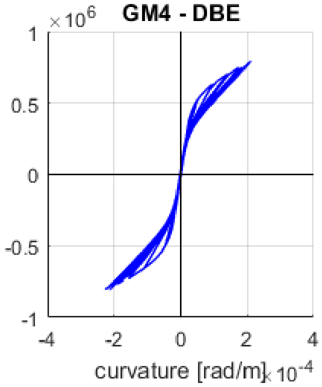

GM4 - DBE

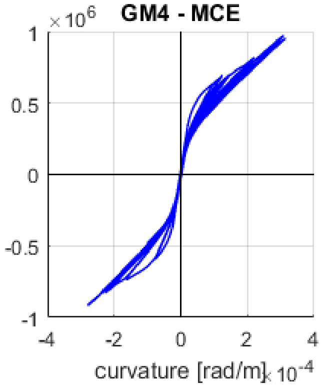

GM4 - MCE

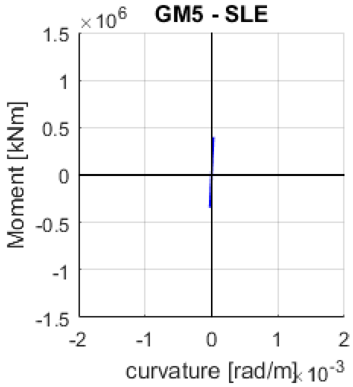

GM5 - SLE

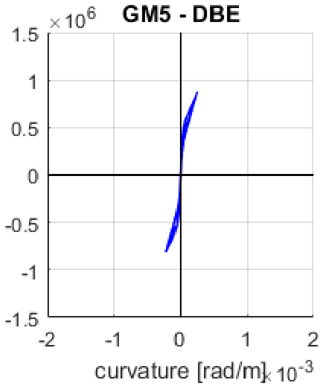

GM5 - DBE

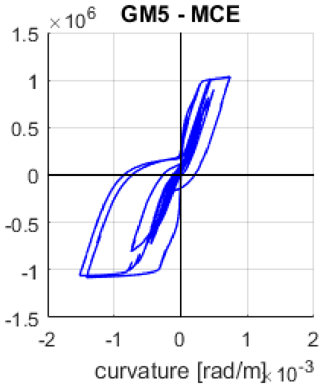

GM5 - MCE

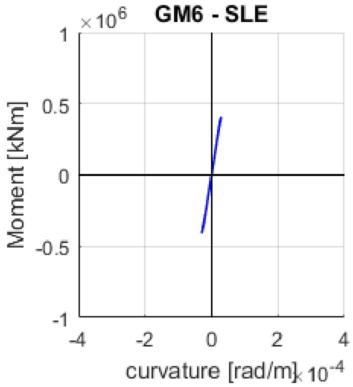

GM6 - SLE

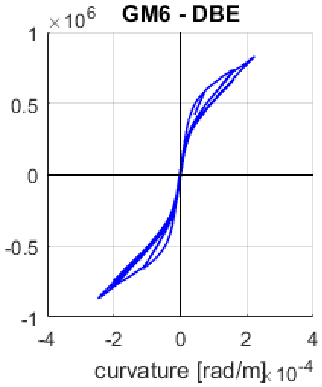

GM6 - DBE

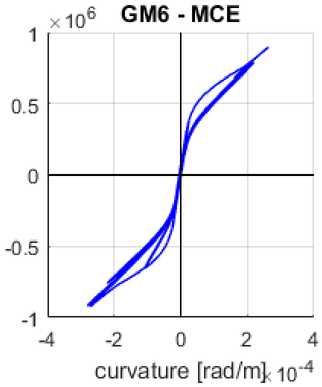

GM6 - MCE

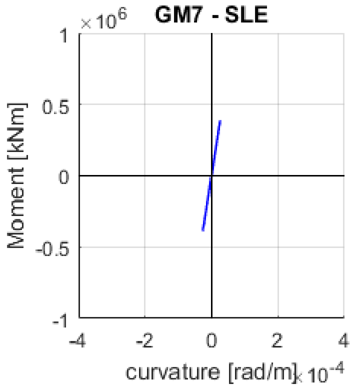

GM7 - SLE

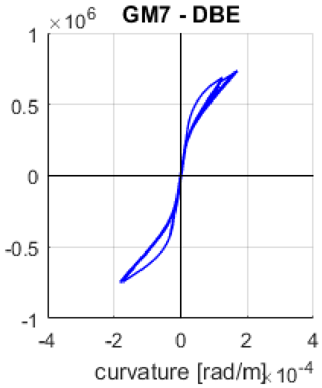

GM7 - DBE

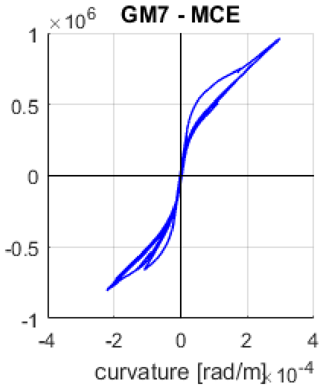

GM7 - MCE

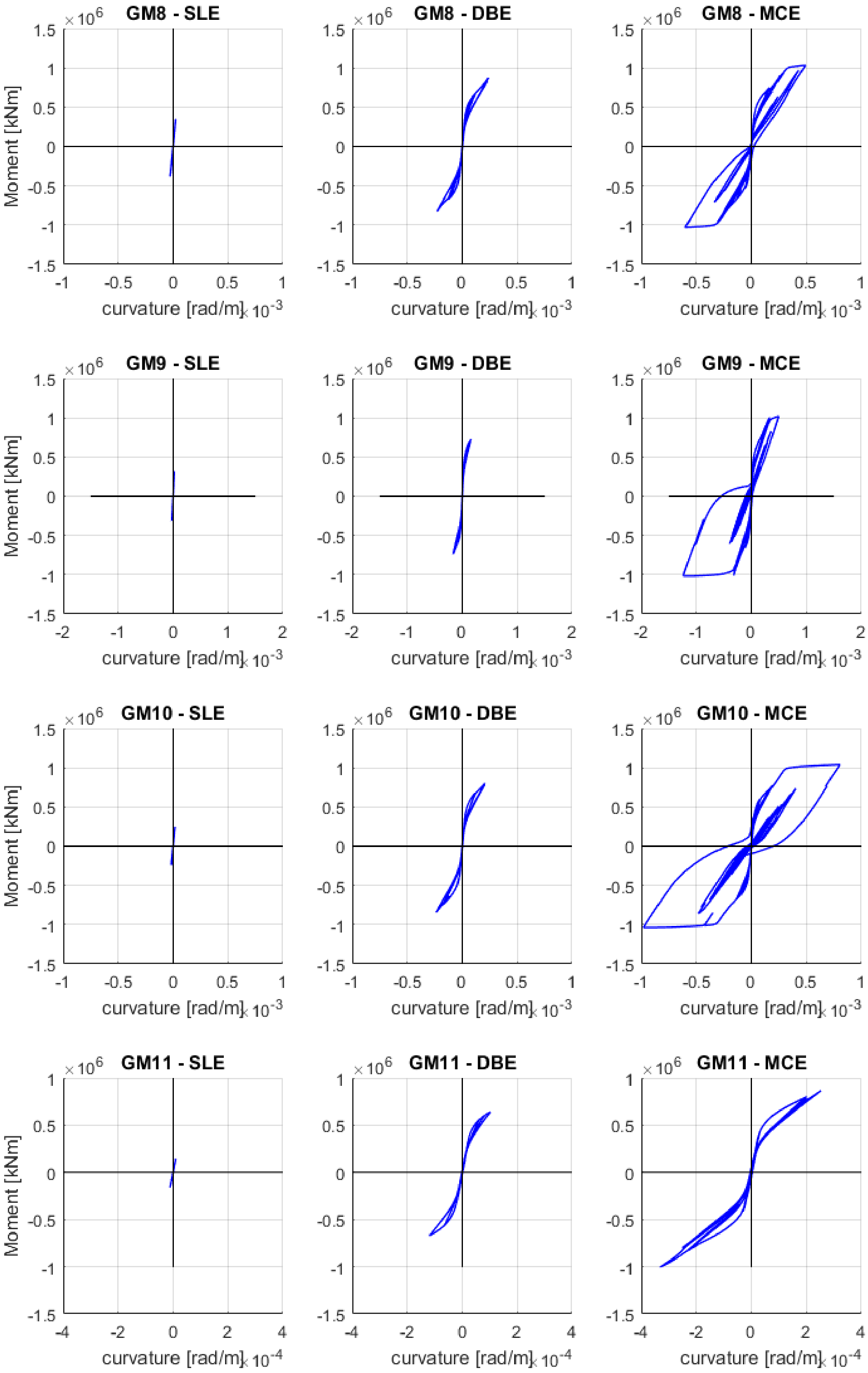
GM8 - SLE
GM8 - DBE
GM8 - MCE
GM9 - SLE
GM9 - DBE
GM9 - MCE
GM10 - SLE
GM10 - DBE
GM10 - MCE
GM11 - SLE
GM11 - DBE
GM11 - MCE
Moment [kNm]
curvature [rad/m]
× 10^6
× 10^-3
× 10^-4
1.5
1
0.5
0
-0.5
-1
-1.5
-4
-2
2
4

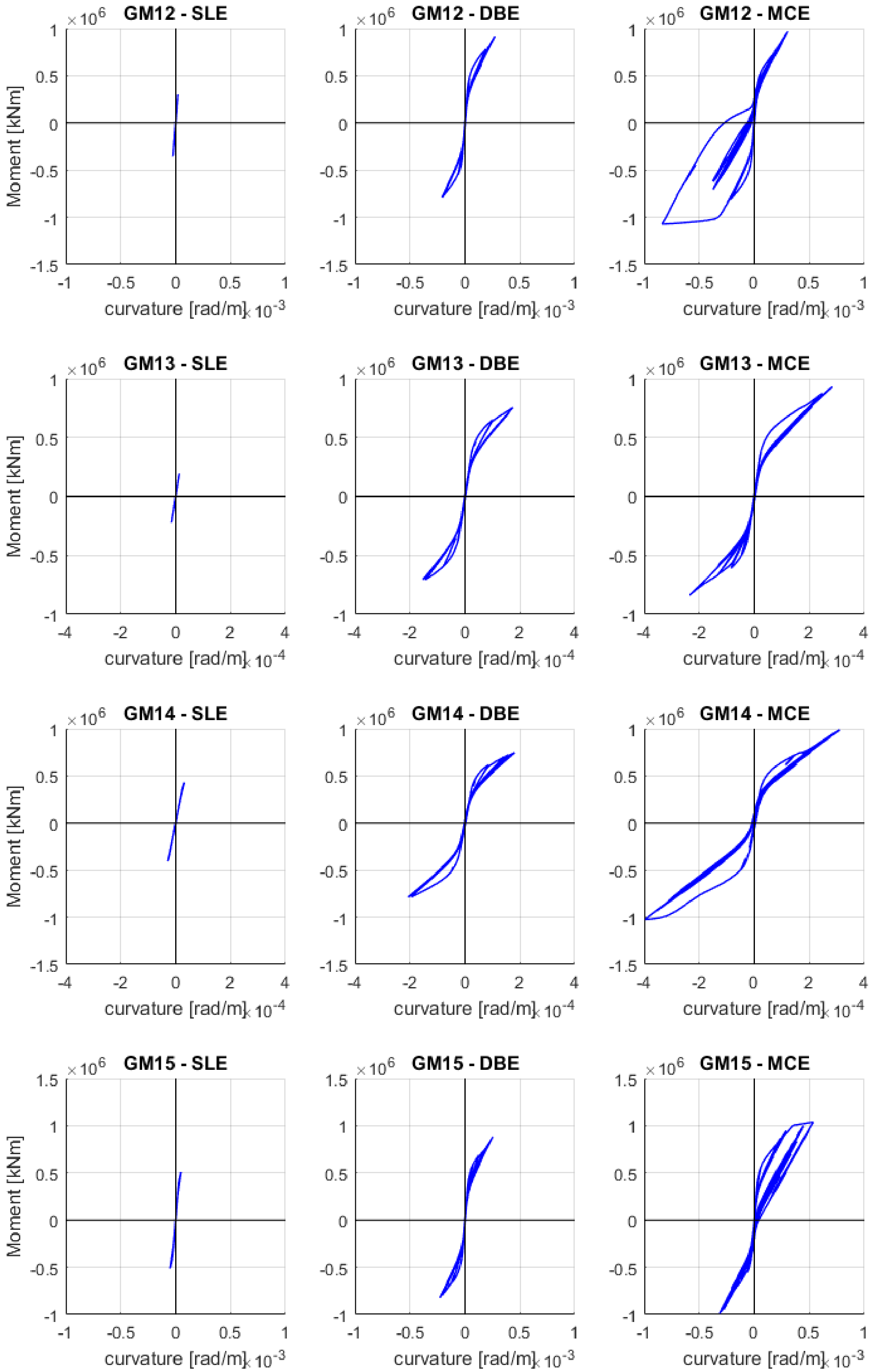
GM12 - SLE
GM12 - DBE
GM12 - MCE
GM13 - SLE
GM13 - DBE
GM13 - MCE
GM14 - SLE
GM14 - DBE
GM14 - MCE
GM15 - SLE
GM15 - DBE
GM15 - MCE
Moment [kNm]
× 10^6
curvature [rad/m]
× 10^-3
× 10^-4
1
0.5
0
-0.5
-1
-1.5
-4
-2
2
4

Moment-curvature response of wall at outrigger from Tower C:

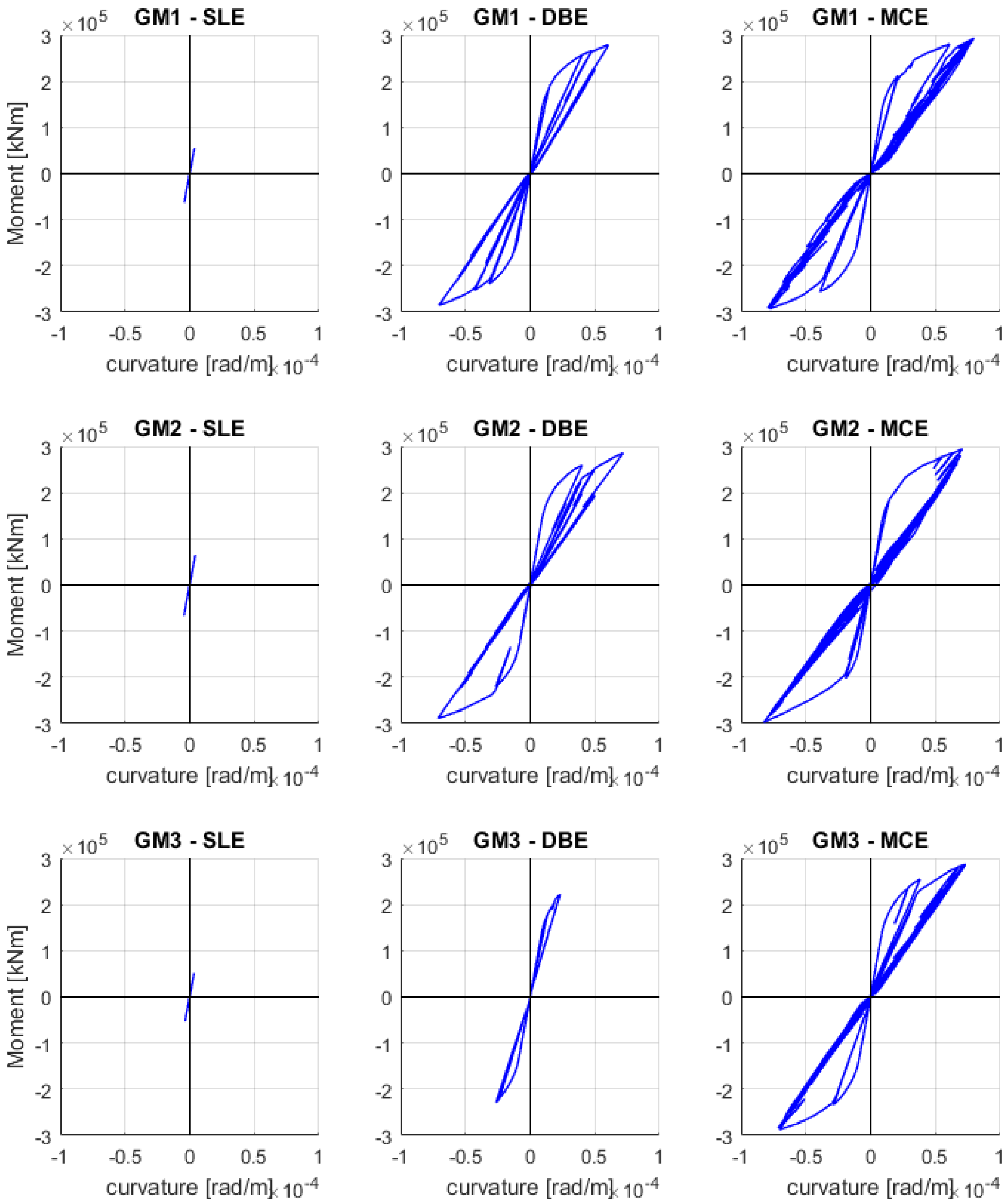

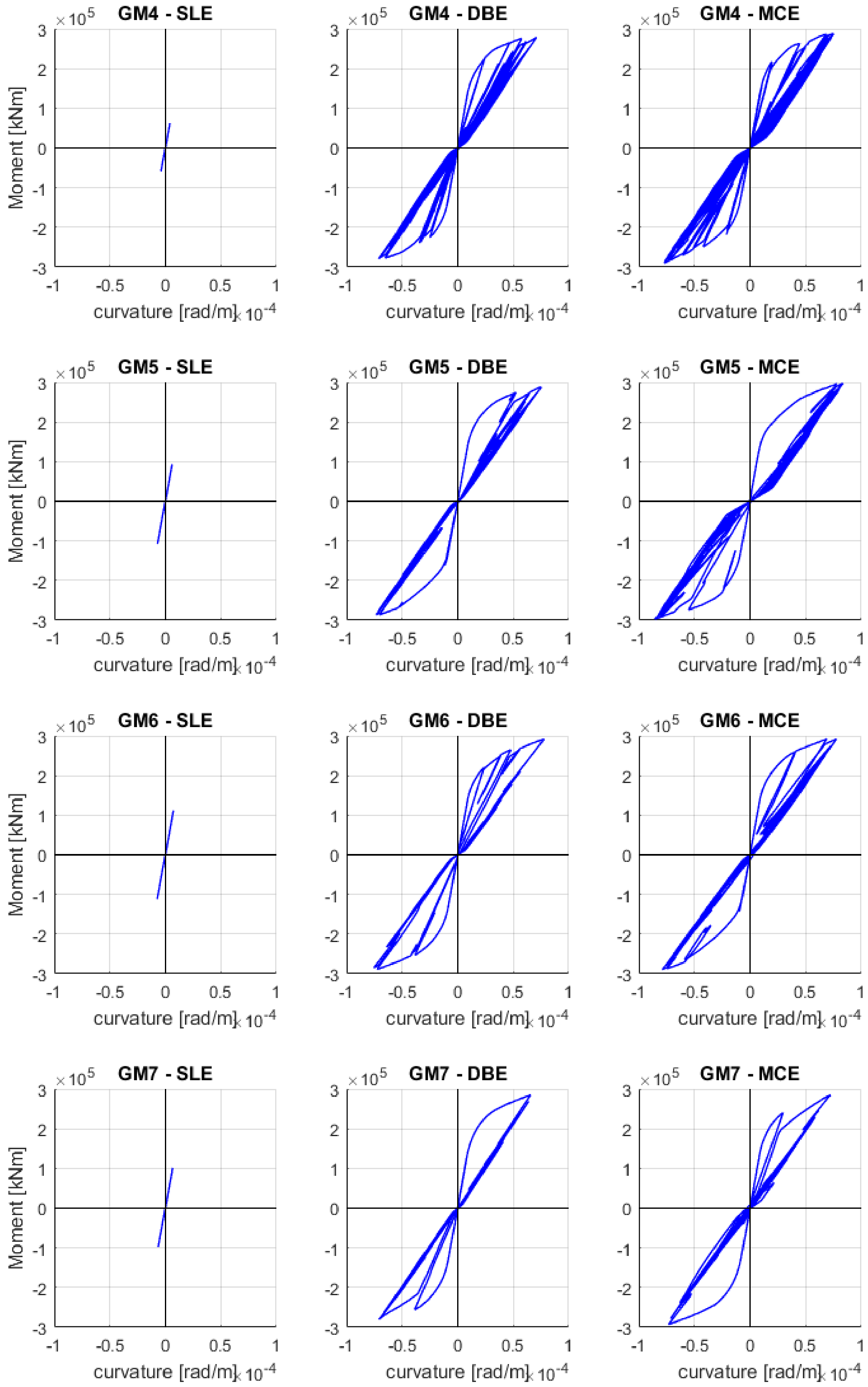
GM4 - SLE
GM4 - DBE
GM4 - MCE
GM5 - SLE
GM5 - DBE
GM5 - MCE
GM6 - SLE
GM6 - DBE
GM6 - MCE
GM7 - SLE
GM7 - DBE
GM7 - MCE
Moment [kNm]
$\times 10^5$
3
2
1
0
-1
-2
-3
curvature [rad/m]
$\times 10^{-4}$
-1
-0.5
0
0.5
1

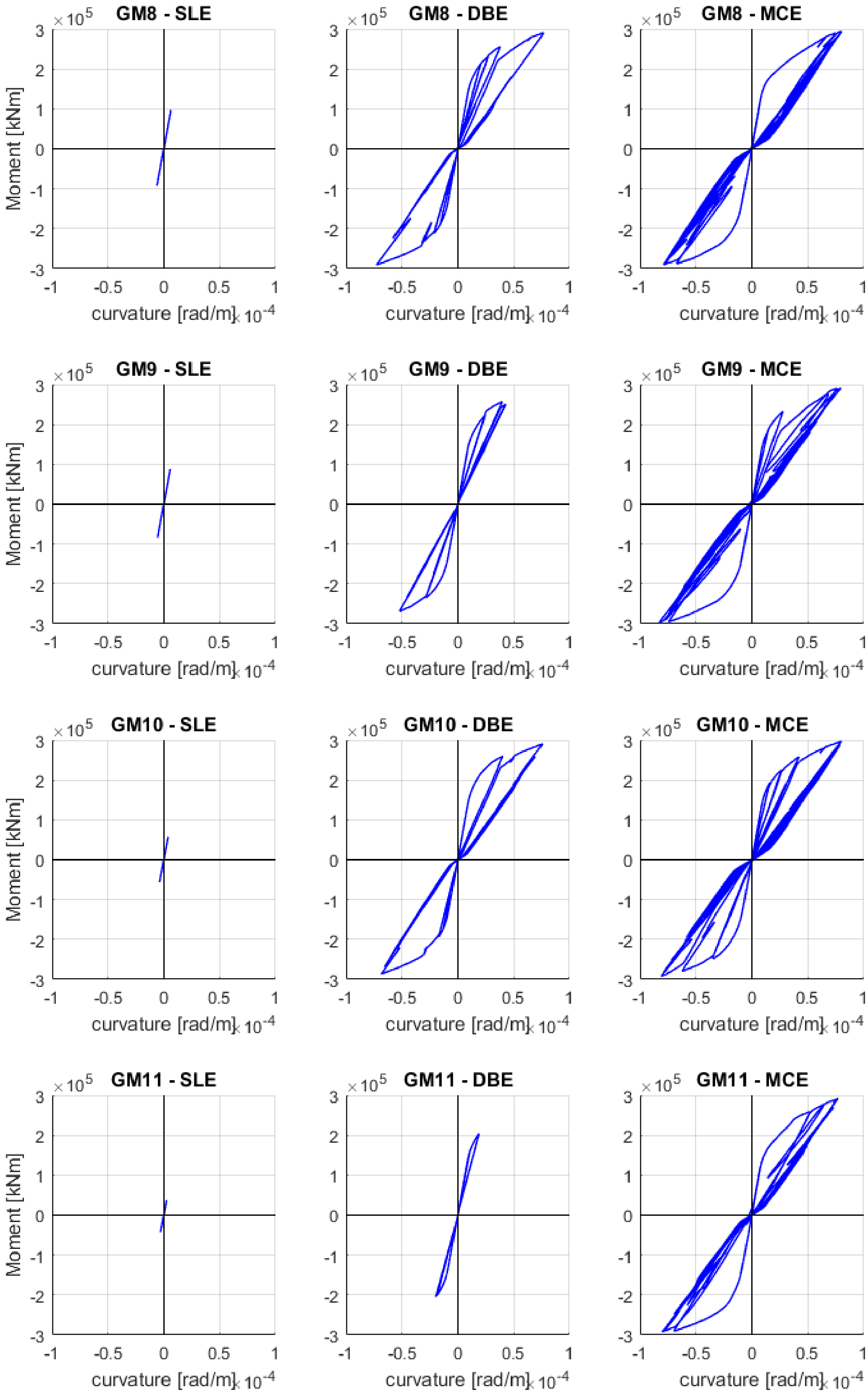
GM8 - SLE
GM8 - DBE
GM8 - MCE
GM9 - SLE
GM9 - DBE
GM9 - MCE
GM10 - SLE
GM10 - DBE
GM10 - MCE
GM11 - SLE
GM11 - DBE
GM11 - MCE
Moment [kNm]
$\times 10^5$
3
2
1
0
-1
-2
-3
curvature [rad/m]
$\times 10^{-4}$
-1
-0.5
0
0.5
1

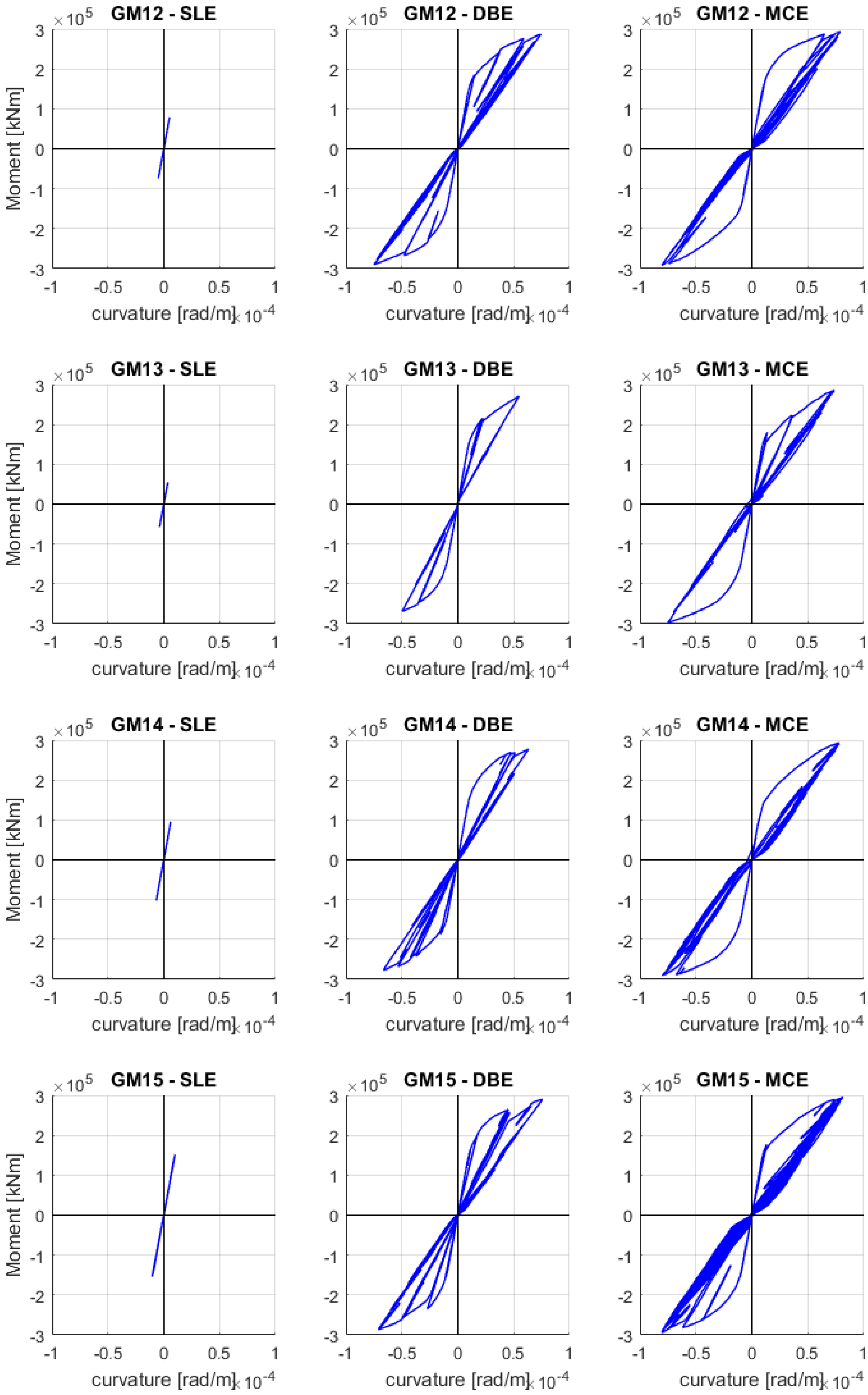
GM12 - SLE
GM12 - DBE
GM12 - MCE
GM13 - SLE
GM13 - DBE
GM13 - MCE
GM14 - SLE
GM14 - DBE
GM14 - MCE
GM15 - SLE
GM15 - DBE
GM15 - MCE
$\times 10^5$
Moment [kNm]
3
2
1
0
-1
-2
-3
curvature [rad/m]
$\times 10^{-4}$
-1
-0.5
0
0.5
1

Outrigger Fuse Hysteresis from Tower C:

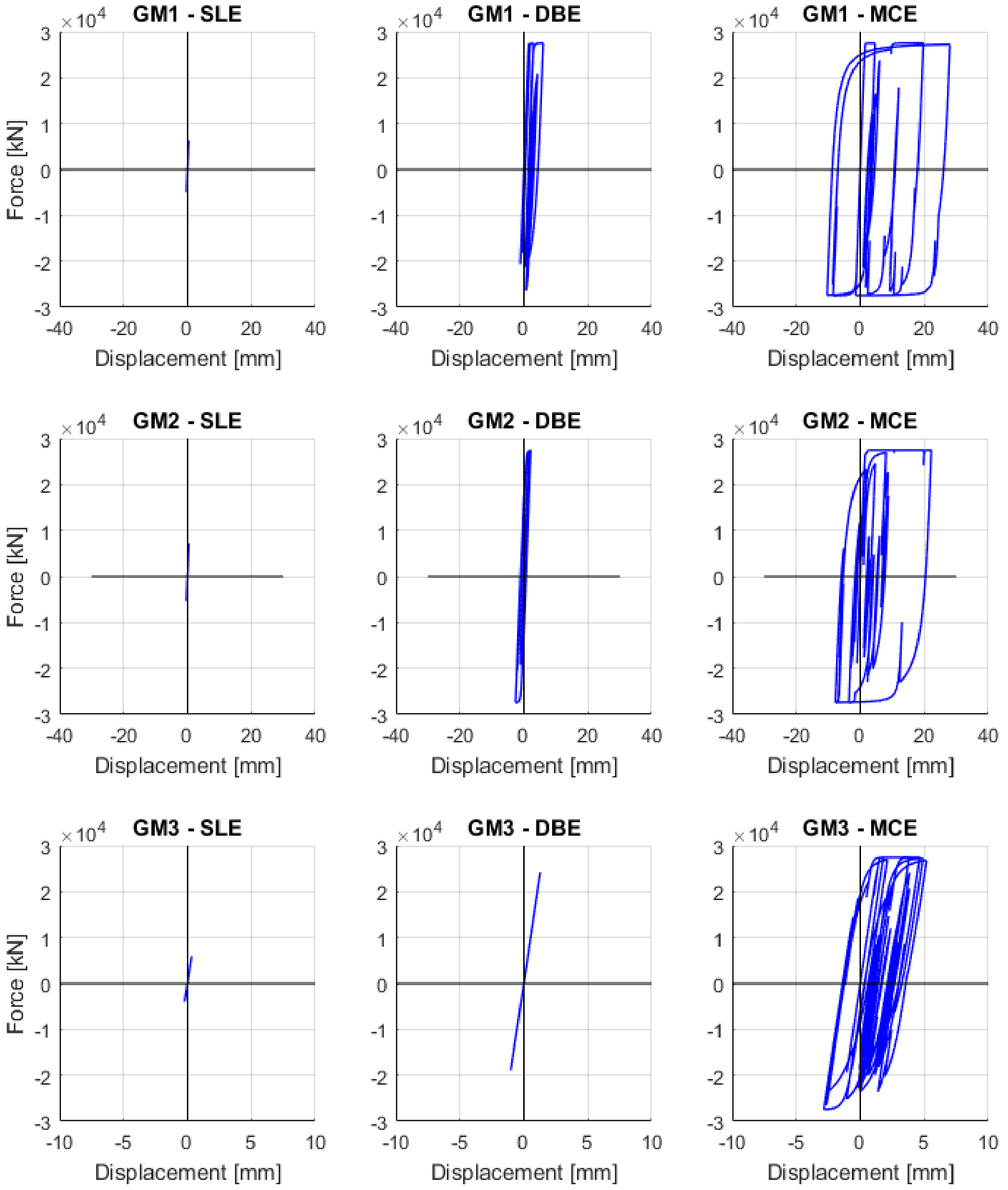

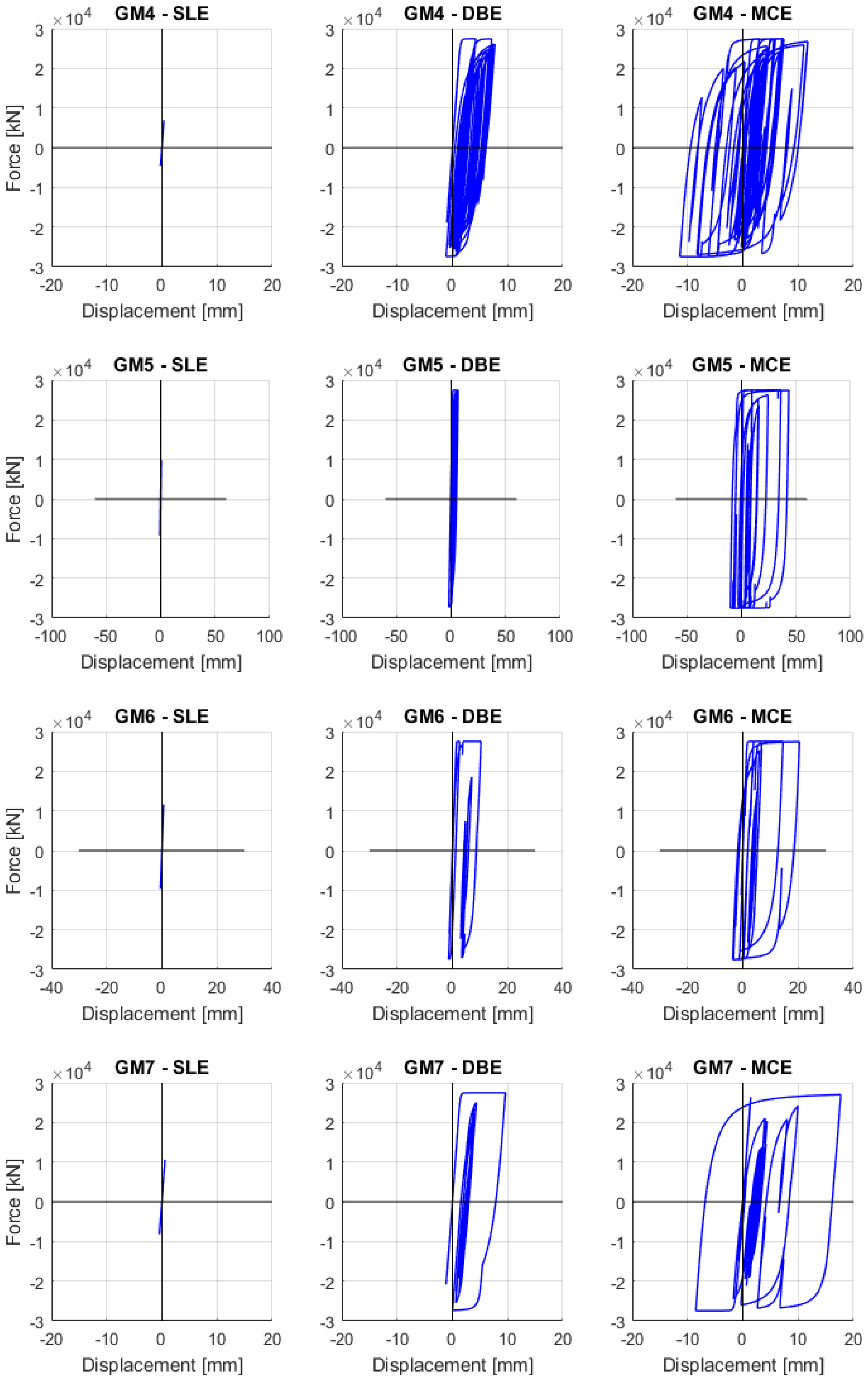
GM4 - SLE
GM4 - DBE
GM4 - MCE
GM5 - SLE
GM5 - DBE
GM5 - MCE
GM6 - SLE
GM6 - DBE
GM6 - MCE
GM7 - SLE
GM7 - DBE
GM7 - MCE
×10^4
Force [kN]
Displacement [mm]
3
2
1
0
-1
-2
-3
-20
-10
0
10
20
-100
-50
50
100
-40
40

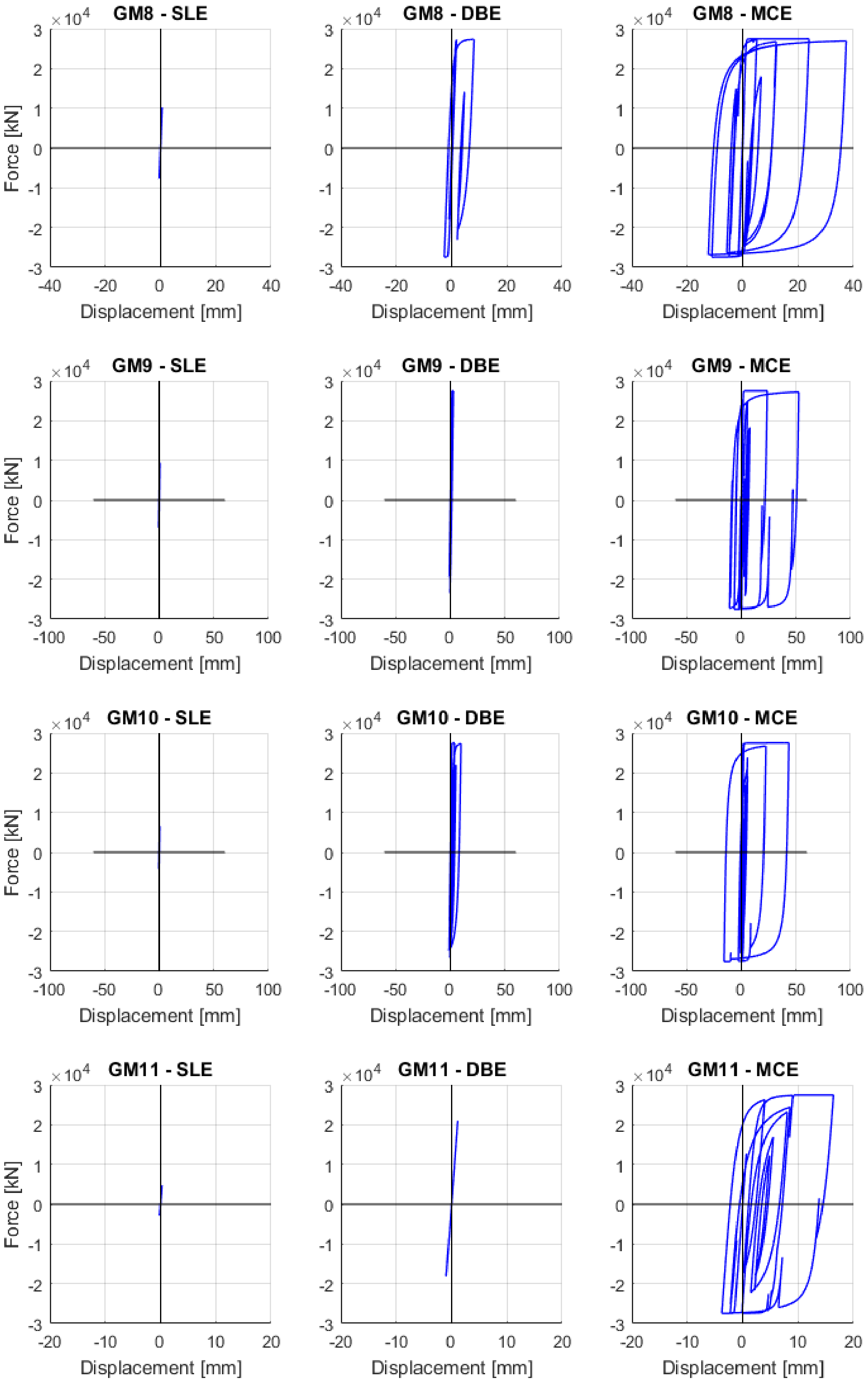
GM8 - SLE
GM8 - DBE
GM8 - MCE
GM9 - SLE
GM9 - DBE
GM9 - MCE
GM10 - SLE
GM10 - DBE
GM10 - MCE
GM11 - SLE
GM11 - DBE
GM11 - MCE
× 10^4
Force [kN]
Displacement [mm]
3
2
1
0
-1
-2
-3
-40
-20
0
20
40
-100
-50
0
50
100
-20
-10
0
10
20

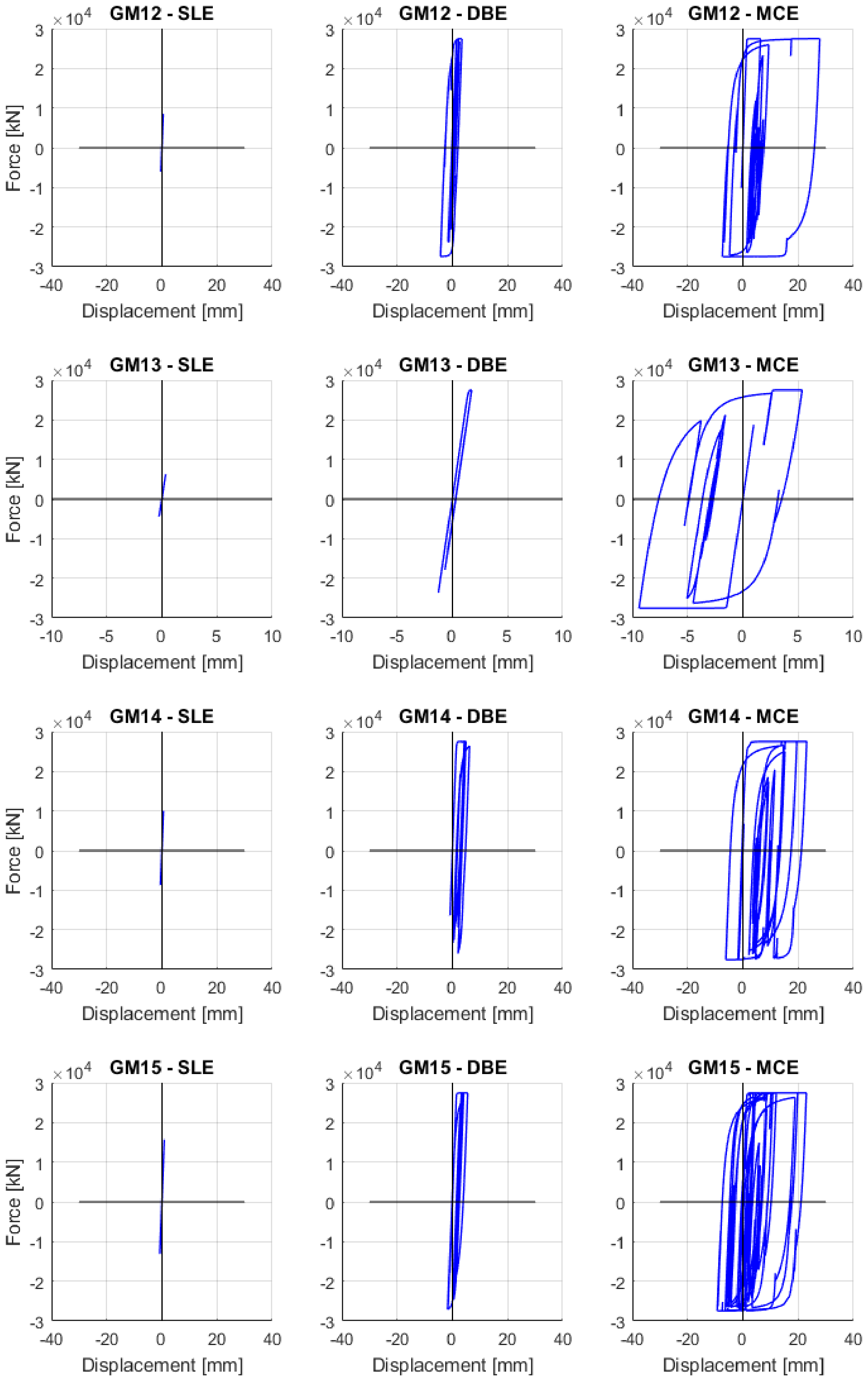
GM12 - SLE
GM12 - DBE
GM12 - MCE
GM13 - SLE
GM13 - DBE
GM13 - MCE
GM14 - SLE
GM14 - DBE
GM14 - MCE
GM15 - SLE
GM15 - DBE
GM15 - MCE
×10^4
Force [kN]
Displacement [mm]
3
2
1
0
-1
-2
-3
-40
-20
0
20
40
-10
-5
0
5
10